

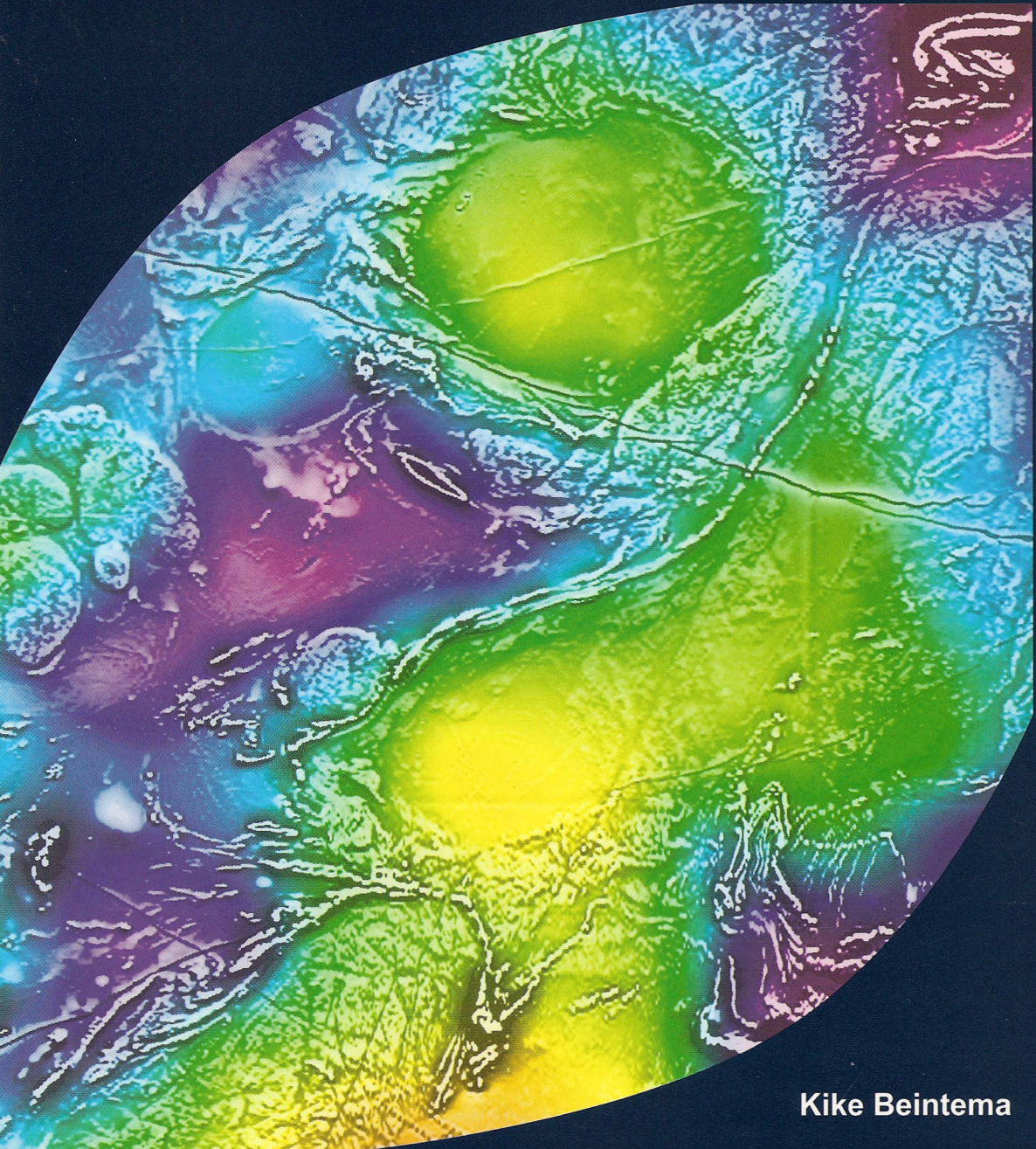
GEOLOGICA ULTRAIECTINA

Mededelingen van de Faculteit Geowetenschappen
Universiteit Utrecht

No. 232

**Geodynamic evolution of the West and Central
Pilbara Craton in Western Australia**

a mid-Archaean active continental margin



Kike Beintema

GEOLOGICA ULTRAIECTINA

Mededelingen van de
Faculteit Geowetenschappen
Universiteit Utrecht

No. 232

**Geodynamic evolution of the West and Central
Pilbara Craton in Western Australia:
a mid-Archaean active continental margin**

Kike A. Beintema

2003

Cover illustration: combined gravity anomaly and short-wavelength magnetic anomaly image of the central part of the Archaean Pilbara Craton in Western Australia (image courtesy AGSO).

The research in this thesis was carried out at the faculty of Earth Sciences at Utrecht University, the Netherlands, under the programme of the Vening Meinesz Research School of Geodynamics (VMSG). The project was funded by the Geodynamisch Onderzoeks Instituut (GOI), part of VMSG. The author acknowledges financial support from the Dr. SchUrmann fund for the field research in the Pilbara with grant numbers 1997114, 1998114, 19991J4a, 2000/14a and 2001/14a, and the Molengraaff fund for their financial support in 1999, 2000 and 2001. The Netherlands Organisation for Scientific Research (NWO) provided support with grant number R75-386, and funding for the Utrecht LA-ICP-MS laboratory.

Faculty of Earth Sciences
Utrecht University
Budapestlaan 4
3584 CD Utrecht
The Netherlands

<http://www.geo.uu.nl>

ISBN: 90-5744-091-1

Geodynamic evolution of the West and Central
Pilbara Craton **in** Western Australia:
a mid-Archaean active continental margin

Geodynamisch model voor de West Pilbara in West Australië:
een Archaïsche actieve continentale marge

(met een samenvatting in het Nederlands)

PROEFSCHRIFT

Ter verkrijging van de graad van Doctor aan de Universiteit Utrecht
op gezag van de Rector Magnificus, Prof. Dr. W.H. Gispen,
ingevolge het besluit van het college voor promoties
in het openbaar te verdedigen op maandag 20 oktober 2003 des middags te 12:45 uur

door

Kike Anneke Beintema
Geboren op 23 juli 1975, te Ede

Promotor:

Prof. Dr. S.H. White
Faculteit Geowetenschappen
Universiteit Utrecht

Co-promotor:

Dr. J.R. Wijbrans
Faculteit Aard- en Levenswetenschappen
Vrije Universiteit Amsterdam

Members of the dissertation committee:

Dr. R.S. Blewett
Geoscience Australia
Canberra, Australia

Prof. Dr. A. Kroner
Universitat Mainz
Mainz, Germany

Prof. Dr. H.N.A. Priem
Universiteit Utrecht
Utrecht, The Netherlands

Dr. R.H. Smithies
Geological Survey of Western Australia
Perth, Australia

Prof. Dr. M.J. de Wit
University of Cape Town
Cape Town, South Africa

Contents

1 Introduction	11
1.1 The Archaean Earth and plate tectonics	11
1.2 The Pilbara Craton in Western Australia	12
1.3 Problem statement	13
1.4 Approach	13
1.5 Outline of this thesis	14
2 The Archaean	15
2.1 Introduction	15
2.2 Granites and greenstones	15
2.3 Tectonic settings of Archaean terrains	17
2.4 Thermal evolution of the Earth	18
2.5 Plate tectonics?	18
2.5.1 Subduction	18
2.5.2 Low angle subduction	20
2.5.3 Geochemical signatures of subduction	21
2.6 Alternative geodynamic models	21
2.7 Impacts	23
2.8 Crustal growth and formation of cratons	23
2.9 Summary	26
3 Geology of the Archaean Pilbara Craton - brief overview	27
3.1 Introduction	27
3.2 Domains, domain boundaries and stratigraphy	27
3.3 The East Pilbara	30
3.3.1 The Nullagine Domain	30
3.3.2 The Marble Bar Domain	32
3.3.3 The Pilgallgoora Domain	33
3.4 The Tabba Tabba Shear Zone	35
3.5 The Central Pilbara	36
3.5.1 Mallina Domain	36

3.5.2 Whim Creek Belt (Sholl-Whim Creek Domain)	39
3.5.3 Sholl Belt (Sholl-Whim Creek Domain)	39
3.6 The Sholl Shear Zone	40
3.7 The West Pilbara	40
3.7.1 The Roebourne Domain	40
3.8 Tectonic models and geodynamics	42
3.9 Summary	45
4 Lithology, structure and geochemistry of the ca 3.5 Ga North Star Basalt in the Marble Bar Greenstone Belt, Archaean Pilbara Craton, Western Australia	47
Abstract	47
4.1 Introduction	47
4.2 Regional Geology	50
4.3 Lithology	52
4.3.1 The extrusive stratigraphy	52
4.3.2 Sills	54
4.3.3 Dykes	55
4.3.4 Metamorphism	55
4.3.5 Lithology - discussion	56
4.4 Geochemistry	57
4.4.1 Analytical methods	57
4.4.2 Results	57
4.4.3 Interpretation of geochemical data	57
4.4.4 Discussion of geochemical data	64
4.5 Structural geology	66
4.5.1 Introduction	66
4.5.2 Shears	66
4.5.3 Folds	67
4.5.4 Brittle faults	67
4.5.5 Discussion of structures	68
4.6 $^{40}\text{Ar}/^{39}\text{Ar}$ Geochronology	68
4.7 Tectonic synthesis	70
4.8 Summary and Conclusions	72
5 Structural, geochronological and geochemical constraints on the tectonic evolution of the West and adjacent Central Pilbara Craton, Western Australia	73
Abstract	73
5.1 Introduction	73
5.2 Regional Geology	74
5.2.1 Domains and domain boundaries	74
5.2.2 Lithology	76
5.3 Structural Geology	80
5.3.1 Introduction	80

5.3.2 The Roeboume Domain	80
5.3.3 Sholl Belt	87
5.3.4 Whim Creek Belt	88
5.3.5 The Sholl Shear Zone	90
5A Geochemistry	100
5.4.1 Introduction	100
5.4.2 Analytical methods	101
5.4.3 Geochemical results	102
5.4.4 Discussion of the geochemical results	102
5.4.5 Summary & conclusions of geochemical results	107
5.5 Geochronology	108
5.5.1 Introduction	108
5.5.2 Results - geochronology	108
5.5.3 Discussion - $^{40}\text{Ar}/^{39}\text{Ar}$ geochronology	111
5.5.4 U-Pb zircon analyses	III
5.5.5 Summary of geochronological results	112
5.6 Tectonic synthesis	114
5.7 Summary and conclusions	117
6 New constraints on the timing of tectonic events in the Archaean Central Pilbara Craton, Western Australia.	119
Abstract	119
6.1 Introduction	119
6.2 Geological setting	120
6.3 Sample descriptions	122
6.4 Analytical procedures	124
6.4.1 Sample preparation	124
6.4.2 Laser ablation ICP-MS U-Pb zircon analysis	124
6.4.3 SHRIMP U-Pb zircon analysis	126
6.4.4 U-Pb data processing	126
6.4.5 Zircon major and trace element analysis	127
6.5 Results	127
6.5.1 Standard data	129
6.5.2 Comparison of laser ablation ICP-MS and SHRIMP results	130
6.6 Discussion	132
6.7 Tectonic implications	137
6.8 Summary and Conclusions	138
7 The Tappa Tappa Shear Zone: its role in the mid-Archaean tectonic evolution of the Central Pilbara Craton, Western Australia	139
Abstract	139
7.1 Introduction	139
7.2 Regional Geology	140

7.3 Lithology and Structural Geology	145
7.3.1 Introduction	145
7.3.2 Lithology and metamorphism	145
7.3.3 Structural geology of the Tabba Tabba Shear Zone	146
7.3.4 Structural geology of the Mallina Basin	158
7.3.5 Summary of deformation history	161
7.4 Geochronology	162
7.4.1 Introduction - geochronology	162
7.4.2 Analytical techniques - $^{40}\text{Ar}/^{39}\text{Ar}$ geochronology	162
7.4.3 Results - geochronology	162
7.4.4 Discussion - geochronology	162
7.5 Geochemistry	166
7.5.1 Introduction - geochemistry	166
7.5.2 Analytical methods	167
7.5.3 Results of geochemical analyses	168
7.5.4 Interpretation of geochemistry	168
7.5.5 Summary of geochemistry	174
7.6 Synthesis	174
7.7 Summary & Conclusions	177

8 The West and Central Pilbara Craton, Australia: a mid-Archaean active continental margin **179**

Abstract	179
8.1 Introduction	179
8.2 Plate tectonics and subduction in the Archaean	181
8.2.1 Subduction - or not?	183
8.2.2 Shallow subduction	185
8.2.3 Subduction-related magmatism	186
8.3 Regional geology of the Archaean Pilbara Craton	186
8.3.1 Domains and domain boundaries	186
8.3.2 Lithology and stratigraphy	188
8.3.3 Geochronology	189
8.3.4 Previous tectonic models for the Pilbara	189
8.4 Tectonic framework for the West and Central Pilbara	191
8.4.1 The Roeboume Domain, West Pilbara	191
8.4.2 The Sholl Shear Zone; boundary between West and Central Pilbara	193
8.4.3 The Sholl Belt, Central Pilbara	193
8.4.4 The Whim Creek Belt, Central Pilbara	193
8.4.5 The Mallina Basin, Central Pilbara	194
8.4.6 The Tabba Tabba Shear Zone: boundary between Central and East Pilbara	194
8.4.7 The role of the East Pilbara	196
8.4.8 Tectonic synthesis	197
8.5 Geodynamic model	198
8.5.1 Introduction	198
8.5.2 ca 3265 Ma	199

8.5.3 ca 3150 Ma	202
8.5.4ca 3150 - 3115 Ma	202
8.5.5 ca 3020 - 3010 Ma	203
8.5.6 ca 2970 Ma	203
8.5.7 ca 2955 - 2925 Ma	203
8.5.8 Discussion and summary	203
8.6 Conclusions	206
References	207
Samenvatting in het Nederlands	219
Het Archaëicum	219
Plaatteconiek	219
Het Pilbara Craton	220
Dit proefschrift	221
Dankwoord	223
Curriculum Vitae	225
Appendices	227

Introduction

1.1 The Archaean Earth and plate tectonics

The Archaean era lasted for about one third of the Earth's history, from ca 4.0 until 2.5 billion years ago. Because the Archaean spans such a long time, knowledge about this era is crucial for understanding the evolution of the Earth until the present day, especially because it is the time of formation of much of the Earth's continental crust. However, because it was a very long time ago, this period is difficult to study; the geological record contains a limited amount of rocks that date from this era.

Hutton's doctrine of uniformitarianism; "the present is the key to the past" may be true in a general sense. The Archaean Earth may have had a structure very much like it does today: it probably had a core, a convecting mantle, a crust, oceans, and an atmosphere. However, on closer inspection there are many differences between the present day and the Archaean Earth. During the Archaean the earliest life on Earth evolved. Geodynamic processes may also have been significantly different and they are the focus of this thesis.

There is still much controversy about whether modern-style plate tectonics, characterized by rigid plates, spreading and subduction of ocean floor, recycling of oceanic crust, generation of continental crust, and continental growth by lateral accretion of terranes, were possible in the Archaean (see papers in Coward and Ries, 1995; De Wit and Ashwal, 1997). Thermal and geodynamical modeling studies have not provided conclusive answers, mainly because the temperature of the interior of the Earth in the Archaean still is a major unknown. Geological field studies can potentially provide the data necessary to constrain the thermal, tectonic and geodynamic regimes of the early, mid and late Archaean.

Modern plate tectonics can be defined by several characteristic features, however, some of these are very difficult to identify in ancient rocks. The main problem is that the ocean floor plays the leading role in the plate tectonic process, but it is this same ocean floor which is continuously recycled, and not preserved and accessible to field studies. We have to look for features that were preserved on the continents. Most diagnostic are those that are directly related to subduction, such as ophiolites (obducted slices of oceanic crust), accretionary tectonic melanges (formed at the leading edge of the overriding plate), and the occurrence of high pressure-low temperature metamorphic rocks at the surface (indicating that rocks have been taken down to great depths and subsequently exhumed).

Other characteristic features are the occurrence of magmatic products from subducted ocean

floor and subduction-modified mantle; the widespread occurrence of intermediate magmatism, and compression-extension tectonic cycles followed by major strike-slip events. These characteristic features have been researched in the Archaean Pilbara Craton in Western Australia, in the context of this PhD thesis focusing on the West and Central Pilbara. A temporally constrained structural-kinematic framework supported by petrology and geochemistry is built, in order to assess possible geodynamic regimes in the mid-Archaean.

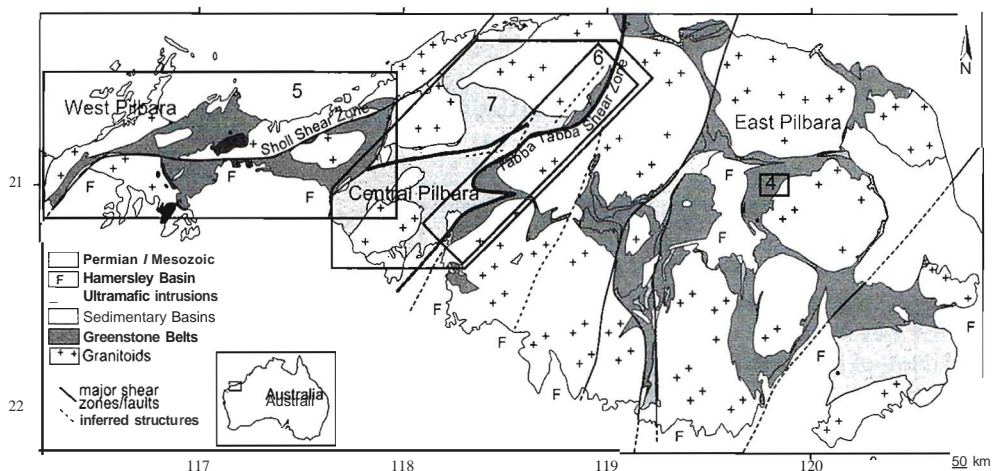


Figure 1.1. The Pilbara Craton in North Western Australia. The study areas and chapter numbers are indicated. Chapter 4: lithology, geochemistry and structure of a possible ophiolitic section of a greenstone belt. Chapter 5: structural, metamorphic, geochemical and geochronological framework for the West Pilbara. Chapter 6: V-Pb geochronology of the Tabba Tabba Shear Zone in the Central Pilbara. Chapter 7: structural, metamorphic, geochemical and geochronological framework for the Central Pilbara. Chapter 8: tectonic synthesis of all of the above.

1.2 The Pilbara Craton in Western Australia

The Archaean Pilbara Craton in the north west of Western Australia comprises two major components: the 3650-2850 Ma North Pilbara Granite-Greenstone Terrain (Hickman, 1983; Hickman, 1999) and the unconformably overlying volcano-sedimentary sequence of the 2775 to 2450 Ma Hamersley Basin (Blake, 1993), which now covers about two thirds of the craton (see Figure 3.1). The early to mid-Archaean granite-greenstone terrain consists of granitoid complexes, greenstone belts, and sedimentary basins. The North Pilbara Granite-Greenstone Terrain is one of the best-preserved Archaean Cratons in the world, mainly because it has suffered less subsequent deformation and metamorphism than other terranes of similar age. It is also one of the best exposed, because it occurs in a semi-desert.

The North Pilbara Granite-Greenstone Terrain consists of several domains separated by major shear zones and it has been suggested that this domainal geometry may reflect a history of accretion (Barley, 1997; Smith et al., 1998). The major transcurrent structures separating the do-

mains in cratons are typical features of continental crust of all ages, and many of these structures have a long history of reactivation. The kinematics of these structures contain important clues to the Archaean tectonic history of the Earth, and they are the main subject of this Ph.D. study, in addition to the intradomainal areas.

Hickman (1983) published a Pilbara-wide model based on a deformation history consisting of five major events, and came forward with a diapiric model (Hickman, 1984). Krapez (1993) developed a model that divided the Pilbara into domains and the greenstone successions into first and second-order sequence stratigraphic units, which were interpreted in a plate-tectonic context (Krapez and Eisenlohr, 1998). Blewett (2002) presented structural data interpreted in terms of far-field horizontal stresses related to plate interactions. Van Kranendonk et al. (2002) presented structural data that are interpreted to further support Hickman's (1984) diapiric model. However, Van Kranendonk et al. (2002) suggest that the western part of the North Pilbara Granite-Greenstone Terrain may be an accreted terrane as proposed by Smith et al. (1998) and Kiyokawa and Taira (1998). Van Kranendonk et al. (2002) suggest that after 3.2 Ga 'microplate tectonics' may have taken over from diapirism. This PhD thesis is mainly concerned with the ca 3.25 Ga and later history of the West- and Central Pilbara and therefore will not elaborate further on the 'vertical versus horizontal tectonics' discussion, which is concerned with the pre 3.25 Ga history of the East Pilbara.

1.3 Problem statement

Structural, kinematic, geochemical and geochronological data are used to build a temporally constrained tectonic framework for the West and Central Pilbara Craton, in order to solve the following problems: 1) Is there evidence for modern type plate tectonics in the Pilbara, i.e. are there ophiolites, high pressure metamorphic terranes, accretionary wedges and subduction-related igneous provinces? 2) Are the proposed accretionary models for the West and Central Pilbara Craton correct? Was the domainal geometry formed by modern-style plate-tectonic processes? 3) Are there alternative geodynamic models, and can those be placed in the context of modern type plate tectonics?

1.4 Approach

This PhD project focuses on the tectonic evolution of the Western and Central parts of the North Pilbara Granite-Greenstone Terrain. By reconstructing a spatially and temporally constrained tectonic model for the mid- to late Archaean evolution of this part of the Pilbara Craton, this project aims to provide another piece of the puzzle of the Archaean Earth and the possible changes in tectonic style that occurred between the Mid and the Late Archaean.

The problems outlined above have been researched in a field-based structural geological project, during several field seasons of two months in the Pilbara Craton in Western Australia. In addition, laboratory research has been carried out at Utrecht University and the Free University of Amsterdam in the Netherlands (geochronology, geochemistry, microstructural and petrological studies). The Pilbara field research was cancelled out in the local winter, as this is the cool and dry season during which most of the area is accessible by dirt roads. Aerial photographs provided by the Geological Survey of Western Australia (GSWA) were extremely useful for locating outcrop, navigation, and geological interpretation. In addition, Landsat TM, regional magnetic and gravity imagery provided by the Australian Geological Survey Organization (AGSO, now Geoscience Australia) were used.

Recently published 1:100,000 geological maps (by GSWAIGSO) were used as a lithological basis. The field research concentrated on the Central and West Pilbara; the purpose of the field studies was to add structural-kinematic data to the map basis, from the domain boundary structures as well the intradomain areas, and to collect samples. These samples were used for microstructural and petrological studies. $^{40}\text{Ar}/^{39}\text{Ar}$ hornblende and muscovite geochronology, and U-Pb zircon geochronology form the second component of this thesis. Major and trace element analyses were done to support the structural-kinematic framework. Finally, all of the data were integrated with the aid of GIS (Esri software).

1.5 Outline of this thesis

Chapter 2 contains an overview of published ideas about Archaean geodynamics, and Chapter 3 provides an introduction to the regional geological background of the North Pilbara Granite-Greenstone Terrain. It summarizes the lithological and geochronological characteristics and previously proposed tectonic models, concentrating on the Central and West Pilbara. This information forms the basis for the main section of the thesis where new data and interpretations are presented.

In Chapter 4 the lithology, geochemistry and structure of a possible ophiolitic section of a greenstone belt in the East Pilbara is investigated. In Chapter 5 a structural, metamorphic, geochemical and geochronological framework, and a new tectonic model are presented for the western part of the Pilbara Craton, which had been interpreted as an accreted island arc by previous studies. Chapter 6 reports the development of a relatively new technique for U-Pb dating of zircons by Laser Ablation ICP-MS at Utrecht University, and the results on samples from the central part of the Pilbara Craton are presented. These data provide firm constraints on the timing of tectonic events in that area. In Chapter 7 these geochronological data are integrated with structural-kinematic data, and supported by geochemical data they are placed in a tectonic framework for the central part of the Pilbara Craton. In Chapter 8 a complete discussion of all data forms the basis for a new geodynamical model for the mid- to late Archaean evolution of the west and central parts of the North Pilbara Granite Greenstone Terrain.

In all chapters, some recommendations are made for the follow-up of this project, as some questions have remained unanswered, and many more have arisen. Chapters 4 to 7 of this thesis have been written for publication as papers. Therefore a degree of repetition is unavoidable, especially in the introductory sections.

The Archaean

2.1 Introduction

This chapter aims to provide a short summary and background of published data, models and speculations on the Archaean Earth, especially its geodynamics and tectonics. The chapter neither aims to give a complete overview, nor does it provide an opinion on the published models at this stage; it is merely intended as a background. The books *Early Precambrian Processes* edited by Coward and Ries (1995) and *Greenstone Belts* edited by De Wit and Ashwal (1997) contain a large collection of papers and reviews and are suggested for further reading. This information will be called upon in the following chapters. In the final chapter the newly presented data collected in the North Pilbara Granite-Greenstone Terrain will be discussed in the context of some of these models. The collected geochemical and structural-kinematic data from the North Pilbara Granite-Greenstone Terrain will then be placed in a geodynamic framework.

2.2 Granites and greenstones

About 10% of the presently exposed continental crust is formed by Archaean rocks, i.e. older than ca 2.5 Ga (Figure 2.1). Geological studies of these rocks are largely confined to the few areas with good outcrop. These well-studied areas are located in Western Australia, Southern Africa and Canada.

Archaean terrains are composed of three main rock type associations. Grey gneisses with a complex structural history form much of the mid- and lower crust, granitoid sheets and plutons are more typical for the upper crust. Greenstone belts are the third component: the term greenstone belt is historically applied to all remnants of mostly Archaean supracrustal and igneous rocks that have experienced a low grade of metamorphism and some are therefore 'green'. Some of these rocks have undergone significant deformation. Greenstone belts are also more typical of the upper crust and are often associated with the granitoids to form the characteristic granite-greenstone terrains.

The areas between the greenstones referred to as granitoid-terrains and in the early- and mid-Archaean terrains they are characterized by tonalite-trondhjemite-granodiorite suites (TTG). Geochemistry and modeling indicate that TTG suites were derived by partial melting of

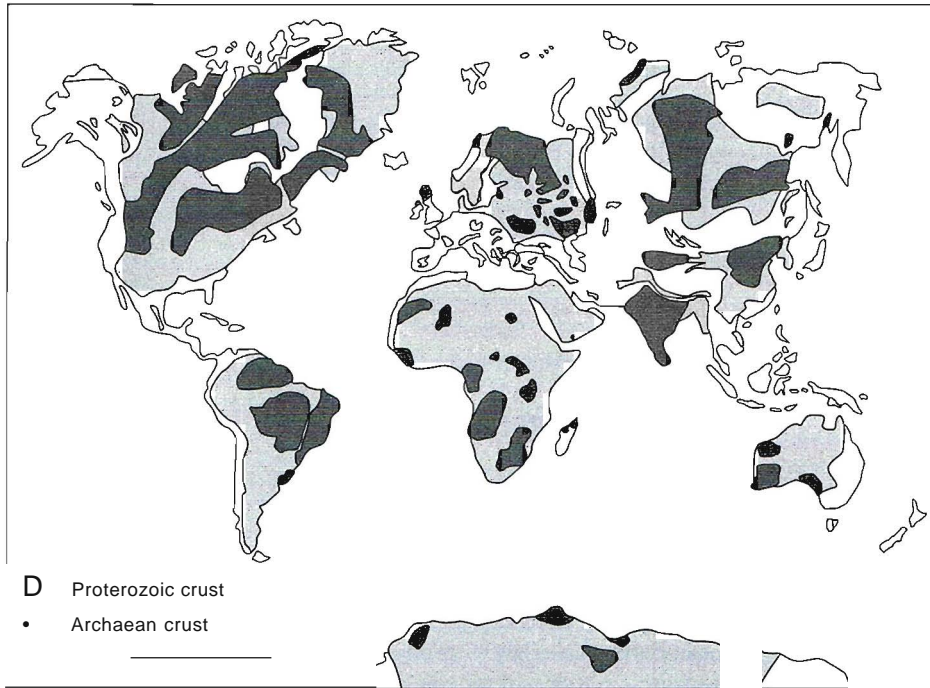


Figure 2.1. Archaean and Proterozoic crust on the present-day continents. After Kusky and Po/ot (1999).

hydrous basaltic crust at pressures high enough for the stability of garnet and amphibole (e.g. Martin, 1994). The 'granitoid terrains' comprise sheeted granite, batholithic granite, migmatite, granulite and amphibolite gneiss.

Detailed mapping and description of the internal features of greenstone belts has revealed that they are not simple sequences with a layer-cake stratigraphy and a synclinal structure (De Wit and Ashwal, 1995). They are often as complex as modern orogenic belts and the rock associations are now interpreted in the context of modern tectonic environments (e.g. the early paper of Bickle et al., 1980; book by Nisbet, 1987).

Greenstone belts were initially thought to be restricted to the Archaean (Condie, 1981), but more recently it has been suggested that they were formed throughout geological time (Condie, 1994). Post-Archaean examples are less common, for example the Ungava Orogen in Quebec (St-Onge et al., 1997), the Yavapai-Mazatzal Orogenic Belt in Arizona (Dann and Bowring, 1997), and the Rocas Verdes Greenstone Belt in the Southern Andes (Stem and De Wit, 1997). Even though there may be a few examples of post-Archaean greenstone belts, it is generally thought that they formed due to geological processes that were dominant in the Archaean.

Most greenstone belts were affected by deformation, but often the degree of deformation has not been extensively quantified. Greenstone belts often have greater stratigraphic than geophysical thickness, which suggests an underestimation of the degree of tectonic stacking (De Wit and Ashwal, 1995). This could be due to difficulties in the evaluation of bulk strain, tectonic discontinuities, sequence stratigraphy and the effect of erosion, and the tendency of stratigraphers to quote maximum

thickness rather than averages. Some gravity, seismic and electrical studies suggest that many greenstone belts are shallow structures (Stettler et al., 1997), others suggest that they go down to mid-crustal levels (Wellman, 1999). The base of greenstone belts remain enigmatic as their contacts with the granitoids at the surface are often tectonic or intrusive, and geophysics has not provided conclusive data about the buried contacts.

2.3 Tectonic settings of Archaean terrains

Tectonic settings of early to mid-Archaean greenstone belts and associated granitoids have been discussed in the context of a wide variety of modern analogues such as continental rifts, convergent plate boundaries, impact settings, submarine plateaus, hot spot type oceanic settings and mid ocean ridges (Platt, 1980; De Wit et al., 1992; Kroner and Layer, 1992; Condie, 1994). The major differences between modern orogens and Archaean terrains are reportedly the lack of high pressure metamorphism (blueschist and eclogite), ophiolite complexes, molasse basins, tectonic melanges and large accretionary wedges (Kroner, 1979; Hamilton, 1998). Hamilton (1998) uses this negative evidence, to rule out modern style plate tectonics for all of the Archaean and the early Proterozoic. However, others have reported some of those components from Archaean terrains: parts of ophiolites (e.g. De Wit et al., 1987b; Fripp and Jones, 1997), molasse basins (e.g. Eriksson, 1981), and many have interpreted Archaean terrains in the context of modern tectonic settings (e.g. Kroner, 1991; Kroner and Layer, 1992; Myers and Kroner, 1994; Myers, 1995; Barley, 1997; Krapez and Eisenlohr, 1998; Windley, 1998).

Greenstone belts commonly contain voluminous volcanic rocks that were erupted in a sub aqueous environment, and consequently greenstone belts have been interpreted to represent Archaean oceanic crust (De Wit and Ashwal, 1995). However, geochemical evidence points to interaction of the magmas with continental crust on their way to the surface (Bickle et al., 1994; Green et al., 2000) indicating that the lavas possibly were erupted onto submerged continents. This may indicate there were large volumes of continental crust present and the ocean basins were either shallower than at present or contained more active ridges or plateaus (Arndt, 1999). It may also indicate that episodes of rapid crustal growth alternated with periods during which supercontinents existed with very little or no freeboard.

Recent models for the formation of greenstone belts tend towards a comparison with modern tectonic settings, as the genetic order of the super sequences in greenstone belts suggests a relation to the opening and closure of ocean basins (Barley, 1997). Recycling of hydrated oceanic crust, possibly through subduction, may have been the source of the earliest continental crust in the form of TTG's (De Wit and Hart, 1993; De Wit, 1998). Greenstone belts may have been produced by short-lived episodes of intra-arc spreading followed by compression (Sleep and Windley, 1986). Alternatively, regional extension may have led to crustal scale boudinage and diapirism (Marshak, 1999) and TTG suites could have formed in intracontinental rift settings (Kroner, 1984). Seismic data have also shown that thin-skinned tectonics and thrusting may have played a major role in the development of many greenstone belts (Stettler et al., 1997).

The domainal geometry of Archaean Cratons has led to a comparison with modern orogens, where this geometry is caused by the lateral accretion of terranes (Coney, 1989). Structural, geochronological and geochemical studies of several different Archaean cratons indicate that granite-greenstone terrains may have grown by terrane accretion, possibly at convergent margins (De Wit et al., 1992; Wilde et al., 1996; Barley, 1997; Sun and Hickman, 1998; Kusky and Polat, 1999; Holttta et al., 2000; Polat and Kerrich, 2001; Dirks et al., 2002).

2.4 Thermal evolution of the Earth

Since its formation 4.56 billion years ago the Earth has continuously been losing heat: primordial heat from the time of formation of the Earth, potential energy from core segregation and radiogenic heat. In the Archaean the rate of radiogenic heat production was approximately three (or up to five) times higher than it is today (Lambert, 1976; Jackson and Pollack, 1984). After the initial accretion process the Earth probably had a completely molten magma ocean at the surface (Abe, 1993). Cooling caused the magma ocean to solidify partially, resulting in chemical differentiation. A thin protocrust probably covered the magma ocean and was frequently recycled by volcanism and impacts. After about 400 Ma solid state convection took over and long-lived crust covered the Earth's surface (Abe, 1993). Evidence for this early crust and possibly oceans was found in the form of ca. 4.2 and even 4.4 Ga old zircons (Mojzsis et al., 2001; Wilde et al., 2001).

The temperature of the mantle in the Archaean is a matter of controversy. The composition of komatiites in Archaean terrains may indicate that the mantle was significantly hotter (200-300 degrees) than it is today (Nisbet et al., 1993). Alternatively, the komatiites were extracted from a 'wetter' mantle rather than hotter (De Wit and Hynes, 1995). The 'Archaean Paradox' is based on the observation that metamorphic conditions in high grade continental terrains were not much different from recent ones. This could either indicate that Archaean mantle temperature may have been similar to the present day mantle temperature (Bickle, 1978; England and Bickle, 1984), or that only the mantle heat flow was comparable to today's. This could point to more efficient heat loss along the mid-ocean ridges (Morgan, 1984), or a greater total ridge-length (Pollack, 1997).

2.5 Plate tectonics?

2.5.1 Subduction

At present, plate tectonics is the most effective mechanism for cooling of the Earth. Oceanic plates are formed by rising magmas at mid-oceanic spreading ridges. These magmas solidify and cool at the surface, and the plates are returned into the mantle through subduction. However, a number of reasons have been suggested why plate tectonics may not, or not as efficiently, have operated in the Archaean, suggesting there were alternative cooling mechanisms and alternative forms of geodynamics. There are also many reasons why plate tectonics may have operated, as pointed out in section 2.3. Some of the arguments will be discussed here, as they will return in other chapters.

All principal geodynamic mechanisms are driven by heat flow from the Earth's interior. If the Earth has been cooling steadily, there are a number of reasons why plate tectonics may not have operated in the Archaean as it does at present. A hotter mantle would have produced more melt as decompression melting would have started at deeper levels, and hence a thicker oceanic crust would have formed (McKenzie and Bickle, 1988). A thick harzburgitic layer would have formed below the crust (Vlaar et al., 1994), that made the oceanic lithosphere more buoyant, stable, and harder to subduct (Vlaar, 1986). Also, a hotter mantle would have convected faster, allowing the oceanic lithosphere less time to cool and to become gravitationally unstable (Davies, 1992). A hypothetical crustal section is shown in Figure 2.2.

The thickness of the oceanic crust and lithosphere (as a function of mantle temperature), the buoyancy, the rate of convergence and the age of the plate at the subduction zone determine the

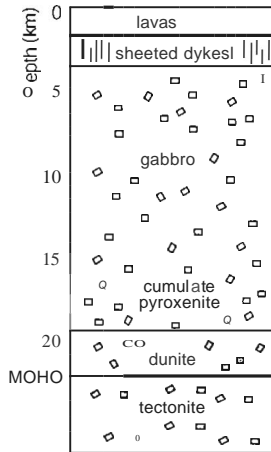


Figure 2.2. Hypothetical Archaean oceanic crustal section. After Bickle (1994).

'subductability' of an oceanic plate. For mantle temperatures of only 50°C higher than at present, the age of neutral buoyancy of plates was greater than the mean age of subduction: the crossover point where plates become 'subductable' may have occurred between 1.4 and 0.9 Ga (Davies, 1992). This timing seems to be disproved now, and there is evidence for plate tectonics and subduction at least after ca. 3.2 Ga (De Wit et al., 1992; Wilde et al., 1996; Barley, 1997; Sun and Hickman, 1998; Kusky and Polat, 1999; Holtta et al., 2000; Polat and Kerrich, 2001; Dirks et al., 2002). Alternatively, obduction may have dominated in early tectonic processes, and the thick thrust stacks of oceanic lithosphere may have started to differentiate internally to generate TTG magmatism (De Wit et al., 1992).

If plate tectonics occurred before the above crossover point, the plates possibly moved slower in order to cool sufficiently to become unstable (Davies, 1992). If that was the case, the mantle was not being cooled efficiently by plate tectonics, and heat must have been removed from the mantle by some other mechanism. Considering that the radiogenic heat production in the Archaean was approximately three times greater than it is today (Lambert, 1976; O'Nions and Pankhurst, 1978; Jackson and Pollack, 1984), plate tectonics in the Archaean may not have been the only process responsible for heat loss.

Heat can also be removed from the Earth's interior by rising plumes. Mantle plumes are assumed to be responsible for continental flood basalts, oceanic plateaus and volcanic oceanic hot spot chains. It has been suggested that mantle plumes could also be responsible for major continental magmatic provinces such as Archaean granite-greenstone terrains, by emplacement of a plume head beneath a continental crust (Hill et al., 1992). But Davies (1992) suggested that plume tectonics is not an alternative for plate tectonics. Mantle plumes arise from a hot, lower boundary layer (e.g. the core-mantle boundary) and plates from a cold upper boundary layer (the surface) (Davies and Richards, 1992). They are complementary rather than alternative processes. At all times, also in the Archaean, a cooling mechanism involving the cool upper boundary layer must have been active (Anderson, 2001). Davies (1992) suggested that if the oceanic crust was not much thicker than it is at present, conductive cooling occurred, possibly making the mantle part of the oceanic plates strong.

In early plate tectonic models of Arndt (1983) and Nisbet and Fowler (1983) the Archaean oceanic crust was of similar thickness as present-day oceanic crust, formed by komatiitic magmas in fast-spreading ridges. The driving forces on plates (ridge push and slab pull) would have been

less than they are today. However, the resistive forces on the plates would also have been much less in the hotter and less viscous Archaean mantle (Nisbet and Fowler, 1983).

A thick Archaean oceanic crust may have behaved in a similar fashion as modern oceanic plateaus which are thicker than normal oceanic crust. When arriving at a subduction zone they cause 'jamming' and possibly reversal of the sense of subduction. Archaean plate tectonics may also be compared to the behavior of young oceanic lithosphere at present: with sufficiently low mantle viscosities and high convergence rate, flat subduction may have been possible under an actively overriding plate (Van Hunen et al., 2000).

In several cratons evidence for sporadic subduction in the Archaean may have been found. Wet sources for komatiites indicate that the mantle was locally enriched by addition of hydrous fluids from subducted slabs (De Wit and Hart, 1993), and the occurrence of Archaean eclogitic xenoliths indicates that it was possible to bring basaltic material down to great depths (Carlson et al., 2000).

The Earth may have experienced episodes of distinctly different tectonic styles. The mantle may have been initially layered, but this layering episodically may have become unstable and broken down via mantle overturn (Stein and Hofmann, 1994; Davies, 1995). During overturns the cool upper mantle in these models was replaced with hotter lower mantle material: this may have caused global episodes of crust formation. According to the models of Davies (1995) plate tectonics could have operated in the Archaean between the overturn events. It has also been suggested that plate movements and catastrophic overturns occurred simultaneously, as expressed by global magmatic episodes (Nelson, 1998).

As opposed to ocean floor, continents however may have been stable for a very long time because the continental upper mantle did not participate in large scale overturn events (De Smet et al., 2000). This may have been due to the low density of the depleted residual peridotite in the continental root. The existence of such a 'keel' is confirmed by data from diamonds (Shirey et al., 2002).

The absence of large volumes of high pressure-low temperature (blue schist) Archaean metamorphic rocks is an argument against catastrophic mantle flush events (Galer and Metzger, 1998) but they may also just indicate that the continents were not affected by such events. Others have suggested that partial convective overturn did occur in the early continental crust (e.g. Collins et al., 1998), however, this concerns a process on considerably smaller scale. Mantle rare-gas evolution is believed to indicate that the lower mantle (below the 660 km discontinuity) has remained an isolated and undegassed reservoir for at least the past 4 Ga (Morgan, 1998), which argues against whole mantle overturns as recurring events.

2.5.2 Low angle subduction

Subduction in modern tectonic settings occurs in many different varieties. Firstly, the types of plates involved in the collision (oceanic or continental) determine the type of subduction. Secondly, the relative velocities and the buoyancy of the downgoing plate determine the angle of subduction. As has been discussed before, the Archaean oceanic crust is expected to be more buoyant than modern oceanic crust, and steep subduction of Archaean oceanic plates is unlikely.

Even though the early and mid-Archaean oceanic crust was probably much thicker and more buoyant than the average modern oceanic crust (Vlaar, 1986), it may still have been subducted involving a 'flat' geometry (Van Hunen et al., 2000). This can be compared to modern very fast subduction zones, subduction of young and buoyant oceanic lithosphere (Drummond and Defant, 1990), or subduction of oceanic plateaus and seamounts (Gutscher et al., 2000; Foley et al., 2003).

An example of modern flat subduction occurs below Peru and Chile in the Central Andes (Figure 8.5). It has been shown that the subducted slab is forced down as deep as the mechanical root of the continent at about 100 kilometers depth (Gutscher et al., 2000), and then continues horizontally for several hundreds of kilometers. It is thought that the cause for flat subduction in this area is the presence of an oceanic plateau in the subducting plate, making it more buoyant.

This 'flat' geometry might apply to subduction in the Early Archaean Earth (Foley et al., 2003). It implies that after the initiation of subduction, there is no thick mantle wedge as in a 'normal' subduction setting, and melt generated in the subducting plate will not interact with the asthenospheric mantle. The geochemical characteristics of the volcanic arc of the upper plate contain important clues to these processes. It is proposed that during the Mid-Archaean there may have been an intermediate stage, during which both types of subduction were possible, or pockets of mantle existed between the two crustal slices, and a large variety of magmatic suites ranging between TTG and arc-magmatism, was created. Similar ideas were developed by Smithies and Champion (2000).

2.5.3 Geochemical signatures of subduction

In a 'normal' subduction regime (subduction angle of at least 25°), fluids are produced as a result of slab dehydration, where the slab reaches a depth of about 110 kilometers (Tatsumi and Eggins, 1995). Interaction of these slab fluids with the overlying mantle wedge results in calc-alkaline basaltic and andesitic volcanism (Schmidt and Poli, 1998) which occurs in a relatively narrow zone.

Subduction of young and hot oceanic lithosphere may result in dehydration of the downgoing slab at very shallow levels. Because magma genesis occurs at deeper levels, the melt generation in the dry slab will involve lower degrees of partial melting and there will be less metasomatism in the mantle wedge (Harry and Green, 1999).

During flat subduction there exists no asthenospheric mantle material between the subducting slab and the bottom of the overriding lithospheric plate. As a consequence, the slab melts do not interact with mantle material. If the hydrated mafic crust still contains amphibole and the melting occurs below the plagioclase stability depth and in the presence of garnet, the resulting magmas are adakitic (Drummond and Defant, 1990).

Smithies (2000) found that TTG's are distinct from adakites, as they show no evidence for interaction with mantle material. Martin and Moyen (2002) noticed that the composition of TTG from the early Archaean through to the Proterozoic reflected a gradual change towards higher Mg numbers and trace element evidence reflecting more interaction with a mantle wedge. These data suggest that during the early Archaean no, or only flat subduction occurred. During the mid and late Archaean subduction at a small to medium angle may have become possible.

2.6 Alternative geodynamic models

Some workers suggest that plate tectonics was not at all possible in the Archaean, others argue that some forms of plate tectonics may have operated. Subduction may have been possible if the crust was scraped off before subduction of the eclogitic part of the lithosphere by mantle decoupling (Park, 1981), as illustrated in Figure 2.3. This is similar to the 'A-type' subduction proposed for the Proterozoic by Kroner (1979; 1983). The thick crustal pile that formed by this process, may have internally differentiated and come to resemble an island arc (De Wit et al., 1987a; Nutman and Collerson, 1991). The eclogite transformation may have increased the rates of plate movement (Figure 2.3). If the mantle was hotter and the crust thicker, the mantle part of the plates may actually

have been soft and more likely to show symmetrical 'dripping' of the eclogitic root (Campbell and Griffiths, 1992), rather than asymmetrical subduction. Delamination and dripping of the eclogitic lower part of the oceanic lithosphere could also spontaneously occur beneath thick ocean plateaus (Kroner 1980, 1981, Zegers and Van Keken, 2001), and this would be followed by uplift, extension and TTG production (Figure 2.3).

A variation of the delamination model is provided by Hoffmann and Ranalli (1988). They proposed that a hotter Archaean mantle and a thicker oceanic lithosphere may have resulted in a 'sandwich' rheology in which the lower crust contains a weak ductile layer. In convergent settings the upper crust may have delaminated, resulting in 'ocean flake tectonics' during which the oceanic upper crust was accreted or obducted onto the overriding plate and the lithospheric mantle was subducted. However, there is geochemical evidence that Archaean hydrated upper crust was subducted along with the lower crust and mantle, resulting in subduction-modified and enriched mantle (Smithies and Champion, 1999) and production of arc-type magmas (Barley et al., 1998).

Not only oceanic lithosphere, but also the continents may have had a weak ductile layer in the lower crust (Bailey, 1999). Consequently, crustal thickening could cause 'overflow' of continental crust onto adjacent ocean basins (Figure 2.3). This would result in a geometry that resembles shallow subduction and could also explain the generation of TTG suites.

Vlaar et al. (1994) proposed a cooling and recycling mechanism involving continental roots as opposed to the recycling models of oceanic lithosphere and they proposed that the Archaean

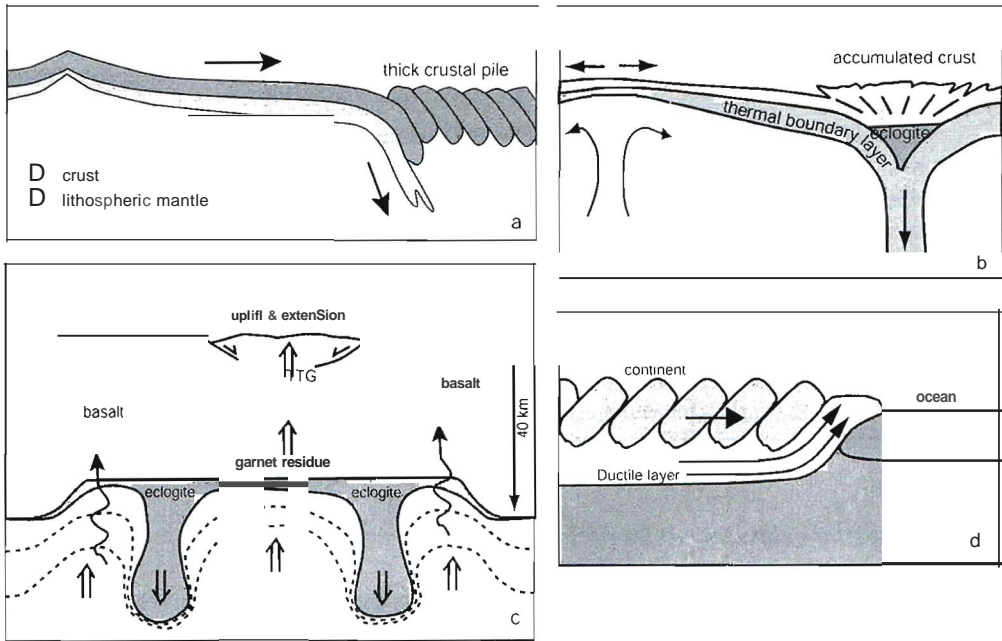


Figure 2.3. Sketches of some of the models discussed in the text. a) Subduction of the mantle part and the lithosphere by decoupling. From Davies (1998). This is similar to the 'A-type' subduction proposed for the Proterozoic by Kroner (1983) b) Eclogite/anaorhesis may have aided in the recycling of From Park (1981). c) Delamination of the eclogitic lower part of the lithosphere beneath thick ocean plateaus, followed by uplift, extension and TTG production. From Zegers and Van Keken (2001). d) Crustal thickening resulting in 'overflow' of continental crust onto adjacent ocean basins. From Bailey (1999).

continents stabilized early on top of a compositionally stratified harzburgitic root. After formation of the stable basalt-harzburgitic layering, recycling of crust may still have occurred as a result of the transformation of basalt in the lower crust to the much denser garnet-granulite and eclogite. New crust may have been generated by eclogite re-melting as well as ongoing decompression melting, explaining the occurrence of both basalt and komatiite in greenstone belts.

Kroner and Layer (1992) proposed a tectonic model for the early Earth similar to that seen in Venus. The heat loss may have occurred mainly through hot spots linked to zones of spreading. Extensive shortening and 'crumpling' may have caused thickening of the early continents and may have caused intracrustal melting to produce TTG magmatism (Kroner, 1980).

2.7 Impacts

The effect of large impacts on the early crust is largely speculative, but by analogy with the other terrestrial planets and moons in our solar system it could be considerable. This subject has been largely overlooked in many discussions about Archaean tectonics, however, it has been suggested that these impacts may have modified whatever crust there was before 3.8 Ga (Grieve, 1980). Impacts may have aided in recycling early crust into the mantle (Warren, 1984; Taylor, 1989). However, very few known Archaean terrestrial rocks bear signs of large impacts, but this could be due to orogenic reworking and erosion of elevated terrains, and recycling of the oceanic crust. The chances of preservation of the effects of an impact decrease with increasing magnitude of the impact and associated thermal effects (Glikson, 1993).

Several formations in the Archaean to Palaeoproterozoic Hamersley Basin in Western Australia contain layers rich in distinctive sand-size spherules of former silicate melt produced by major bolide impacts. Some of these layers may be correlated to similar layers in South Africa, indicating a world-wide event (Simonson et al., 1999). The episodic nature of worldwide tectonic and magmatic events has been discussed in the context of mantle convection (Davies, 1995), but it may also be explained by mega-impacts as shown in Figure 2.4 (Glikson, 1995; Glikson, 1996; Glikson, 2001). Many Phanerozoic major impact events correspond to formation of major volcanic flood basalts, and this may be true for Archaean rock-forming events (3.45, 3.25, 3.00, 2.70 Ga) as well, especially because these 250 Ma cycles correspond to the galactic rotation period. This could indicate the Earth was subjected to clustered meteorite showers. Mega-impacts could induce asthenospheric updoming, melting and diapirism, radial dyke swarms, continental rifting and sudden changes in plate motions (Glikson, 1996). Supercontinent cycles have also been linked to extraterrestrial effects (Barley and Groves, 1992).

2.8 Crustal growth and formation of cratons

Growth of continental crust over geological time is still controversial because this process is very difficult to quantify. At present, continents grow mainly due to magmatic and accretionary processes at convergent margins, through accretion of oceanic plateaus, magmatic arcs, back-arc basins and microcontinents. The modern rate of crustal growth (production minus recycling) cannot be measured accurately because of the uncertainty in recycling rates; extrapolation of crustal growth rates back through time is even more difficult. Many different models have been proposed, varying between two extremes, see Figure 2.5. In the first end member model, the continents may have differentiated from the mantle at a very early stage, and have been continuously recycled since then, resulting in a

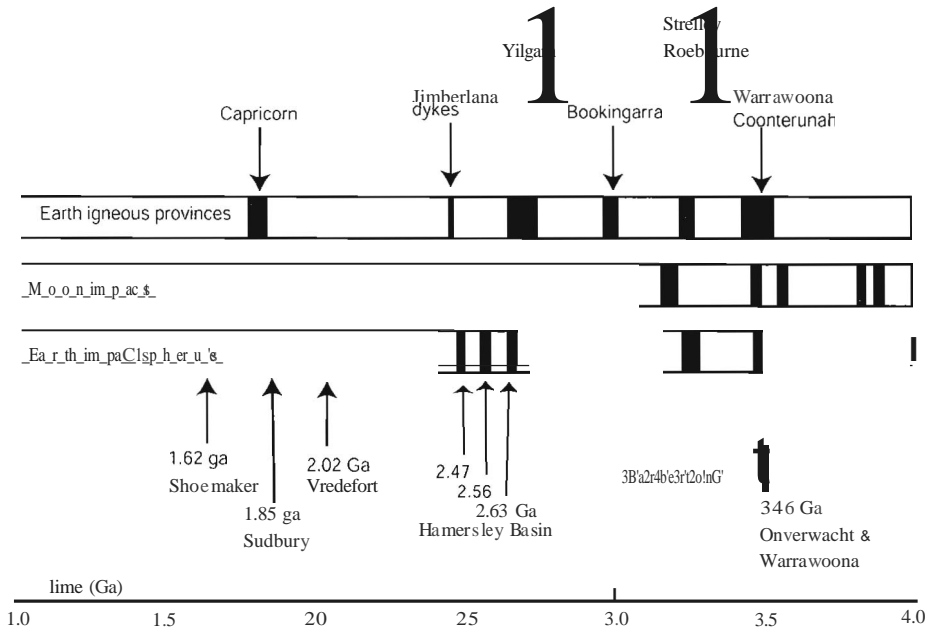


Fig. 2.4. Ages of terrestrial igneous provinces in the range 0/1.0-4.0 Ga, the ages of terrestrial impact spherules, lunar impact event peaks, and major mafic-ultramafic igneous events in the Pilbara and Yilgarn Cratons, Western Australia. From Glickson (2001).

constant volume of continental crust since the early Archaean (Armstrong, 1968; Armstrong, 1981). This steady-state model is compatible with a wide range of observed isotopic data (Armstrong, 1991). The other end-member model proposes continuous continental growth (e.g. Reymer and Schubert, 1984). In the generally accepted models the majority of continental crust had formed by 2.5 Ga, but growth continues until the present day (Hurley, 1968). In these models the crust is only partially recycled (Dewey and Windley, 1981; Reymer and Schubert, 1984). Isotopic observations may indicate a gradual increase of the volume of preserved continental crust (Bowring and Housh, 1995) and is consistent with the accretion of juvenile crust (Kusky and Polat, 1999).

Cooling of the Earth is thought to have led to a thinner oceanic crust, and therefore to deepening of the ocean basins, fall in sea level and exposure of the continents to erosion (Vlaar, 2000). Studies of these early sediments have revealed that zircons older than 3900 Ma are quite rare (Nutman, 2001), indicating that crustal growth may have dominated over recycling in the early Archaean. Nevertheless, the presence of 4.2 Ga (Froude et al., 1983), 4.3 Ga (Mojzsis et al., 2001) and even 4.4 Ga year old zircons (Wilde et al., 2001) in Archaean metasediments is interpreted to indicate the presence of (possibly continental) silica-saturated crust at that time. In addition, oxygen isotopes indicate there may have been oceans. However, if there were large volumes of continental crust in the Archaean, it is strange that we do not observe much of it at the surface today. Possibly the geological record is strongly biased towards the 'accidentally' stabilized continental fragments of abnormal thickness.

There is much disagreement on the mechanism of crustal accretion, because lateral magmatic accretion, as in modern arcs and along active continental margins, is only possible in modern plate

tectonic settings. It is suggested that vertical accretion by plume-induced magmatic underplating has been a dominant process (Kroner, 1980; Kroner and Layer, 1992). Thickening of the lithosphere may have taken place by addition of low-density depleted peridotite, from which komatiites and basalts were extracted (Herzberg, 1999), possibly also trapping the high density residue from which felsic melts were extracted. The density difference would have inhibited recycling of this early crust.

McCulloch and Bennett (1994) argued that the continents grew episodically and it was shown that the distribution of juvenile crust is indeed episodic (Condie, 1998; Condie, 2000). In such models episodic penetration of subducted slabs through the 660 km seismic discontinuity during 'slab avalanche' events causes the mode of convection in the mantle to change from layered to whole mantle convection (Stein and Hofmann, 1994; Davies, 1995). These episodes correspond to major periods of crustal formation and the assembly of supercontinents, which could be explained by attraction of continental fragments by the major downwelling directly over a slab avalanche (Peltier et al., 1997).

The first continental crust is represented by tonalite-trondhjemite-granodiorite suites (TTG) and is believed to have formed by melting of amphibolite or eclogite, either in a subduction setting (Drummond and Defant, 1990; Barley et al., 1998; Foley et al., 2002) or by melting of the base of a thick basaltic crust (Kroner, 1985). When the primary basaltic crust was replaced by more felsic material, thermal blanketing enhanced stabilization of the underlying harzburgitic root (De Smet et al., 1999). The depleted continental root may have grown by episodic injection of small diapiric upwellings from the undepleted mantle. Long term stability of continents was enhanced by a density gradient related to the degree of depletion in the continental root (De Smet et al., 1998). The great lithospheric thickness of Archaean cratons could be due to the large amounts of crustal extraction, and this is used as evidence for crustal growth models with a high rate of crust production in the Archaean (Abbott et al., 2000).

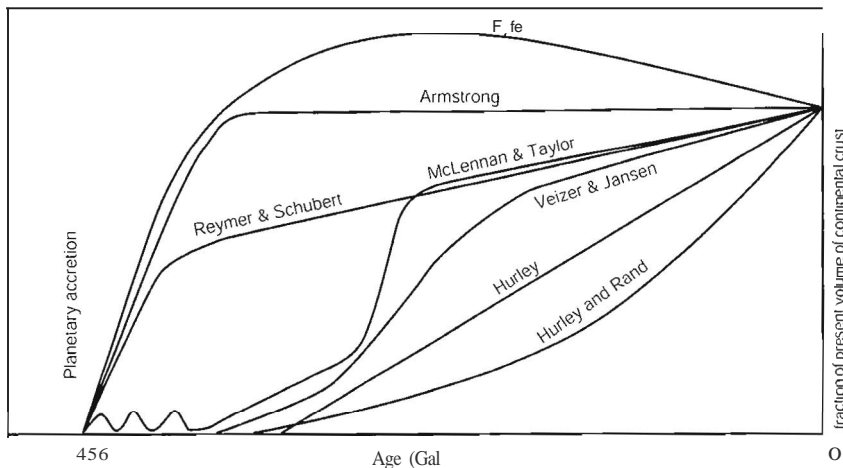


Figure 2.5. Crustal growth models. After Taylor and McLennan (1985).

2.9 Summary

The main driving force for all tectonic processes is heat: the flow of heat from the interior of the Earth to the surface. Heat has become progressively less available since the Archaean as the Earth cooled. In the early Archaean, recycling of basaltic crust and generation of tonalite-trondhjemite-granodiorite suites may have been possible by delamination and recycling of the eclogitic part of the lower crust. An alternative is flat subduction, which may have occurred sporadically. Modern style plate tectonics and high angle subduction were probably not possible until the mid or late Archaean due to the buoyancy of the oceanic plates. The details of Archaean tectonics and geodynamics will probably not be understood until a full understanding of the modern regimes has been developed.

Geology of the Archaean Pilbara Craton - brief overview

3.1 Introduction

This chapter aims to provide a summarized overview of the regional geology of the Archaean Pilbara Craton in Western Australia. Detailed geological introductions are also given in each of the following chapters. The classical geological data and tectonic models will be summarized, and recent developments will be discussed and compared. The Archaean Pilbara Craton in the north west of Western Australia (Figure 3.1) comprises two major components: the 3650-2850 Ma North Pilbara Granite-Greenstone Terrain (Hickman, 1983; Hickman, 1999) and the unconformably overlying volcano-sedimentary sequence of the 2775 to 2450 Ma Hamersley Basin (Blake, 1993), which now covers about two thirds of the craton. This study is concerned with the granite-greenstone terrain, which is a 'typical' Early to Mid-Archaean terrain consisting of granitoid complexes and greenstone belts. The North Pilbara Granite-Greenstone Terrain is one of the best-preserved Archaean Cratons in the world, mainly because it has suffered less subsequent deformation and metamorphism than other terrains of similar age.

3.2 Domains, domain boundaries and stratigraphy

Previous studies have shown that the North Pilbara Granite-Greenstone Terrain consists of elongate domains (Figure 3.1, Figure 3.2) (e.g. Krapez and Barley, 1987; Krapez, 1993; Krapez and Eisenlohr, 1998) and it has been suggested that this domainal structure reflects a history of accretion (e.g. Barley, 1997). Major transcurrent structures separating domains in Archaean cratons are common features in continental crust of a) Iages, and many of these structures have a long history of reactivation (De Wit, 1998). The kinematics of these structures contain important clues to the Archaean tectonic history of the Earth; in addition to the deformation history of the intradomainal areas, they are the main subject of this Ph.D. study.

A tabular stratigraphy for the greenstone successions in the Pilbara was originally proposed (Hickman, 1983; Horwitz, 1990), but with the recognition of the domain boundary structures this interpretation has been revised (e.g. Hickman, 1999; Van Kranendonk et al., 2002). The greenstone successions of the different domains cannot or only partially be correlated across domain boundaries.

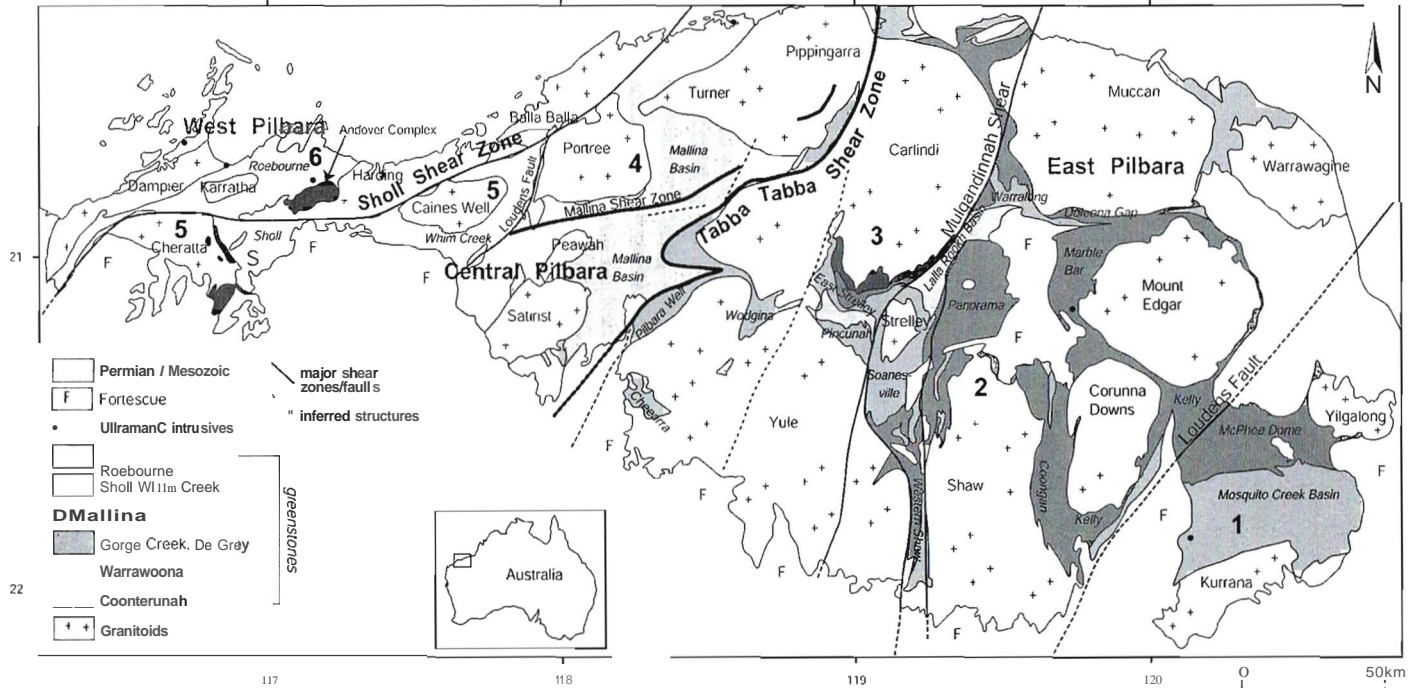


Figure 3.1. The Pilbara Craton in North Western Australia. See Figure 3.2 for a combined gravity-magnetic image of the craton. The six domains of Krapez and Eisenlohr (1998) are also indicated: 1 = Nullagine Domain, 2 = Marble Bar Domain, 3 = Pilgangoora Domain, 4 = Mallina Domain, 5 = Sholl-Whim Creek Domain, 6 = Roebourne Domain. Van Kranendonk et al. (2002) include the Sholl Belt (5) in the West Pilbara. Blewett (2002) and this study consider the Sholl Shear Zone to be the boundary between the West and Central Pilbara. The Tabba Tabba Shear Zone is the boundary between the Central and East Pilbara. Names in small regular font indicate names of granitoid batholiths. Names in small italic font indicate names of greenstone belts.

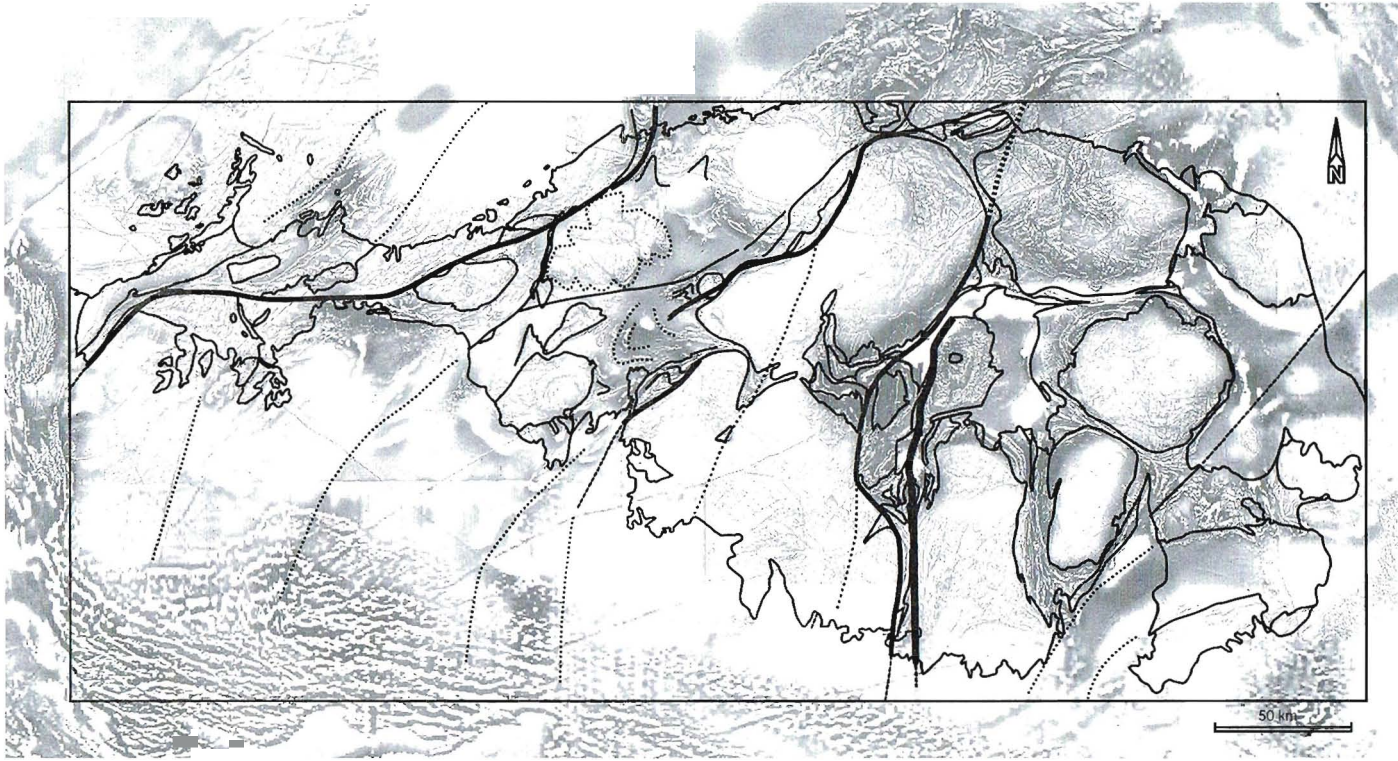


Figure 3.2. Grayscale version of the short-wavelength magnetic Gnomal' image superimposed on Bouguer gravity anomaly image composed by Blewett et al. (2000). Outline of simplified geology as shown in Figure 3.1 is superimposed on the image. Thick lines: major structures. Thin lines: minor structures and lithological contacts. Dashed lines: no outcrop - interpretation of this image.

After the recognition of domains and their boundary faults in the Pilbara, the nomenclature of the different areas has changed. Krapez and Eisenlohr (1998) recognized six tectonostratigraphic domains (see Figure 3.1) which they claimed were consistently younging towards the west. Smithies (1999) and Hickman (1999) proposed a division into an East and West Pilbara, separated by a Central Pilbara. Recently Van Kranendonk et al. (2002) adopted this division, however, the Sholl Belt was included in their 'West Pilbara', but they do not describe a major structure separating it from the Whim Creek Belt (Figure 3.1). Blewett (2002) used a division in which the Sholl Shear Zone is regarded as the boundary between the West and Central Pilbara. That division is adopted in this PhD thesis.

The East Pilbara comprises the ca 3.51 Ga Coonterunah Group, the ca 3.47-3.43 Ga Warrawoona Group, the ca 3.23 Ga Sulphur Springs Group, the un-dated Gorge Creek Group and the ca 2.95 Ga De Grey Group (section 3.3). A detailed overview of the most recently published East Pilbara stratigraphy is given in Table 3.1. The West Pilbara comprises a ca 3.26 Ga succession in the Roebourne Domain, and an undated mafic sequence of possibly oceanic origin (section 3.7). The Central Pilbara comprises the 3.12 Ga volcanics in the Sholl Belt, a ca 3.01-2.97 Ga volcano-sedimentary succession in the Whim Creek Belt, and 2.97 Ga continental sediments in the Mallina Basin (section 3.5). A detailed overview of the most recently published West and Central Pilbara stratigraphy is given in Table 3.2. This Ph.D. thesis is mainly concerned with the post 3.25 Ga history of the West- and Central Pilbara.

After stabilization of the Pilbara Craton and slow uplift and erosion, the ca 2.77 - 2.45 Ga volcano-sedimentary successions of the Hamersley Basin was deposited over a large part of the craton. This was the result of an event that involved the breakup of a continental plate which contained the Pilbara Craton (Blake and Barley, 1992).

The deep structure of the Pilbara has remained enigmatic. Drummond (1979; 1981) found through seismic studies, that the crustal thickness in the Pilbara is 28-33 kilometers, about 10 kilometers thinner than adjacent crust to the south, and 20 kilometers thinner than the crust in the Archaean Yilgarn Craton. The Pilbara has an upper crust of about 13 kilometers thick, consisting of felsic to intermediate rocks (Drummond, 1979). The base of the greenstone belts in the Pilbara is inferred to be about 14 kilometers, and a similar average thickness was modeled for the granitoid complexes (Wellman, 1999). The outlines of the granitoid complexes, greenstone belts and sedimentary basins can be seen very clearly in the combined gravity anomaly and short-wavelength magnetic anomaly image in Figure 3.2, also in the poorly exposed areas in the West and Central Pilbara. (from Blewett et al., 2000).

3.3 The East Pilbara

3.3.1 The Nullagine Domain

The Nullagine Domain consists of three main tectono-stratigraphic divisions; the northern McPhee Dome and Yilgalong Granitoid Complex, the central Mosquito Creek sedimentary basin, and the southern Kurrana Complex (Figure 3.1).

The Mosquito Creek Basin comprises mainly metasediments, and its age remains controversial. It was correlated to the Gorge Creek Group by Krapez (1993) and is now included in the De Grey Group (Table 3.1). The McPhee Dome consists mainly of mafic volcanics and is ascribed to the lower Warrawoona Group. Barley et al. (1998) found that the geochemistry of ca 3430 to 3417 Ma calc-alkaline basalts, andesites and dacites of the Warrawoona Group in the McPhee Dome

Table 3.1. Supracrustal sequences in the East Pilbara Granite-Greenstone Terrain. Compiled from Van Kranendonk et al. (2002) and references therein. The timing and occurrence of granitoid intrusions can be seen in Figure 3.3. Numbers in the left column refer to the domains shown in Figure 3.1.

Group	Formation	Lithology	age (Mal)	thickness (km)
De Grey (1,2,3,(4))	Lalla Rookh Sandstone	Sandstone, conglomerate, shale	ca 2950	
Gorge Creek (1,2,3)	Pyramid Hill Honeyeater Basalt Paddy Market Corboy Pincunah Hill	Banded iron formation (BIF) Basalt shale, chert sandstone, mudstone, conglomerate shale, BIF, sandstone, felsic volcanics	<3235	max 3.5
Sulphur Springs (2,3)	Kangaroo Caves Kunagunarrina Leilira	tholeiitic mafic to felsic volcanics, chert, BIF pillow basalt, high-Mg basalt, chert wacke, rhyolite, sandstone, mudstone, chert	3238-3235	max 1.5 max 2.4
(3)	Golden Cockatoo	BIF, rhyolite, quartzite, metapelite	>3238	
(2)	Budjan Creek	conglomerate, sandstone, siltstone, felsic volc	3308	max 1.2
W Kelly	Charteris Basalt	komatiite, basalt		
A Subgroup	Wyman	felsic volcanics	3325	max 1.1
R (1,2,3)	Euro	tholeiitic and komatiitic pillow basalt and chert		max 9.4
R Salgash	Strelley Pool Chert	quartzite, chert, stromatolites		
A Subgroup	Panorama	felsic volcanics, tuffaceous sandstones	3459-3434	1.5
W (1,2,3)	Apex	altered basalts, chert		max 4
0	Towers	blue, black, white layered chert	<3463	
0 Taiga Taiga	Duffer	dacitic tuff, agglomerate	3471-3463	max 5
N Subgroup	MtAda	basalt and chert		2
A (1,2,3)	Dresser McPhee North Star Basalt	stromatolitic barite-chert felsic schist basalt	ca 3490 3477	0.5
Coonerunah	Double Bar	Basalt, volcanogenic seds	3508	
(3)	Coucal Table Top	Mafic and felsic volcanics, chert, BIF basalt, komatiite	3515	max 6

reflects intracrustal fractional crystallization of a mantle-derived magma combined with assimilation of older crust.

The Kurrana Complex is a granitoid gneiss complex. The presence of a shear zone between the Mosquito Creek Block and the Kurrana Complex has been reported by Tyler et al. (1992): the structure has the characteristics of a suture zone and possibly represents the boundary between two geochemically distinct terranes; the Kurrana Domain and the Nullagine Domain.

Blewett et al. (2002) recorded late regional north-south shortening in the Mosquito Creek Basin. Zegers (1996) reported that the Lionel Fault, the western boundary of the Nullagine Domain, (Figure 3.1) is a brittle structure with a main dextral component of displacement: its last major movement during a 3000 - 2850 event was dextral transcurrent with associated N-NE verging thrusts and transpressive P-shears. White et al. (1998) found that structural trends vary across the Lionel Fault and they suggested that it is a late terrane boundary. Late normal movement on the Lionel Fault has been reported, with vertical displacement in the Mt Roe Group (Hamersley Basin) of over one kilometer (Blake and Barley, 1992).

3.3.2 The Marble Bar Domain

The Marble Bar Domain (Figure 3.1) is the largest and most intensely studied area of all domains in the Pilbara Craton. It comprises several granitoid complexes and greenstone belts. Most of the rocks of the greenstone belts in this domain have been included in the Warrawoona Group (Barley, 1993). The Coonterunah Group lies stratigraphically below the Warrawoona Group (Table 3.1) but its presence in the Marble Bar Domain has not been confirmed. Results of U-Pb geochronological studies of the Warrawoona Group (e.g. Thorpe et al., 1992, Nelson, 1995-2002) indicate that most of it was deposited during the period between ~3480 and ~3430 Ma. These ages are very similar to those of some of the granitoid phases (Figure 3.3) of the Shaw and Mount Edgar Granitoid Complexes (Williams and Collins, 1990; Zegers et al., 2001). Williams and Collins (1990) suggested that the greenstones and the granitoids formed at the same time and from the same source.

Considerable geochemical variation has been found within the Warrawoona Group (Barley et al., 1998). The Kelly Belt dacites have the characteristics of melt derived from subducted mafic crust (Barley et al., 1998). Barley et al. (1998) also concluded that the granites and greenstone belts in the eastern Pilbara are not strictly coeval. They proposed a model of growth for the eastern Pilbara in a convergent tectonic setting, in which pulses of extension were alternated by periods of crustal thickening and intrusion of granitoids. Barley and Pickard (1999) and Collins (1993) found that in addition to recycling of basaltic crust, Archaean *TTG* continental crust was recycled as early as 3.3 Ga. Green et al. (2000) suggested that even earlier Archaean (3.5-3.4 Ga) continental crust was recycled.

A number of structural studies have been carried out in the Marble Bar Domain. An early collisional event has been recorded in the Coonterunah Group (White et al., 1998; Van Kranendonk et al., 2002). While the Marble Bar Domain has been regarded the classical example of vertical tectonics and diapirism (e.g. Collins, 1989; Williams and Collins, 1990; Collins and Kranendonk, 1998), others have interpreted the geology in terms of horizontal tectonics. The first widely recognized event was observed within the Warrawoona Group. It involved east-west extension during deposition of the Duffer Formation between 3470 and 3450 Ma (Zegers et al., 1996; Zegers, 1996; Nijman et al., 1998; Van Haaften and White, 1998; White et al., 1998; Kloppenburg et al., 2001). This extension resulted in the development of core complexes, intrusion of granitoids, mafic and felsic volcanism and deposition of sediments (Zegers et al., 1996; Nijman et al., 1998; Kloppenburg et al., 2001; 2001). However, the role of extension has been questioned by White and Hickman (public discussion at 4IAS, Perth, 2001).

This extensional phase is followed by a compressional event, resulting in folding and thrusting between 3450 and 3310 Ma (White et al., 1998; Kloppenburg et al., 2001). During this event crustal scale north-south trending transcurrent structures developed. A late phase of thrusting occurred

between 3000 and 2900 Ma. It records north-northwest-south-southeast directed transport and it is suggested that this event records accretion of terranes onto the western margin of the East Pilbara Craton (Barley, 1997; Smith et al., 1998; White et al., 1998). Bickle et al. (1980) suggested that horizontal tectonics were responsible for the fold and thrust geometry in the Western Shaw area, and that the uplift of the granitic domes occurred relatively late in the structural evolution of the area. This was in contrast to the diapiric models proposed by Hickman (1983) and others.

Because of the domal geometry of its granitoids (Figure 3.1) the Marble Bar Domain has been put forward as the classical type area for Archaean solid-state diapirism (Hickman, 1984; Collins, 1989; Collins et al., 1998; Van Kranendonk et al., 2002). However, recent studies have shown that major shear zones occur in this area, and the unidirectional lineations suggest a plate tectonic process caused the observed structural-kinematic patterns (Kloppenburg et al., 2001). Blewett (2002) also suggested that the domal geometry is caused by successive horizontal tectonic events rather than granite-driven diapirism.

Davids et al. (1996) dated a regional metamorphic event in the Coongan Belt at 3240 Ma, which is similar to the results of Wijbrans et al. (1987) who dated a regional metamorphic event in the Western Shaw Belt at 3200-3300 Ma. A metamorphic event of similar age is reported by Zegers et al. (1998; 1999) and may be related to a regional compression, without associated magmatism. Boulter et al. (1987) recognized a tectonic event of that age in the western margin of the Shaw Granitoid Complex, and estimated the metamorphic conditions at 4-7 kbar and 500-700°C. They interpreted it as an orogenic event with associated crustal thickening.

Davids et al. (1996) dated north-south striking shear zones in the Coongan Belt at ~2940, which is coeval with a major intrusive event in the East Pilbara. This coincides with ~2950 Ma dates of Wijbrans et al. (1987) in the Western Shaw Belt, which they related to updoming of the Yule Granitoid Complex in the Pilgangoora Domain (next section). They also found a post-tectonic overprint in the area of the Shaw Granitoid Complex of 2840-2900 Ma, indicating either prolonged high temperatures or a late thermal pulse related to intrusion of post-tectonic granitoids (Figure 3.3).

The Mulgandinnah Lineament forms the western boundary of the Marble Bar Domain (Figure 3.1). It consists of a 5-20 kilometers wide north-trending subvertical anastomosing shear zone network and is traceable for over 80 kilometers. Rotated clasts consistently indicate a sinistral sense of shear, locally overprinting thrust structures in the Tambourah Belt (Zegers et al., 1998). The Mulgandinnah Shear Zone must have been active at 2934 Ma as this is the SHRIMP U-Pb zircon age of a syn-kinematic granitic dyke (Zegers et al., 1999, 2001). Krapez et al. (1987) and Van Kranendonk and Collins (1998) attributed the formation of the Lalla Rookh Basin to pull apart in a releasing bend in the Mulgandinnah Shear Zone, during a regional sinistral transpressional phase at about 2950 Ma.

There is no compelling evidence that the Mulgandinnah Lineament forms a tectono-stratigraphic terrane boundary, even though it must have accommodated considerable displacement (Zegers et al., 1998). There is no significant difference between the stratigraphy, and the metamorphic and tectonic history of the domains on either side of the lineament (Van Kranendonk and Collins, 1998). However, the Coonterunah Group has only been reported in the Pilgangoora Domain (Buick et al., 1995).

3.3.3 The Pilgangoora Domain

The oldest greenstone assemblage of the Pilbara Craton, the Coonterunah Group (Table 3.1), occurs in the Pilgangoora Domain (Buick et al., 1995). It is located at the southern edge of the Carlindi Granitoid Complex (Figure 3.1). Green et al. (2000) performed a geochemical study of the mafic

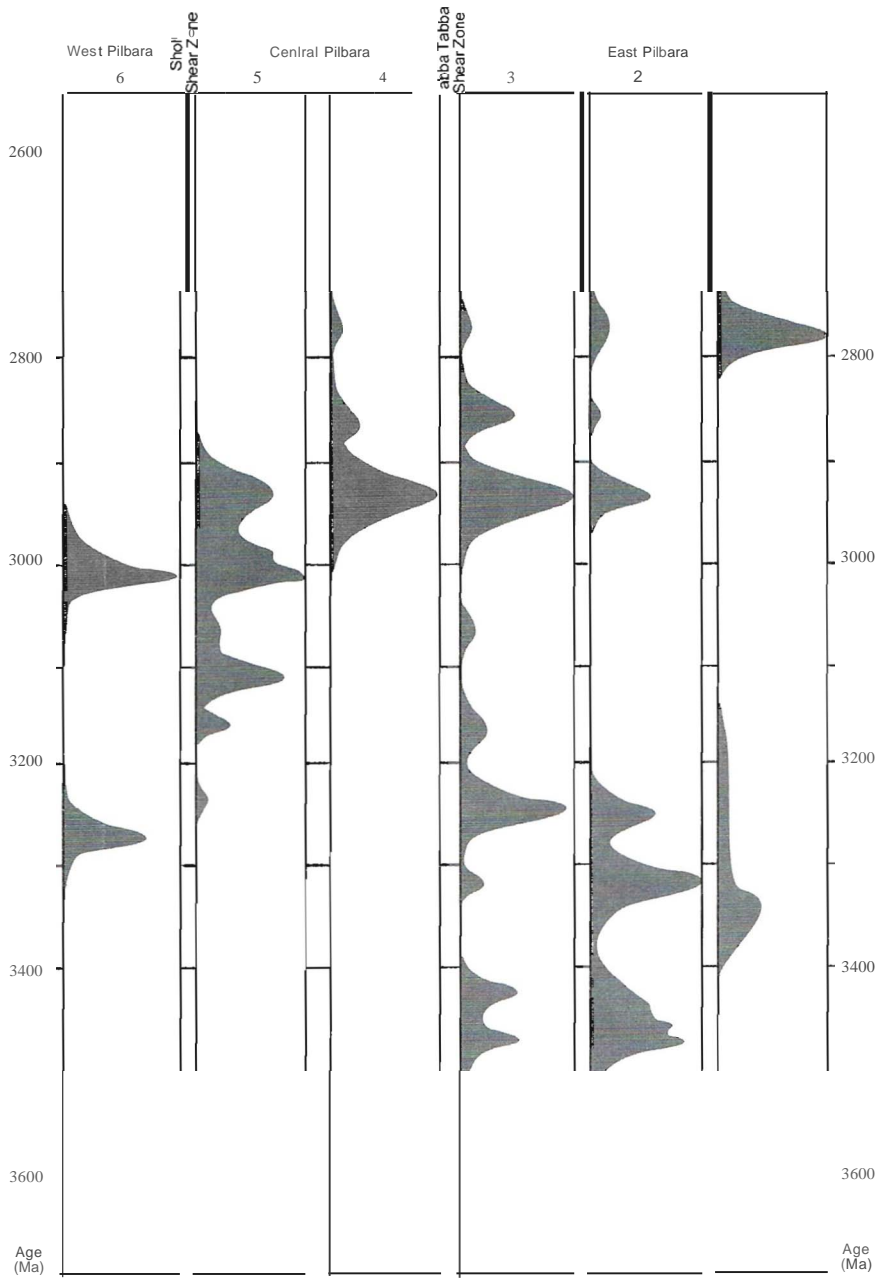


Figure 3.3. Cumulative probability diagrams. One column per domain (domain numbers refer to Figure 3.1). Based on all 169 published SHRIMP ages. Peak height indicates number of samples, which not necessarily reflects the volume of rock. See text for discussion and references.

volcanics in the Coonterunah and Warrawoona Groups. They concluded that the two are very similar and that their compositions can be explained by different degrees of contamination by felsic crustal material. Bolhar et al. (2002) question their modeling methods but Green et al. (in press) replied that the mismatch of their model is minor and does not allow for any other interpretation. The remainder of the greenstones sequences in the Pilgangoora Domain are correlated to the Warrawoona Group, Golden Cockatoo Formation, Sulphur Springs Group and Gorge Creek Group (Table 3.1).

Between the East Strelley Belt and the Yule Granitoid Complex (Figure 3.1), the Golden Cockatoo Formation occurs in the Abydos Belt. These rocks are described (Blewett, 2002; Van Kranendonk et al., 2002) as metamorphic pelite, quartzite, BIF and rhyolite, must have been deposited on >3312 Ma rocks, and are crosscut by 3240 Ma granites. A temporally distinct province is formed by the Sulphur Springs Group (Table 3.1) and Strelley Granite (Buick et al., 2002). Most felsic volcanism in this area occurred at ~3235 Ma. The Strelley Granite has a similar geochemistry and age, and is reported to be a syn-volcanic laccolith.

The structure of the East Strelley Belt is dominated by the Pilgangoora syncline. Baker et al. (2002) found a five-phase deformation history, and Blewett (2002) describes a nine-phase deformation history, illustrating that it is a structurally very complex area.

The age of gold mineralization in the Mt York district in the East Strelley Belt is about 2890 Ma (Neumayr et al., 1998; Baker et al., 2002), indicating that mineralization and the associated structural and metamorphic events post-dated the main magmatic evolution in both the East and the West Pilbara Craton; major mineralization coincided with late deformational events along strike-slip shear zones in the West Pilbara and late syn- to post-tectonic granitoids and associated metamorphism in the East Pilbara (Neumayr et al., 1998; Baker et al., 2002). An ~2860 Ma phase of granite and pegmatoid intrusions (Figure 3.3) and associated mineralization seems to be much more voluminous than previously thought (Sweetapple and Collins, 2002) and was associated with regionally elevated temperatures.

3.4 The Tabba Tabba Shear Zone

The Tabba Tabba Shear Zone (Figure 3.1) has been interpreted as the major division in the Pilbara Craton because of the different tectono-thermal histories of the bordering domains (Barley, 1997). The domains to the west have no pre-3.3 Ga history: the >3.5 Ga Coonterunah Group and the 3.47-3.43 Ga Warrawoona Group (see section 3.3) do not occur to the west of this shear zone, and the 3.45 and 3.3 Ga tectonic events recorded in the East Pilbara (White et al., 1998) have not been recognized in the West Pilbara. Zegers (1996) reported that the Tabba Tabba lineament consists of intensely sheared volcanics and intrusives with a subvertical foliation, down-dip stretching lineations and a NW up sense of shear. White (1998) suggested that the Tabba Tabba Lineament is the boundary along which the West Pilbara Super Terrane was accreted onto the East Pilbara Super Terrane at about 2.9 Ga. The Tabba Tabba Shear Zone forms a major boundary and its structure and geochronology have not previously been studied in detail; it is one of the main subjects of this PhD study.

Table 3.2. Supracrustal sequences in the West and Central Pilbara Granite Greenstone Terrains. the Roebourne Group in the Roebourne Domain (West Pilbara), the Whundo Group in the Sholl Belt (Central Pilbara), Cleaverville Formation which occurs both north and south of the Sholl Shear Zone, the Whim Creek and Bookingarra Groups in the Whim Creek Belt (Central Pilbara), and the Mallina Basin (Central Pilbara). Compiled from Hickman et al. (2001) and references therein. The timing and occurrence of granitoid intrusions can be seen in Figure 3.3. Numbers in the left column refer to the domains shown in Figure 3.1. In domain 5: WC = Whim Creek Belt, S = Sholl Belt

Group (Occurrence)	Formation	Lithology	age (Ma)	Thickness (km)
Mallina (4)	Mallina Fm	sandstone, slate	ca 2975	
	Constantine Sandstone	conglomerate, sandstone	ca 2975	
Bookingarra (5-WC)	Kialrah Rhyolite	rhyolite	ca 2975	
	Negri + Louden Volcanics	mainly mafic volcanics		2
	Cistern Fm + Rushall Slate	clastic sediments	ca 2978	
Whim Creek (5-WC)	Mons Cupri Dacite	dacitic intrusions	ca 3010	0.2
	Red Hill Volcanics	andesite, rhyodacite, sandstone, breccia	ca 3010	0.3
	Warambie Basalt	basalt, minor seds		0.2
	(4,5,6)	Cleaverville Fm	chert, BIF, basalt and felsic volcanics	ca 3020-3015
Whundo (5-S)	Woodbrook Fm	basalt and felsic volcanics	ca 3115	
	Bradley Basalt	basalt, minor felsic volcanics	ca 3115	>4
	Tozer Fm	basalt, rhyolite, sediments and chert	ca 3120	2.5
	Nallana Fm	basalt, minor ultramafics, pyroclastics	ca 3125	2
Roebourne (6)	Regal Fm	komatiites, basalt	not known	2
	Nickol River Fm	volcanogenic sediments, chert	ca 3270-3250	0.1-0.5
	Ruth Well Fm	basalt, talc schist, chert	ca 3270	1-2

3.5 The Central Pilbara

3.5.1 Mallina Domain

The Mallina Basin is a major lithological and structural feature in the Central Pilbara (Figure 3.1). It was an active depocentre between ca 3010 and 2970 Ma, and has long been recognized as a major basin (Krapez and Barley, 1987; Krapez, 1993; Eriksson et al., 1994). However, its significance in the geological evolution of the North Pilbara Granite Greenstone Terrain was only recently highlighted (Smithies et al., 1999; Huston et al., 2000; Smithies et al., 2001; Blewett, 2002; Van Kranendonk et al., 2002). The Mallina Basin was intruded by many felsic to mafic intrusions, and is intensely folded,

3.5.1.1 *Mallina Basin fill*

The Mallina Basin in the Central Pilbara is important in the evaluation of the tectonic history of Pilbara Craton; it is thought to overlie the boundary between the East and West Pilbara Granite Greenstone Terrains (Smithies et al., 1999; Smithies et al., 2001; Van Kranendonk et al., 2002).

The Cleaverville Formation at 3020-3015 Ma (Table 3.2), possibly forms the base of the Mallina Basin (Smithies et al., 2001). The Mallina Basin fill consists of complete submarine flat-ramp-fan systems including turbidites, breccias, sandstones, and mudstones (Hickman, 1983; Eriksson et al., 1994). The lower, generally coarser unit is the Constantine Sandstone, the upper is the Mallina Formation (Table 3.2). The main accumulation in the Mallina Basin occurred between 2970 and 2955 Ma (Smithies et al., 1999; Huston et al., 2000; Smithies et al., 2001), and these authors suggested that the basin developed in a rifted intracontinental setting. It implies that at least part of the Mallina sediments are the lateral equivalent of the ca 2955 Ma Bookingarra Group in the Whim Creek Belt (section 3.5.2) (Smithies et al., 2001). A late rhyolitic sill in the Mallina Basin is quoted by Van Kranendonk and Collins (1998) to have a crystallization age of 2950 Ma.

SHRIMP V-Pb zircon ages of detrital grains show that turbidites of the Mallina Basin have source rocks of 3250-3150 Ma (Nelson, 1997; Smithies et al., 2001) and these were derived from the east as well as the west. A young detrital zircon population of ca 2940 Ma in the northern part of the basin and renewed extension along some of the faults suggest a second stage of basin development shortly after 2940 Ma (Smithies et al., 2001).

Boninite-like rocks have recently been found in the south of the Mallina Basin, near the base of the succession (Smithies, 2002). Boninites (high-Mg rocks of basaltic to andesitic composition with U-shaped REE patterns) are traditionally thought to be restricted to Phanerozoic convergent margins, specifically island arcs (Crawford, 1989). This was because they are thought to originate from a mantle source depleted by previous basalt extraction, and subsequently hydrated and enriched in incompatible trace elements by infiltration by a subduction-derived fluid or melt.

The boninites described by Smithies (2002) form a schistose assemblage of actinolite-chlorite-tremolite and epidote-talc-plagioclase-quartz. Locally the original igneous textures such as quench textures and olivine cumulate textures have been observed. No evidence for extrusion was found, but the layers are parallel to the sedimentary bedding and are interpreted as shallow sills. The units have experienced the major phase of folding that occurred in the Mallina Basin and must therefore be between 2970 and 2955 Ma old. The Negri and Loudon Volcanics in the Whim Creek Belt are the same age as the boninite-like rocks and are also LREE and LILE-rich and high in Mg, and high in Si. Even though the boninites are compositionally very similar to modern boninites, they are different in their intracontinental setting and the lack of coeval subduction (Smithies, 2002). The LREE and LILE enrichments could alternatively be caused by and partial melting of a previously enriched mantle source and contamination with continental crust (Smithies, 2002).

3.5.1.2 *Intrusions in the Mallina Basin*

The Mallina Basin was intruded by several suites of granitoids (Figure 3.3). By a suite of high-Mg diorites intruded along a linear belt parallel to the basin axis (Figure 3.1), and by large volumes of alkaline granites in the northern part of the basin (Champion and Smithies, 1998; Smithies and Champion, 1999). The felsic members of the intrusive high-Mg diorite suite have high Mg, Cr and Ni, and are enriched in incompatible trace elements (Smithies, 2000). They post-date the boninites and the ~2955 Ma phase of folding of the Mallina Basin, but are thought to be related to the same

processes in the source region as the boninites (Smithies et al., 2001). The mafic members of the high-Mg diorite suite have very high Cr and Ni and are extremely enriched in LILE and LREE. Similar rocks of 2700 Ma in the Superior Province in Canada have been called sanukitoids and are thought to have formed by partial melting of a subduction enriched mantle source, with no crustal contamination (Stem et al., 1989). Smithies et al (2001) used the constant LILE concentrations across a range of SiO_2 and Mg values as evidence against assimilation of felsic crust. One of these intrusions is the Peawah Granitoid, which is a hornblende tonalite and has an age of 2948 ± 5 Ma (Nelson, 1997).

After a late phase of basin development at 2940 Ma the Mallina Basin was intruded by a suite of monzogranites at approximately 2935 Ma (Smithies et al., 2001). The Satirist Granitoid is a composite granodiorite, which intrudes the Mallina Basin, the Peawah Granitoid and the Millinditula mafic-ultramafic suite. No published dates of the Portree and Turner Granitoids exist (Figure 3.1).

Throughout the Central and East Pilbara a suite of 'younger granites' has been emplaced between 2890 and 2830 Ma (Smithies and Champion, 1998). Rare metal pegmatites are genetically related to this suite of 'younger granites' (Sweetapple and Collins, 2002, and references to abstracts and reports therein). The majority of the pegmatites are spatially associated with major faults and lineaments. The Opaline Well Granitoid, intruding on the contact between the Whim Creek Belt and the Mallina Basin (Figure 3.1), is significantly younger than the other units of Mallina Domain and is a genetic component of the Fortescue Group, because it has an age of 2765 ± 5 Ma (Nelson, 1997).

3.5.1.3 Structure of the Mallina Basin

The Mallina Basin has been reported to record three phases of folding. Krapez and Eisenlohr (1998) describe an early, overprinted set of folds that was originally east-west trending. The southeast dipping axial planar cleavage of these folds has been refolded by the later phase. The second generation are closed folds with southeast dipping, north-trending axial planes. This phase of folding created anticlines that expose the Constantine Sandstone in their cores, and also affected the Millindinna Suite. According to Smithies et al. (2001) the Mallina Basin experienced a phase of folding on north-trending axes at approximately 2955 Ma, immediately followed by intrusion of the high-Mg diorites. A third and final deformation phase resulted in east-northeast trending regional scale folds, and occurred during and after intrusion of granites between 2940 and 2930 Ma (Nelson, 1998a; Nelson, 1999; Nelson, 2000).

The Mallina Shear Zone runs east-northeast along the axis of the Mallina Basin (Figure 3.1). Because it is such a prominent feature on aeromagnetic images (Figure 3.2) the Mallina Shear Zone is interpreted to be a reactivated structure in the basement. The surface expression consists of very low grade, intensely folded and sheared metasediments. The structures record south-side-up movement and are related to the main phase of northeast-trending folds in the Mallina Basin. Later structures record several phases of minor strike-slip movement (Hickman et al., 2001).

Recent publications (e.g. Blewett, 2002; Pike et al., 2002; Van Kranendonk et al., 2002) refer to the Mallina Basin and the Whim Creek Belt as the Central Pilbara (Figure 3.1). As a consequence, the Loudens Fault that separates the Mallina Basin from the Whim Creek Belt, is no longer considered to be a terrane boundary, in contrast to previous interpretations (Krapez and Eisenlohr, 1998). During a late phase of deformation in the Pilbara Craton, with the opening of the Hamersley Basin, the Loudens Fault was a northwest-up brittle structure.

3.5.2 Whim Creek Belt (Sholl-Whim Creek Domain)

The Whim Creek Belt (Figure 3.1) contains two main supracrustal components: the ~3010 Ma Whim Creek Group and the ~2975 Ma Bookingarra Group (Table 3.2). The basement on which it was deposited unconformably, is formed by the Whundo Group in the western part, and the Caines Well Granitoid. The extent of the Whim Creek Belt is defined by the Sholl Shear Zone in the northwest, and the Loudens fault in the southeast. The Whim Creek Belt locally extends into the Roebourne Domain, as volcanics and sediments on the north side of the Sholl Shear Zone were interpreted to belong to the Whim Creek Belt (Smithies, 1996). The Whim Creek Belt may form the lower part of the Mallina Basin (Smithies et al., 1999).

The base of the Whim Creek Group is formed by the dominantly subaqueous Warambie Basalt, accompanied by minor sediments (Table 3.2). The overlying Red Hill Volcanics are dominated by andesite and rhyodacite, dated at 3009 ± 4 Ma (Nelson, 1998a). These rocks are interpreted to represent subaqueous sedimentation of volcanoclastics by turbidity currents and debris flows (Pike et al., 2002). The Mons Cupri Dacite is a single, large-volume unit of dacite emplaced as a high-level intrusion into the Red Hill Volcanics. The dacite is interpreted to be the source of mineralizing fluids that formed base metal deposits in the area (Pike et al., 2002). Pike and Cas (2002) suggest that the early volcanics of the Whim Creek Group could be related to a continental arc, based on basalt geochemistry. However, there is no direct evidence for subduction associated with the basin development.

The Bookingarra Group is the second component of the Whim Creek Belt (Table 3.2). It comprises the sedimentary Cistern Formation and Rushall Slate with maximum depositional ages of 2978 ± 5 Ma (Nelson, 2000), and the dominantly mafic volcanic Mount Negri and Loudens Volcanics and the Kialrah Rhyolite with an age of 2975 ± 4 Ma (Nelson, 1998a). Krapez et al. (1993) described four fining-up depositional cycles thought to reflect volcano-sedimentary cycles in a back-arc basin (Barley, 1987).

The Caines Well Granitoid (Figure 3.1), which has tectonic contacts with the Whim Creek Belt, consists of several phases. The oldest phase was dated at 3093 ± 4 Ma, with xenocrysts on 311 ± 13 Ma (Nelson, 1997), indicating the presence of basement of the same age as the Whundo Group (Figure 3.3). The main phase is a monzogranite with an age of 2990 ± 5 Ma (Nelson, 2000). Most of the contacts of the Caines Well Granitoid are sheared but intrusive contacts with amphibolite-grade Whundo Group basalts have been reported (Barley, 1987; Krapez and Eisenlohr, 1998; Pike et al., 2002). The Whim Creek Belt and margin of the Caines Well Granitoid Complex are also intruded by mafic-ultramafic sills and dykes of the Opaline Well and Sherlock Intrusions.

3.5.3 Sholl Belt (Sholl-Whim Creek Domain)

The supracrustals in the Sholl Belt (Figure 3.1) comprise the four units of the Whundo Group, and the Cleaverville Formation (Table 3.2). The ~3125 Nallana Formation consists mainly of basalt, and minor ultramafics and intermediate pyroclastics. The Tozer Formation consists of a range of extrusives from basalt to rhyolite, and minor metasediments and chert. The Bradley Basalt is a succession of massive and pillowed basalts with high-Mg basalt present near the base, and minor felsic tuffs near the top which were dated at 3115 ± 5 Ma (Nelson, 1996). The top of the Whundo Group is formed by the basalts and rhyolites of the Woodbrook Formation, dated at 3117 ± 3 Ma (Nelson, 1998a). These volcanic rocks were derived from juvenile crust, possibly in a back arc setting (Smith et al., 1998) in a subduction zone environment (Sun and Hickman, 1998). The stratigraphic sequence (Horwitz and Pidgeon, 1993) was interpreted to be consistent with a back-

arc rift environment (Krapez, 1993). The Sholl Belt shows evidence of folding on northeast trending axial planes (Krapez and Eisenlohr, 1998; Hickman et al., 2001). The entire belt is of low greenschist metamorphic grade.

The Cheratta Granitoid Complex (Figure 3.1) occurs to the west of the Sholl Belt and consists of at least three generations of granitoid. All generations have intrusive eastern contacts with the Sholl Belt. The oldest component has an age of 3114 ± 5 Ma (Smith et al., 1998), which is coeval with the felsic volcanics within the Sholl Belt (Horwitz and Pidgeon, 1993; Nelson, 1996; Nelson, 1997). These old granites have crustal feldspar-bearing sources that are interpreted to have formed in a continental back-arc setting (Smith et al., 1998). The middle phase of the Cheratta Granitoid is dated at 3014 ± 4 Ma (Smith et al., 1998) and is coeval with a rhyolitic sill intruding the Sholl Belt with an age of 3014 ± 6 Ma (Nelson, 1997). These granitoids have geochemical characteristics of a garnet-bearing mafic source in an arc environment, possibly related to continental back-arc compression accompanying low angle subduction and underplating of the West Pilbara by oceanic lithosphere (Krapez and Eisenlohr, 1998). The main and youngest phase of the Cheratta Granitoid has an age of 2994 ± 2 Ma (Nelson, 1997), and a thermo-tectonic event was recorded by post-magmatic zircons with an age of 2925 ± 11 Ma (see granite age diagram in Figure 3.3). Small inliers thought to be part of the Cheratta Granitoid in the Fortescue River valley have been dated at 3236 Ma (Nelson, 1999).

The Sholl Belt is intruded by a number of mafic-ultramafic bodies. One component, the Munni Munni Complex, which intrudes the Whundo Group as well as the Cheratta Granitoid, has an age of 2925 ± 16 Ma (Arndt et al., 1991). It was emplaced at an estimated 3.5 - 5 kbars and at a temperature between 1050° and 1100°C (Hoatson and Sun, 2002).

3.6 The Sholl Shear Zone

The Sholl Shear Zone runs from west to east approximately parallel to the coastline for over 150 kilometers. Its width varies around 1 km. The Sholl Shear Zone has only recently been recognized as a terrane boundary structure (Smith et al., 1998). The Sholl Shear Zone separates the Sholl-Whim Creek Domain from the Roebourne Domain, and the Central Pilbara from the West Pilbara (Figure 3.1). A tonalitic granitoid intrusive along strike into the Sholl Shear Zone, has a SHRIMP U-Pb in zircon age of 3024 ± 4 Ma (Smith et al., 1998). This granitoid is derived from the melting of garnet-bearing mafic amphibolite possibly in an arc setting (Smith et al., 1998). Hickman et al. (2001) interpreted that a very large (200-300 km) sinistral displacement occurred on the Sholl Shear Zone, probably between 3050 and 3020 Ma. This is overprinted by the measurable 40 kilometers of dextral displacement which took place after deposition of the Whim Creek Group (Smithies, 1996).

3.7 The West Pilbara

3.7.1 The Roebourne Domain

The Roebourne Domain (Figure 3.1) comprises the Roebourne Group and the Cleaverville Formation (Table 3.2). The oldest formation is the Ruth Well Formation, which comprises basalt, talc schist and chert. The formation has not been dated but it must be older than the conformably overlying Nickol River Formation, which consists of clastic sediments, felsic volcanics and chert, and has an

age of 3251 ± 6 Ma (Nelson, 1998a). It must also be older than the Karratha Granodiorite by which it is intruded (Blewett, 2002) and which has been dated at 3265 Ma (Nelson, 1998b; Smith et al., 1998).

The undated Regal Formation is separated from the underlying Ruth Well and Nickol River Formations by a tectonic contact, the Regal Shear Zone (Hickman et al., 2001). The Regal Formation consists of komatiites, basalt and minor chert, and is reported to have MORB affinities (Sun and Hickman, 1999). Ohta et al (1996) suggested that chert and clastics associated with the basalts represent an accretionary complex generated by the scraping off of the subducted oceanic crust. The Ruth Well, Nickol River and Regal Formations and the Karratha Granodiorite occur exclusively to the north of the Sholl Shear Zone.

The Cleaverville Formation has an age 00020–3015 Ma (Nelson, 1998a) and consists of BIF, chert, volcanogenic sediments and minor felsic and mafic volcanics, all metamorphosed to lower greenschist facies. Detrital zircon populations in the Cleaverville Formation have ages similar to the ages of magmatic zircons found in the Nickol River Formation and Karratha Granitoid (ca 3265 Ma), indicating crust of this age must have been exposed at the time of deposition. Interestingly Nelson (1998a) found one detrital zircon with an age on 461 ± 8 Ma, which is a common age of the Warrawoona Group in the East Pilbara. This may indicate that East Pilbara crust was close by and exposed at 3020 Ma, or it may be a contaminant in the sample. The minimum age of the Cleaverville Formation is constrained by a granitic intrusion with an age of 3014 ± 6 Ma (Nelson, 1997), and detrital zircons of 3014 ± 6 Ma (Nelson, 1998a). The Cleaverville Formation has a Sm-Nd Tm Model age of 3110–3210 Ma (Sun and Hickman, 1998). In much of the West Pilbara the Regal Formation stratigraphically underlies the Cleaverville Formation, but their contact is always tectonic.

The Karratha Granitoid (Figure 3.1) has a zircon age of 3261 ± 4 Ma and the geochemistry of the tonalites to granodiorites indicates that it may have formed in an arc environment (Smith et al., 1998). Nd model ages of 3480–3420 Ma (Sun and Hickman, 1998) indicate that magma generation involved older crust. This is confirmed by the presence of old cores of similar age in zircons (Smith, 2003). A different suite intrudes the Ruth Well Supracrustal Unit and is geochemically identical to the Karratha Granitoid. It has a zircon age of 3265 ± 4 Ma (Smith et al., 1998), and is interpreted to be part of the same island arc setting as the Karratha Granitoid.

The Harding Granitoid (Figure 3.1) comprises two generations of granitoid (Figure 3.3). The oldest suite of the Harding Granitoid consists of tonalitic plutons and is coeval with high-level felsic intrusions in the Ruth Well Supracrustal Unit. These tonalitic plutons occur in the eastern and southern parts of the Harding Granitoid. They have ages on 3014 ± 3 Ma (Nelson, 1997), 3024 ± 4 Ma and 3031 ± 6 Ma (Smith et al., 1998).

The Dampier Granitoid consists mainly of granite-granodiorite and an age of 2997 ± 3 Ma (Nelson, 1998a) has been obtained. The Balla Balla Granitoid (Figure 3.1), which was included in the Harding Granitoid by Hickman et al. (2001), comprises a main phase of monzogranite and compositionally banded granodiorite (Hickman et al., 2001). It has been dated at 3014 ± 3 Ma (Nelson, 1997) and has a Nd model age of 3276 Ma (Sun and Hickman, 1998). Banded gneiss in the Sholl Shear Zone was dated at 2995 ± 11 Ma (Nelson, 1997) and gave a Nd model age of 3246 Ma (Hickman et al., 2001).

The Andover Complex (Figure 3.1) is a layered mafic-ultramafic intrusion, consisting of serpentinized peridotite, gabbro and dolerite dykes (Hoatson and Sun, 2002). It intrudes the Harding Granitoid as well as the Ruth Well Formation. An early phase of magmatism is indicated by the 3016 ± 4 Ma age obtained by Nelson (2001), but it is thought that the main portion of the complex correlates to the other mafic-ultramafic intrusions in the West Pilbara that have ages of about 2925 Ma (Hoatson and Sun, 2002).

Table 3.3. The tectonic evolution of the Pilbara as proposed by Hickman (1983), who remarked that the absolute ages were not firmly established at that time.

Timing (Ga)	geology	tectonics
2.6	conjugate folding and faulting due to east-west compression	
2.95-2.6	uplift and erosion, intrusion of post-tectonic granites	
2.95	deformation causes domes and synclines	
3.4-2.95	interfolding of granites and greenstones, granite intrusion and migmatization, partial melting of lower crust. basin formation	main solid state diapiric deformation phase regional metamorphism (greenschist-amphibolite)
ca 3.4	tabular succession of tholeiitic basalts, local felsic volcanism	stable conditions
3.55-3.45	local deformation, calc-alkaline volcanism, granodiorite intrusion	local volcanic centers possibly related to subduction or down warping
ca 3.6	subaqueous tholeiitic basaltic extrusion, erosion and partial melting of crust	
3.9-3.6	gneisses: relics of volcanism, sedimentation, granitic intrusion	
4.6-3.9	speculative: core formation, mantle differentiation, protocrust formation	catastrophic meteorite bombardment

The sheared contacts between the different units of the Roebourne Domain are interpreted as thrust faults on which high grade blocks in the south were emplaced structurally over lower grade units in the north. When structurally restored, the Roebourne Domain was interpreted to resemble an ophiolite complex in a setting that might be similar to a modern immature island-arc (Kiyokawa and Taira, 1998; Krapez and Eisenlohr, 1998; Kiyokawa et al., 2002),

Low-angle thrusts such as the Regal Thrust are interpreted to have accommodated southward displacement of units in the Roebourne Domain prior to 3130 Ma (Hickman et al., 2000). This possibly occurred at the time of a thermal disturbance at 3150-3160 Ma recorded by K-Ar dating (Kiyokawa and Taira, 1998; Smith et al., 1998). These structures do not occur in the Whundo group, indicating they must predate 3130 Ma. The large scale regional northeasterly trending folds were probably formed at about 2950 Ma, as they may correlate to folds with the same orientation in the Mallina Basin (Hickman et al., 2001).

3.8 Tectonic models and geodynamics

As discussed in Chapter 2, there is still much controversy on whether modern-style plate tectonics, characterized by spreading and subduction of rigid ocean floor, and continental growth by lateral accretion of terranes, were possible in the Archaean. Geodynamical modeling has not provided

Table 3.4. Sequence stratigraphic evolution of the Pilbara as proposed by Krapez (1993). Numbers in the leji column refer to the domains shown in Figure 3.1.

Timing (Ga)	geology	tectonics
megacycle		
2.95-2.77	granites and pegmatites	back arc magmatism
Negri (4,5)	mafic volcanism, terrigenous seds	intra-cratonic graben
3.11-2.95	hiatus	microplate orogeny
Roebourne	clastic seds, mafic volcanism	strike-slip graben, transtensional rift
(6)	hiatus	microplate orogeny
	clastic seds, mafic and felsic volcanism	back arc magmatism, folding, thrusting
	hiatus	microplate orogeny
(2-5)	BIF	oceanic platform
	felsic volcanoclastics	fore arc
	mafic volcanoes	allochthonous oceanic islands
3.34-3.11	metamorphism, fold and thrust belt	back arc, continental accretion
Gorge Creek	turbidites, BIF	foredeep, marginal basin
(2-5)	marine volcanoclastics and sediments	extensional continental back arc
	metamorphism, fold and thrust belt	back arc, continental accretion
(1)	molasse and flysch sedimentation	fore arc basin
	calc-alkaline volcanism and tholeiitic basalts	volcanic arc and intra-arc basins
349-334	migmatite gneiss	arc accretion
Warrawoona	mafic volcanic platform	marginal basin
(1,2,3)	bimodal volcanics	near-arc basin
	mafic volcanics	allochthonous oceanic island

conclusive answers, mainly because the temperature of the interior of the Earth in the Archaean still is a major unknown.

Most tectonic interpretations of Archaean terrains can be placed in either of two end-member models. The first is a 'vertical' tectonic regime dominated by diapirism (e.g. Hickman, 1984; Collins and Kranendonk, 1998; Hamilton, 1998). The second is a 'horizontal' tectonic regime dominated by plate interactions (e.g. Bickle et al., 1980; De Wit, 1998; Krapez and Eisenlohr, 1998; Blewett, 2002). Most studies in the Pilbara have concentrated on limited areas, and mainly in the East Pilbara; they have been summarized above. Few studies report models that involve the whole of the craton.

Hickman (1983) was the first to publish a Pilbara-wide model. It was based on a deformation history consisting of major events (Table 3.3). This involved magmatism, volcanism, metamorphism and deformation between 3600 Ma and 2950 Ma and focused on diapiric processes. Krapez (1993) presented a model that divided the Pilbara greenstone successions into first and second-order sequence stratigraphic units (Table 3.4). He recognized four first-order cycles which he interpreted in terms of fore-arc, arc, and back-arc tectonic evolution in settings that he directly related to convergent margins in Wilson and Supercontinent cycles. This model was refined (see Table 3.5) for the West and Central Pilbara by Krapez and Eisenlohr (1998).

Table 3.5. Tectonic evolution of the West and Central Pilbara (called West Pilbara Block, before definition of the Central Pilbara), as proposed by Krapez and Eisenlohr (1998).

Timing (Ma)	Domain 6	Domain 5	Domain 4
2860-2770	uplifted plateau	uplifted plateau	uplifted plateau
2900-2860	collision orogen	collision orogen	collision orogen
2950-2900	back arc basin, plume event	back arc basin, plume event	back arc basin, plume event
3000-2950	hinterland margin	transtensional basin	hinterland plateau
3050-3000	back arc magmatic belt	back arc magmatic belt	back arc magmatic belt
3090-3050		back arc thrust belt	retro arc basin, remnant ocean
3140-3090		back arc basin, plume related	
3180-3140	collision orogen	collision orogen	collision orogen
3230-3180	compressive basin	arc orogen	arc orogen
3270-3230	intra arc basins	back arc basin	back arc basin
3325-3270	island arc, ophiolites		

Table 3.6. Tectonic evolution of the Pilbara Craton as proposed by Blewett (2002). Numbers in the left column refer to the domains shown in Figure 3.1.

Timing	geology	tectonics
3.02-2.85 Ga (4,5,6)	continuous magmatism, basin development. accretion of new crust	convergent margin
ca 3.1 Ga (4,5)	development of the Central Pilbara, new crust generation, rifting	subduction zone setting, back-arc spreading
3.25-3.2 Ga (1,2,3,4,5,6)	Pilbara-wide magmatic and deformation events, compression from NW	arc and back-arc settings
3.5-3.3 Ga (1,2,3)	development of the domal geometry in the East Pilbara, intracrustal generation and recycling of TIG	chocolate-tablet style extension and compression due to horizontal tectonics

Table 3.7. Tectonic evolution of the Pilbara as proposed by Van Kranendonk et al (2002).

Timing	geology	tectonics
3.15-2.93	widespread deformation	onset of microplate tectonics
3.30-3.07 Ga	diachronous volcanism across Pilbara	rifting, back arc
3.53-3-31 Ga	continuous volcanism in East Pilbara, recycling of lower mafic crust and generation of TIG	mantle plumes main phase of diapiric deformation
3.72-353 Ga	early crust formation: sialic basement	?

Blewett (2002) presented structural data that may indicate that the 'dome and basin geometry', characteristic of the East Pilbara and used by many as evidence for diapirism, was established as a result of far-field horizontal stresses related to plate interaction, in a chocolate-table style of deformation. He interpreted the entire structural history of the Pilbara in terms of extensional and compressive events (Table 3.6), and suggested that granite-driven diapirism is at best a modifying factor. He reinterpreted the vertical lineations in a 'zone of sinking' (see Collins and Kranendonk, 1998) as intersection lineations. Van Kranendonk et al. (2002) presented structural data (Table 3.7) that they interpreted to contradict the 'horizontal' structural models published for the Marble Bar area (see section 3.3.2 for references) and further support Hickman's (1984) diapiric model. However, they suggest that after about 3.2 Ga a form of micro plate tectonics became a dominant process. This Ph.D. thesis is concerned with the post-3.25 Ga history of the West- and Central Pilbara and therefore will not elaborate on the 'vertical vs. horizontal tectonics' discussion.

3.9 Summary

The Pilbara Craton in western Australia contains one of the oldest, best preserved and best exposed Archaean granite-greenstone terrains. It has a long active geological history spanning between ca 3.6 and 2.9 Ga, and an even longer subsequently history as a stable craton. The classical domal geometry of the granitoids, particularly in the East Pilbara, have led to the development of models in which solid-state diapirism was a dominant tectonic process, however, this is still a matter of debate. The advocates of diapirism in the Pilbara have restricted their models to the pre-3.25 Ga history of the East Pilbara. Because the Pilbara Craton consists of several elongate domains, accretionary models have been developed in a modern tectonic context. In the recent literature, all authors agree that after about 3.25 Ga, at least some form of (micro-) plate tectonics was active and responsible for the formation of the observed rocks and structures.

Lithology, structure and geochemistry of the ca 3.5 Ga North Star Basalt in the Marble Bar Greenstone Belt, Archaean Pilbara Craton, Western Australia

Abstract

This study was undertaken to investigate a possible oceanic origin for the North Star Basalt in the Marble Bar Belt. This is the lowermost formation of the Warrawoona Group and one of the oldest greenstones sequences in the Archaean Pilbara Craton in Western Australia. It consists mainly of pillowed and massive basalts, minor gabbro, and comprises a large number of mafic and ultramafic dykes. Geochemical studies have shown that the upper part of the North Star Basalt comprises enriched tholeiitic basalts, probably due to contamination of the magmas by assimilation of crustal material. They do not resemble modern MORB. The lower, ultramafic part of the stratigraphy may not be part of the North Star Basalt, as indicated by its different trace element geochemistry. A $^{40}\text{Ar}/^{39}\text{Ar}$ cooling age of about 3.47 Ga indicates that these rocks may be the same age as the Taiga Taiga Subgroup of the Warrawoona Group, to which the North Star Basalt belongs. Only a small fraction of the dykes that occur in the area, is genetically related to the extrusive pile; the majority has been emplaced later, probably during regional extension at ca 3.3 Ga. Granite intrusions at ca 3.3 Ga post-date emplacement of all of the dyke suites, and have destroyed the lower section of the greenstone sequence. There is no firm evidence for large displacements on any of the structures within the unit. Therefore the Taiga Taiga Anticline may still be a suitable type area for the North Star Basalt, but the presence of low angle unconformities should not be disregarded.

4.1 Introduction

The Marble Bar Greenstone Belt is located in the Archaean Pilbara Craton in Northwestern Australia (Figure 4.1). The Pilbara Craton is an early to mid-Archaean terrane comprising granitoids and greenstone belts (e.g. Hickman, 1983), overlain by the late Archaean volcano-sedimentary sequence of the Hamersley Basin. The studied area is located about 25 km north of Marble Bar and 150 km to the southeast of Port Hedland (Figure 4.1). It is well accessible, and the outcrop is generally good.

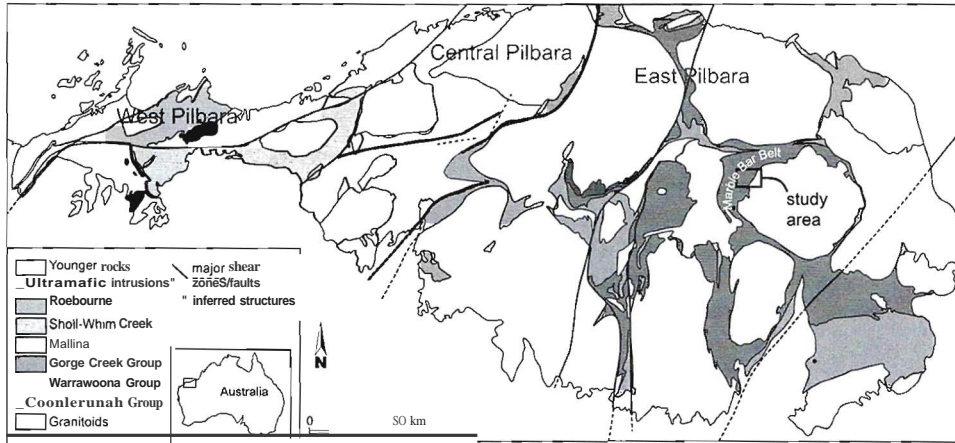


Figure 4.1 The Pilbara Craton in Western Australia. The study area is indicated.

The basal Warrawoona Group forms an anticlinal structure in the Marble Bar Belt, west of the Mount Edgar Granitoid Complex. This structure is referred to as the Taiga Taiga Anticline (Figure 4.2) and hosts the type area for the Taiga Taiga Subgroup (Hickman, 1977; 1983). The local stratigraphy is summarized in Table 4.1. The basal formation of the Taiga Taiga Subgroup is the North Star Basalt which comprises a ca 1 km thick sequence of dominantly basalt.

The North Star Basalt is thought to be a potential ophiolitic sequence (see comment in De Wit (1998)). Zegers (1996) suggested it was part of the Coonterunah Group. If it does belong to either the Coonterunah or Warrawoona Groups, correlation with the work of Green et al. (2000)

Table 4.1. The stratigraphy of the Coonterunah and Warrawoona Groups in the Marble Bar Domain of the East Pilbara Craton. After Van Kranendonk et al (2002) and references therein.

Group	Formation	Lithology	age (Ma)	thickness (km)
W	Kelly	Charteris Basalt		
A	Subgroup	Wyman	3325	max 1.1
R		Euro		max 9.4
R	Saigash	Strelley Pooli Chert		
A	Subgroup	Panorama	3459-3434	ca 1.5
W		Apex		max 4
O		Towers	<3463	
O	Taiga	Duffer	3471-3463	max 5
N	Taiga	MtAda		ca 2
A	Subgroup	Dresser	ca 3490	
		McPhee	3477	ca 0.5
		North Star Basalt		ca 1
Coonterunah	Double Bar	Basalt, volcanogenic sed	3508	
	Coucal	Mafic and felsic volcanics. chert. BIF	3515	max 6
	Table Top	basalt, komatiite		



Figure 4.2. Landsat TM image showing the regional setting of the North Star Basalt, the Taiga Taiga Alltcline and the Mounl Edgar Batholith in the lower right corner.

suggests that it cannot be oceanic. Green et al. (2000) indicated that the basalts of the Coontenmah and upper Warrawoona groups were deposited in a continental environment. This would indicate that the East Pilbara has been a stable continental block since at least the deposition of the ca 3515 Ma Coonterunah Group. The long term stability of the East Pilbara has implications for the evolution of the West and Central Pilbara and is important to the central theme of this thesis.

In this paper the results of a detailed lithological, structural and geochemical study of the North Star Basalt are presented. The study is based on mapping (Figure 4.3) and was undertaken to investigate the tectonic setting in which the extrusive pile was formed. The possibility of an oceanic

origin for the North Star Basalt will be discussed after an investigation into the extent to which it has been structurally disturbed. In fact, Trendall (1995) suggested that the North Star Basalt presents an area that potentially contains some answers to important questions about the geological history of the Pilbara Craton.

4.2 Regional Geology

The Warrawoona Group in the East Pilbara is the most wide spread greenstone sequence in the East Pilbara Craton; it unconformably overlies the Coonterunah succession (see Table 4.1). U-Pb zircon ages indicate the Warrawoona Group was deposited between ca 3475 and 3435 Ma (e.g. Thorpe et al., 1992, Nelson 1996-2002). It comprises mainly volcanic assemblages that were possibly deposited in volcanic-arc and near-arc environments (Barley, 1997). In most of the East Pilbara the Gorge Creek Group unconformably overlies the Warrawoona Group. It consists mainly of clastic sediments, pillow basalts and minor komatiites.

The North Star Basalt is the basal formation of the Taiga Taiga Subgroup and also of the Warrawoona Group. The lower boundary of the North Star Basalt in the Marble Bar Belt (Figure 4.1) is the intrusive contact with the Mount Edgar Granitoid Complex. Its stratigraphic position and regional correlations have been the subject of debate, because its age is not well constrained. The mafic rocks of the Taiga Taiga Subgroup have a Sm-Nd model age of approximately 3560 ± 32 Ma (Hamilton et al., 1981) or 3712 ± 98 Ma (Gruau et al., 1987), however, it is not clear exactly which rocks suites have been included in the calculations for these model ages. In the most recently published stratigraphy of the east Pilbara Craton (Van Kranendonk et al., 2002) the North Star Basalt is still regarded as the oldest formation of the Taiga Taiga Subgroup (see Table 4.1).

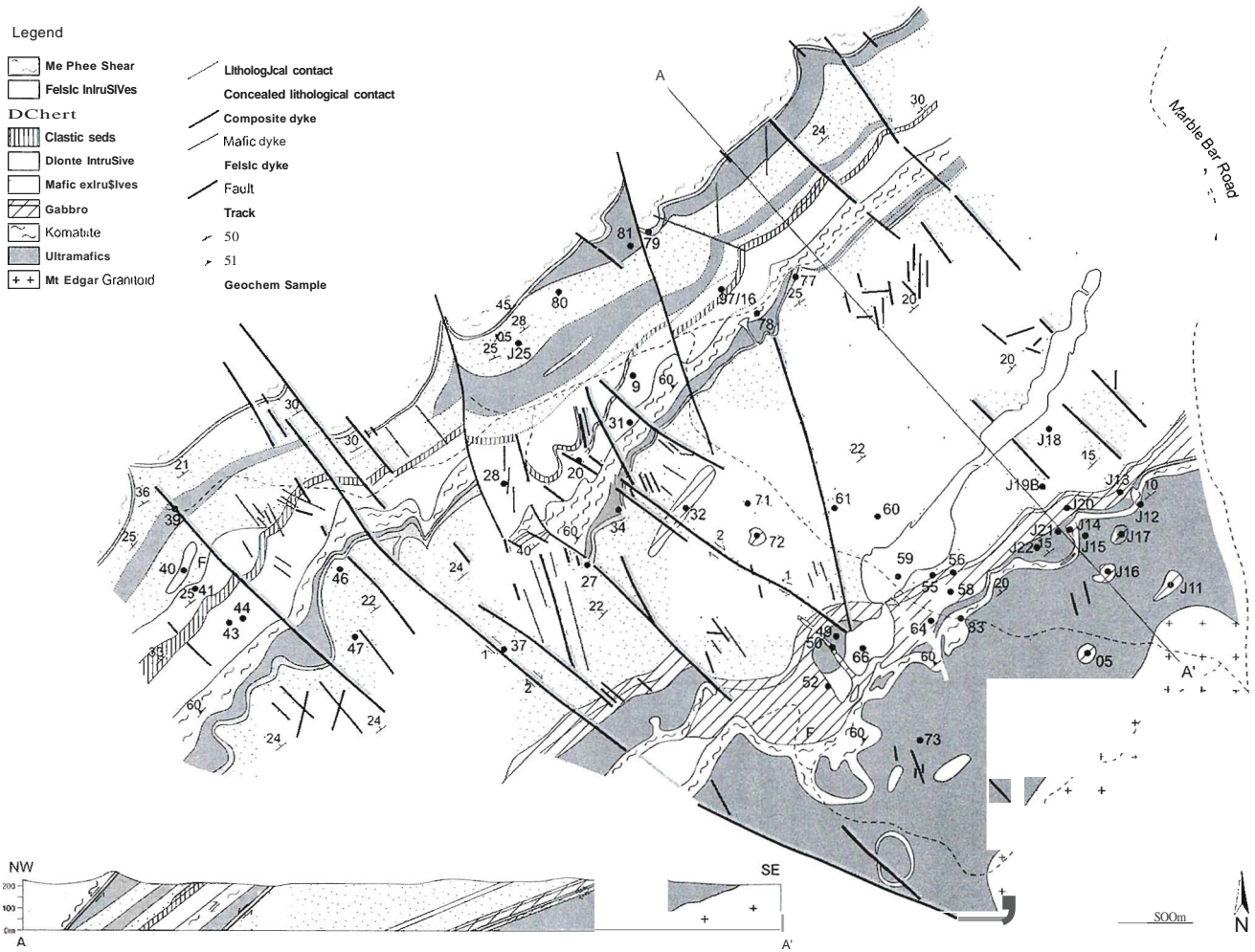
Nowhere a conformable lower contact has been observed for the North Star Basalt (or the base of the Warrawoona or Coonterunah Group for that matter), so the nature of the basement onto which the sequence was extruded, remains enigmatic. However, Barley (1986) reported crustal contamination of the Warrawoona basalts, and Green et al. (2000) reported granitic xenoliths in basalts of the upper Warrawoona Group, suggesting those basalts were extruded onto a continental basement.

A pillow basalt near the top of the North Star Basalt was reported to contain zircons with ages of 3326 ± 10 Ma, and a syn-volcanic dolerite sill has been dated at 3238 ± 6 Ma (McNaughton et al., 1993), but these zircons most likely have a hydrothermal origin. The stratigraphic locations of these published data are indicated in Figure 4.4. Nelson (2000) has dated a rock from the overlying McPhee Formation (Table 4.1). A rock described as a vitric tuff, but with a petrographic description of a cherty mylonitic schist, gave an age of 3477 ± 2 Ma. A felsic lens in the overlying Mount Ada Basalt (Table 4.1) was dated at 3469 ± 3 Ma (Nelson, 2000). In this paper the results of $^{40}\text{Ar}/^{39}\text{Ar}$ dating in the North Star Basalt will be presented.

Zegers et al. (1996) suggested that the Warrawoona Group was deposited during a phase of continental extension based on interpretation of syn-depositional extensional brittle faults in the Duffer Formation in the Coongan Greenstone Belt (Figure 4.1). They related these structures to ductile detachment shears observed at deeper levels in the stratigraphy and within batholiths, in an architecture similar to modern extensional core complexes. Although similar observations have been made in the North Pole Dome and Marble Bar Belt by Nijman et al. (1998), the role of extension has been questioned by White and Hickman (public discussion at 4IAS, Perth, 2001).

Van Haafden and White (1998) reported a major east-directed thrusting event during which they suggest Taiga Taiga Anticline was formed by thrust stacking, and therefore suggested that the

Figure 4.3 Map (this study) of the North Star Basalt the Taiga Taiga area.



The North Star Basalt

area is not suitable as a type section for the Taiga Taiga subgroup. However, van Kranendonk et al (2001) commented that there is no evidence for large displacement on the structures found by Van Haafden and White (1998), and they suggest that the Taiga Taiga Anticline was formed by diapiric activity of the Mount Edgar Granitoid Complex (as did Hickman, 1984; Collins, 1989).

4.3 Lithology

4.3.1 The extrusive stratigraphy

The Taiga Taiga area was mapped at a scale of 1:5000 with the aid of aerial photographs and Landsat imagery. A detailed map is shown in Figure 4.3 and the stratigraphic column is given in Figure 4.4. The basal unit of the North Star Basalt is the Lower Ultramafic Unit. The lower part of the unit consists of fine-grained massive mafic rocks, doleritic and gabbroic patches. Several lenses of up to 100 m long and 10 m thick occur on small hills: these lenses have a pyroxenite texture but their mineralogy consists mainly of actinolite, chlorite, epidote, serpentine and carbonates. The main lithologies of this unit are fine grained massive mafic rocks, composed of 30% chlorite, 20% magnesio-carbonates, 10% plagioclase and accessory titanite and opaques. The top of the unit is formed by a ca 30-50 m thick talc-carbonate-serpentine schist with a greenish-white appearance, which dips ca 20 degrees to the northwest, as shown in the map and cross section in Figure 4.3. Locally altered olivine spinifex textures up to 30 cm long are preserved (Figure 4.5), indicating that those rocks are not strongly deformed. These rocks are composed of chlorite, dolomite, magnesite, serpentine and opaque. On the basis of geochemistry (section 4.4) and texture, this unit is interpreted to be a komatiite.

The Main Basalt (Figure 4.4) forms the dominant lithology of the North Star Basalt. The sequence contains massive flows and pillows. Individual flows are up to several meters thick. The pillows and flows contain amygdales that consist of a quartz rim and chlorite center. The rocks contain mainly actinolite, albite, chlorite and minor quartz. The basaltic lavas have low vesicle contents, however, primary igneous textures are still preserved. In the pillows the vesicles form a radiating pattern, in flows they are locally elongated. The concentration of vesicles is greater in the top of flow and pillows, than in the bottom. This was used to establish that the Main Basalt has a consistent younging direction to the northwest. The unit dips 15-25 degrees to the northwest, as shown in the map and cross section in Figure 4.3.

The Thin Chert overlies the Main Basalt. It is a 5-10 m thick banded chert that dips 25-35 degrees to the northwest. This is slightly steeper than the bedding below, but parallel to the bedding above. The lower contact is obscured by schistose and strongly weathered rocks. The chert consists of very finely laminated quartz and opaques. It could possibly be a silicified slate horizon. This chert is overlain by the Middle Ultramafic Unit. The lower part of this unit consists of massive ultramafic rocks. The upper part of this unit is a carbonate-serpentine schist.

The Middle Ultramafic Unit (Figure 4.4) is overlain by a Clastic Sedimentary Unit with variable thickness and composition. The Clastic Sediments display two distinct sub-units. A fine grained lower sub-unit consists of dark colored, very finely laminated slaty material. This sub-unit forms a marker bed throughout the area, and is about 10 m thick. The upper sub-unit consists of a very coarse matrix-supported breccia. Locally the breccia coarsens upward, but in most outcrops the size of the clasts varies randomly. The breccia contains a wide variety of clasts. Chert clasts are angular to subrounded, mostly elongated, and 1-30 cm in length. Basaltic clasts are typically rounded and 1 to 15 cm in size. The matrix of the breccia is silicified. A weak foliation sub-parallel to the

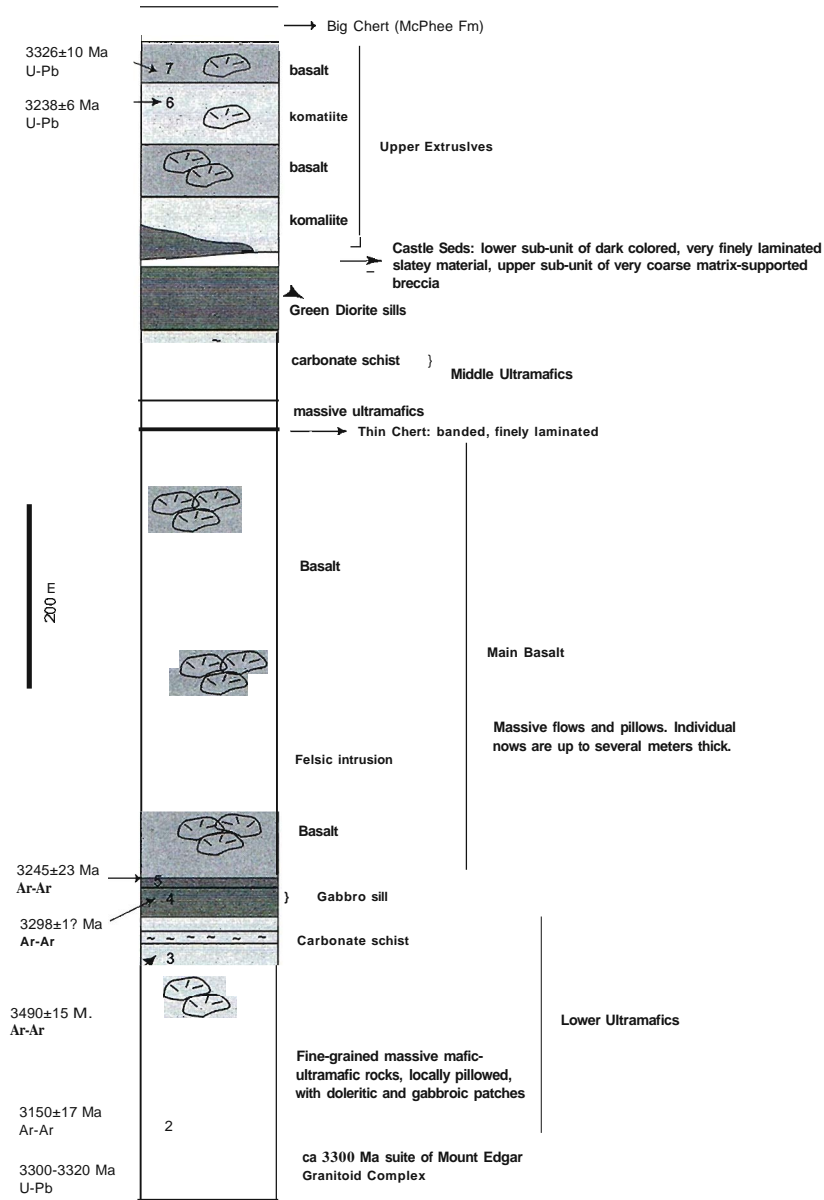


Figure 4.4. Stratigraphic column (this study) of the North Star Basalt, showing published geochronological data. 1: (Collins, 1993; Williams et al., 1983), 2, 3, 4 and 5: (this study), 6 and 7: (McNaughton et al., 1993).

bedding is defined by a preferred orientation of the clasts. Locally the upper sub-unit reaches a maximum thickness of 60 meters, while in other localities it is absent.

The top of the North Star Basalt is formed by the Upper Extrusive Unit (Figure 4.4), which contains alternating massive flows and vesicular pillow basalt. The rocks are locally altered to serpentine-carbonate schist, while in other places they are relatively unaltered basalt. Altered and unaltered packages alternate in this unit. A 20 m thick banded chert, the Big Chert, unit caps the formation. Like the Thin Chert halfway in the stratigraphy, the Big Chert overlies foliated and weathered rocks and dips at a slightly steeper angle than the bedding below. It forms the base of the overlying McPhee Formation (Figure 4.4).

4.3.2 SiUs

Low in the stratigraphy, between the Lower Ultramafics and the Main Basalt, a gabbroic sill has been emplaced (Figure 4.4). This sill is internally differentiated: it has a melanogabbroic main body now consisting of mainly actinolite, plagioclase, epidote and relics of pyroxene, and a leucogabbroic top which is richer in plagioclase and contains magmatic hornblende which has been dated (section 4.6). Green Diorite Sills have intruded the contact of the Middle Ultramafic Unit and the Clastic Sedimentary Unit. The diorite locally crosscuts the clastic sediments, and diorite sills up to 20 m thick occur above the Clastic Sedimentary Unit (Figure 4.4). A felsic unit was emplaced at a small angle in the Main Basalt, and its system of feeder dykes have intruded the Lower Ultramafic Unit

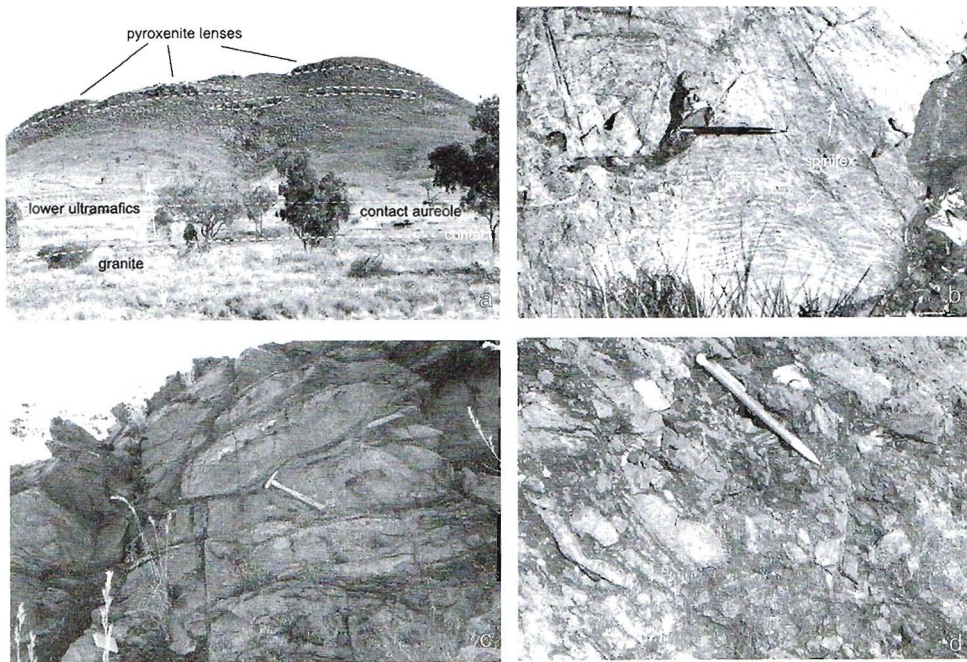


Figure 4.5 Field photographs of the North Star Basalt in the Taiga area a) Hill in the lower part of the stratigraphy: altered pyroxenite lenses of the Lower Ultramafic Unit are visible on the hillside. b) Spiral texture in the serpentine-carbonate schist in the Lower Ultramafic Unit c) Pillow basalts at the Main Basalt. d) Coarse breccia in the Clastic Sedimentary Unit.

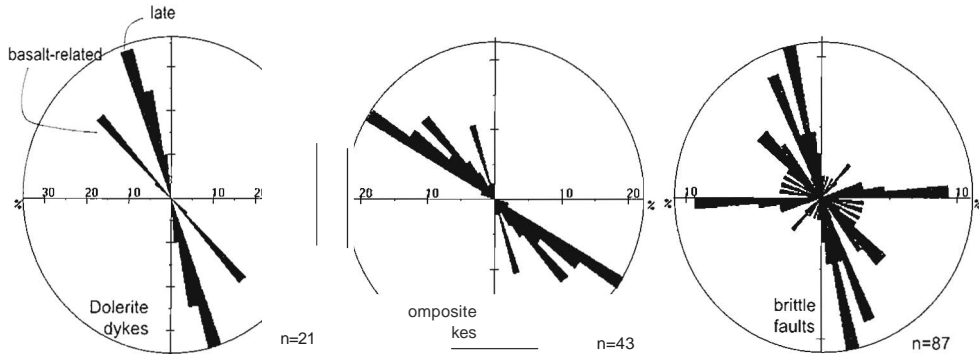


Figure 4.6. a, b. The orientation of dykes in the North Star Basalt plotted in frequency-azimuth Rose-Diagrams. c. Rose Diagram of the orientation of late brittle faults in the main basalt and lower lithramajics.

and the Gabbro (see Figure 4.3). The felsic unit is the youngest intrusion in this area. It is related to the ca 3300-3320 Ma granite suite of the Mount Edgar Granitoid Complex which forms the lower contact of the North Star Basalt (McNaughton et al., 1993).

4.3.3 Dykes

The North Star Basalt is crosscut by several suites of mafic dykes. Some of the dykes form composite systems of mafic and ultramafic dykes, whereas others form separate sets of only dolerite dykes. All dykes are sub-vertical; their orientations are shown in Figure 4.6a and b. It is shown that the separate dolerite dykes form two sets, with a main trend of 340 and a minor trend at 320. The minor set are small and thin (up to 50 cm) and occur at a right angle to the basaltic bedding. They are interpreted to be the local feeders of the basalt, because some of the dykes have been observed to be connected to flows. The other set of dolerite dykes is younger. The composite dyke suite also forms separate sets. The trend of the main set is 300. In Figure 4.3 it can be observed that the composite dykes cut not only the volcanic stratigraphy but also the later diorite sills. None of the dyke suites cut the granite or the felsic sill, so they all pre-date ca 3320 Ma (McNaughton et al., 1993). Importantly the dykes in the North Star basalt form several distinct suites that formed at different times in the geological history.

4.3.4 Metamorphism

Some of the alteration of the rocks may have occurred at an early stage in the history of the North Star Basalt. Yardley (1989) suggested that hydration and alteration are characteristic of basalts that have experienced sea floor alteration at low greenschist facies conditions. However, the greenschist facies metamorphism has been recorded throughout the area (Hickman, 1983). This thermal event may also be related to the regional emplacement of large granitic bodies. Zegers et al. (1996) suggested that this kind of metamorphism in greenstones could be the effect of the emplacement of mid-crustal rocks against the greenstones along a detachment fault in a setting similar to modern metamorphic core complexes. They associated the observed metamorphic event with a phase of continental extension at ca. 3.46 Ga.

The mineral assemblages of the metamorphic, formerly mafic and ultramafic rocks (epidote, chlorite, carbonate, serpentine) indicate greenschist grade metamorphism (Miyashiro, 1994). There is no variation in the metamorphic grade throughout the study area, except towards the contact with the granite. This indicates no significant gaps or duplications of the metamorphic field gradient and consequently no significant tectonic disturbance of the section post-dating the metamorphic event.

The contact of the North Star Basalt with the Mount Edgar Granitoid Complex (see map in Figure 4.3) is mostly exposed, however, the general dip of the contact could not be determined, due to the irregular intrusive nature of the contact. It is interpreted to be quite steep, based on the limited extent of the contact aureole. The structural effect of the intrusion is intense fracturing of the lower 10 meters of the mafics, allowing granitic melt and fluids to penetrate and silicify this bottom part of the section intensely. This effect drops off further away from the contact. The contact aureole shows a steep gradient from hornfelsing very close to the contact, to very limited overprinting about 500 meters away from the contact.

Contact metamorphism also occurred adjacent to the Green Diorite sills in the top of the stratigraphy. Thin section studies have shown that a greenschist metamorphic assemblage of albite, actinolite and epidote is overprinted by chlorite and calcite due to the heat and fluid flux associated with the intrusion. This contact metamorphic aureole reaches up to 30 meters into the host rock.

4.3.5 Lithology - discussion

A summary stratigraphic column is shown in Figure 4.4. The Lower Ultramafics were formed by extrusion in water, as indicated by the presence of pillows. Komatiites (now carbonate schists) were extruded, or emplaced as a shallow sill. This was followed by the deposition of the Main Basalt, accompanied by the formation of its own feeder dykes in the lower and central part of the exposed basalt sequence. During a period of quiescence, the Thin Chert was deposited on a low angle unconformity. This chert is now deformed and foliated and is interpreted to represent silicified and ferruginized slate. The quiet period is followed by the extrusion of an alternation of ultramafic and mafic lavas forming the Upper Extrusives. The North Star Basalt is capped by a chert unit of the overlying McPhee Formation, following a second phase of quiescence and subsidence accompanied by syn-depositional faulting (at a high angle to the bedding) resulting in a low-angle unconformity at the top of the formation (see map in Figure 4.3.). This chert is now deformed and foliated and is interpreted to represent silicified and ferruginized slate. The gabbro sill low in the stratigraphy was emplaced early in the history, the diorite sills and the felsics were emplaced later as indicated by crosscutting relationships with the dykes (see map in Figure 4.3.)

Three dyke suites were recognized. The first are a set of minor and thin dolerite dykes in the lower and central part of the stratigraphy, that appear to be associated with the Main Basalt as local feeders. This is confirmed by their geochemistry (section 4.4). The second are a suite of composite (mafic-ultramafic) dykes which have a northwest trend. They are up to 10 meters wide and can be traced through all structures in the North Star Basalt and into overlying formations, but not into the Mt Edgar Granitoid Complex. A clearly later and separate set of dolerite dykes has a northwest trend. They are up to 1 meter wide and have been observed to cut the older two sets and all older structures, but cannot be traced into the Mount Edgar Granitoid Complex. They are approximately orthogonal to the extensional direction in the upper plate at ca 3300 Ma, when the Mount Edgar Marginal Shear was under extension (Kloppenburg et al., 2001). That is, they are the result of a phase of continental extension rather than extension associated with a mid-ocean ridge. They can therefore not all be part of an ophiolite complex.

4.4 Geochemistry

4.4.1 Analytical methods

Fifty-four representative samples were selected for geochemical analysis. All mafic lithologies in the North Star Basalt are represented and the least weathered samples were selected. The samples were located away from faults and fractures. Any secondary quartz and carbonate veins were removed before grinding. XRF analyses were performed on pressed powder pellets for the VK-samples, on fused glass discs for the JW-numbered samples. The XRF analyses were carried out at the Free University of Amsterdam, on a Philips PWI404110 spectrometer. ICP-MS trace element analyses were performed at ACTLAB in Ontario, Canada.

4.4.2 Results

Sample locations and petrographic descriptions can be found in Appendix 4.A.1. All samples show evidence for low greenschist grade metamorphism, however, in most rocks the original igneous textures can still be observed. Rocks containing amphiboles, albite, epidote, chlorite and quartz are interpreted to be metamorphosed mafic rocks.

The major element data (Appendix 4.A.2) are given in weight %, recalculated to a total dry sum of 100% and with total Fe represented as Fe_2O_3 . The uncorrected total sum for all major element analyses deviated no more than 2% from 100%. The trace element data can be found in Appendix 4.A.3. To check the reliability and reproducibility of the analyses, in-house and internationally certified standards (BAS I, BHVO-2) were measured as well as sample duplicates. Analytical errors are reported with the data.

4.4.3 Interpretation of geochemical data

4.4.3.1 Introduction

Alteration and metamorphism will have affected the geochemistry of the analyzed rocks. Of the major elements only Al, Ti, Mn and P can be regarded as immobile. Therefore, classification of the rocks on the basis of major elements is problematic. The LILE elements (Rb, Ba, K, Th, U, Sr) are expected to be most affected by alteration. The other trace elements (HFSE and REE) are expected to have remained immobile (Rollinson, 1993). Certain trace element ratios can be used to check for the degree of alteration. Sr and Ba are less mobile than Rb, which is extremely mobile. Alteration commonly results in anomalously high Ba/Rb ratios and low Rb/Sr ratios. In general Ba/Rb ratios >15 and Rb/Sr ratios <0.03 are an indication of severe alteration (Hofmann and White, 1983). In Figure 4.7 these ratios are normalized and plotted; it can be observed that some of the samples show signs of loss of mobile elements. The LOI values also give an indication of the degree of alteration, as especially in ultramafic rocks the unstable mineral assemblages may have been altered to hydrous minerals. Early hydration under greenschist conditions appears to have been important. Metamorphic processes have changed the mineral assemblages but this does not necessarily imply that the bulk rock chemistry has changed. The recognition of primary igneous textures in the field and in thin section, and primary igneous trends in terms of Al_2O_3 and TiO_2 versus MgO (Figure 4.8) is an indication of isochemical changes.

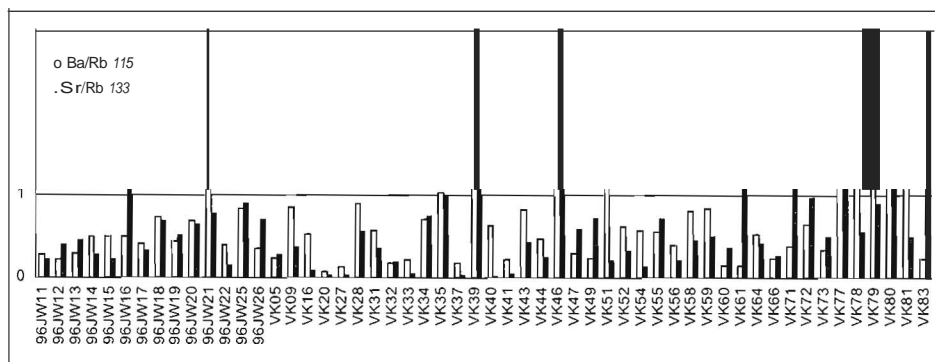


Figure 4.7. *Ba/Rb* ratios >15 and *Rb/Sr* ratios <0.03 are an indication of the degree of alteration (Hofmann and White, 1983). Values > 1 indicate moderate to severe alteration.

In order to interpret the geochemical data, the following approach was taken. The samples have been ordered into groups, based on the field lithology as shown in the stratigraphic column (Figure 4.4). On the basis of REE patterns some of these groups have been re-combined (Figure 4.10). Primitive mantle-normalized trace element patterns are shown (Figure 4.11), and MORB-normalized spidergrams of incompatible elements are used to determine the similarities and differences between the basaltic samples, and E-type and N-MORB rocks (Figure 4.12). Furthermore, selected trace elements are used to place further constraints on the tectonic regime and associated petrological processes (Figure 4.9, Figure 4.13).

The AFM major element diagram (Figure 4.9) is used to distinguish between tholeiitic and komatiitic rocks (Irvine and Baragar, 1971). Two representative major element variation diagrams, of Al_2O_3 and TiO_2 versus MgO , are used to investigate fractionation trends in the basaltic series (Figure 4.8). The minor element oxides TiO_2 , MnO and P_2O_5 can also be used to subdivide basalts. These elements are regarded immobile in hydrothermal alteration and metamorphism up to lower amphibolite facies (Mullen, 1983). In addition, the trace elements La, Y and Nb can be used to discriminate between different types of basalt (Cabanis and Lecolle, 1989). Altered and metamorphic rocks may show some distortion relative to the La apex, because La is not fully immobile under greenschist metamorphic conditions.

It should be noted that the discrimination fields in the presented diagrams are based on modern tectonic regimes. Their use for Archaean studies may be limited, because the Archaean crust and mantle were probably different in their chemical and thermal properties. Firstly, the samples have experienced alteration and metamorphism, although it is shown that this is limited. Furthermore, tectonic and crustal processes may have been different in the Archaean. The geochemical signature of a rock records the physical-chemical condition of the source region, i.e. the composition of the source and the temperature, depth and degree of melting at which the melt was formed, and possibly contamination that occurred during magma migration. A similar geochemical signature does not necessarily imply a similar tectonic regime as is the modern case.

4.4.3.2 Basal/

All basaltic samples plot in the tholeiitic field on the AFM diagram (Figure 4.9.3). Their spread relative to the A apex may be caused by mobility of the alkali components. In terms of their Mn-Ti-P variation, the basalts they plot in the arc tholeiitic field (Figure 4.9.b), whereas the Y-La-Nb

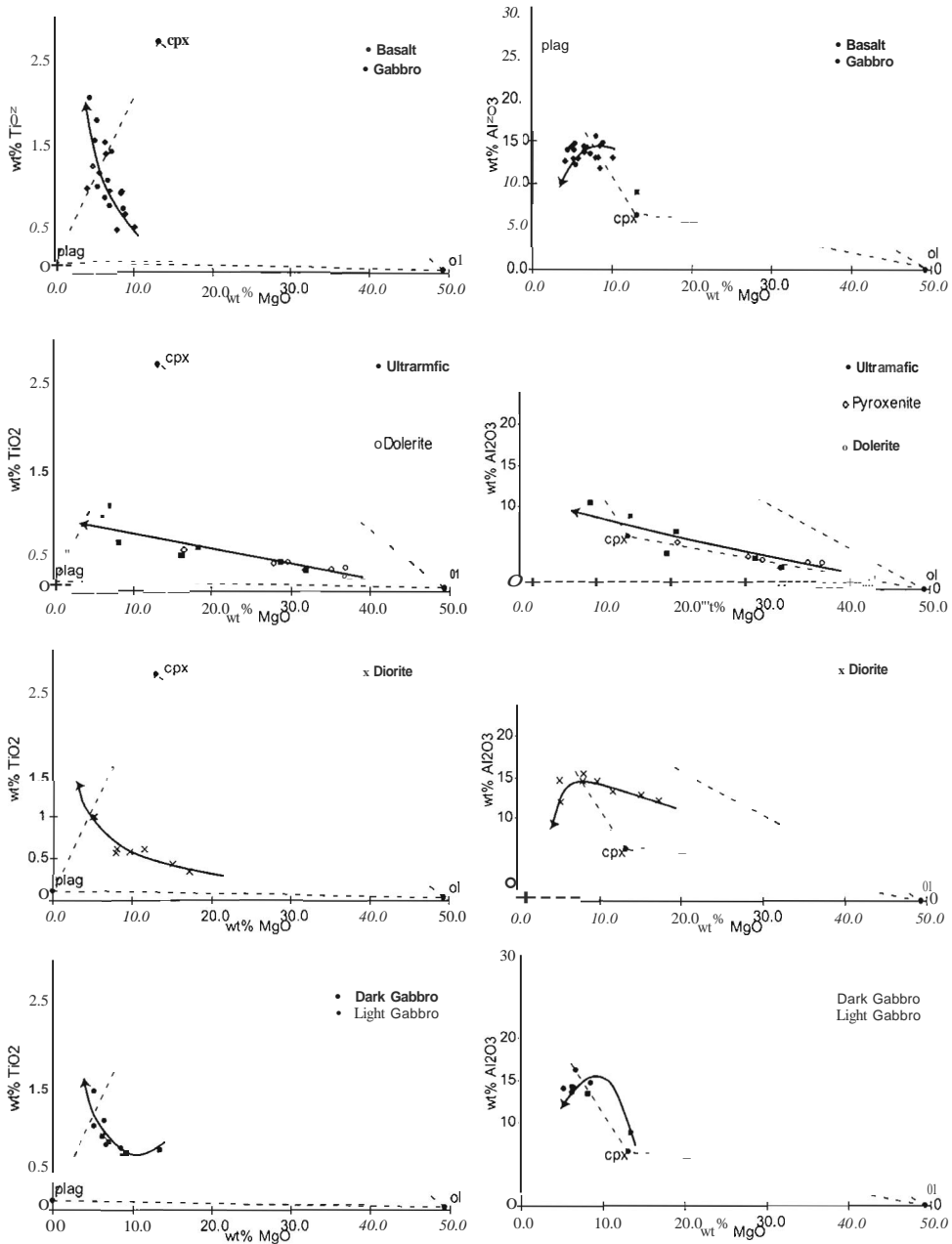


Figure 4.8. Major element variation diagrams for different lithologies. Left: Al₂O₃ vs MgO, right: TiO₂ vs MgO. The compositions of olivine, clinopyroxene and plagioclase, and fractionation trends are indicated.

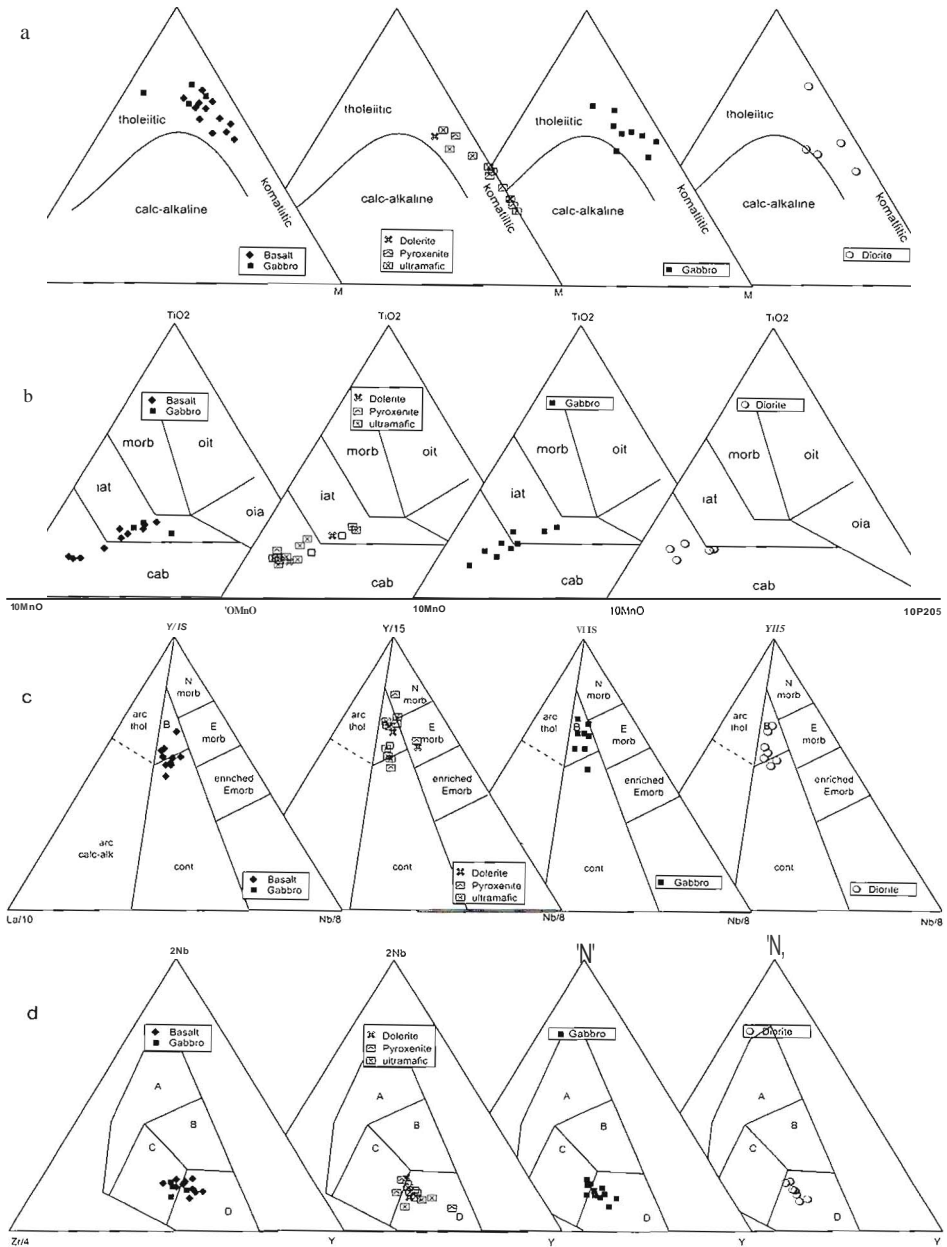


Figure 4.9. Triplots. a) AFM diagram (Irvine and Baragm; 197/). b) MnO-TiO₂-P₂O₅ diagram: cab = calc-alkaline basalt. oia = alkaline basalt. oit = oceanic island tholeiitic basalt, morb = mid ocean ridge basalt, iat = island arc tholeiitic (Mullen, 1983). c) La₁₀-Y₁₅-Nb₈ diagram. B = back arc basalt (Cabanis and Lecolle, 1989) d) Zr₄-2Nb-Y diagram. A = Intraplate alkali basalts, B = plume and E-type MORB, C = Intraplate tholeiites, D = normal MORB. Volcanic arc basalts plot in areas C and D.

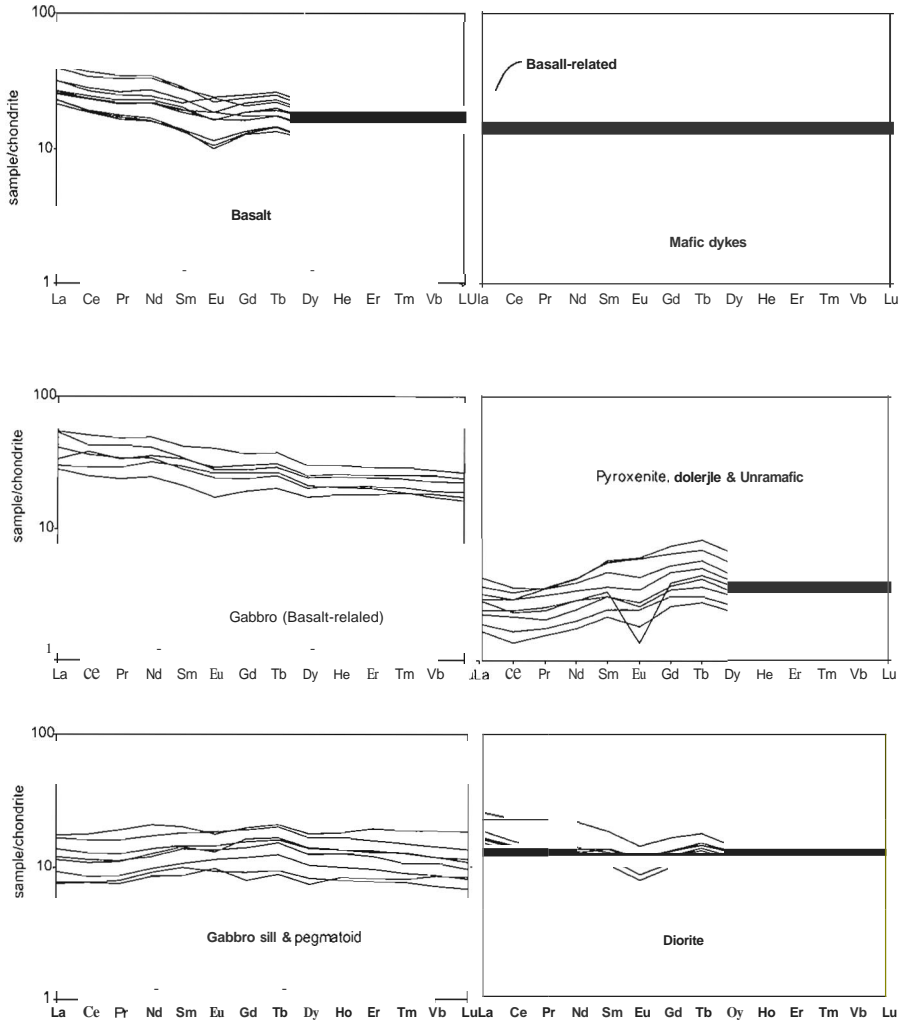


Figure 4.10. Chondrite normalized REE patterns for all lithologies. Normalizing values from McDonough and Sun (1995).

composition points to the continental to back-arc field (Figure 4.9.c). The Y-Nb-Zr compositions plot in the MORB and intraplate-tholeiite fields (Figure 4.9.d). An evolution of minor olivine followed by mainly plagioclase fractionation can be recognized in the major element variation diagrams (Figure 4.8). The Ni content of these rocks is relatively high for basalts (70 ppm).

All basalts, irrespective of their stratigraphic position, are slightly LREE enriched and show a Eu and Sr anomaly confirming plagioclase fractionation (Figure 4.10). The primitive mantle normalized pattern (Figure 4.11) is relatively flat, but overall enriched. The N-MORB normalized trace element pattern shows a slope, however, the E-MORB is flat around a value of 1 (Figure 4.12). The messy appearance on the left side of these diagrams is caused by the mobility of these LILE elements, however, there may in fact be some real enrichment in fluid

Chapter 4

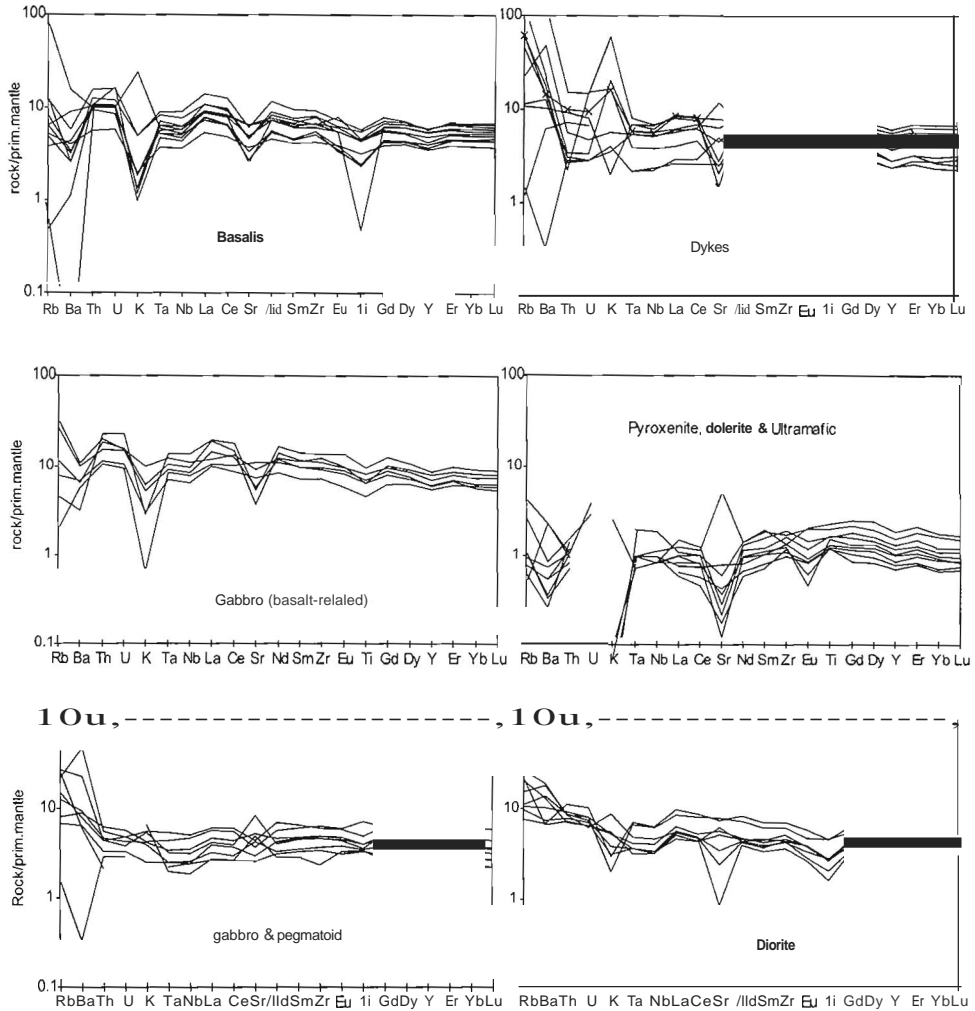


Figure 4.1 Primitive mantle normalized trace element patterns/lithologies. Normalizing values from McDonough and Sun (1995). The variable Sr anomalies are interpreted to be caused by the mobility of Sr in carbonate alteration during greenschist metamorphism.

mobile elements. The trace element geochemistry of these basalts of the North Star Basalt shows resemblance to modern E-MORB, however, there are distinct negative Ta, Nb and Ti anomalies. This points to crustal contamination. This is also shown in Figure 4.12.a, where the basalts are plotted against a background of the values found by Green et al. (2000), who suggested continental crustal contamination for the upper Warrawoona Group. In Figure 4.12.b the data are plotted against continental flood basalts, showing a difference in enrichment.

4.4.3.3 Ultramafics

On the basis of similar REE patterns (Figure 4.10), the pyroxenite, dolerite and ultramafics are grouped into one suite. The Lower Ultramafic Unit is peridotitic-komatiitic: it has a MgO contents between 15% and 35% and all samples plot in the komatiitic field on the AFM diagram (Figure 4.9.a). These extremely high MgO contents are characteristic of olivine and pyroxene cumulates. The series shows an evolution of olivine crystallization, followed by minor pyroxene and plagioclase at the end of the fractionation process (Figure 4.8). Small negative Sr and Eu anomalies confirm minor plagioclase fractionation. In the field pyroxene cumulate lenses have been observed (Figure 4.5.a). In Figure 4.9.b (Mn-Ti-P) the samples plot in the arc tholeiitic field, in Figure 4.9.c (Y-La-Nb) in the continental to back-arc field, and in Figure 4.9.d (Y-Nb-Zr) in the MORB and intraplate-tholeiitic fields. Their scatter largely overlaps with that of the basalts, suggesting a common source.

The ultramafic suite does not have the negative Nb, La and Ti anomalies observed in the primitive mantle normalized spidergrams of the basalts (Figure 4.11). The Upper Extrusive unit contains an ultramafic series that has slightly lower MgO contents, but shows a similar evolution. The Upper Extrusive Ultramafics and the ultramafic dykes have slightly higher trace element concentrations than the lower units. All ultramafic rocks have extremely high Ni and Cr contents. The overall concentration of trace elements is low, indicating that the melts were extracted from their source by a high degree of partial melting (Figure 4.11).

4.4.3.4 Gabbro

The gabbroic suite can be divided in two groups based on the chondrite normalized REE patterns. One group has LREE enrichment, the other group has a flat to slightly LREE depleted pattern and is overall less enriched (Figure 4.10). The smaller patches of gabbro identified in the field, show more LREE enrichment than the larger gabbroic bodies. The LREE enriched group is interpreted to be genetically related to the main basaltic stratigraphy (sub-volcanic sills). The second group is interpreted to represent a separate suite of intrusions.

These separate gabbros show large variation in their major element compositions, but they all fall within the tholeiitic field (Figure 4.9.a). The other triplots again suggest a common source, but they do confirm that the separate gabbro is overall less enriched than the basalt. In Figure 4.8 a fractionation pattern of olivine and pyroxene followed by plagioclase fractionation can be recognized. The primitive mantle normalized trace element pattern for the separate suite of gabbro does not show the negative Nb and Ti anomalies recognized in the gabbro that is similar to the basalt (Figure 4.11).

4.4.3.5 Diorite

The dioritic rock suite is represented by the diorite sills and their feeder dykes. They show a large amount of variation in their MgO values, but the trends are interpreted to be of magmatic origin. They plot as a range of tholeiites in Figure 4.9.a. The early magma evolution is dominated by olivine fractionation, later followed by plagioclase fractionation (Figure 4.8). This is confirmed by their slight negative Eu and Sr anomalies. The primitive mantle normalized trace element pattern shows even more strongly developed negative Nb and Ti anomalies than those recognized in the basalt (Figure 4.11).

4.4.3.6 Dykes

The ultramafic parts of the composite dykes have been included in the ultramafic suite. In the mafic dykes, two groups can be recognized on the basis of the chondrite-normalized REE pattern (Figure 4.10). The first group is identical to the basaltic rocks in the area, and is interpreted to be genetically

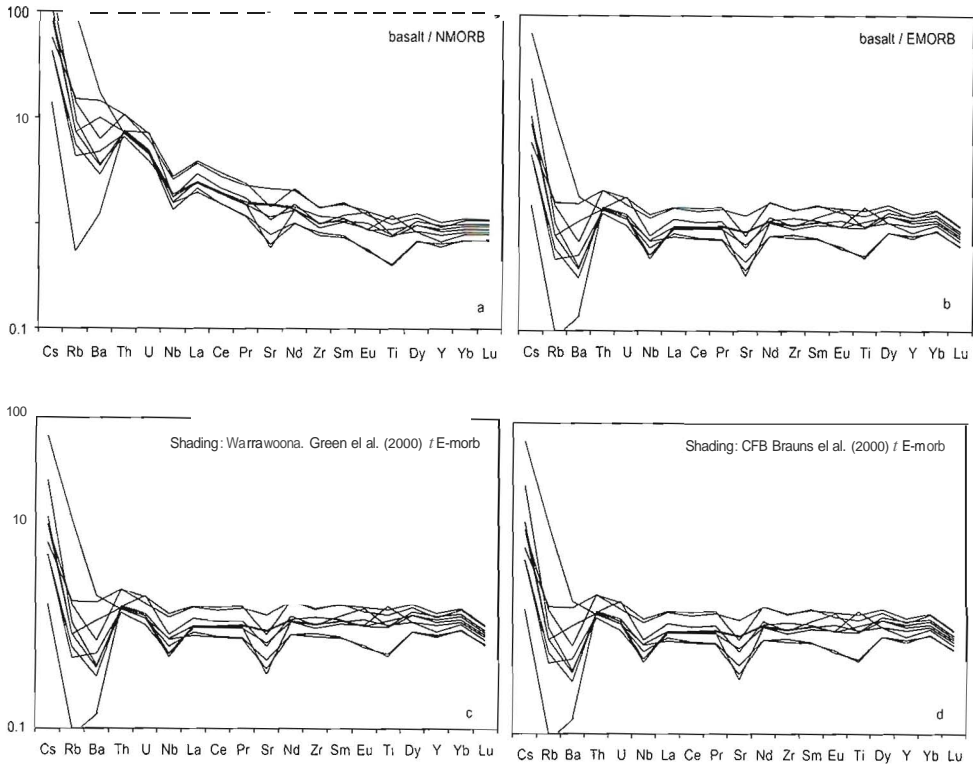


Figure 4.12. a) N-MORB normalized incompatible element diagram of the basalt samples. b) E-MORB normalized incompatible element diagram of the basalt samples. c) E-MORB normalized incompatible element diagram for the basalt samples. Shaded area indicates the data for the Upper Warrawoona Gabbro from Green et al. (2000). d) E-MORB normalized incompatible element diagram of the basalt samples, shaded area indicates the range of continental flood basalts (eFB). Data from Brauns et al. (2000). Normalizing values from (Sun and McDonough, 1989).

related. This is confirmed by the field relations (section 4.3.3). The second group is different in its flatter pattern and slight LREE depletion, and lack of negative Nb and Ti anomalies (Figure 4.11). It is similar to the Gabbro Sill and interpreted to be genetically related to that gabbro.

4.4.4 Discussion of geochemical data

The basalts and related dolerite feeder dykes and gabbro sills of the North Star Basalt are typical Archaean tholeiites. They are slightly LREE enriched with a weak negative Eu anomaly. The negative La, Nb and Ti anomalies reflect that the magmas have been enriched by a crustal component (Thompson et al., 1984). This is also illustrated with incompatible element ratios (Figure 4.13.b and c). This suggests that the magmas were either derived from a subduction-related enriched mantle source, or that the crustal component was added by assimilation during passage of the magma through continental crust. Our results are very similar to the data published by Green et al. (2000) for the Coonterunah and upper Warrawoona Groups in the Pilgangoora Belt, as illustrated in Figure

4.12.c. They showed by REE modeling that assimilation is a good explanation for the observed geochemistry, confirming what Barley (1986) has also suggested. In addition, they found granitic xenoliths. Therefore it may be concluded that the North Star Basalt was erupted onto a chemically evolved silicic basement. However, the Main Basalt is less enriched than modern continental flood basalts (Figure 4.12.d).

The Lower Ultramafics including the pyroxenite are distinct in their geochemistry, especially the very high Mg contents. Differentiation trends are characteristic of olivine fractionation. Low incompatible trace element concentrations and LREE depletion (Figure 4.10) indicate a large degree of partial melting of a source already depleted by removal of clinopyroxene. High Ni and Cr contents also indicate these rocks formed by a large degree of partial melting (Figure 4.13.a).

The Lower Ultramafics are interpreted to have a different magma source than the main basalts in the stratigraphy. The ultramafics were differentiated at greater depth as indicated by the absence of Eu and Sr anomalies indicative of plagioclase fractionation. Their difference from the basalts is confirmed by incompatible trace element ratios (Figure 4.13). The Lower Ultramafics have no negative Nb and Ti anomalies, so they somehow did not assimilate much crustal material during magma migration. They can be classified as Barberton-type (low-AI) komatiites (Nesbitt and Sun, 1976; Amdt and Brooks, 1980). We suggest that the Lower Ultramafics are not related to the Main

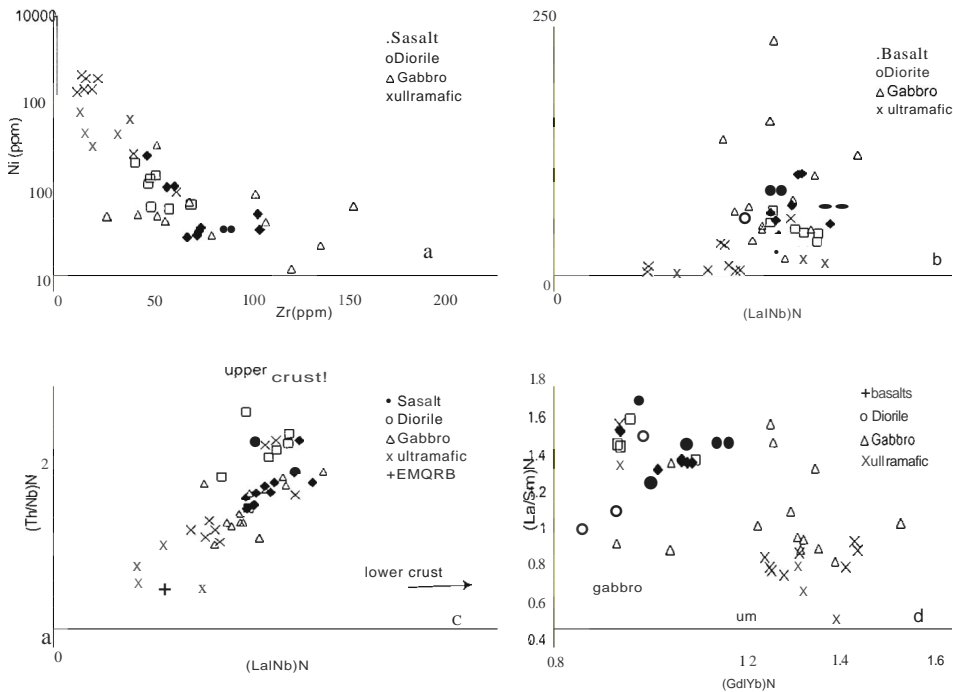


Figure 4.13. Incompatible element ratios plotted/or the different lithologies. a) logarithmic scale for Ni. The differences between the different lithologies are evident. b) The primitive mantle normalized (McDonough and Sun, 1995) La/Nb ratio is an indication of the negative Nb anomaly: addition of crustal material leads to increased values. c) The primitive mantle normalized (McDonough and Sun, 1995) Th/Nb and La/Nb ratios give an indication of addition of crustal material: this leads to increased values. E-MORB is plotted for reference. The different trends of the lithologies indicate different sources. d) Chondrite normalized (Sun and McDonough, 1989) La/Sm and Gd/Yb ratios. The different trends of the lithologies indicate different sources.

Basalt, and therefore they may not be part of the North Star Basalt *sensu stricto*. Unfortunately, Green et al. (2000) could not distinguish between the Coonterunah and Warrawoona Basalts on the basis of major or trace elements, and therefore we cannot determine whether the Lower Ultramafics belong to the Coonterunah or Warrawoona Group.

The gabbroic sills and later north-northwest trending dykes with flat REE patterns, and the dioritic intrusions, are interpreted to be genetically unrelated to the extrusive stratigraphy. They show much stronger characteristics of crustal contamination, which again can be explained either by a subduction-enriched source or crustal assimilation. In the incompatible element plots (Figure 4.13.c and d) they plot distinctly separate from each other, and from the basalt and the ultramafics. Therefore it is thought that they come from different sources.

4.5 Structural geology

4.5.1 Introduction

On a regional scale, the lower Marble Bar Belt is folded in the Taiga Taiga Anticline, as can be seen on the Landsat image (Figure 4.2). Away from the core of the anticline, the limbs are increasingly destroyed by intrusions of the Mount Edgar Granitoid Complex (see map in Figure 4.3). Generally, the greenstones on the western side of the mount Edgar Granitoid Complex dip radially away from the granite. In the area studied the average dip of the bedding is between 20 and 35 degrees to the northwest. The dips steepen towards the northwest.

4.5.2 Shears

The North Star Basalt contains two bedding-parallel zones of foliated rock consisting of serpentine-carbonate schist. The foliation within the schist has a variable orientation. The average strike of the foliation is same as the strike of the bedding, but the foliation dips more steeply than the bedding, at 45-65°. From this it may be concluded that the schistose zones are in fact shear zones in which case there may have been west-block-up thrust movement along them (in the present orientation). However, the local preservation of primary igneous (spinel) textures (Figure 4.5) indicates that the amount of strain in these zones may not be very large. The fact that the S-foliation within the high strain zones still occurs at an angle to the shear plane, is also an indication that the amount of strain is low.

Thin Chert and the Big Chert dip 10-20° steeper than the bedding of the underlying rocks. This disconformity may be caused by vertical movement and reorientation of the extrusive pile before deposition of the cherts. This vertical movement could either be related to magmatism, e.g. effects of cooling of the extrusive pile or the underlying magma chamber, or it is caused by regional scale deformation of the basement during or just after formation of the North Star Basalt. This can not be resolved at the scale of this study.

Just below the both chert units, the underlying basalts are foliated. The geometry of the foliation in the field indicates normal movement occurred along the cherts: the foliation curves from subhorizontal, i.e. with a normal sense, into the cherts. The relative timing of movement within the carbonate schists and the chert units cannot be resolved, because the structures have no cross cutting relations.

The composite dyke systems are sheared. The foliation at the edges of the dykes indicates that they are sinistral strike slip shears: together they form an array with the vertical main shears

striking ca 310 and vertical minor shears striking ca 340 (Figure 4.6). Kinks folds in the foliation at the sides of the dykes indicate dextral overprinting.

4.5.3 Folds

The Thin Chert contains meso-scale cylindrical, open folds with a wavelength of about 2m. Their fold axes plunge to the northwest. In two locations a different type of folding was found within the Thin Chert: these folds have horizontal fold axes parallel to the strike of the bedding. They are asymmetrical; when looking towards the southwest they are Z-shaped. This may indicate normal movement occurred along the chert, as was also concluded from the foliation described above.

In the Clastic Sedimentary Unit a variety of folds can be observed: in many locations the finely laminated sub-unit is folded at cm-, dm-, and m-scale: the folds are open to tight. The fold closures occur in all directions, some are dismembered, and locally the layers are weakly boudinaged. These folds are interpreted to be slump folds.

Minor folds in the ultramafic part of the composite dyke systems are closed, cylindrical and symmetric, they locally have a box shape. Their fold axes are sub-vertical. The asymmetry of these folds as well as the offset of lithological units show that these structures have a large dextral offset. This dextral phase overprints the sinistral movement, and is interpreted to have occurred at the same time as the development of the dextral faults.

4.5.4 Brittle faults

In the lower massive ultramafics and in the main basalt two sets of small vertical faults were observed. The faults are 1-20 cm wide. Some are filled with quartz, which very occasionally shows slickensides plunging 40° to the northwest. The largest faults of this type are traceable for no more than 100-200m. The orientation of faults is shown in Figure 4.6.c. Within these faults different elements of the brittle Riedel Array can be recognized; most faults strike due west and show a dextral sense of shear. The set striking northwest show a sinistral sense of shear. These sets form a conjugate system, and the lineations indicate the NW block was brought up relative to the southeast. The amount of displacement on these structures could not be determined as they occur only in homogeneous parts of the stratigraphy.

A number of subvertical northwest trending faults were observed in the Upper Extensive Unit (see map in Figure 4.3). These structures have a dextral strike-slip component. Some of them do not displace the Big Chert and must therefore be synvolcanic, formed before formation of the Big Chert (McPhee Formation). A second set of large faults occurs in the top of the stratigraphy: they do displace the Big Chert by 1-20m. As they are located in small valleys the outcrop of the actual faults could not be observed. The absolute sense of shear could not be determined, but the relative displacement of the Big Chert in the present orientation indicates that there was a dextral strike slip component. Some of these faults coincide with composite dykes, but there are also a number of faults that are separate.

The margins of the mafic dykes show evidence for both the dextral as well as sinistral movement. This indicates that this set of mafic dykes as well as the ultramafic dykes both predate the initial sinistral movement on the shear zones. The late set of dolerite dykes is undeformed, indicating it postdates the last deformation. However, its emplacement is interpreted to be related to regional northeast-southwest extension (Kloppenborg et al., 2001), forcing them in this orientation and creating the stepped outcrop pattern.

4.5.5 Discussion of structures

The relative timing of structures is constrained by field relations. The first structures that developed were northwest trending vertical faults in the Upper Extrusives, that do not cut the Big Chert. They can either be interpreted as synvolcanic faults or as normal faults related to regional extension.

The relative timing of the next two events (east-west extension and east-west compression) has not been determined because there are no cross-cutting relations. An east-west extensional event led to deformation along the chert units. The foliation in the rocks adjacent to the cherts is interpreted to be associated with these structures and indicates normal movement. Small scale folds in the clastic sedimentary unit indicate normal movement occurred on planes approximately parallel to the bedding. It is interpreted that movement in the cherts and the clastic sediments occurred during the same event. This east-west extensional event is possibly related to an early phase of extension at about 3.46 Ga as proposed by Zegers et al. (1996), but the extent of this event has been questioned by White and Hickman. The increase of the dip of the stratigraphy across the chert units is interpreted to be a primary feature: the cherts are thought to be deposited on low angle unconformities. This is also shown on the map (Figure 4.3).

Two ductile layer-parallel shears were observed in the komatiitic units, now carbonate schists. The foliation is steeper than the bedding and is interpreted as an S-fabric, indicating reverse movement occurred on the shears. This is interpreted to be related to a regional east-west compressional event that occurred between 3460 and 3350 Ma (Van Haaften and White, 1998). The thrusts are bedding-parallel and have not been observed to cross-cut the stratigraphy. Because primary igneous features such as spinifex textures can locally be recognized in the schist, and the foliation occurs at an angle to the shear plane, the amount of displacement was probably minor.

After these events, shears were initiated in the composite dykes, first with a sinistral shear sense; then the principal stresses shifted resulting in shear reversal on the sheared composite dyke system. The last tectonic event resulted in the formation of a conjugate set of small brittle faults due to northwest-southeast directed compression.

4.6 $^{40}\text{Ar}/^{39}\text{Ar}$ Geochronology

Sample descriptions are summarized in Table 4.2. The mineral separation and 4°ArP9Ar step heating experiments were carried out at the isotope laboratory of the Vrije Universiteit van Amsterdam. We followed the analytical methods developed by Wijbrans et al. (1995).

Age spectra of the samples are shown in Figure 4.14. A hornblende-pyroxene lens in the Lower Ultramafics has an $^{40}\text{Ar}/^{39}\text{Ar}$ cooling age of 3472 ± 21 Ma, which falls within the generally accepted age of the Warrawoona Group (Table 4.1). The Gabbro Sill low in the stratigraphy has cooling ages of 3290 ± 18 Ma and 3272 ± 21 Ma. This may record slow cooling of the ca 3300 Ma granitoids nearby (McNaughton et al., 1993; Nelson, 2000). Alternatively this may correspond to tectonothermal events recorded elsewhere in the Pilbara Craton, in the Sulphur Springs and Roebourne Groups (Van Kranendonk et al., 2002). Another sample from the Lower Ultramafics has a strongly disturbed age spectrum with a semiplateau at 3127 ± 77 Ma. This does not appear to be related to any known intrusions in the area, however, it is a widespread $4\text{Ar}/^{39}\text{Ar}$ resetting age throughout the Pilbara Craton (see Figure 8.2).

Table 4.2. Sample description and location of the $^{40}\text{Ar}/^{39}\text{Ar}$ geochronology samples. For position in the stratigraphy see figure 4.4.

sample	East	North	rock type	mineral	Age (Ma) $\pm 2\sigma$	% ^{39}Ar	MSWD	total fusion (Ma) $\pm 2\sigma$
96JW011	0796570	7673290	komatiite (LU)	hornblende	3127	77	73.43	3.59
96JW017	0796306	7673430	gabbro sill	hornblende	3290	28	82.8	0.80
96JW019b	0795985	7673686	gabbro sill	hornblende	3260	39	100	74.64
96JW022	0795935	7673414	pyroxenite (LU)	hornblende	3472	21	98.91	1.93

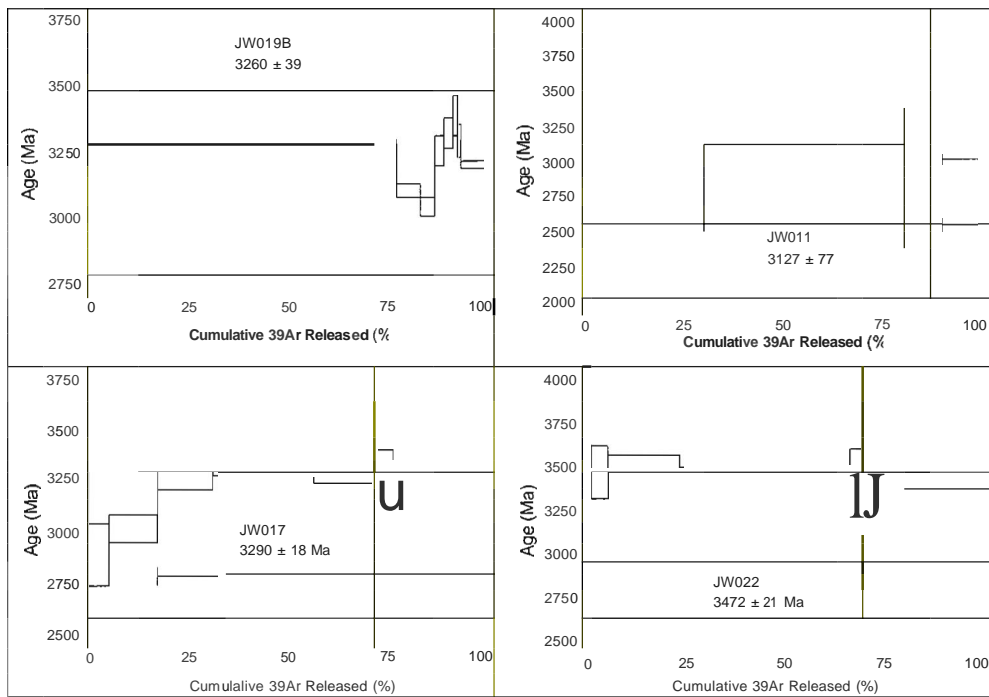


Figure 4.14. $^{40}\text{Ar}/^{39}\text{Ar}$ step heating spectra.

4.7 Tectonic synthesis

The origin of Archaean granitoid-greenstone terrains has been discussed in the context of a wide variety of modern analogues such as continental rifts, continental margins, oceanic island-arcs, submarine plateaus, hot spot type oceanic settings and mid ocean ridges (Kroner and Layer, 1992; Condie, 1994; De Wit and Ashwal, 1997). One of the aims of this study was to investigate a possible ophiolitic origin of the North Star Basalt. Modern ophiolites are an association of allochthonous rocks that, while typically found on continents, are interpreted to represent oceanic crust and upper mantle. A complete ophiolite sequence as defined by the Geological Society of America is several kilometers thick. It is an allochthonous complex consisting of peridotite tectonite, cumulate gabbro, a mafic sheeted dyke complex and a mafic volcanic complex (Anonymous, 1972).

Processes of oceanic crust formation in Archaean times may have differed from those at modern oceanic spreading centers (De Wit et al., 1992; Vlaar et al., 1994) and consequently oceanic crust may have had a different composition and stratigraphy (Bickle et al., 1994). Considering that Archaean oceanic crust is thought to be substantially thicker than present-day oceanic crust (Bickle et al., 1994), the thickness of the North Star Basalt of ca 1 kilometer is not great enough to contain a complete ophiolite. The absence of a peridotite tectonite sequence may be explained by the fact that the lower contact of the North Star Basalt is the intrusive contact with the Mount Edgar Granitoid Complex. Geochemistry has shown that most of the gabbro in the area is genetically unrelated to the Main Basalt sequence, but are later mafic intrusions. Finally, even though in the North Star Basalt a large number of mafic and ultramafic dykes is present, this does not represent a sheeted dyke complex. Field relations and geochemistry have shown that very few of them are genetically related to the basaltic sequence and they only account for a small percentage of the total volume of rock. The dykes were formed as a result of distinct tectonic events: they are not the product of a single phase of extension at a mid ocean ridge. Even though the North Star Basalt does not resemble a modern ophiolite, the rocks did form in an under water environment as recorded by the presence of pillowed basalts.

The major and trace element geochemistry of the extrusive pile and related dykes and sills resembles that of EMORB. The higher degree of partial melting in the Archaean mantle, in combination with a higher fertility, may have resulted in a higher Fe and REE content than in modern MORB (Ohta et al., 1996). However, the LREE enrichment and negative Nb and Ti anomaly indicate some involvement of more evolved rocks. This suggests that the magmas were either derived from a subduction-related enriched mantle source, or that the crustal component was added by assimilation during passage of the magma through continental crust. Green et al. (2000) came to similar conclusions for the Coonterunah and Upper Warrawoona Groups in the Pilgangoora Belt. They showed by REE modeling that assimilation is a good explanation for the observed geochemistry, confirming what Barley (1986) has also suggested. Bickle et al. (1994) showed that demonstrably continental sequences contain successions resembling ocean floor, with mafic lavas and gabbroic, peridotitic and dunitic cumulates in intrusive bodies. It may be concluded that the North Star Basalt was erupted onto a chemically evolved silicic basement.

Trace element geochemistry suggests that the lower part of the stratigraphy (the Lower Ultramafics) may not be part of the North Star Basalt as presently defined. The stratigraphic position of the Lower Ultramafics below the Main Basalt of the North Star Basalt could lead to the suggestion that it may actually be part of the Coonterunah Group. However, Green et al. (2000) showed that the Upper Warrawoona and Coonterullah Groups are geochemically very similar. Therefore it is concluded that the Lower Ultramafics represent a distinct volcanic sequence. However, an $^{40}\text{Ar}/^{39}\text{Ar}$ cooling

Table 4.3. Summary of magmatic and tectonic events that affected the North Star Basalt.

Phase	Timing	Event
		Slow uplift and erosion
	ca 3300 Ma	intrusion of felsic sill and dykes. Emplacement of Mt Edgar Granitoid Complex destroying lower part of North Star Basalt. Regional emplacement of large granitic bodies, regional greenschist metamorphism.
05		NW-SE directed compression: Late conjugate set of brittle faults
04		NNW-SSE directed compression shear reversal in the composite dike systems
03		WSW-ENE directed compression Initiation of shears in the composite dike systems with sinistral shear sense
	ca 3434 Ma	Emplacement of northwest trending dolerite dykes Emplacement of ultramafic-mafic composite dykes Intrusion of diorite sill along clastic sed Intrusion of gabbro low in the stratigraphy
02		E-W directed compression, reverse movement in carbonate schists
01	ca 3450 Ma	E-W directed extension, normal movement along cherts Quiescence and deposition of big chert (Mc Phee Fm) Extrusion of basalt and komatiites of upper extrusives + feeder dykes Deposition of clastic sediments Extrusion and shallow sills of middle ultramafics Quiescence and deposition of thin chert Extrusion of Main Basalt and co-genetic dykes and sills
	ca 3500 Ma	Extrusion and shallow sills of Lower Ultramafics

age of about 3470 Ma suggests the lower ultramafics are age equivalent of the lower Warrawoona Group.

Structures in the North Star Basalt record five tectonic events (see Table 4.3) which can be dated by previously published geochronology. The oldest structures are vertical faults at a high angle to the bedding, They offset the extrusive pile which has an angular upper contact with the overlying chert of the McPhee Formation. The relative timing of the next two events is unclear. The formation of strike parallel normal faults adjacent to or in the chert units. These are possibly associated with a phase of continental extension (Zegers et al., 1996) involving regional greenschist grade metamorphism. This was followed by east-west directed compression that resulted in the activation of bedding parallel thrusts in komatiitic units, and the formation of the Taiga Taiga antiform (Van Haaften and White, 1998). However, this study has shown that displacement on these structures (within the North Star Basalt) was probably minor. After the compression, a set of northwest-trending composite dykes was emplaced, cross cutting older structures.

The next deformational event, which post-dates the emplacement of the composite dykes, was directed west-southwest east-northeast and initiated sinistral strike slip shears in the composite dykes. These sheared dykes were reactivated as dextral shears. The last event has created a conjugate set of minor brittle shears due to NW-SE directed compression, Finally, a set of north-northwest trending dolerite dykes was intruded. This possibly occurred during southwest-northeast extension at a time when the Mount Edgar Marginal Shear was under extension (Kloppenbng et al., 2001). Major granitic intrusions at 3.3 Ga (McNaughton et al., 1993) post-date emplacement of all of the dike suites, and have destroyed the lower section of the greenstone sequence.

4.8 Summary and Conclusions

The North Star Basalt comprises five different components based on lithological and geochemical characteristics. The lower part of the stratigraphy consists of LREE depleted Barberton-type komatiites and pyroxene cumulates. They are genetically not related to the overlying basalts, and it is not known whether they belong to the Coonterunah Group or the Warrawoona Group. The main basalt stratigraphy is LREE enriched with negative Nb and Ti anomalies. The basalts are interpreted to be contaminated tholeiites, enriched with continental crustal material during magma migration. This is similar to the findings of Green et al. (2000) for the Coonterunah and upper Warrawoona Group in the Pilgangoora Belt. Gabbro dykes and sills, and dioritic intrusions make up two minor components of the North Star Basalt, and they are interpreted to be genetically unrelated to the extrusive stratigraphy. Two chert units are interpreted to be silicified slaty sediments. Some displacement occurred along them.

Lithologically and geochemically the North Star Basalt does not resemble a modern ophiolite, however, the rocks were erupted in water as recorded by the pillowed basalts. The majority of the dykes in the area were emplaced during distinct regional events, few are genetically related to the basalt. The complex structural history of the area involved syn-depositional faulting, regional extensional and compressional events at ~3450 Ma and ~3300 Ma respectively. Therefore the Taiga Taiga Anticline may still be a suitable type area for the North Star Basalt, but the presence of low angle unconformities should not be disregarded. Early normal faults developed along these unconformities, however, the displacement on all structures in the area was probably minor.

Acknowledgements

The field research was funded by grant 1997/14 of the Dr. Schürmann Fund. Marije van Koolwijk participated in the mapping and carried out the geochemical analyses as part of her M.Sc. project in 1997. She is thanked for making her geochemical data available for this paper. I would like to thank Dr. Kim Hein for reviewing an early version of this manuscript.

Structural, geochronological and geochemical constraints on the tectonic evolution of the West and adjacent Central Pilbara Craton, Western Australia

Abstract

The early to mid-Archaean granite-greenstone terrain of the Pilbara Craton in Western Australia consists of a number of domains separated by major transcurrent shear zones. The Sholl Shear Zone is one of those major structures and it has been reported to be the boundary of an accreted terrane, based mainly on significant differences in the geochemistry and age of the bordering domains.

In this paper a combined structural, geochronological and geochemical study of the West Pilbara, the Sholl Shear Zone, and the adjacent Central Pilbara is reported. The oldest components of the West Pilbara are possibly arc-related volcanic and intrusive rocks of ca 3265 Ma, overlain by an over-thrust oceanic unit of unknown age. The West Pilbara was affected by north-directed thrusting associated with amphibolite-grade metamorphism at ca 3150 Ma. This might have been due to a collisional or subduction event.

The Whundo Group was then deposited at about 3120 Ma south of the Sholl Shear Zone, in a continental transtensional setting. One hundred million years later renewed transtension resulted in the formation of the Mallina Basin in the Central Pilbara. This involved sinistral transtension on subvertical crustal scale structures. The whole area was affected by a major compressional event after 2930 Ma and became a north-west verging fold and thrust belt. This might have been due to a collisional or subduction event.

5.1 Introduction

Tectonic settings of Archaean greenstone belts and granitoids have been discussed in the context of a wide variety of modern analogues such as continental rifts, continental margins, oceanic island-arc, submarine plateaux, hot spot type oceanic settings and mid ocean ridges (e.g. Kroner and Layer, 1992; Condie, 1994; De Wit and Ashwal, 1997). Recent tectonic models for the Pilbara Craton are based on the growing belief that the rock record in greenstone successions can be compared to that in modern tectonic settings (e.g. Barley, 1997; Kiyokawa and Taira, 1998; Smith et al.,

1998). These models place the Roebourne and Sholl-Whim Creek Domains (Figure 5.1) respectively in an island-arc and back arc setting, and are largely based on geochemical data. In addition, it has been proposed that the structural and deformation record preserved in the Pilbara Craton can be explained by horizontal tectonic processes (Blewett, 2002).

Domains separated by major transcurrent structures are typical features of cratons of all ages, and many of these boundary structures have a long history of reactivation. The kinematics of these structures in the Pilbara Craton may contain important clues to the Archaean tectonic history of the Earth. In this study, the thermo-tectonic evolution of the two domains adjacent to the Sholl Shear Zone is investigated, as well as this major shear zone itself. The aim is to place further constraints on the extent to which the observed crustal processes (rock-forming events and regional deformation and metamorphism) are related to plate tectonics. The results of field mapping, structural-kinematic analyses, geochemical analyses, $^{40}\text{Ar}/^{39}\text{Ar}$ and V-Pb zircon geochronology are presented here. A tectonic model for the evolution of the West Pilbara and adjacent Central Pilbara, is presented.

5.2 Regional Geology

5.2.1 Domains and domain boundaries

The mid-Archaean Pilbara Craton has a domainal structure, and it has been suggested that this geometry reflects a history of accretion (e.g. Krapez and Barley, 1987; Barley, 1997; Kiyokawa and Taira, 1998; Krapez and Eisenlohr, 1998; Smith et al., 1998; Blewett, 2002; Van Kranendonk et al., 2002). Hickman (1983) originally proposed a tabular stratigraphy for the greenstone successions in the Pilbara. However, as a result of the detailed mapping in the North Pilbara Mapping Accord of AGSO/Geoscience Australia and GSWA, and the recognition of the domain boundary structures, this interpretation has been revised (e.g. Hickman, 1999; Van Kranendonk et al., 2002). The greenstone successions of the different domains cannot or only partially be correlated across domain boundaries. A simplified compilation of the most recently published general stratigraphy of the Western part of the Pilbara greenstone stratigraphy is summarized in Table 5.1.

Table 5.1. Distribution of supracrustal sequences in the Western part of the Pilbara Craton. Adapted from Blewett (2002) and references therein,

Age (Ma)	Stratigraphy	Occurrence	Lithology
2760-2690	Fortescue Group	Pilbara-wide	Basalt, rhyolite, sandstone
2850	Granites and pegmatites	Central & East Pilbara	Granites and pegmatites
2925	Mafic-Ultramafic intrusions	West & Central Pilbara	Ultramafic layered intrusions and granite
2970-2940	De Grey Group (Mallina Fm) and a range of granites	Pilbara-wide (Central Pilbara)	Clastic basin fill and granites
2975	Bookingarra Group	Central Pilbara	Clastic sediments, basalt, rhyolite
3010	Whim Creek Group	Central Pilbara	Basalt, rhyolite, sandstone
3020	Cleaverville Fm	Pilbara-wide	Banded ironstone, shale, basalt, felsic volcano.
3120	Whundo Group	Central Pilbara	Calc-alk felsic and mafic volcanics
3260-3270	Roebourne Group	West Pilbara	Basalt, chert, volc seds & granodiorite

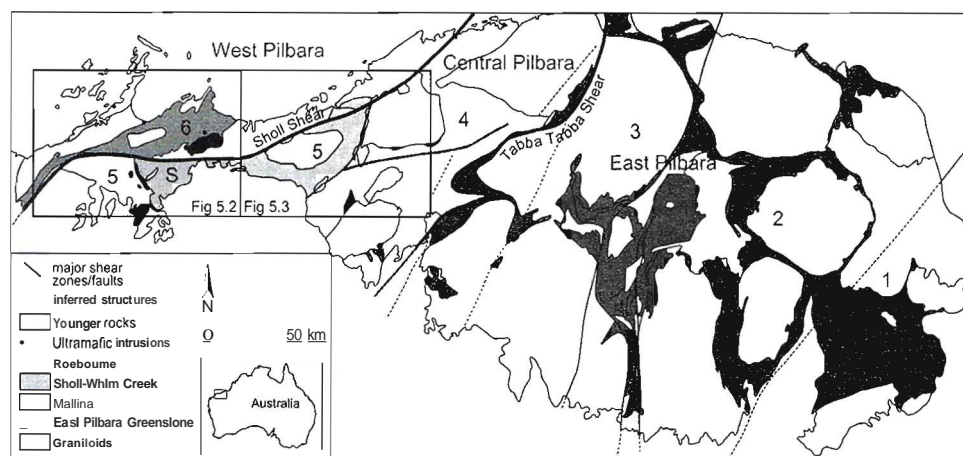


Figure 5.1. The Archaean Pilbara Craton in Western Australia. The study areas are indicated. The six domains of Krapez and Eisenlohr (1998) are also shown: 1 = Nulagine Domain, 2 = Marble Bar Domain, 3 = Pilgangoora Domain, 4 = Mallina Domain, 5 = Sholl-Whim Creek Domain, 6 = Roebourne Domain. Van Kranendonk et al. (2002) include the Sholl Belt (S) in the West Pilbara. Blewett (2002) regards the Sholl Shear Zone as the boundary between the West and Central Pilbara. The latter is used in this study.

The geographic names West, Central and East Pilbara, as shown in Figure 5.1, refer to the respective Superdomains and need some clarification. Van Kranendonk et al. (2002) use a division where they include the Sholl Belt as part of the West Pilbara. However, it has not been shown that there is a major structure separating the Sholl Belt from the Whim Creek Belt, which is in the Central Pilbara. In addition, the Whundo Group of the Sholl Belt unconformably underlies the Whim Creek Belt. Therefore, in this study, the Sholl Shear Zone will be regarded as the boundary between the West and Central Pilbara. Blewett (2002) also used this division. The Tappa Tappa Shear Zone forms the boundary between the East and Central Pilbara.

On aeromagnetic and gravity imagery the Sholl Shear Zone can be traced as a major, roughly east-west running structure for more than 150 kilometers through the northwestern Pilbara (Blewett et al., 2000). Previous workers (Barley, 1987; Krapez, 1993; Krapez and Eisenlohr, 1998; Smith et al., 1998; Hickman et al., 2000; Hickman et al., 2001; Van Kranendonk et al., 2002) have suggested that the Sholl Shear Zone experienced a major phase of sinistral shearing early in its history. A dextral event post-dating deposition of the Whim Creek Group, and with a displacement of approximately 40 kilometers, has been recognized (Smithies, 1997a; Hickman et al., 2001; Blewett, 2002; Van Kranendonk et al., 2002).

This paper is concerned with the West Pilbara and the western part of the Central Pilbara. The West Pilbara comprises the Roeboume Domain (domain 6 in Figure 5.1) and its lithological characteristics will be discussed in the next section. The Central Pilbara comprises the Sholl-Whim Creek Domain (domain 5 in Figure 5.1) and the Mallina Basin (domain 4 in Figure 5.1), which will

is not included in this study. The Sholl-Whim Creek Domain comprises the Sholl Belt, and the Whim Creek Belt. Their lithologies will be discussed in the next section.

5.2.2 Lithology

5.2.2.1 Roebourne Domain

The stratigraphy of the Roebourne Domain is given in the lower part of Table 5.2. All rocks are metamorphosed to at least greenschist facies metamorphic grade, but the prefix meta will be omitted from here on for convenience. Most of the lithological contacts in the domain are sheared, only the oldest and lowest two formations have a conformable contact. The oldest formation is the Ruth Well Formation, which comprises basalt, talc schist and chert. The formation has not been dated but it must be older than the overlying Nickol River Formation, which consists of clastic sediments, felsic volcanics and chert, and has a U-Pb zircon age of 3265 Ma (Nelson, 1998a). It must also be older than the Karratha Granodiorite (Figure 5.2) by which it is intruded (Blewett, 2002) and which has been dated at 3265 Ma (Nelson, 1998b; Smith et al., 1998).

The undated Regal Formation is separated from the underlying Ruth Well and Nickol River Formations by a tectonic contact, the Regal Shear Zone (Hickman et al., 2001). The Regal Formation consists of komatiites, basalt and minor chert, and is reported to have MORB affinities (Sun and Hickman, 1999). Ohta et al (1996b) suggested that chert and clastics associated with the basalts represent an accretionary complex generated by the scraping off the subducted oceanic crust. The Ruth Well, Nickol River and Regal Formations and the Karratha Granodiorite occur exclusively to the north of the Sholl Shear Zone.

The Cleaverville Formation has an age of 3020-3015 Ma (Nelson, 1998a) and consists of BIF, chert, volcanogenic sediments and minor felsic and mafic volcanics, all metamorphosed to lower greenschist facies. Detrital zircon populations in the Cleaverville Formation have ages similar to the ages of magmatic zircons found in the Nickol River Formation and Karratha Granitoid (ca 3265 Ma), indicating crust of this age must have been exposed at the time of deposition. Interestingly Nelson (1998a) found one detrital zircon with an age of 3461 ± 8 Ma, which is a common age of the Warrawoona Group in the East Pilbara. This may indicate that East Pilbara crust was close by and exposed at 3020 Ma, or it may be a contaminant in the sample. The minimum age of the Cleaverville Formation is constrained by a granitic intrusion with an age of 3014 ± 6 Ma (Nelson, 1997), and detrital zircons of 3014 ± 6 Ma (Nelson, 1998a). The Cleaverville Formation has a Sm-Nd T_{DM} Model age of 3110-3210 Ma (Sun and Hickman, 1998). In much of the West Pilbara the Regal Formation stratigraphically underlies the Cleaverville Formation, but their contact is purely tectonic.

The Karratha Granitoid has a SHRIMP U-Pb in zircon age of 3261 ± 4 Ma and the geochemistry of the tonalites to granodiorites indicates that it may have formed in an arc environment (Smith et al., 1998). Nd model ages of 3480-3420 Ma (Sun and Hickman, 1998) indicates that magma generation involved older crust. This is confirmed by the presence of old cores in zircons (Smith et al., 1998). A different suite intrudes the Ruth Well Supracrustal Unit and is geochemically identical to the Karratha Granitoid. It has a SHRIMP U-Pb in zircon age of 3265 ± 4 Ma (Smith et al., 1998), and is interpreted to be part of the same island arc setting as the Karratha Granitoid.

The Harding Granitoid comprises two generations of granitoid. The oldest suite of the Harding Granitoid consists of tonalitic plutons and is coeval with high-level felsic intrusions in the Ruth Well Supracrustal Unit. These tonalitic plutons occur in the eastern and southern parts of the Harding Granitoid-Gneiss Complex. They have SHRIMP U-Pb in zircon ages of 3014 ± 3 Ma (Nelson, 1997), 3024 ± 4 Ma and 3031 ± 6 Ma (Smith et al., 1998).

Table 5.2. Stratigraphy of the Roebourne Group in the Roebourne Domain, the Whundo Group in the Sholl Belt, Cleaverville Formation which occurs both north and south of the Sholl Shear Zone, and the Whim Creek and Bookingarra Groups in the Whim Creek Belt. Adapted from Hickman et al. (2001) and references therein.

Group	age (Ma)	Formation	Thickness (km)	Lithology
Bookingarra Group	ca 2975	Kialrah Rhyolite		rhyolite
		Negri + Loudon Volcanics	2	mainly mafic volcanics
	ca 2978	Cistern Fm + Rushall Slate		clastic sediments
Whim Creek Group	ca 3010	Mons Cupri Dacite	0.2	dacitic intrusions
	ca 3010	Red Hill Volcanics	0.3	andesite, rhyodacite, sandstone, breccia
		Warambie Basalt	0.2	basalt, minor seds
		Cleaverville Fm	1.5	chert, BIF, basalt and felsic volcanics
Whundo Group	3020-3015			
	ca 3115	Woodbrook Fm	1	basalt and felsic volcanics
	ca 3115	Bradley Basalt	>4	basalt, minor felsic volcanics
	ca 3120	Tozer Fm	2.5	basalt, rhyolite, sediments and chert
	ca 3125	Nallana Fm	2	basalt, minor ultramafics, pyroclastics
Roebourne Group	not known	Regal Fm	2	komatiites, basalt
	ca 3270-3250	Nickol River Fm	0.1-0.5	volcanogenic sediments, chert
	ca 3270	Ruth Well Fm	1-2	basalt, talc schist, chert

The Dampier Granitoid consists mainly of granite-granodiorite and an age of 2997 ± 3 Ma (Nelson, 1998a) has been obtained. The Balla Balla Granitoid (included in the Harding Granitoid by Hickman et al. (2001)) comprises a main phase of monzogranite and compositionally banded granodiorite (Hickman et al., 2001). It has been dated at 3014 ± 3 Ma (Nelson, 1997) and has a Nd model age of 3276 Ma (Sun and Hickman, 1998). Banded gneiss in the Sholl Shear Zone was dated at 2995 ± 2 Ma (Nelson, 1997) and gave a Nd model age of 3246 Ma (Hickman et al., 2001).

The Andover Complex (Figure 5.2) is a layered mafic-ultramafic intrusion, consisting of serpentized peridotite, gabbro and dolerite dykes (Hoatson and Sun, 2002). It intrudes the Harding Granitoid-Gneiss Complex as well as the Ruth Well Supracrustal Unit. An early phase of magmatism is indicated by the 3016 ± 4 Ma age obtained by Nelson (2001), but it is thought that the main portion of the complex correlates to the other mafic-ultramafic intrusions in the West Pilbara that have ages of about 2925 Ma (Hoatson and Sun, 2002).

5.2.2.2 Sholl-Whim Creek Domain - Sholl Belt

The stratigraphy of the Sholl-Whim Creek Domain is shown in Table 5.2. The Sholl Belt lies to the south of the Sholl Shear Zone. It comprises the four units of the Whundo Group, and the Cleaverville Formation, all metamorphosed to very low greenschist grade (Hickman et al., 2001). The ca 3125 Ma Nallana Formation consists mainly of basalt, minor ultramafics and intermediate pyroclastics. The overlying Tozer Formation consists of a range of basalt to rhyolite, and minor sediments and chert. The Bradley Basalt is a succession of massive and pillowed basalt with high-Mg basalt present near the base, and minor felsic tuffs near the top which were dated at 3115 ± 5 Ma (Nelson, 1996). The top of the Whundo Group is formed by basalt and rhyolite of the Woodbrook Formation, dated

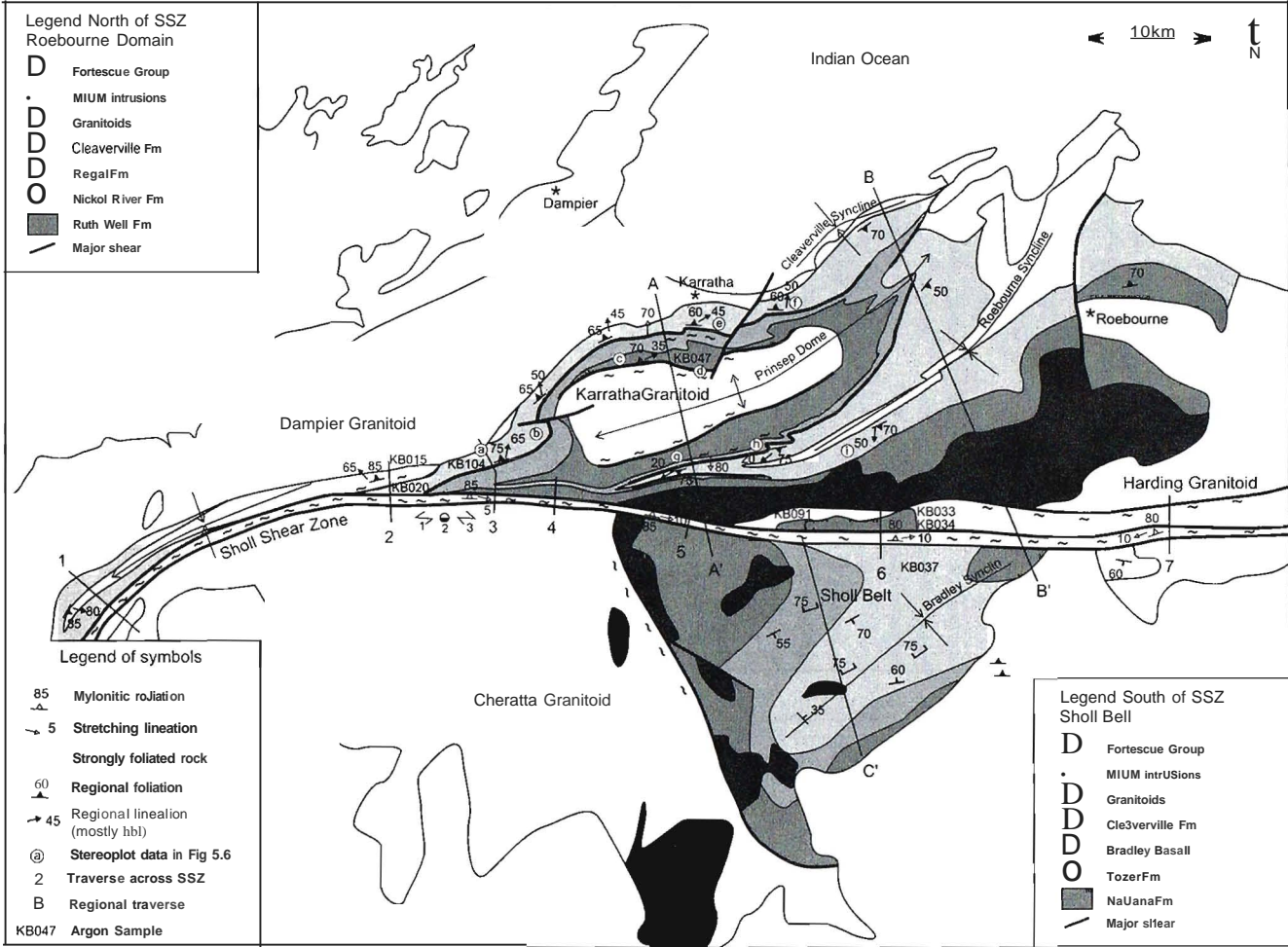


Figure 5.2. The Roebourne-Karratha area. Lithology based on Dampier and Roebourne 1:100,000 geological maps (Hickman, 1997; Hickman, 2000) Location indicated in Figure 5.1 Locations of traverses A, B and C are shown.

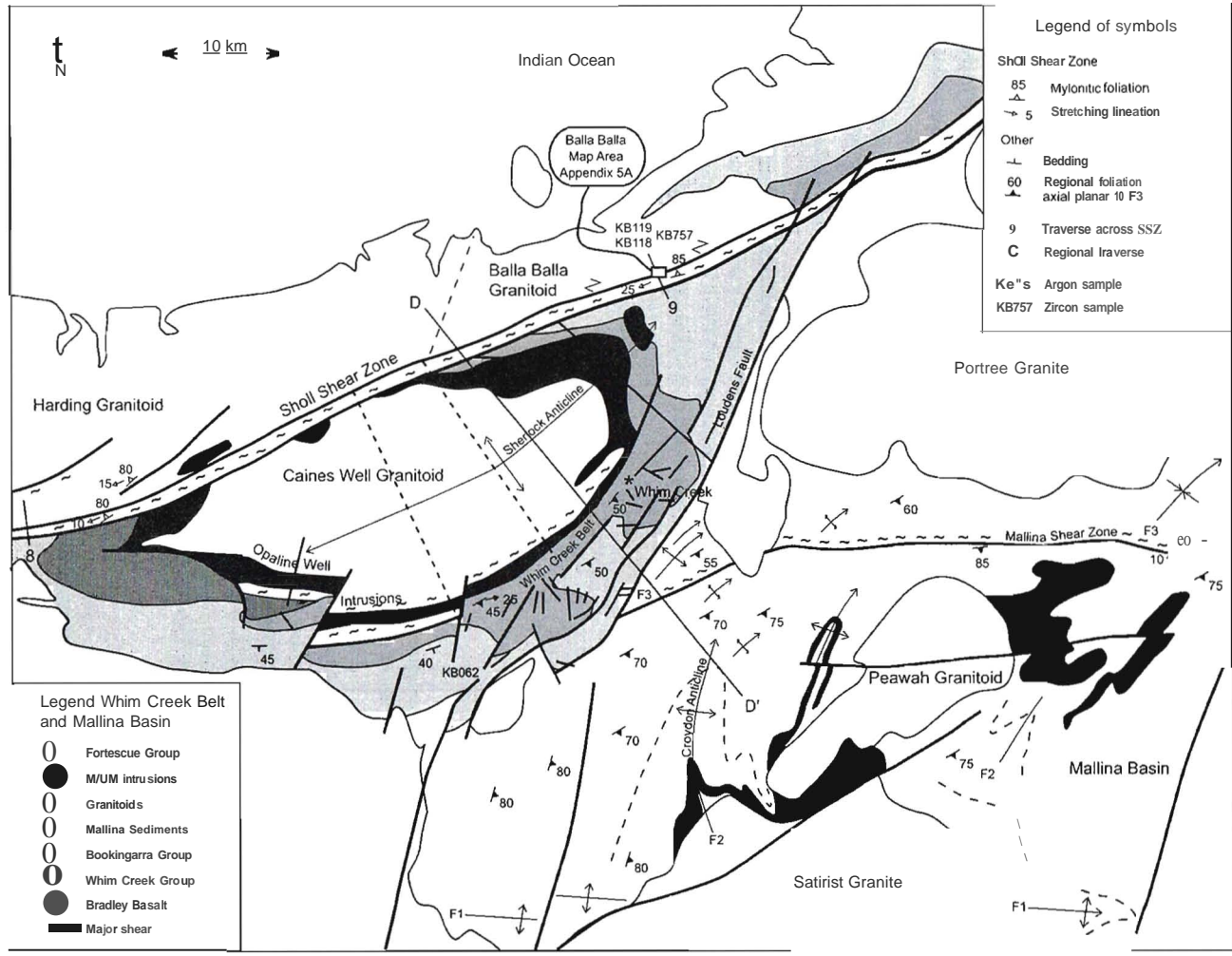


Figure 5.3. The Whim Creek area. Lithology based on Roebourne and Sherlock 1:100 000 geological maps (Hickman 2000; Smithies, 1997b). Location indicated in Figure 5.1.

at 3117 ± 3 Ma (Nelson, 1998a). These volcanic rocks were derived from juvenile crust, possibly in a back arc setting in a subduction zone environment (Smith et al., 1998; Sun and Hickman, 1998). The stratigraphic sequence, described in detail by Horwitz and Pidgeon (1993), was interpreted to be consistent with a back-arc rift environment (Krapez, 1993).

5.2.2.3 Sholl-Whim Creek Domain - Whim Creek Belt

The rocks of the Whim Creek Group unconformably overlie the Whundo Group. They are metamorphosed to low greenschist grade, and the stratigraphy is summarized in Table 5.2. The base of the Whim Creek Group is formed by the dominantly subaqueous Warambie Basalt, which is locally pillowed and is accompanied by minor sediments. The overlying Red Hill Volcanics are dominated by andesite and rhyodacite, dated at 3009 ± 4 Ma (Nelson, 1998a). These rocks are interpreted to represent subaqueous sedimentation of volcanoclastics, turbidity currents and debris flows (Pike et al., 2002). The Mons Cupri Dacite is a single voluminous unit of dacite emplaced as a high-level, syndepositional intrusion into the Red Hill Volcanics. There is no direct regional evidence for subduction associated with the basin development but Pike and Cas (2002) suggested that the early volcanics of the Whim Creek Group could be related to a continental arc, based on basalt geochemistry.

The second component of the Whim Creek Belt is the Bookingarra Group (Table 5.2). It comprises the sedimentary Cistern Formation and Rushall Slate with maximum depositional ages of 2978 ± 5 Ma (Nelson, 2000), and the predominantly extrusive Mount Negri and Loudon Volcanics, and Kialrah Rhyolite with an age of 2975 ± 4 Ma (Nelson, 1998a). Krapez et al. (1993) described four fining-up depositional cycles thought to reflect volcano-sedimentary cycles in a back-arc basin (Barley, 1987).

5.3 Structural Geology

5.3.1 Introduction

The structural-kinematic relationships of the Roebourne and Sholl-Whim Creek Domains were studied by field traverses, local mapping, and microstructural analysis of thin sections. Two main traverses were made across the Roebourne Domain. Traverse A was made across the Prinsep Dome and through the town of Karratha (Figure 5.2), Traverse B was made through the town of Roebourne (Figure 5.2). Several other locations were visited in the Roebourne Domain, and their structural data have been included in the figures and their interpretation. The Sholl Shear Zone, which separates the West from the Central Pilbara, was studied on several traverses. The Sholl Belt was studied on Traverse C and several other locations (Figure 5.2). The Whim Creek Belt was studied on Traverse D and spot checks (Figure 5.3). The results are reported below.

5.3.2 The Roebourne Domain

5.3.2.1 Traverse A part 1: south-north through north side of Prinsep Dome.

The northern margin of the Karratha Granitoid is formed by a sheared contact with mafic and felsic schists (map in Figure 5.2, cross section in Figure 5.4 and stereoplots of structural data in Figure 5.5.a-t). The schists have a north-dipping foliation, and generally north-plunging hornblende mineral lineations (Figure 5.5.d). Within the contact zone, sheets of granite occur parallel to the foliation. They are strongly foliated, and have stretching lineations parallel to the hornblende mineral lineation

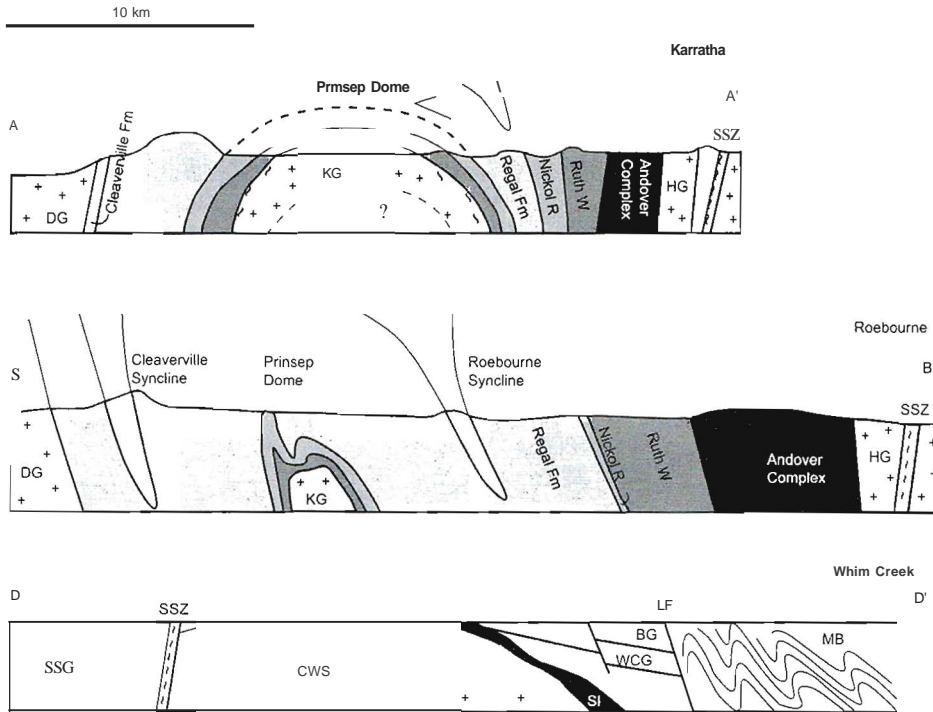


Figure 5.4. Sketch cross sections. A) Section through Karratha. B) Section through Roebourne. D) Section through Whim Creek. Locations indicated in Figure 5.2 (A and B) and Figure 5.3 (D). DG = Dampier Granitoid. KG = Karratha Granitoid: its structure at depth is interpreted to be a sheet-form, in order to facilitate folding of the Prinsep Dome. HG = Harding Granitoid. CWB = Caines Well Batholith. SI = Sherlock Intrusion, SSZ = Sholl Shear Zone. BBG = Balla Balla Granitoid. WCG = Whim Creek Group, BG = Bookjarra Group. LF = Loudens Fault. MB = Mallina Basin

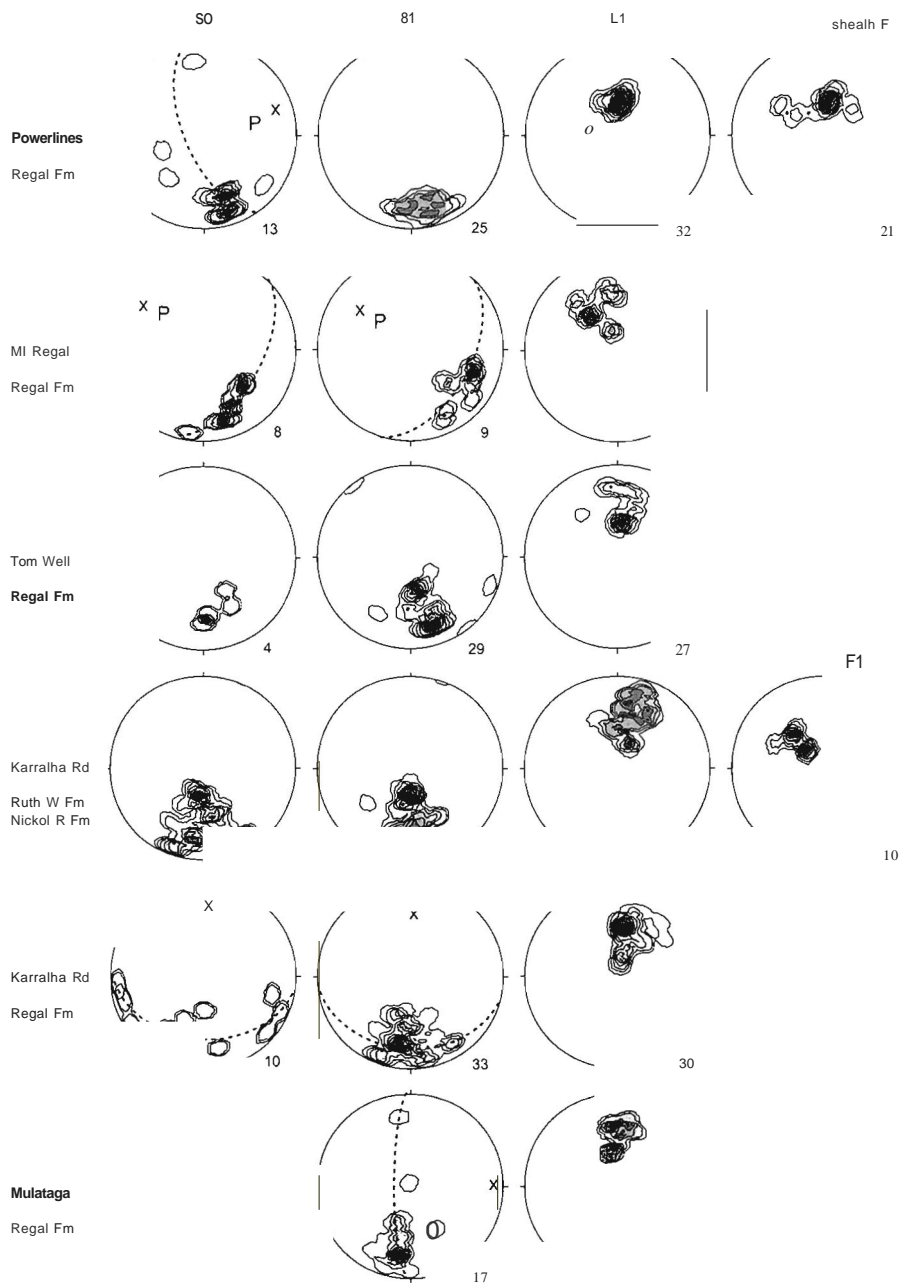
in the schist, i.e. northeast plunging (Figure 5.5.d) and dextral normal shear bands, and are therefore interpreted as shear zones. This amphibolite grade shear zone is cut by slightly more steeply north dipping shears, that have north-east plunging chlorite streak lineations and dextral normal shear bands. These steeper zones contain chlorite, indicating greenschist metamorphic grade. The similar kinematics are interpreted to indicate that the transition from amphibolite to greenschist occurred during deformation, and are consistent with having formed during exhumation.

There is no clear contact aureole surrounding the Karratha Granitoid. This may be due to the intense shearing, or overprinting by regional amphibolite grade and greenschist grade metamorphism. Alternatively, the contact with the schists is purely tectonic. However, Blewett (2002) reported intrusive contacts of the Karratha Granitoid with the Ruth Well Formation.

North of the contact, meter-scale asymmetrical folds with northwest plunging fold axes have been observed in the lower Ruth Well Formation on the north side of the Prinsep Dome (S-folds in figure 5.6.e). The orientation of the FI fold axes is shown in Figure 5.5.d. They are accompanied by a subhorizontal to moderately south-dipping axial planar cleavage. When the folds are rotated back to eliminate the fact that they occur on the northern limb of the Prinsep Dome

Chapter 5

Locations: north side of Prinsep Dome (Traverse A, part 1)



Locations: south side of Prinsep Dome (Traverse A, part 2)

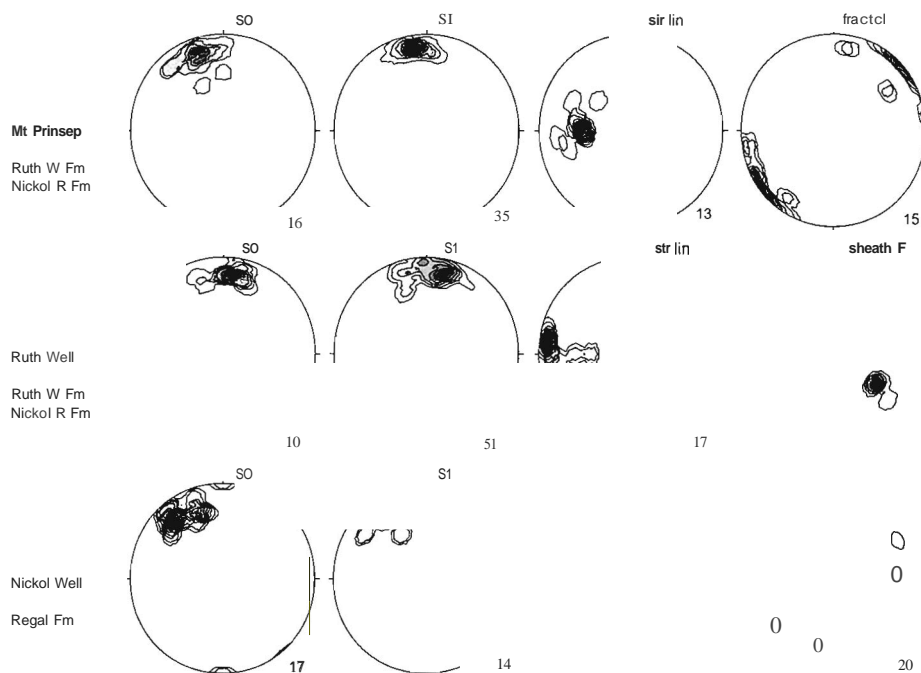


Figure 5.5. part I (previous page). Structural data of the Roebourne Domain, north side of the Prinsep Dome (Traverse A part I), represented in lower hemisphere equal area stereoplots (bin size of density contours adjusted to max 8 levels). Locations are indicated in Figure 5.2. SO = bedding. S1 = regional pervasive amphibolite grade foliation. LI = regional pervasive amphibolite grade lineation. Fract cl = pervasive fracture cleavage. sheath F = fold axes of intrafolial folds within bedding parallel shears. FI = north-verging first generation folds. 'x' indicates reconstructed (old axis: 'P' indicates the Prinsep Dome). Figure 5.5 part II (this page). Structural data of the Roebourne Domain, south side of the Prinsep Dome (Traverse A, part 2). SO = bedding. S1 = regional pervasive amphibolite grade foliation. str lin = stretching lineations in bedding parallel shears. Fract cl = pervasive fracture cleavage. Sheath F = fold axes of intrafolial folds within bedding parallel shears.

(Figure SA.A), they still have a north-verging asymmetry. This is interpreted to record an early north-verging compressional event.

All principal lithological contacts on the northern limb of the Prinsep Dome are tectonized as indicated by the foliated contacts. In chert in the upper Nickol River Formation isoclinal folds with steeply north-plunging axes have been observed, near the contact with the overlying Regal Formation. They are interpreted to be sheath folds and are parallel to steeply north-plunging quartz stretching lineations: the chert is interpreted to be a mylonite. The Regal Formation overlies the shear zone at the top of the Nickol River Formation. It consists of massive and pillowed basalt and thin gabbroic sills, all metamorphosed to amphibolite facies metamorphic grade. A pervasive hornblende

mineral lineation plunges to the northeast (Figure 5.5.e). The lineation plunges more steeply than the lineation close to the margin of the Karratha Granitoid (compare Figure 5.5.d and e).

In the far western limit of the exposed Roebourne Domain, the Cleaverville and Regal Units are exposed. Both units are folded to form a tight syncline on the northwestern side of the Sholl Shear Zone. It is interpreted to be the continuation of the Cleaverville Syncline (see Figure 5.2). The Regal Formation is of amphibolite metamorphic grade in this area, and contains subvertical hornblende mineral lineations (see Traverse I across Sholl Shear Zone).

5.3.2.2 *Traverse A part 2: north-south through south side of Prinsep Dome*

On the southern side of the Prinsep Dome, the Ruth Well and Nickol River Formations are cut by numerous bedding-parallel shears. Most of these structures are strongly altered and weathered, however, abundant sinistral shear bands and folds can still be observed (Figure 5.6.f). They are interpreted to be related to late stages of deformation as they refold a subhorizontal stretching lineation within the schist. The contact of the Nickol River Formation with the overlying Regal Formation is tectonized and silicified, and has subhorizontal plagioclase stretching lineations and hornblende mineral lineations (Figure 5.5.g, h).

In this area, the Regal Formation consists of upper amphibolite facies metamorphic mafic rocks, containing hornblende and plagioclase. Locally migmatitic textures, pegmatitic blobs and melanosomes occur. The pervasive hornblende lineation that occurs in the northern limb of the Prinsep Dome has not been recognized here. A shear zone, with moderately west plunging hornblende mineral lineations, forms the contact of the Regal Formation with the Nickol River Formation. In the top of the Nickol River Formation about 50m of metasediments occur, with em-sized garnets and minor K-feldspar growing at the expense of white mica and quartz, indicative of high amphibolite metamorphic grade in excess of 550°C (Yardley, 1989).

The top of this metasedimentary unit in the Nickol River Formation is formed by a band of lined chert, interpreted to be a silicified shear zone. Within this mylonitic chert isoclinal intrafolial folds with subvertical axes have been observed (Figure 5.6.g). To the south of this chert, the bedding dips to the north. The shear zone is interpreted to form the sheared axial plane of a tight syncline. A thin strip of the Ruth Well Formation occurs on the southern limb. The remaining section towards the Sholl Shear Zone in the south, consists of mafic and ultramafic intrusive rocks of the Andover Complex (see map in Figure 5.2, and cross-section A in Figure 5.4). The Andover Mafic-Ultramafic Complex is a late intrusive unit, however, its margins are deformed.

5.3.2.3 *Traverse B: west of Roebourne*

The main structural history of the section through Roebourne (see map in Figure 5.2, and cross-section B in Figure 5.4) is similar to that observed on the Prinsep Dome. However, the metamorphic grade in the Regal Formation decreases from amphibolite grade on the Prinsep Dome, to greenschist facies towards the northeast. A regional, generally steeply north or south plunging hornblende mineral lineation was observed mainly in the Regal, but also in the Nickol River and Ruth Well Formations. The fact that this lineation occurs over a relatively large area, indicates that it is associated with a major regional event. It does not occur in the Cleaverville Formation and it is interpreted to have formed during an early north-directed thrusting event and associated amphibolite grade metamorphism.

Deformation within the Cleaverville Formation was studied in the area west of Roebourne (see map in Figure 5.2). Some bedding-parallel zones were observed that internally consist of chaotically deformed chert beds. These are interpreted to be syn-sedimentary to diagenetic slump structures. Deformation in this part of the Cleaverville Formation is dominated by northwest-directed

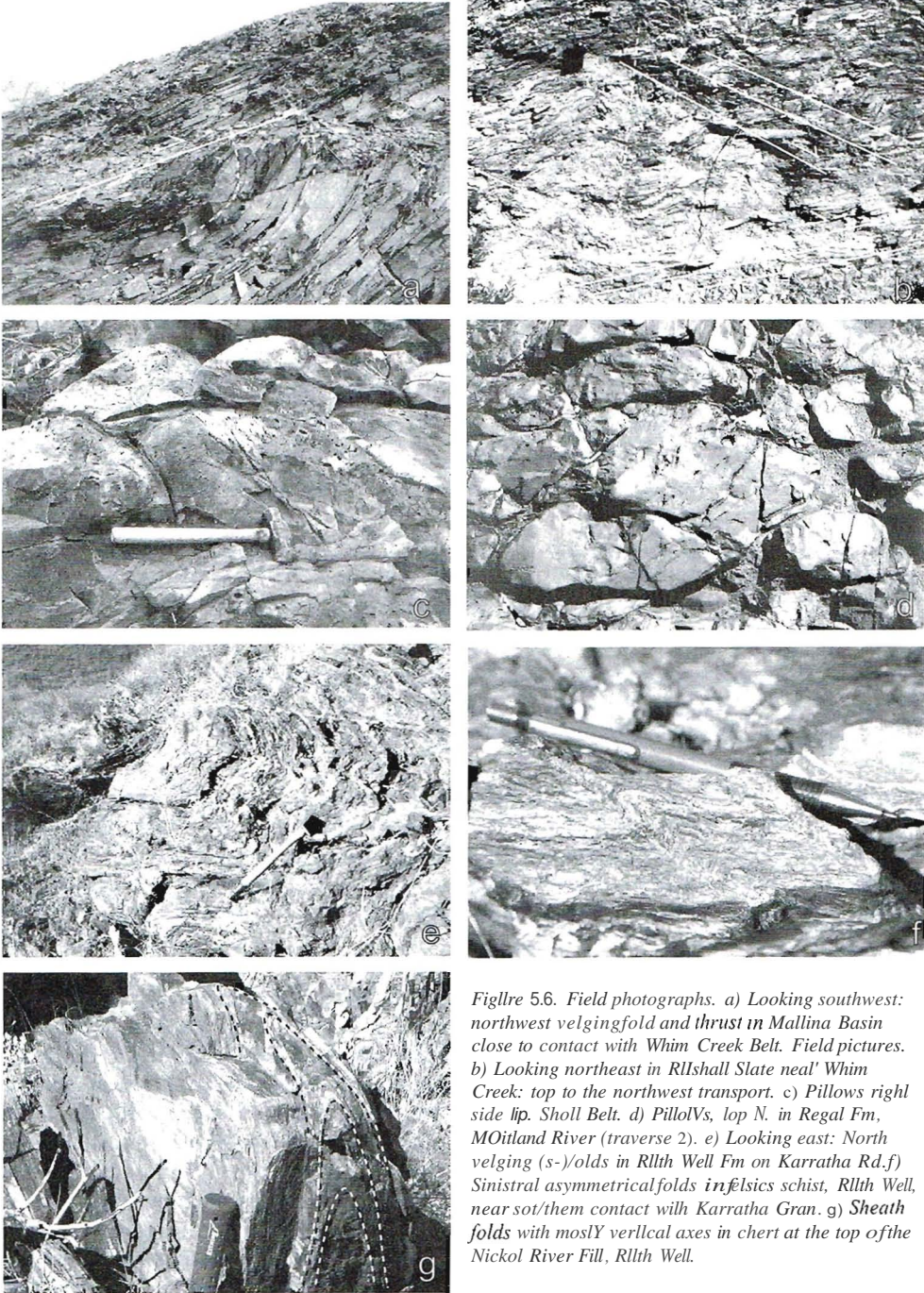


Figure 5.6. Field photographs. a) Looking southwest: northwest verging fold and thrust in Mallina Basin close to contact with Whim Creek Belt. Field pictures. b) Looking northeast in Rllth Well near Whim Creek: top to the northwest transport. c) Pillows right side lip. Sholl Belt. d) Pillows, top N. in Regal Fm, MOitland River (traverse 2). e) Looking east: North verging (s-)olds in Rllth Well on Karratha Rd. f) Sinistral asymmetrical folds in felsic schist, Rllth Well, near contact with Karratha Gran. g) Sheath folds with mostly vertical axes in chert at the top of the Nickol River Fill, Rllth Well.

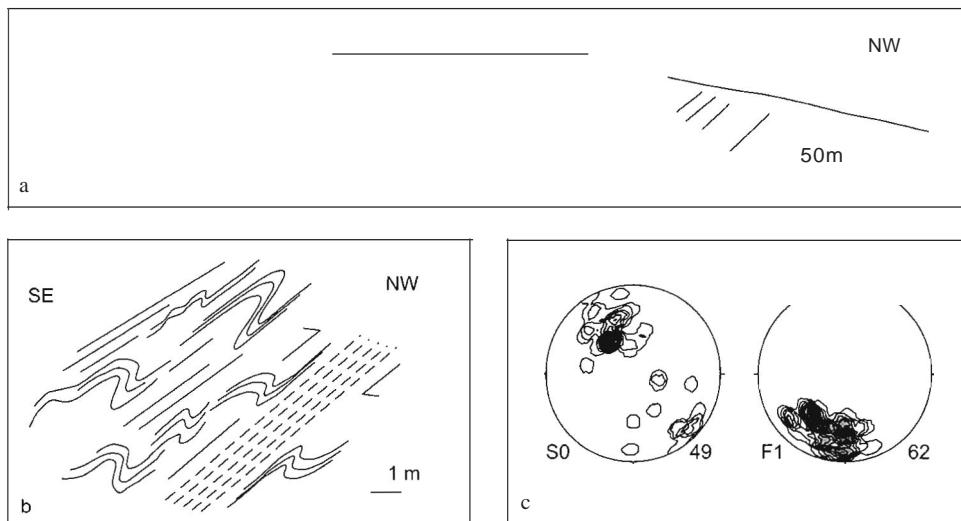


Figure 5.7. a) Field sketch of the north-west directed thrust structures and associated folds in the Cleaverville Formation, in a hill side near Roebourne b) Field sketch of meter-scale north-west verging folds and fault zone near Roebourne c) Lower hemisphere equal area stereoplots of bedding (S0) and fold axes (F1).

thrusting and associated asymmetrical folding, as shown in the field sketch in Figure 5.7.a and b. The asymmetrical folds plunge moderately to the south-southwest (Figure 5.7.c). At a few locations, small southeast-directed thrusts were observed; they are interpreted to be backthrusts in the same system.

The entire Cleaverville Formation is folded by the Roebourne Syncline, Prinsep Dome, and Cleaverville Syncline (see map in Figure 5.2 and cross-section B in Figure 5.4). The thrust structures described above and these large amplitude regional folds are interpreted to have formed during the same north-west verging compressive event. Throughout the Roebourne Domain, northeast trending brittle faults occur. Internal Riedel arrays indicate that the displacement on these structures is dextral.

5.3.2.4 Summary of deformation history of the Roebourne Domain

The deformation history of the Roebourne Domain is summarized in Table 5.3. The first regional event recognized (D1), is a tectono-metamorphic event affecting the older components of the Roebourne Domain. It was associated with north-directed thrusting and the formation of a hornblende lineation throughout the area, and local folding in the Ruth Well and Nickol River Formations. The timing of this event is poorly constrained at ~3150 Ma by K-Ar dating (Kiyokawa and Taira, 1998) and Ar-Ar dating (see section 5.5 on geochronology). The event must post-date the formation of the older units, which is ca 3265 Ma for the Ruth Well and Nickol River Formations and the Karratha Granitoid. The absolute age of the Regal Formation is not known, and as it is separated from the underlying formations by a tectonic contact, its relative age is also unknown. It is also affected by the metamorphism so it must be older than 3150 Ma. An ancestral Prinsep Dome and Roebourne Syncline may have formed at this time. The ca 3020 Ma Cleaverville Formation has not seen the amphibolite grade metamorphism and must therefore post-date the event.

Table 5.3. Deformation history of the Roebourne Domain.

Timing	Event	Roebourne Domain
2760 Ma	D5	dextral movement on NE trending brittle faults: N-S extension Hamersley Basin
post 2930 Ma	D4	Dextral deformation in most east to northeast trending shears
	D3	Regional scale folding on northeast trending axes, steepening of all structures, northwest directed thrusting in Cleaverville.
3020 Ma		Deposition of Cleaverville Fm across West (and Central) Pilbara, intrusion of granites.
	D2	Sinistral deformation in marginal shear Karratha Granite, bedding parallel shears in Ruth Well and Nickol River Fm's
-3150 Ma	D1	Folding in Ruth Well, Nickol River and Regal Formations, regional amphibolite grade metamorphism
pre 3150 Ma		Deposition of Regal Fm (in oceanic environment) possibly pre-3265 Ma
3265 Ma		Intrusion of Karratha Granodiorite (in subduction setting)
3265 Ma		Deposition of Nickol River Fm
pre 3265 Ma		Deposition of Ruth Well Fm

Before deposition of the Cleaverville Formation, sinistral strike-slip shearing occurred at amphibolite metamorphic grade in bedding-parallel shears in the Ruth Well and Nickol River Formations, and along most lithological contacts (D2). This deformation phase is only observed on the southern side of the Prinsep Dome. This is interpreted to be associated with sinistral deformation in the Sholl Shear Zone at that time (see section 5.3.5 on the Sholl Shear Zone).

After deposition of the ca 3020 Ma Cleaverville Formation, the now complete stratigraphy of the Roebourne Domain was folded on a regional scale, on northeast trending axes (D3). The Cleaverville Syncline, Prinsep Dome, and Roebourne Syncline were formed and tightened at this time.

The most prominent deformation in the northern and southern contacts of the Karratha Granodiorite was dextral, with moderately east-plunging lineations and dextral shear bands (D4). This is interpreted to be associated with dextral deformation in the Sholl Shear Zone at ca 2930 Ma (see section 5.3.5 on the Sholl Shear Zone). The last deformation event in the Roebourne Domain is represented by northeast-trending brittle shears with a dextral component of displacement (D5), interpreted to be associated with the initiation of the Hamersley Basin.

5.3.3 Sholl Belt

The Sholl Belt was studied on Traverse C (Figure 5.2). The Sholl Belt consists of mainly mafic and minor intermediate and felsic volcanics, and is of greenschist metamorphic grade, as indicated by the abundance of chlorite and epidote. Flow top breccias, vesicles and pillows indicate that the stratigraphy is not overturned (Figure 5.6.c). The Sholl Belt shows evidence for one phase of folding. These folds are regional scale open folds with northeast trending fold axes. One major syncline, the Bradley Syncline, dominates the Sholl Belt. A penetrative subvertical northeast-trending fracture-cleavage is axial planar to this fold. Structural data are presented on the map (Figure 5.2) and in stereoplots (Figure 5.8).

The Sholl Belt is affected by brittle faulting; a set of NE trending faults occurs throughout the area. Displacement on these structures is dextral, with slightly northeast-plunging epidote slickensides on fault surfaces. A northwest-trending localized fracture cleavage has been observed

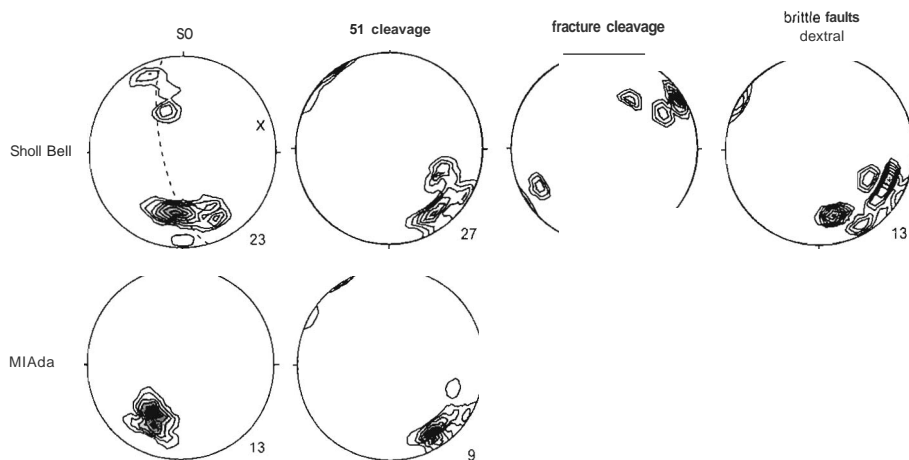


Figure 5.8. Structural data for the Sholl Belt represented in lower hemisphere equal area stereoplots.

which possibly represents the conjugate fault set of the dextral faults. Alternatively it is caused by a separate compressive event without associated folds. The western margin of the Sholl Belt is a sheared contact with the Cheratta Granitoid. These events are summarized and correlated with events in the Whim Creek Belt in Table 5.4. The connection between the two areas lies in the correlation of the D4 folds.

5.3.4 Whim Creek Belt

The Caines Well Granitoid has a sheeted and tectonized contact with quartz-muscovite and quartz-muscovite-biotite schists near Whim Creek (Figure 5.3). The *elongate* Opaline Well mafic intrusions occur at the margins of the Caines Well Granitoid, and their margins are also deformed and schistose. Shear bands and stretching lineations in these marginal shears indicate oblique sinistral nonnal movement (Figure 5.9.a.1). This is interpreted as D2 and/or D1 (Table 5.4). This is overprinted by dextral reverse kinks (Figure 5.9.a.2). These kinks are in turn overprinted by subvertical brittle sinistral faults with a northwesterly trend (Figure 5.9.a.3). The regional-scale outcrop pattern of the Caines Well Granitoid and surrounding units is determined by the northeast-trending Sherlock anticline (Figure 5.3), which formed due to northwest-southeast compression (O4) after the major activity in the Caines Well Marginal Shear. Cleavage of similar orientation occurs in the Rushall Slate near Whim Creek (Figure 5.9.b). It overprints a set of north-trending folds which therefore is interpreted as O3. The slates near Whim Creek show a locally very well-developed pencil cleavage, resulting from intersection of the D3 and O4 cleavages.

The dominant structures in the eastern part of the Whim Creek Belt are northeast-trending and steeply to moderately southeast dipping faults that run parallel to the Loudens Fault (see map in Figure 5.3). These faults are brittle structures with epidotized slip surfaces and gouge zones. Slickensides, tension gashes and step-structures indicate a sinistral-normal movement (D5). Major activity on these structures is interpreted to have occurred during or after the opening of the Hamersley Basin, and involved east side-down movement in the order of hundreds of meters as indicated by the preserved thickness of the basal Fortescue Group on the downthrown side (Smithies, 1996).

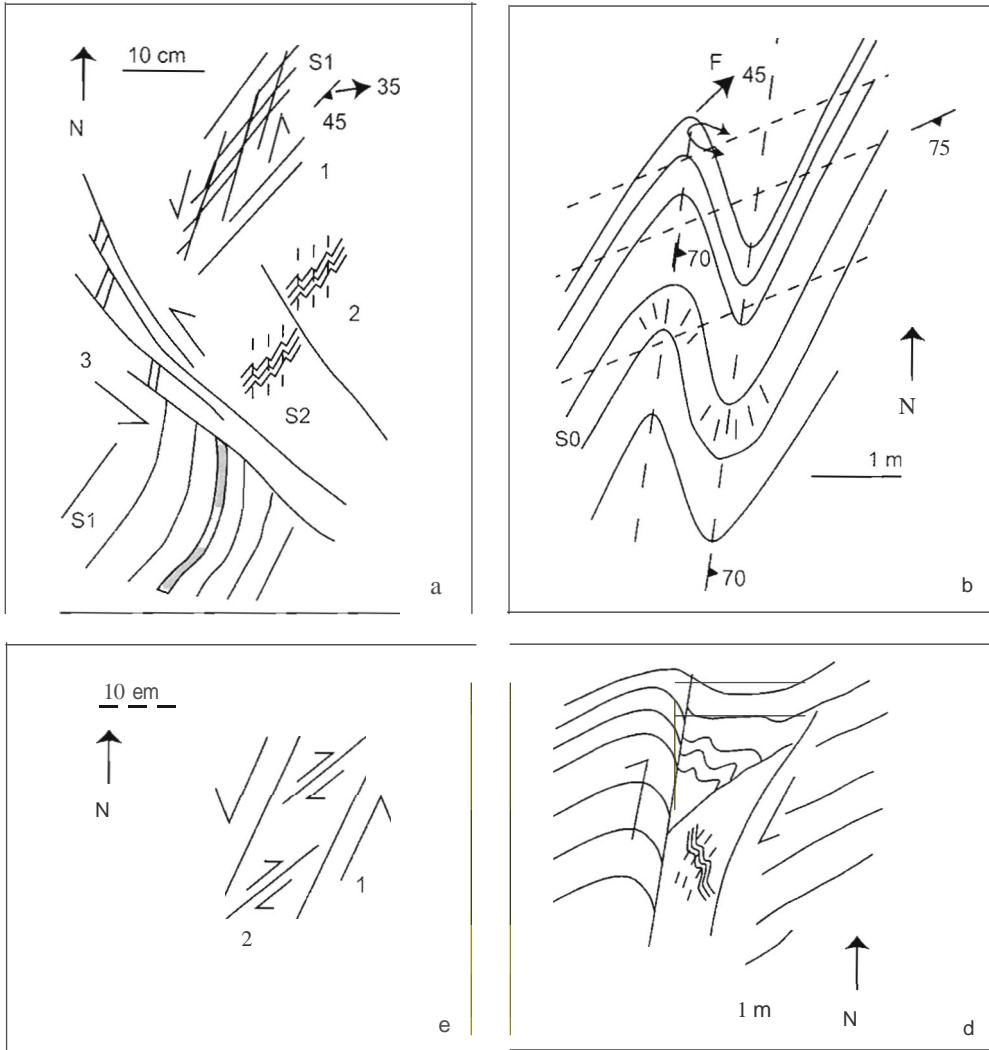


Figure 5.9. Schellmieu representation of the observed deformation events in the Whim Creek Belt and Caines Well Marginal Shear: a) Caines Well Marginal Shear: Initial sinistral normal movement overprinted by brittle dextral movement and late sinistral movement. b) Folds in Rushed Slate near Mons Cupri Mine overprinted by northeast-trending cleavage. c) Sinistral brittle faults overprinted by dextral movement through Whim Creek Belt. d) Dextral Faults in Malina Fm near Whim Creek. e) Another view of the Caines Well Marginal Shear showing sinistral brittle faults overprinted by dextral movement.

Table 5.4. Deformation history of the Sholl-Whim Creek Domain. Schematic representation of the deformation phases in the Caines Well Marginal Shear is shown in Figure 5.9. References for geochronology: a: Blake and Barley (1992), b: Smithies et al. (2001), c: Pike et al. (2002), d: Nelson (2000), e: Nelson (1997)./ Nelson (1998a).

Timing	D	Sholl Belt	Caines Well Marginal Shear	Whim Creek Belt
post 2770 Ma	06	Dextral movement on NE brittle faults		Dextral/normal movement in NE trending structures
post 2770 Ma (a)	D5		Sinistral/normal movement	Sinistral/normal movement in NE trending structures
post 2930 Ma (b)	04	NE trending folds	Reverse/dextral movement	NE trending, NW verging folds and thrusts
pre 2950 Ma (b)	03			N trending folds
2970 Ma (c)	02		Sinistral/normal movement	Deposition of Bookingarra Group and Mallina Sediments
2990 Ma (d)			Intrusion of main phase of Caines Well Granitoid	
3010 Ma (c)	D1		Sinistral/normal movement	Deposition of Whim Creek Group unconformably on Whundo and Caines Well
3020-3015 Ma (e)		Cleaverville Fm	Cleaverville Fm	Cleaverville Fm
3095 Ma (e)			Whundo Group intruded by Caines Well early phase.	
3115 Ma (f)		Deposition of Whundo Group		Deposition of Whundo Group

Internally, these fault zones show evidence for a (D6) dextral overprint (Figure S.9.c). Dextral brittle faults also occur throughout the Mallina Basin as the last deformation phase. The deformation history in the Whim Creek area is summarized in Table 5.4. A sketched cross-section of the Whim Creek area is shown in Figure S.4.c.

5.3.5 The Sholl Shear Zone

5.3.5.1 Traverses

The Sholl Shear Zone forms the boundary between the West and Central Pilbara. It is a major structure running parallel to the North Pilbara coastline, its maximum width is approximately 2 kilometers. The shear zone has a length of more than 200 kilometers as can be seen on aero-magnetic and gravity imagery (Blewett et al., 2000). In areas of poor outcrop, these images were used to locate the structure (see Figure 3.2). At a number of locations traverses were made across the structure.

Traverse I

At the westernmost exposure of the West Pilbara (traverse I, Figure 5.2) amphibolite grade schistose mafic rocks, interpreted to belong to the Regal Formation, have a northeasterly trend and dip steeply

to the southeast. They display a steeply east-plunging hornblende lineation. To the southeast several prominent northeast trending chert ridges occur in which a steeply east plunging stretching lineation was observed (Figure 5.1 O.a). East of this high-strain zone, shallowly west-dipping andesites of the basal Fortescue Group occur.

Traverse 2

At traverse 2 across the Sholl Shear Zone, at the Maitland River (Figure 5.2, Figure 5.11.a), the most prominent feature is an east-trending subvertical ridge of banded chert, which can be traced along strike into the Cleaverville Formation. To the north of the chert, greenschist grade mafic schists occur, intruded by coarse muscovite-rich pegmatites, interpreted to be associated with the Dampier Granitoid. These are deformed by dextral meter-scale shear bands. Locally hornblende randomly overgrows the greenschist grade actinolite-chlorite foliation of the mafic schist, indicating a post-tectonic thermal disturbance.

To the south of the chert, amphibolite-grade hornblende-plagioclase schists occur, with anastomosing high-strain zones with steeply northwest-plunging actinolite-hornblende mineral lineations and plagioclase stretching lineations (Figure 5.1 O.b). Some very well developed centimeter to meter-scale sheath folds with subvertical fold axes were observed (Figure 5.12.a). These fold axes are parallel to the sub-vertical mineral and stretching lineations in the amphibolite grade shears (Figure 5.10.b), interpreted to indicate that these structures formed during the same event. The high-strain zones form anastomosing bands of one to several meters wide and occur over a total width of a little less than one kilometer (Figure 5.11.a). Thin section analysis has shown a north-side up sense of shear, which makes the now steeply north-dipping Sholl Shear Zone a thrust during this event. Locally the less-deformed amphibolites show pillow structures (Figure 5.6.d).

Traverse 3

Northeast of Karratha Station (traverse 3, Figure 5.2), a few outcrops of the Sholl Shear Zone were studied. They consist of mafic schists, with the greenschist-facies mineralogy of chlorite and actinolite. The foliation dips steeply to the north. Within the schist dextral shear bands were observed. A number of amphibolite grade mafic boudins is present within the greenschists. They do not possess a long axis and, as they may have been rotated during later deformation, their orientation can not be interpreted to be representative of earlier deformation.

Towards the south, many thin granitic sheets alternate with the schist. The schist contains hornblende overgrown by randomly oriented actinolite. The granitic sheets are mylonitized; they have very fine grain sizes and strongly developed quartz and plagioclase stretching lineations. In the coarser-grained parts of these granitic mylonites the stretching lineation plunges 70-80° to the north-west, in the finer grained zones the stretching lineation is subhorizontal (Figure 5.10c). Locally lineations with intermediate plunge angles occur. This is interpreted to indicate a transition from reverse movement at amphibolite grade conditions, to dextral strike-slip movement at greenschist grade conditions, during a single event.

Traverse 4 and 5

A few kilometers to the west of the Hamersley Rail Road (traverse 4, Figure 5.2) a small outcrop of the Sholl Shear Zone occurs. The foliated granite displays very strongly developed quartz and plagioclase stretching lineations and dextral shear bands. The foliation dips 60-80° to the north and the mineral lineation plunges 0-10° to the east. At this locality a large 20 m wide north-east trending undeformed dolerite dyke cross cuts the Sholl Shear Zone.

Locations: Sholl Shear Zone, Western Section

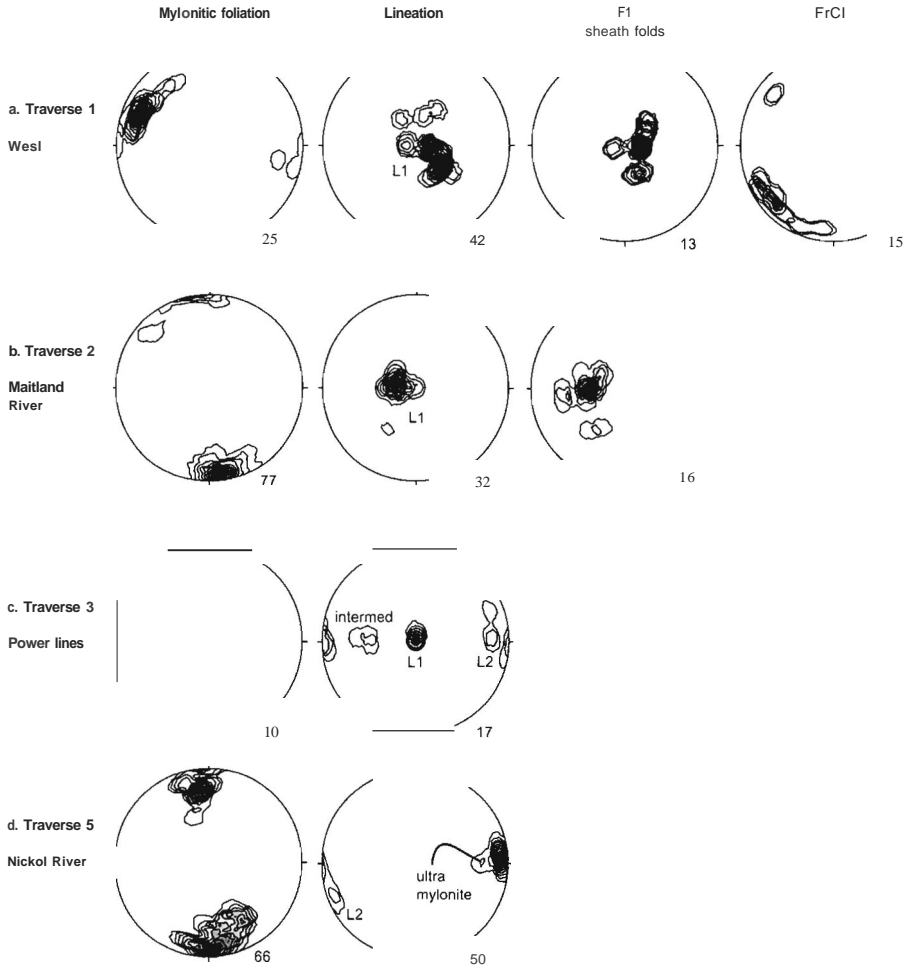


Figure 5.1. Structural data of the Sholl Shear Zone (western section) represented in lower hemisphere equal area stereoplots (bin size/or contours adjusted to max 8 levels). Locations (traverses) are indicated in Figure 5.2. Lineations are shear-related lineations occurring only within the Sholl Shear Zone. L1 are steeply plunging hornblende mineral lineations associated with north-block-up kinematics. F1 are sheath folds with axes parallel to L1. L2 are subhorizontal stretching lineations associated with dextral kinematics. At Traverse 3 an intermediate lineation has been observed. At Traverse 5 the stretching lineation in thin ultramylonite zones (picture in Figure 5.1/b) plunges more steeply to the east than that in the mylonite.

Locations: Sholl Shear Zone, Eastern Section

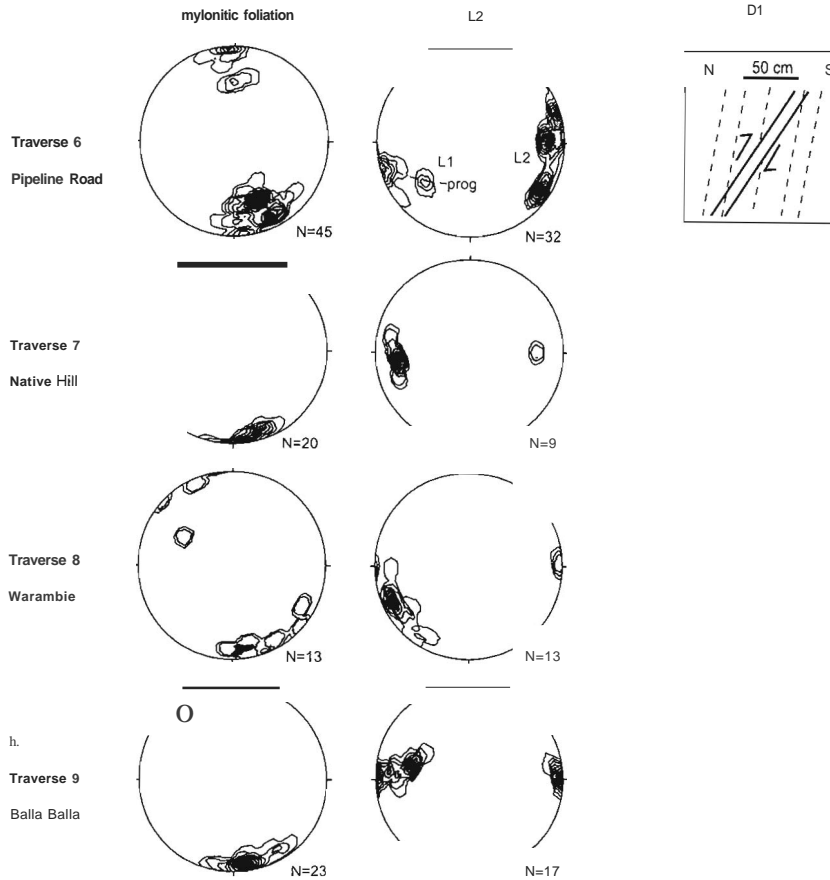


Figure 5.10. part II Structural data of the Sholl Shear Zone (SSZ) eastern section, represented in lower hemisphere equal area stereoplots. Locations (traverses) are indicated in Figure 5.2. and Figure 5.3. Lineations are shear-related lineations occurring only within the Sholl Shear Zone. L1 has not been observed in the eastern section of the SSZ. L2 are subhorizontal stretching lineations associated with dextral kinematics. At Traverse 6 a small side-view of the structure is shown, indicating north-side-up movement.

Granite with strongly developed subhorizontal quartz and plagioclase stretching lineations is exposed in the bed of the Nickol River (traverse 5, Figure 5.2). In the central section, ultramylonite bands with extremely small grain sizes (less than $10\ \mu\text{m}$) occur within this mylonitic granite (picture in Figure 5.12.b). The lineations in these ultramylonite bands plunge about 25° to the east. Dextral shear bands and asymmetrical folds are abundant. The stretching lineation is subhorizontal (picture in Figure 5.12.c, stereoplot in Figure 5.1 O.d) In outcrop as well as in thin-section, sinistrally rotated clasts were found within the mylonitic zone, interpreted to be remnants of an earlier, overprinted, deformation phase. To the south, a weakly foliated, non-metamorphosed basalt of the Sholl Belt occurs. The minimum total width of the Sholl Shear Zone at the Nickol River is estimated at 800 meters.

Traverse 6

Along the Pipeline Road (traverse 6 in Figure 5.2, and Figure 5.II.b) undeformed gabbro, diorite and pegmatitic patches occur to the north of the Sholl Shear Zone. Mafic schists surrounding these intrusions have a northwest-dipping foliation. Shear zones, dipping at a shallower angle to the north than the main foliation, indicate that the northern block has moved up relative to the southern block (sketch in Figure 5.1 O.e). Continuing the traverse to the south, mafic schists with northeast trending and northwest dipping foliation are exposed. They contain the amphibolite-grade metamorphic assemblage of hornblende and plagioclase. A weak hornblende mineral-lineation plunges steeply to the northwest. Towards the south, these amphibolite grade rocks are progressively overprinted by a schistosity defined by chlorite. The steeply north-dipping foliation trends northeast, and is cut by steeply north-dipping dextral shear bands trending east-northeast.

Thin sheets of foliated granite occur within the mafic schist. On steeply south-dipping surfaces these sheets have moderately southwest-plunging quartz-plagioclase stretching lineations. Further to the south they have subhorizontal lineations (Figure 5.1 O.e). Within the greenschist grade schists, amphibolite-grade boudins were preserved. These boudins contain hornblende and plagioclase, an amphibolite-grade metamorphic assemblage. The boudins have a moderately west-plunging hornblende mineral lineation. The upper surfaces of the boudins display a kinked chlorite foliation, with kink-axes at a right angle to the hornblende lineation. The asymmetry of these kinks records dextral/reverse movement.

To the south of these mafic greenschists, foliated granite with strongly developed quartz and plagioclase stretching lineations is exposed (Figure 5.11.b). The mylonitic foliation is steeply north-dipping, quartz-plagioclase stretching lineations are subhorizontal. Decimeter- and centimeter-scale shear bands and folding of the mylonitic foliation indicate dextral movement (Figure 5.12.d). In the field and in thin section sinistrally rotated K-feldspar clasts were observed, indicating early sinistral deformation in the Sholl Shear Zone. South of the Cheratta Road no more outcrop has been observed (Figure 5.11.b), giving the main mylonite a minimum thickness of 300 meters and the total Sholl Shear Zone a minimum thickness of 1 kilometer.

Traverse 7 and 8

At Native Hill (traverse 7, Figure 5.2) and Warambie (traverse 8, Figure 5.3 and Figure 5.11.c) the structure is very similar. Two major shear zones run parallel and east-west. The northern strand shows evidence only for subhorizontal dextral movement as observed elsewhere: dextral shear bands and asymmetrical folds. The southern strand forms the northern margin of the Whim Creek Belt (Warambie Basalt). The area between the two structures is strongly foliated and consists of northeast trending sheets of granite and mafic schists, cut by northeast trending minor shear zones (Figure 5.II.c).

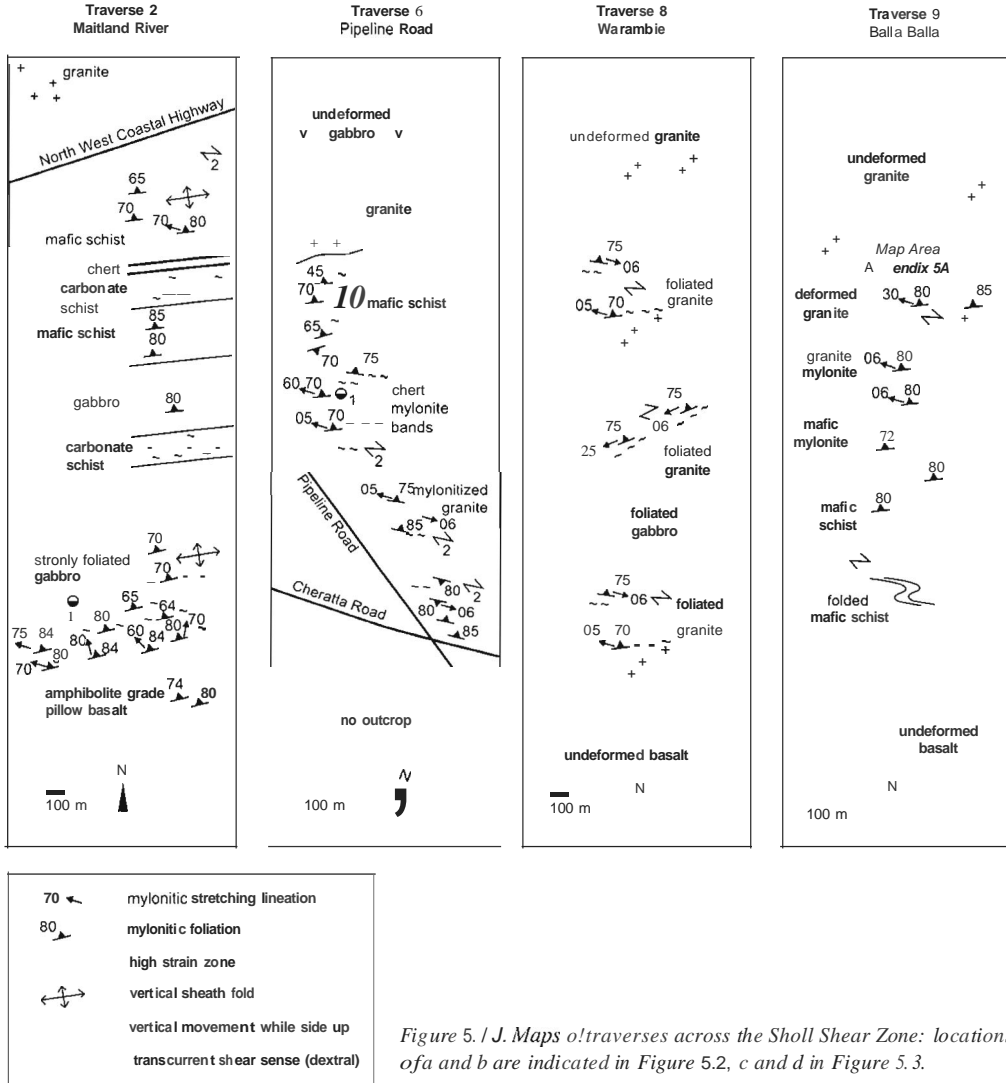


Figure 5.10. Maps of traverses across the Sholl Shear Zone: locations of a and b are indicated in Figure 5.2, c and d in Figure 5.3.

Towards the south the strain increases. In the granitic components of this shear zone sinistral shear bands and rotated clasts occur. The shears contain subhorizontal stretching lineations (Figure 5.10. [and g]), dextrally rotated clasts, subvertical northeast trending dextral shear bands and dextral asymmetrical folds. A pervasive northeast trending foliation is seen in the granite between the two main shear zones, and locally dextral displacement occurred on these foliation planes. These northeast-trending shears have a dextral shear sense, and stretching lineations plunging 20-30° to the southwest. Between Warambie and Balla Balla no outcrop of the Sholl Shear Zone has been found (Figure 5.3).

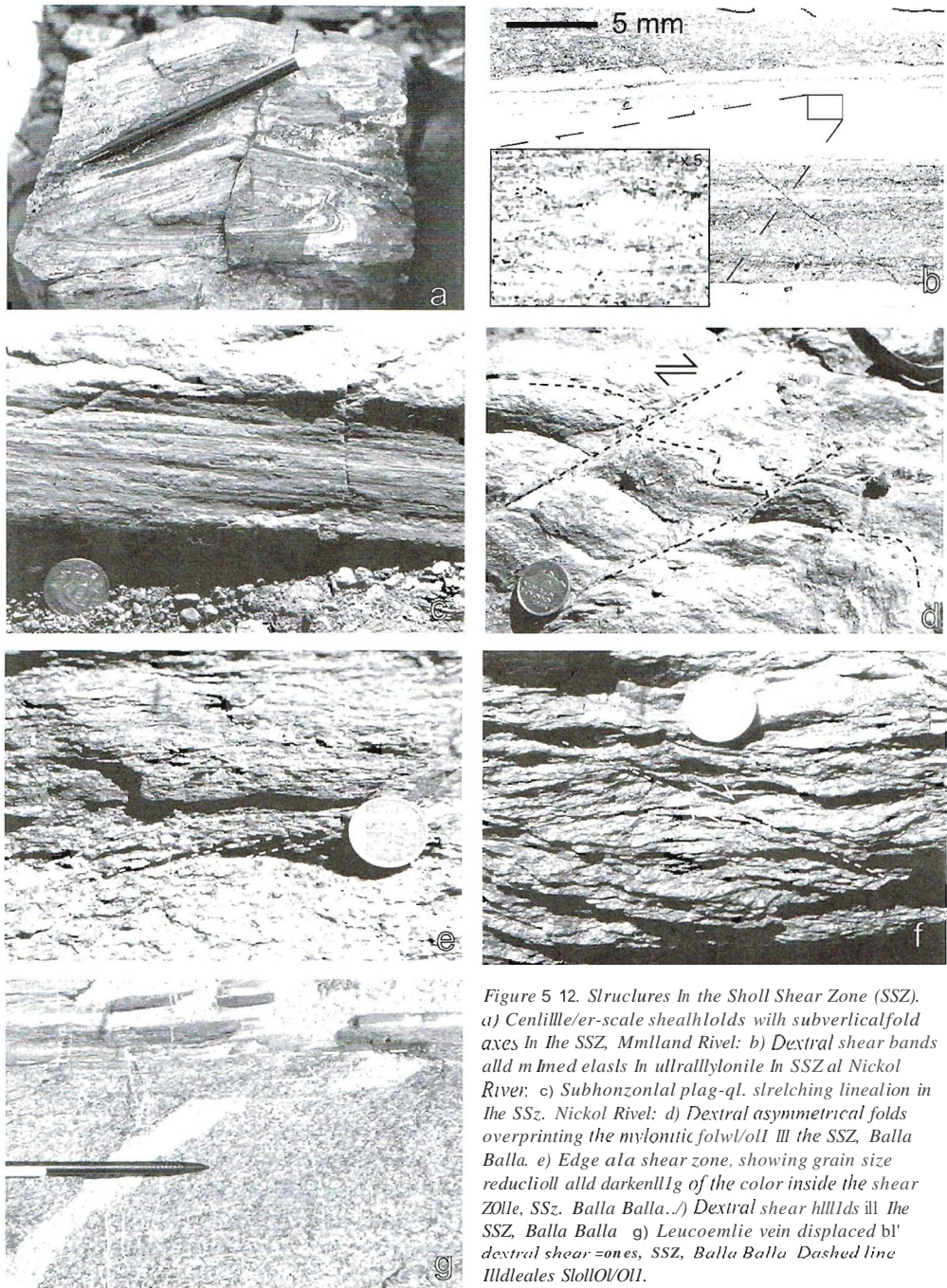


Figure 5.12. Structures in the Sholl Shear Zone (SSZ). a) Centimeter-scale sheathfolds with subvertical fold axes in the SSZ, Mmland River; b) Dextral shear bands and mylonitic bands in ultramylonite in SSZ at Nickol River; c) Subhorizontal plagioclite stretching lineation in the SSZ, Nickol River; d) Dextral asymmetrical folds overprinting the mylonitic foliation in the SSZ, Balla Balla; e) Edge area shear zone, showing grain size reduction and darkening of the color inside the shear zone, SSZ, Balla Balla; f) Dextral shear hills in the SSZ, Balla Balla; g) Leucomelie vein displaced by dextral shear zones, SSZ, Balla Balla. Dashed line indicates original position.

Traverse 9

The granodiorite at West Balla Balla Beach has a migmatitic texture. A pink leucocratic phase was produced and extracted into veins, leaving behind a hornblende-bearing melanosome. Numerous east-trending shear zones occur in the outcrop. These structures show evidence for one deformation phase involving dextral displacement. The traverse at East Balla Balla Beach (traverse 9, Figure 5.11.d) starts in the north in the migmatitic Balla Balla Granodiorite with pink leucocratic veins. This leucocratic phase was sampled for V-Pb dating (see section 5.5). The granodiorite is cut by numerous anastomosing shear zones, which have been mapped and described in detail (see section 5.3.5.8). Biotite stretching lineations in these shear zones plunge moderately to the west.

Over an interval of 200 meters the abundance of these shear zones increases until the rock is completely mylonitized. This main mylonite zone has subhorizontal quartz, plagioclase and biotite stretching lineations. After 300 meters the granodioritic mylonite gives way to mylonitic mafic schist which continues for another 200 meters. The schist has subhorizontal quartz and chlorite stretching lineations. The strain-intensity decreases towards the south and folds can be recognized within the mafic schist. Their fold axes plunge steeply to the west, and their asymmetry indicates dextral movement. The Negri Volcanics of the Whim Creek Belt occur immediately south of the Sholl Shear Zone (Figure 5.11.d). They consist of a felsic conglomerate and massive and spinifex textured basalts of low greenschist metamorphic grade, as indicated by the abundance of chlorite.

5.3.5.2 Meso-scale structures in the Sholl Shear Zone at Balla Balla

At Balla Balla Beach (northern end of traverse 9), north of Whim Creek, two water-washed outcrops of the northern side of the Sholl Shear Zone have been studied in detail (see Figure 5.3 for location). The eastern outcrop has been mapped at a scale of 1:100; the result of this mapping project can be found in Appendix 5.A (on CD-ROM). The outcrop consists of a granodiorite which has been intensely deformed by an anastomosing network of shear zones. Early leucocratic veins and later mafic dykes intrude the granodiorite, and a number of mafic xenoliths is exposed. One of the leucocratic veins has been the subject of V-Pb zircon dating, and several samples were taken for $^{40}\text{Ar}/^{39}\text{Ar}$ dating (see section 5.5).

The displacement across the shears, of the leucocratic veins as well as the mafic dykes is clearly dextral (Figure 5.12.e and Appendix 5.A). On the meso-scale a large number of shear sense indicators is present. In the moderately to highly deformed parts of the granodiorite dextral kinks and shear bands are locally very well developed (examples are shown in Figure 5.12.d, e and f). Micro-scale shear sense indicators such as microscopic shear bands and rotated clasts have been observed in thin sections, and they also consistently indicate a dextral shear sense (see also Figure 5.13). No evidence for sinistral deformation was found, neither in outcrop nor in thin section. The shear zones in the granodiorite have a much darker appearance than the undeformed granodiorite (Figure 5.6). Thin section analysis has shown that the dark color results from grain size reduction and loss of quartz within the shear zones (Figure 5.13). A weak stretching lineation plunges to slightly the west (Figure 5.10h).

For the purpose of the calculations below, it is assumed that the average lineation is horizontal: if there was a large component of vertical displacement along a significant length of the Sholl Shear Zone, this would have been expressed in a difference in metamorphic grade across the shear zone. This is not the case: on both sides the rocks are of greenschist metamorphic grade.

In Figure 5.14 the displacement is plotted against the width of a number of shear zones in the grid area. The minimum displacement of the shear zones is marked by the line: displacement = 10 x width. This seems to be a good description over a wide range of widths and displacements, and if extrapolated to the entire width (1 km) of the Sholl Shear Zone this would give a total minimum

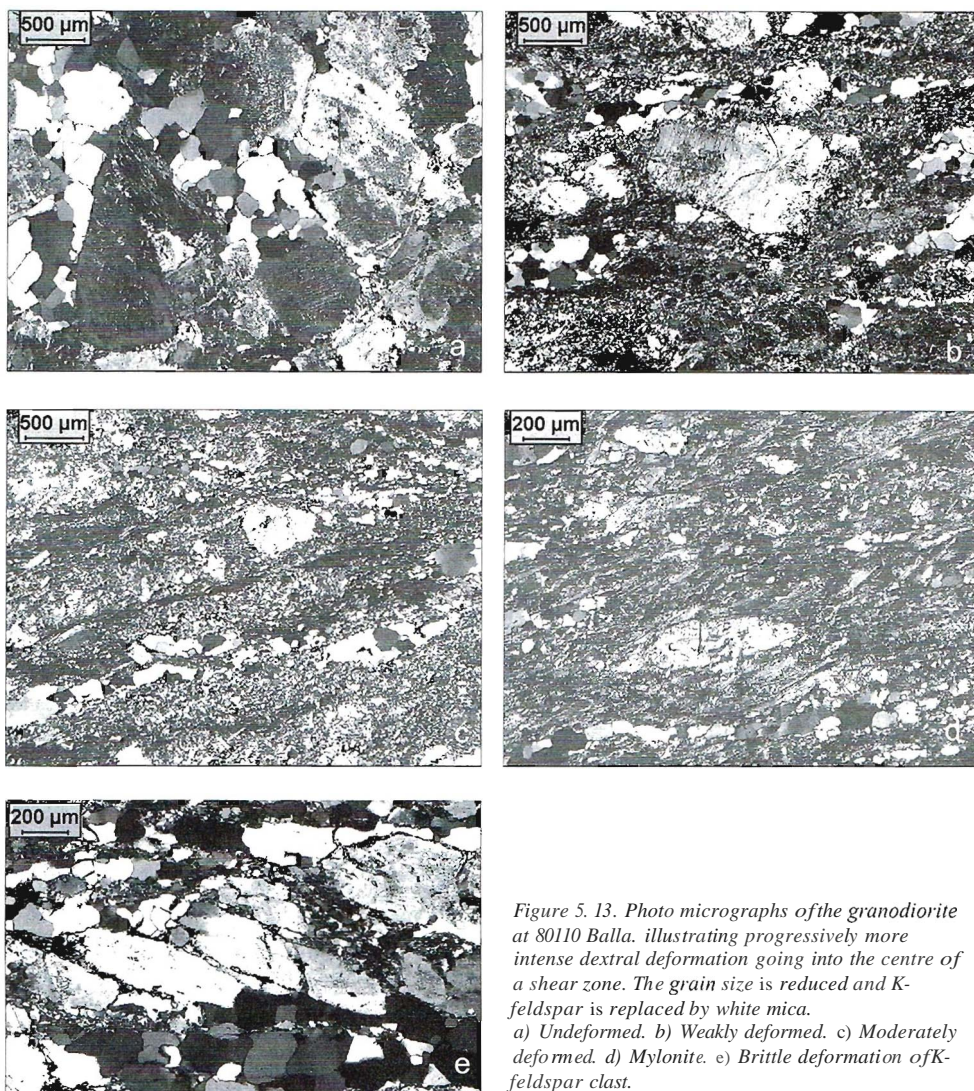


Figure 5.13. Photo micrographs of the granodiorite at 80110 Balla, illustrating progressively more intense dextral deformation going into the centre of a shear zone. The grain size is reduced and K-feldspar is replaced by white mica. a) Undeformed. b) Weakly deformed. c) Moderately deformed. d) Mylonite. e) Brittle deformation of K-feldspar clast.

dextral displacement of 10 kilometers. Since many of the shear zones are discontinuous (meaning that passive markers cannot be traced continuously across the shear zone, as shown in Figure 5.15), the displacement is much larger and no longer directly related to the width of the shear zone. The displacement along discontinuous shear zones is up to 100 times larger than the width. The average relation is approximately: displacement = 40 x width, see Figure 5.14. This gives the total Sholl Shear Zone in this area a dextral displacement component of 40 kilometers. This correlates very well to the 40 kilometers of dextral displacement of the Whim Creek Belt as shown in Figure 5.3.

It is not known why this relationship exists between the width and the displacement along these shear zones. Other studies (e.g. Clark and Cox, 1996) have reported relationships between length of shears and faults and the displacement, but not on the relationships between the width and

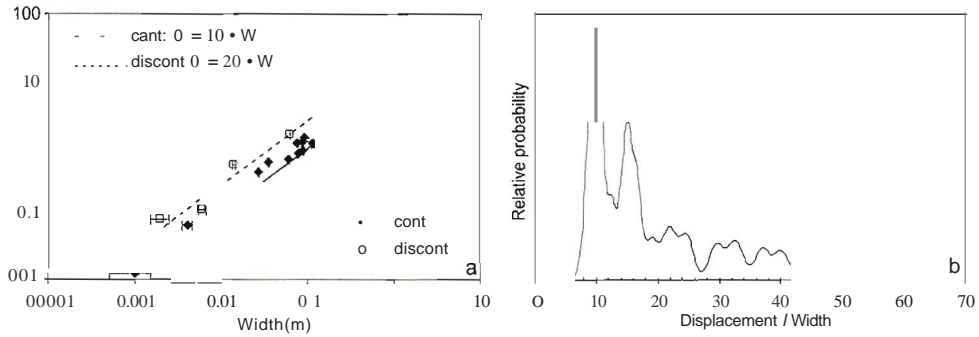


Figure 5./4. a) Plot of width versus displacement for a large number of dextral shears in the Sholl Shear Zone at Balla Balla. b) Cumulative probability plot of the displacement/width ratio. The jagged curve is the result of poor statistics due to low numbers of data.

displacement. The relationship implies that the shear strain is constant in continuous shear zones of all sizes. This can only be done by imposing a maximum strain which is reached relatively quickly, possibly by work hardening. Microstudies of these rocks (pictures of several stages of deformation are shown in Figure 5.13) have not revealed any unusual microstructures. K-feldspar is replaced by muscovite and the grain size is greatly reduced at higher strain. This is expected to result in strain weakening and consequently in strain localization (e.g. Ramsey and Hubert, 1983). The observed effect is the opposite and it cannot be explained by the microstructure. This is a target for further research.

5.3.5.3 Summary of the deformation history of the Sholl Shear Zone

The deformation history of the Sholl Shear Zone is summarized in Table 5.5. The Sholl Shear Zone is a major structure with a long history of activity, separating terranes with significantly different lithology, geochronology and geochemistry. It likely formed early in the history of the West Pilbara. At ca. 3150 Ma a deformation event occurred in the Roebourne Domain, and the Sholl Shear Zone is interpreted to have been formed and active at that time (DI).

Before deposition of the ca 3020 Ma Cleaverville Formation, and before intrusion of the ca 3015 Ma granitoids at Balla Balla (Nelson, 1997; Beintema et al., in press), sinistral displacement

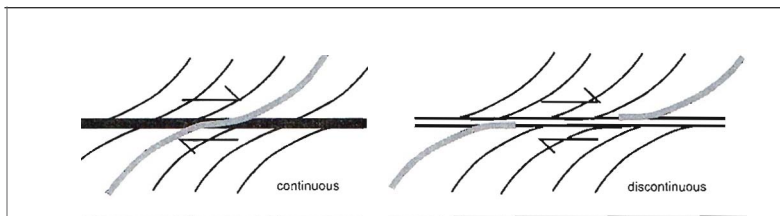


Figure 5./5. Illustration showing the difference between a continuous (left) and a discontinuous shear zone (right). Passive markers can be traced continuously through continuous shear zones. They are displaced along very thin (semi-brittle) zones within the shear in discontinuous shear zones.

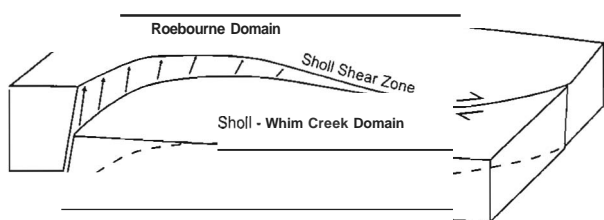


Figure 5.16. Sketch block diagram/or the ca 2930 Ma deformation phase 0/ the Sholl Shear Zone. The curved geometry caused initial thrusting in the western section while strike-slip occurred in the eastern section. During the later stages of this event, this changed to subhorizontal strike-slip in the central section.

occluded along the Sholl Shear Zone (D2), Cryptic evidence for this deformation phase was found in the older granites within the western section of the shear. Structures with similar orientation and kinematics are present in the Roebourne Domain, adjacent to the Sholl Shear Zone,

The Sholl Shear Zone experienced reverse (north side up) movement (O3) in the western section of the structure. There is no evidence for much vertical displacement in the eastern section of the Sholl Shear Zone. This is interpreted to be due to the curved geometry of the structure as illustrated in Figure 5.16. A major phase of dextral deformation occurred (D4) after intrusion of the

Table 5.5. Deformation history of the Sholl Shear Zone.

Timing	Event	Sholl Shear Zone
post 2930 Ma	O4	Dextral deformation, 40 km displacement, greenschist metamorphic grade
pre 2930 Ma	O3	Reverse movement going to dextral.
pre 3020 Ma	O2	Sinistral deformation, unknown amount of displacement
-3150 Ma	O1	formation of ancestral Sholl Shear

ca 3015 Ma granitoids, probably at ca 2930 Ma as indicated by regional correlations as will be discussed in section 5.6. The transition from reverse to strike-slip movement occurred during a single event, while the metamorphic grade decreased from amphibolite to greenschist facies. This happened after deposition of all of the rocks in the Whim Creek Group and Mallina Basin, because they have been displaced dextrally across the Sholl Shear Zone by 40 kilometers (Smithies, 1997b).

5.4 Geochemistry

5.4.1 Introduction

As discussed above, the West and Central Pilbara consist of three domains (Figure 5.1) which have been suggested to have formed by accretion and subduction processes (e.g. Krapez and Eisenlohr, 1998; Smith et al., 1998; Kiyokawa et al., 2002). The present geochemical study was undertaken to investigate the possible role of subduction, accretion, or intracontinental rifting in the formation and deformation history of the West and adjacent Central Pilbara and their characteristic mafic rock suites. The mafic rocks in the Roebourne Domain and Sholl Belt were sampled in order to determine the nature and conditions of their source regions. These rocks cover a time span of more than 300 million years; they have ages between 3265 and 2925 Ma. The Whim Creek Belt has recently been studied and described in detail by Pike and Cas (2002) and Pike et al. (2002).

It should be noted that the discrimination fields in the presented diagrams are based on modern tectonic regimes. Their relevance for Archaean studies may be limited. Firstly, the samples have experienced alteration and metamorphism, although it will be shown that the effects are limited. Furthermore, tectonic and crustal conditions and processes may have been different in the Archaean, such as the geothermal gradient, source rock chemistry, and the type and angle of subduction. The geochemical signature of a rock records the physical-chemical condition of the source region and migration path, i.e. the composition of the source and the temperature, depth and degree of melting at which the melt was formed. This does not necessarily imply a similar tectonic regime as is the modern case.

5.4.2 Analytical methods

Sampling for this project focused on mafic and ultramafic rock types. The least deformed rocks were selected and 2-4 kg of the freshest appearing rock was sampled with a sledge hammer. Whole rock analysis requires powdered (<10 μ m) rock samples. The samples were prepared by removing weathered parts and veins, crushing in a rock splitter and jaw crusher, and ground in a Tungsten-Carbide ring mill. They were dried at 120 degrees before analysis of the LOI values in a TGA automated setup. Glass discs for XRF major element analysis were prepared by adding a LiB₄O₇ flux to about 500 mg of sample powder, followed by melting in a platinum crucible. The melt was homogenized at 1000°C for ten minutes, before slow cooling to form a glass disc in 10 minutes. The XRF major element analyses were carried out with a Siemens SRS 3440 spectrometer, at Utrecht University, the Netherlands.

For trace element analysis by rCP-MS, 0.1 g of sample powder was dissolved in 4 ml HNO₃, 3 ml HClO₄, and 5 ml HF acid, in Teflon bombs. They were heated to 180 degrees for 5 hours, followed by a check for un-dissolved minerals such as zircon. None of the samples needed secondary treatment. Trace elements were measured at Utrecht University, on an Agilent 7500a ICP-MS instrument.

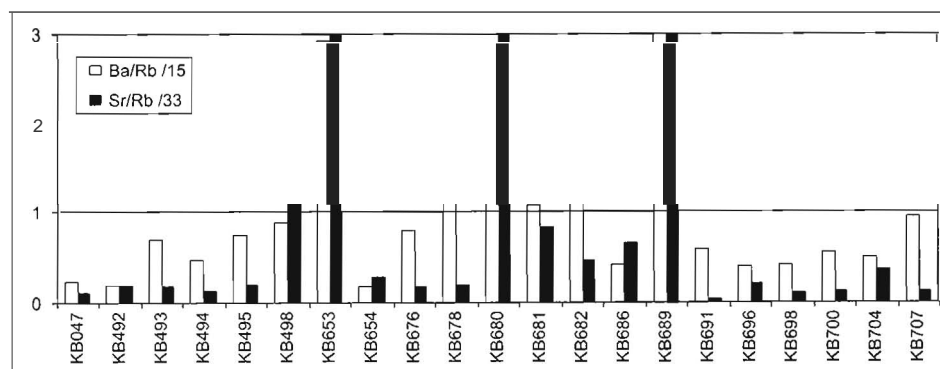


Figure 5.17. Plot of $Ba/Rb/15$ and $Sr/Rb/33$ ratios which give an indication of the degree of alteration (White, 1983). Normalized values >1 indicate moderate to severe alteration.

5.4.3 Geochemical results

In most rocks the original igneous textures can still be observed, implying that deformation was minimal, however, alteration and metamorphism may have affected the geochemistry of the analyzed rocks. The Ruth Well and some of the Regal samples from the Roeboume Domain have experienced amphibolite-grade metamorphism, all other samples have experienced greenschist-grade metamorphism. At all locations the least deformed samples were selected. Sample locations and descriptions have been summarized in Appendix 5.B.1 (on CD-ROM), petrographic descriptions in Appendix 5.B.2 (on CD-ROM).

The results of the major element analyses are given in Appendix 5.B.3 (on CD-ROM), the trace elements are presented in Appendix 5.B.4 (on CD-ROM). The major element data are given in weight %, recalculated to a total dry sum of 100% and with total Fe represented as Fe_2O_3 . The uncorrected total sum including the volatiles deviated no more than 2% from 100% for any of the analyses. To check the accuracy and reproducibility of the analyses, internationally certified standards (BAS-I, OU4, BN02, BR, BHVO-2) were measured as well as sample duplicates. All agreed within standard deviation, except for the ICP-MS analyses of Cr and V. Because the REE do give reproducible results, this is interpreted to be due to sample inhomogeneity.

As alteration and metamorphism are expected to have affected the geochemistry of the analyzed rocks, the interpretation of the geochemical analyses has to be treated with caution. Of the major elements Al, Ti, Mn and P have been regarded as relatively immobile (Mullen, 1983). The LILE elements (Rb, Ba, K, U, Sr) are expected to have been most affected by metamorphism and alteration; the other trace elements (HFSE and REE) are expected to have remained immobile (Rollinson, 1993).

Certain trace element ratios can be used to check for alteration. Sr and Ba are less mobile than Rb, which is extremely mobile. Alteration commonly results in anomalously high Ba/Rb ratios and low Rb/Sr ratios. In general Ba/Rb ratios > 15 and Rb/Sr ratios < 0.03 are an indication of severe alteration (Hofmann and White, 1983). In Figure 5.17 these ratios are plotted and it can be observed that some of the samples show signs of loss of mobile elements (values > 1 indicate moderate to severe alteration). The most affected samples are vesicular volcanics (KB686 and KB689), thin sills (KB680, KB682), or strongly foliated rocks (KB498, KB653, KB681).

5.4.4 Discussion of the geochemical results

5.4.4.1 Introduction

For the presentation of the geochemical data of the mafics rock samples, the following approach was taken. The AFM major element diagram is used to distinguish between tholeiitic and calc-alkaline rocks (Irvine and Baragar, 1971). The minor element oxides TiO_2 , MnO and P_2O_5 can also be used to subdivide basalts and basaltic andesites. These elements are regarded immobile in hydrothermal alteration and metamorphism up to lower amphibolite facies (Mullen, 1983). In addition, the trace elements La, Y and Nb can be used to discriminate between different types of basalt (Cabanis and Lecolle, 1989). Altered and metamorphic rocks may show some distortion relative to the La apex, because La is not fully immobile under metamorphic conditions. The Regal Formation is the only lithology of which sufficient samples were available to study fractionation trends, based on the major element oxides. Two representative variation diagrams, of Al_2O_3 and TiO_2 versus MgO, are used.

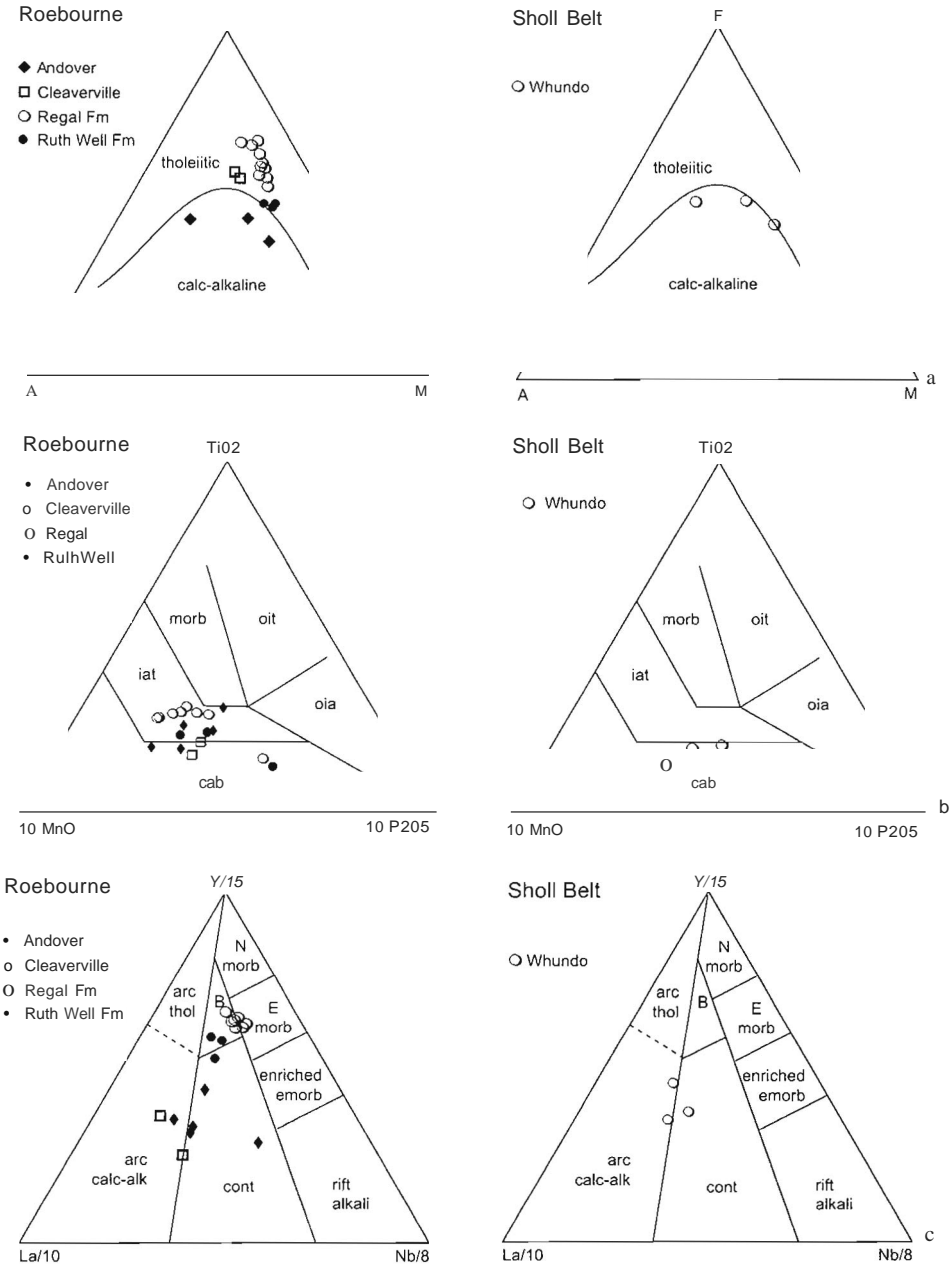


Figure 5.18. a) AFM diagrams (frvifle alld Baragar, 1971). b) IV/nO-TiO₂-P₂O₅ diagrams (Mul/ell, 1983). cab = calc-alkaline basalt, oia = oceanic island alkaline basalt, oit = oceanic island tholeiitic basalt. morb = mid ocean ridge basalt. iat = island arc tholeiite. c) La/10 - Y15 - Nb/8 diagrams (Cabanis and Lecolle, 1989). B = back arc basin.

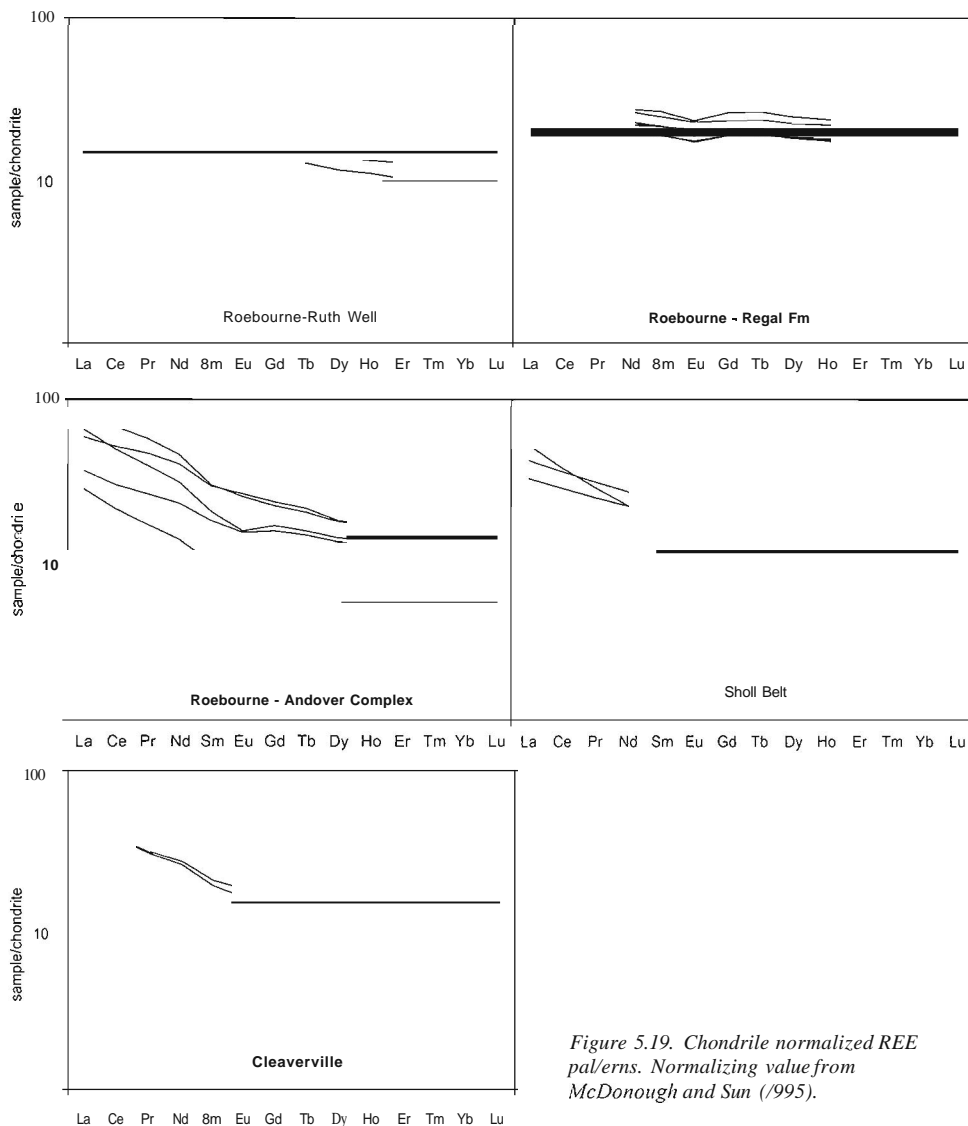


Figure 5.19. Chondrite normalized REE patterns. Normalizing value from McDonough and Sun (1995).

The trace element data are firstly discussed on the basis of REE patterns. This provides information about the mineral-melt equilibria that were present in the course of magma generation and crystallization. However, contamination may play a major role but this is difficult to distinguish from other processes. REE data normalized to chondritic values are useful in determining the amount of fractionation relative to the samples. MORB-normalized spidergrams of incompatible elements are used to determine the similarities and differences between the samples and MORB rocks. Furthermore, some selected trace elements are used to place further constraints on the tectonic regime and associated petrological processes.

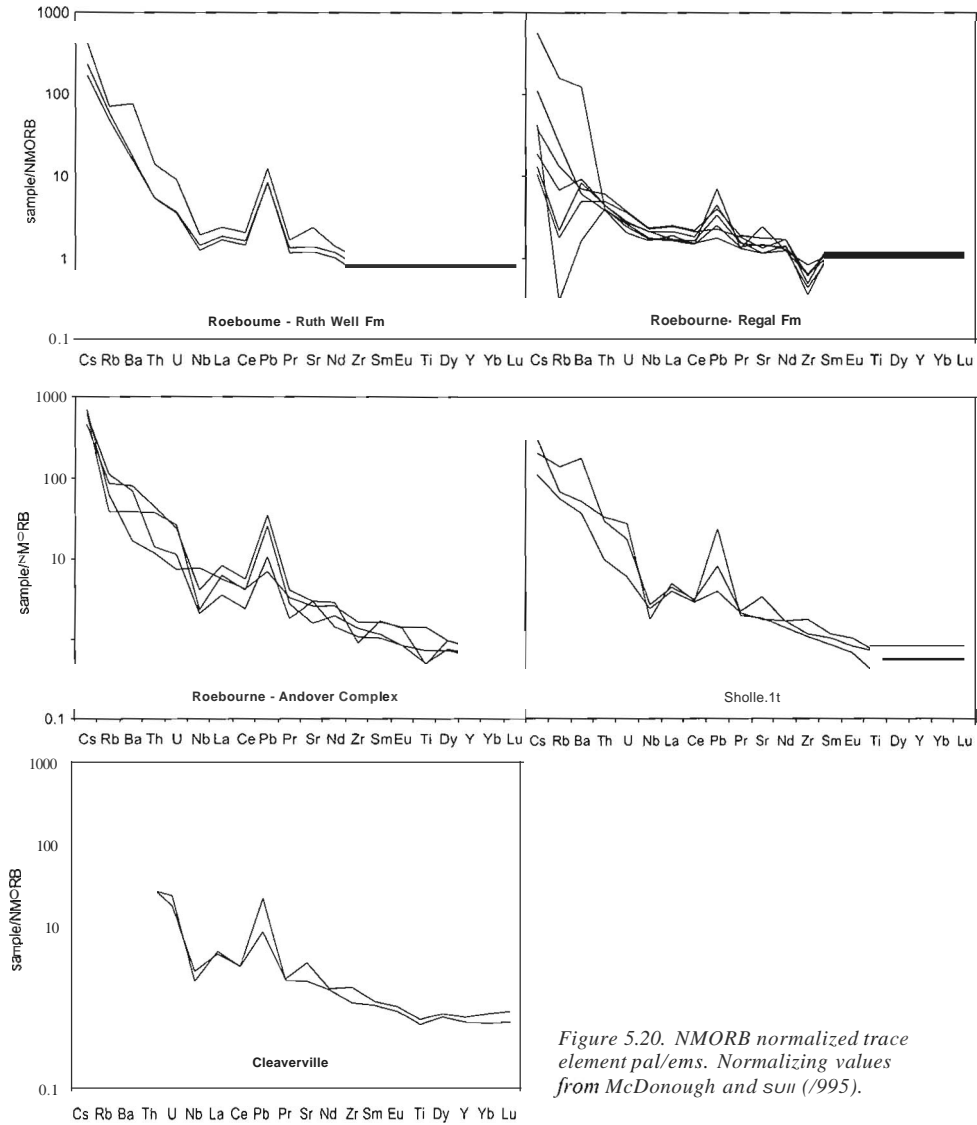


Figure 5.20. NMORB normalized trace element patterns. Normalizing values from McDonough and sun (1995).

5.4.4.2 Roebourne Domain

The Ruth Well Formation represents a series of basalts on the borderline of the tholeiitic and calc-alkaline field (Figure 5.18.a). On the Mullen (1983) triplot (Figure 5.18.b) they are classified as island arc tholeiites. The one anomalous sample comes from the contact with the Karratha Granodiorite and contact metamorphism may explain its higher P_2O_5 content. On the diagram of Cabanis and Lecolle (1989) the Ruth Well rocks plot on the borderline of arc-basalts, continental basalts and back-arc basalts (Figure 5.18.c). However, they have very low alkali contents and MgO of about 9%. This may indicate that their formation involved recycled primitive basaltic crust in combination with mantle material, to explain the high MgO, Ni and Cr contents (Appendix 5.8.4).

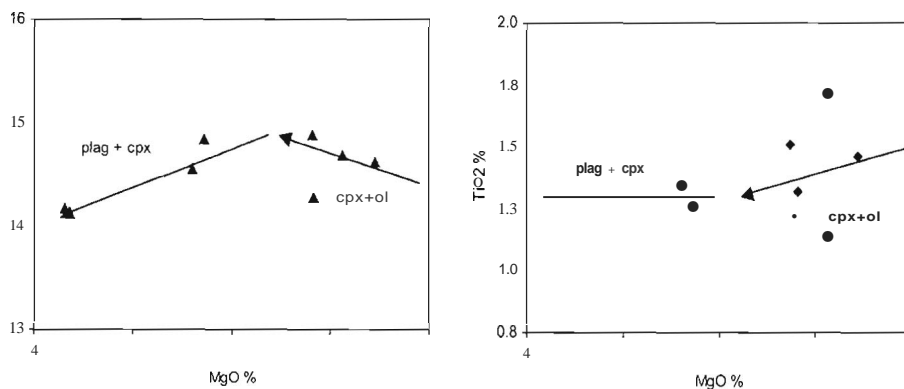


Figure 5.2/ a) Al_2O_3 vs. MgO for the samples from the Regal Formation in the Roeboume Domain.
 b) TiO_2 vs MgO for the Regal Formation.

The Ruth Well samples are slightly LREE enriched (Figure 5.19). The NMORB-normalized spidergram shows weakly negative Nb and Ti anomalies indicative of subduction zone magmatism (Figure 5.20). The fluid mobile (LILE) elements are enriched, but known to be mobile during alteration and metamorphism. The Nickol River Formation was not sampled, as it contains no mafic volcanic rocks.

The Karratha Granodiorite formed simultaneously with the Ruth Well Formation. It is HREE depleted, indicating the presence of garnet in the residue, i.e. depths greater than approximately 80 kilometers (Smith et al., 1998; Smith, 2003). They interpreted these rocks to be subduction-related. The negative Nb anomaly and positive Pb anomaly (although Pb is quite mobile) are also characteristic of subduction zone magmatism (Smith et al., 1998).

The samples of the Regal Formation form a series of Fe-rich tholeiitic basalts to basaltic andesites (Figure 5.18.a). In Figure 5.21.a and b the magma evolution shows a olivine plus clinopyroxene fractionation trend, followed by clinopyroxene plus plagioclase. In the Mullen (1983) diagram (Figure 5.18.b) the Regal Formation plots in the island arc tholeiitic field, but with higher TiO_2 levels than the Ruth Well Formation, closer to the MORB field. In the diagram of Cabanis and Lecolle (1989) the Regal Formation plots on the borderline of the enriched MORB field and back arc basalts (Figure 5.18.c). The basalts from the Regal Formation have flat REE patterns (Figure 5.19), but are overall somewhat more enriched than the rocks of the Ruth Well Formation. The more enriched samples have slightly negative Eu anomalies, which corresponds very well to the fractionation trends shown in Figure 5.21, which indicate that plagioclase fractionation started at a later stage.

The Regal Formation is overall slightly less enriched in REE than modern MORB, possibly as a result of a higher degree of partial melting in combination with a higher fertility of the mantle (Ohta et al., 1996a). The high field strength (HFS) elements show a relatively flat pattern in the NMORB-normalized diagram (Figure 5.20), except for a markedly negative Zr anomaly. These rocks do not have Nb or Ti anomalies. The positive Pb anomaly is possibly caused by the mobility of Pb; all samples show this anomaly. The LILE elements are strongly disturbed, but on average less enriched than those of the Ruth Well Formation.

The mafic rocks from the Andover Complex plot in the calc-alkaline field, and their major element composition is quite variable (Figure 5.18.a). In the Mullen (1983) diagram (Figure 5.18.b) they plot between the island arc tholeiitic and calc-alkaline basaltic fields. In the diagram of Cabanis and Lecolle (1989) the Andover Complex plots in the continental to calc-alkaline fields (Figure 5.18.c). They are strongly LREE enriched suggesting small melt fractions in the source rock (Figure 5.19). One sample has a positive Eu anomaly indicative of plagioclase accumulation. The negative Nb and Ti anomalies in Figure 5.20 is indicative of a source region affected by subduction zone metasomatism.

The samples from basalt of the Cleaverville Formation are tholeiitic (Figure 5.18.a), but slightly more calc-alkaline than the Regal Well Formation (Figure 5.18.b) and have arc-affinity (Figure 5.18.c) They are strongly LREE enriched (Figure 5.19). These rocks have no Eu anomaly, indicating their generation took place below the stability field of plagioclase, or under conditions of extremely high oxygen activity (Drake and Weill, 1975). Negative Nb and Ti anomalies (Figure 5.20) suggest a subduction setting. This is similar to the findings of Kiyokawa and Taira (1998).

5.4.4.3 Sholl Belt, Sholl-Whim Creek Domain

The samples from the Whundo Group in the Sholl Belt plot on the border of the tholeiitic and calc-alkaline fields in the major element plot (Figure 5.18.a). Their minor element composition indicates a calc-alkaline affinity (Figure 5.18.b) and the trace elements place them between calc-alkaline and continental basalts. They are LREE enriched (Figure 5.19) and have a weak negative Eu anomaly, indicating plagioclase fractionation. They are interpreted to have formed in an intracontinental setting. This is supported by the structural and field relations and is in accordance with the findings of Smith (2003) on coeval granites in the Sholl Belt.

5.4.4.4 Whim Creek Belt- Sholl-Whim Creek Domain

In this study no samples from the Whim Creek Belt were analyzed, because of the recent research of Pike et al. (2002). They suggested that the Whim Creek Group was formed in a continental volcanic arc setting. The slightly younger Bookingarra Group is more tholeiitic and has enriched LREE patterns, similar to the Whundo Group. They interpreted it to have formed in an intracontinental rift setting.

5.4.5 Summary & conclusions of geochemical results

The Ruth Well Formation are high-Mg arc tholeiites with a negative Nb anomaly. Combined with the reports of an island-arc affinity for the coeval Karratha Granitoid (Smith et al., 1998), it is interpreted that all ca 3265 Ma components of the Roeboume Domain were formed in a subduction zone setting.

The Regal Formation has characteristics that may indicate it has MORS-affinity. The higher degree of partial melting in the Archaean mantle, in combination with a higher fertility (Ohta et al., 1996a), may have resulted in a higher Fe and REE content. Its age is not known, and it presently occurs as a thrust sheet in the Roeboume Domain. It has been metamorphosed to amphibolite grade at ca 3150 Ma (see below) and is overlain by the essentially un-metamorphosed Cleaverville Formation of ca 3020 Ma. Therefore it must have been emplaced before ca 3150 Ma.

The basalts of the bimodal Whundo Group in the Sholl Belt has characteristics between calc-alkaline and continental. Field relations and the association with continental extensional granites (Smith, 2003) suggest they have formed in an intracontinental setting. Because they are more than

125 Ma younger than the arc-rocks in the Roebourne Domain, a back-arc setting for the Whundo Group during the same tectonic event is ruled out. However, the back-arc signature may be the result of modification of the mantle source during the earlier subduction event at ca 3265 Ma.

The Cleaverville Formation occurs in a large area in the West and Central Pilbara. The basalts are tholeiitic, but with calc-alkaline and arc-characteristics in their minor and trace elements. Their field relations and geochemistry do not provide a consistent clue to their origin.

5.5 Geochronology

5.5.1 Introduction

In this project, geochronology was applied to obtain temporal constraints on tectonic and thermal evolution of key areas identified from structural-kinematic analysis of the major and regional structures in the West and Central Pilbara. U-Pb zircon dating was applied to obtain information on the primary crystallization history of the area, and $^{40}\text{Ar}/^{39}\text{Ar}$ geochronology to obtain constraints on the late thermo-tectonic evolution.

Samples for $^{40}\text{Ar}/^{39}\text{Ar}$ laser probe geochronology were selected on the basis of suitability of location, structural relations and mineralogy. Sample description, location and reason for sampling can be found in Table 5.6. The selected samples were crushed, sieved and washed before mineral separation. Sieve fractions of 250-500 μm and 125-250 μm were selected. A roll magnet was used for hornblende separation. Sheet silicates were separated with a Faul-table separator. The remaining fractions were cleaned ultrasonically in demineralized water. Between one and fifteen clean single crystals of hornblende, biotite, or muscovite were selected per sample by handpicking under a microscope. Aluminium trays loaded with flux monitor standards and samples were stacked in an aluminium can and irradiated with high-energy neutrons for 75 hours in a rotating setup (RODEO) with a cadmium shield, in the ECNIEU high flux research nuclear facility in Petten, The Netherlands. The step-heating degassing experiments were carried out with an argon laserprobe as described by Wijbrans et al. (1995).

Zircons from only one sample from Balla Balla Beach was analyzed for U and Pb by laser ablation ICP-MS, at Utrecht University, the Netherlands. We used an adapted form of the method of Hom et al. (2000). Details on analytical methods and data reduction can be found in Beintema et al. (in press, see chapter 6). The sample description is given in Table 5.7. It was selected because it shows only evidence for dextral deformation on the Sholl Shear Zone: it's age will provide a minimum age for the sinistral deformation phase and a maximum age for the dextral deformation phase of the Sholl Shear Zone.

5.5.2 Results - geochronology

Sample descriptions and the results of all $^{40}\text{Ar}/^{39}\text{Ar}$ analyses are summarized in Table 5.6, sample locations are indicated in Figure 5.2 and Figure 5.3, and age spectra are shown in Figure 5.22. Detailed tables of the individual step-heating experiments can be found in Appendix 5.C (on CD-ROM). The identification of a plateau age is done according to the following criteria: a minimum of three contiguous steps of ages within 2σ error is required; these steps should yield a well-defined isochron; and a significant portion of the ^{39}Ar release must be during these steps (McDougall and Harrison, 1999).

Table 5.6. $^{40}\text{Ar}/^{39}\text{Ar}$ geochronology sample descriptions and results (2s errors). Semi plateau age and total fusion age in Ma. CPS localities in UTM, zone 50K, ACD66.

sample	location	expected cooling age result	GPS	min	semi-plateau	2s	% ^{39}Ar	total fusion	25
KB47	Ruth Well Fm: Karratha Road: contact aureole margin of Karratha	contact aureole Granodiorite	0484475	hbl	2940	37	60.9	2877	54
KB104	Regal Fm: Karratha Sialion: amph grade mafics hbl ml 295/68	amph grade metamorphic event in Roebourne Domain	0470501 7696179	hbl				2832	12
KB15	SSZ: Maitland River: late syntectonic pegmatite	late thermal overprint	0460060 7694323	mu				2895	8
KB20	SSZ: Maitland River: gabbro, vertical hbl lin	gneissic amphibolite grade north-side-up event in SSZ	0459970 7693405	hbl				2462	13
KB91	SSZ: Nickol River: deformed act diorite, act lin	syn-kinematic intrusion during dextral def.	0490430 7689470	act				1955	52
KB33	SSZ: Pipeline Road: granite	mylonitic dextral shearing	0499198 7689359	mu				1322	9
KB34	SSZ, Pipeline Rd, amp boudin, hbl lin	amphibolite grade north-side-up event in SSZ	0499413 7689195	hbl	3144	35	739	3125	50
KB37	Sholl Bell: Pipeline Rd: coarse andesite with actinolite	deposition of andesite	0501346 7687060	act				1767	52
KB119A	SSZ: Balla Balla: sheared granodiorite, tectonic muscovite	dextral shearing	0585785 7710100	mu	2831		94.9	2829	10
KB119B	SSZ: Balla Balla: sheared granodiorite, chloritized biotite	dextral shearing	0585785 7710100	bi				2704	10
KB118	SSZ: Balla Balla: undeformed granodiorite, chloritized biotite	granite intrusion	0585785 7710100	bi				2522	10
KB62	Whim Creek Belt, Sherlock River: gabbro	emplacement age of gabbro (late thermal event)	0573193 7680008	hbl				2979	34

It can be observed that very few samples have yielded good age plateaus. Many samples have yielded moderately to strongly disturbed age spectra, indicating that the area as a whole was disturbed in post-Archaeon times. The results seem to have suffered from the effects of excess argon, yielding anomalously high ages in the first few steps. This is a commonly observed feature in Archaeon hornblends. When compared to the results from earlier work in the East Pilbara (e.g. Wijbrans and McDougall, 1987; Davids et al., 1996; Zegers, 1996), more often severely disturbed spectra have been observed, showing evidence for Proterozoic overprinting. However, this effect seems to be much stronger in the West Pilbara. Plateaus and poor semi-plateaus were found in KBO15, KBI04, KBI19A, KB034 and KB047, whereas KB062 also yielded a late Archaeon minimum age. The results support a general late Archaeon cooling age for the area, with severe overprinting during the Proterozoic. The cumulative probability trend of all step heating analyses (Figure 5.23) shows maxima and 2750 Ma.

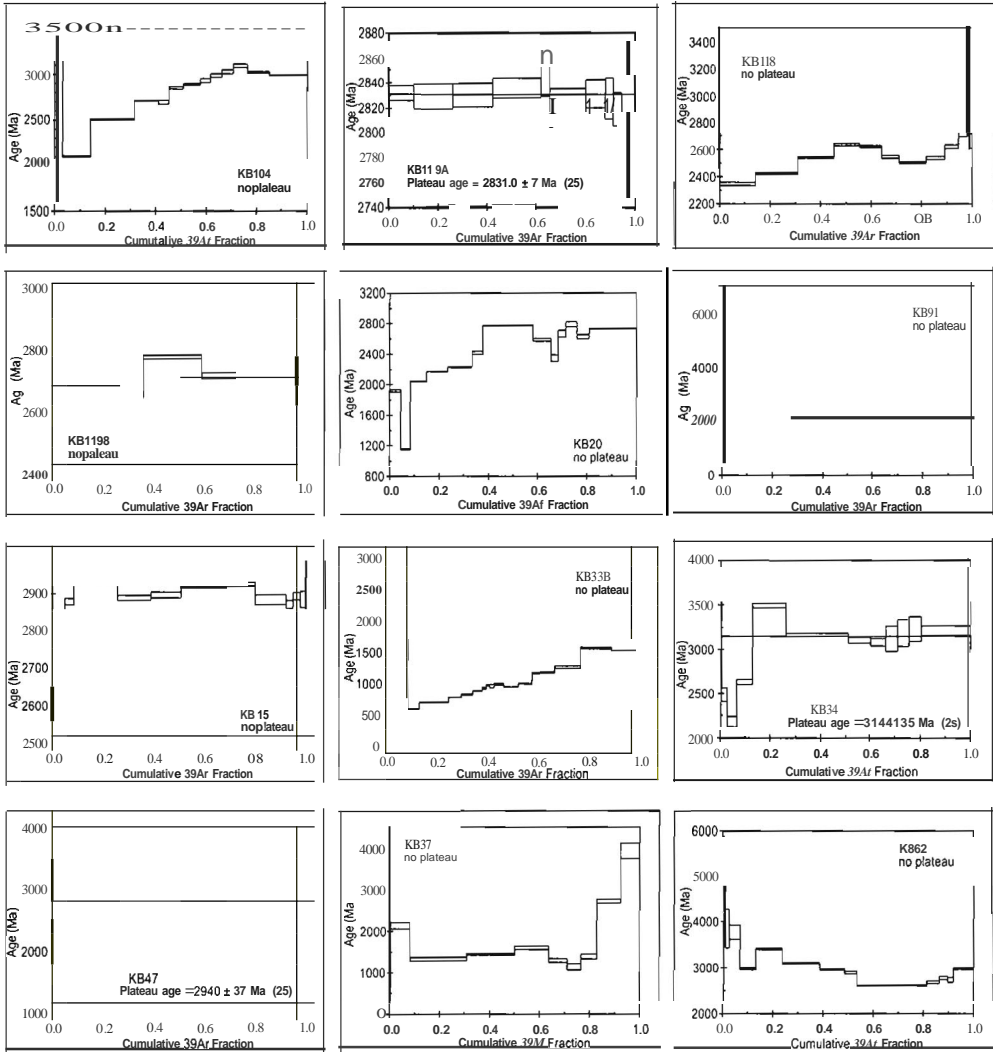


Figure 5.22. Age spectra of the $^{40}\text{Ar}/^{39}\text{Ar}$ analyses of samples from the West Pilbara.

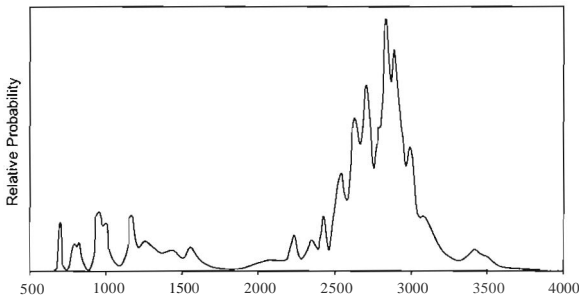


Figure 5.23. Combined cumulative probability pOI for all $^{40}\text{Ar}/^{39}\text{Ar}$ step-heating experiments performed on all samples from the Western Pilbara.

5.5.3 Discussion - $^{40}\text{Ar}/^{39}\text{Ar}$ geochronology

Sample KB034, from an amphibolite grade boudin within the deformed Ruth Well Unit just north of the Sholl Shear Zone, has yielded a semi-plateau at 3144 ± 35 Ma. This is interpreted as the cooling age of an amphibolite grade metamorphic event and simultaneous thrusting (D1) in the Roebourne Domain (see Table 5.3). Sample KB047, from the northern marginal shear of the Karratha Granodiorite, has an age 2940 ± 37 Ma, indicative of the time of cooling from dextral normal shear (and exhumation) activity on the shear zone.

None of the remaining analyses have yielded a plateau age. The combined trend of all analyses is plotted in Figure 5.23 and shows maxima at ca 2870 Ma and 2700 Ma. The first is interpreted to be related to thermal disturbance of the area at about 2860 Ma, which coincides with the intrusion of granites and pegmatites in the Central Pilbara (Blewett, 2002), although this seems a bit far away to cause a significant thermal effect in the West Pilbara. The second disturbance coincides with the subsidence of the Hamersley Basin and the intrusion of northeast-trending mafic dykes in the region.

The elevated curve between 2500 and 2000 may due to resetting at approximately 1900 Ma during the Capricorn Orogeny which involved deformation, metamorphism and magmatism due to collision of the Pilbara Craton with the Yilgarn Craton to the south (Tyler, 2000). Furthermore, there are mid- and late-Proterozoic disturbances at approximately 1200 and 900 Ma. The ca 1200 Ma disturbance corresponds to Grenville age activity which is also seen throughout Rodinia, and 900 Ma may correspond to very early Pan-African activity in East Gondwana (Rogers et al., 1995).

5.5.4 V-Ph zircon analyses

Zircon sample KB757 is a leucocratic vein from a granodioritic gneiss in the Sholl Shear Zone, collected at Balla Balla Beach Figure 5.3. The veins are the product of migmatization of the granodioritic gneiss. A few kilometers to the west, in situ generated melt has been observed. The veins are displaced by dextral shears within the gneiss. At this location Nelson (1997) dated a porphyritic gneiss at 3014 ± 3 Ma, which was interpreted as the age of the precursor granite. There is no evidence for sinistral deformation in the Sholl Shear Zone at any of these locations. Sample location is indicated in Figure 5.3; description and zircon morphology are summarized in Table 5.7.

The results of the laser ablation ICP-MS zircon dating of the sample from Balla Balla (Figure 5.3) is summarized in Table 5.7 and the Concordia plot is shown in Figure 5.24. The results of the

Table 5.7. U-Ph zircon geochronology sample description and results (2s errors). GPS locations in UTM, zone 50K, AGD66. The sample was selected to place a minimum age on the sinistral deformation and a maximum age on the dextral deformation on the Sholl Shear Zone.

Sample	KB757
location	0585771 Nt 7710142 E
description	leucocratic vein in granodiorite
zircon morphology	euhedral, some cracks and inclusions
color	milky, pink
size	60-120 μm
U/Pb Concordia age (# grains)	3014 ± 16 Ma (57)
$^{207}\text{Pb}/^{206}\text{Pb}$ (# grains)	3019 ± 12 Ma (57)
overprint (# grains)	2851 ± 40 Ma (8)
xenocrysts (# grains)	3167 ± 84 Ma (5)

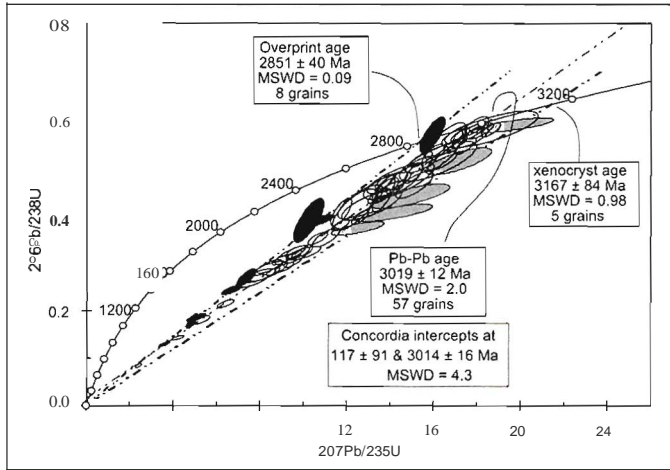


Figure 5.24. Concordia diagram of the LA-ICP-MS U-Pb analyses of sample KB757: main population of zircons is shown in open ellipses.

single analyses can be found in Appendix 5.D (on CD-ROM). The main population of zircons has an age of 3019 ± 12 Ma. This can either be interpreted to represent the migmatization event (if the zircons formed during migmatization) or it could be the time of igneous crystallization of the granodiorite (if the zircons in the leucocratic phase are all xenocrysts from the parent granodiorite). In either case, this provides a maximum age estimate for the dextral deformation phase in the Sholl Shear Zone, and a minimum age estimate for sinistral phase on the Sholl Shear Zone (see Table 5.3).

Sample KB757 has yielded a small population of zircon xenocrysts with a grouped age of 3167 ± 84 Ma. They could either represent the age of the granodiorite (from which the leucocratic vein was extracted) or they may originate from a precursor rock (the source of the granodiorite). This xenocrystic age approximately coincides with the age of the amphibolite grade metamorphic event in the Ruth Well, Nickol River and Regal Formations, and the inferred age of early north-directed thrusting within the Roebourne Domain (Kiyokawa and Taira, 1998). Smith (2003) reports voluminous granitoids of this age south of the Sholl Shear Zone.

5.5.5 Summary of geochronological results

Several studies have reported good Archaean $^{40}\text{Ar}/^{39}\text{Ar}$ ages from the East Pilbara (e.g. Wijbrans and McDougall, 1987; Davids et al., 1996; Zegers et al., 1999). However, the $^{40}\text{Ar}/^{39}\text{Ar}$ analyses presented here, have not yielded many plateaux of Archaean age. The possibility that this is due to sampling technique or the analytical methods has been excluded by running different batches and duplos. The data indicate that the West Pilbara was affected by either thermal, fluid alteration, or deformation events that reset its $^{40}\text{Ar}/^{39}\text{Ar}$ ages throughout the Proterozoic. It is interpreted to be caused by the geographical position of the West Pilbara, closer to the edge of the craton than the East Pilbara.

The LA-ICP-MS sample is part of a project that shows that laser ablation is a suitable method for *V-Pb* dating of Archaean zircons (Beintema et al., in press). The ca 3020 Ma age of the Balla Balla granitoid was previously unknown and has put a useful minimum age on sinistral deformation on the Sholl Shear Zone.

Table 5.8. Summary of tectonic history of the West Pilbara and adjacent Central Pilbara. Hypothetical tectonic scenarios are sketched in Figure 5.26.

Timing (Ma)	Regional stress regime	Event In West Pilbara	Tectonic setting	Roebourne Domain	Sholl Shear Zone	Sholl -Whim Creek Domain
ca 2760		06	continental extension	Dextral northeast trending brittle faults		Dextral northeast trending brittle faults
		05				Sinistral northeast trending brittle faults
ca 2930		04		Dextral deformation in lithological contact shears	Dextral Shear	
ca 2930		03	continental compression	Regional northeast trending folds	Thrusting	Regional northeast trending folds
ca 2970			continental extension	none		Deposition of Bookingarra Group and Mallina sediments
ca 2990						Main phase of Caines Well Granitoid
ca 3010			continental arc	granitoid intrusion		Deposition of Whim Creek Group
ca 3020			quiescence	Deposition of Cleaverville		Deposition of Cleaverville
pre 3020 ca 3120		D2	continental extension	Sinistral shear in lithological contacts	Sinistral shear	Deposition of Whundo Intrusion of granites
ca 3150		01		Folding and regional amphibolite grade metamorphism		
ca 3265			Subduction setting: active continental margin	Deposition of Ruth Well and Nickol R Fm Intrusion of Karratha Granodiorite Emplacement of Regal Fm (Ophiolite)		

5.6 Tectonic synthesis

The geological synthesis is summarized in Table 5.8. The oldest rocks in the West Pilbara are represented by the meta-basalt, talc schist and minor cherts of the Ruth Well Formation. The mafic rocks in this formation are high-Mg arc-type volcanics that share characteristics with calc-alkaline basalts and tholeiites. They are interpreted to have formed at a continental margin above a subduction zone. They are overlain by the metasediments, felsic volcanics and chert of the ~ 3265 Ma Nickol River Formation, which is coeval with intrusion of the Karratha Granodiorite which also has a subduction signature (Smith et al., 1998).

The major and trace element geochemistry of the pre-3150 Ma Regal Formation in the Roebourne area suggest it may represent Archaean ocean floor; however, it differs from modern MORB in its higher Fe and REE content, and lower Ti. This might be explained by a higher fertility of the mantle, and a higher degree of partial melting which started at greater depth than at present, and is what would be expected in the Archaean at a higher potential mantle temperature (see also Ohta et al., 1996a). The fact that these rocks occur as a thrust sheet in the Roebourne Domain suggests that they may have been emplaced as an ophiolite. The Regal Formation has not been dated. It may either have been emplaced during the ca 3265 Ma subduction event, or it may have been emplaced during the compressional and metamorphic event at ca 3150 Ma, described below. Absolute ages for the Regal Formation could potentially resolve this issue. In Figure 5.25 is argued that if the arc-setting is correct, most likely the West Pilbara was an active continental margin with subduction towards the south, at ca 3265 Ma, rather than a (later) accreted island arc.

The Ruth Well, Nickol River and Regal Formations were metamorphosed to amphibolite grade during a northwest directed phase of thrusting and crustal thickening at about 3150 Ma (Table 5.8). All lithological contacts became sheared at this time, and it is interpreted that the Sholl Shear Zone was formed and active at this time. There are no known extrusive or sedimentary rocks of this age or older, south of the Sholl Shear Zone. It is possible that they are not exposed due to down-dropping of the area south of the Sholl Shear Zone, during deposition of the 3120 Ma Whundo Group. However, Smith (2003) has reported extensive granite intrusion between 3160 Ma and 3130 Ma in the area south of the Sholl Shear Zone. Possibly these are associated with collapse following the 3150 Ma compressional event recognized in the Roebourne Domain, and the onset of intracrustal rifting associated with the deposition of the Whundo Group (Figure 5.26). The tholeiites of the Whundo Group are interpreted to have formed in a continental extensional setting (Table 5.8). The geochemistry of the accompanying granites supports this (Smith, 2003).

A phase of sinistral deformation affected the Sholl Shear Zone at an unknown time. The 3020 Ma rocks in the Sholl Shear Zone at Balla Balla show no evidence for sinistral deformation, indicating it took place prior to 3020 Ma. It is interpreted that it occurred earlier, at ca 3130-3115 Ma, creating a sinistral transtensional basin in which the Whundo Group was deposited (Figure 5.26). The vertical displacement on the Sholl Shear Zone may be as much as several kilometers. The eastern margin of this basin is presently unexposed, but it is interpreted that the Tabba Tabba Shear Zone, or structures now concealed in the Central Pilbara played a role in this. This will be further investigated in chapter 8.

The ca 3020 Ma Cleaverville Formation was deposited over a large area spanning the West and Central Pilbara. It occurs in the western part of the Whim Creek Belt at Mount Ada, and forms the youngest stratigraphic unit in the Roebourne area. Granites of similar age are abundant on either side of the Sholl Shear Zone, and have also intruded into the shear. The nature of this rock-forming event remains enigmatic, as on the one hand the Cleaverville Formation seems to suggest a period

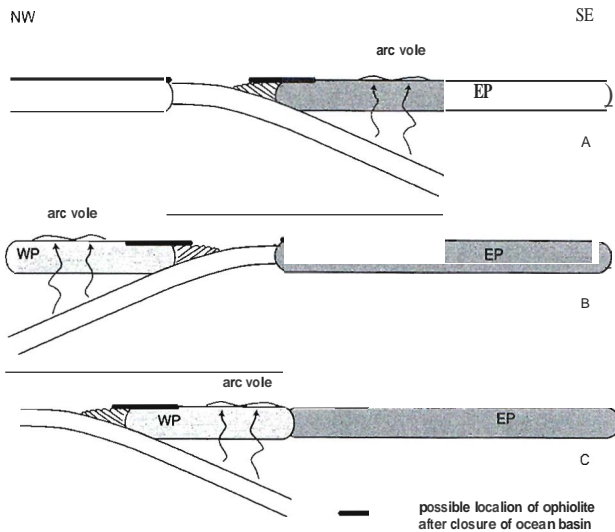


Figure 5.25. Possible tectonic scenarios at ca 3265 Ma. Accretion of the West Pilbara (WP) onto the East (and/or Central) Pilbara (EP) implies that an ocean basin was destructed in the middle. This can be done by southeast-directed subduction as indicated in A), but this would have resulted in ca 3265 Ma arc-like rocks and possibly ophiolites in the East Pilbara. This is not the case. In the case of north west-directed subduction as shown in scenario B) the arc-like rocks and ophiolites are in the correct place (the West Pilbara) but there should have been an accretion wedge between the West and Central Pilbara. In scenario C) the western part of the Pilbara was an active continental margin: all rock type associations are in the correct place. This is proposed as a working hypothesis.

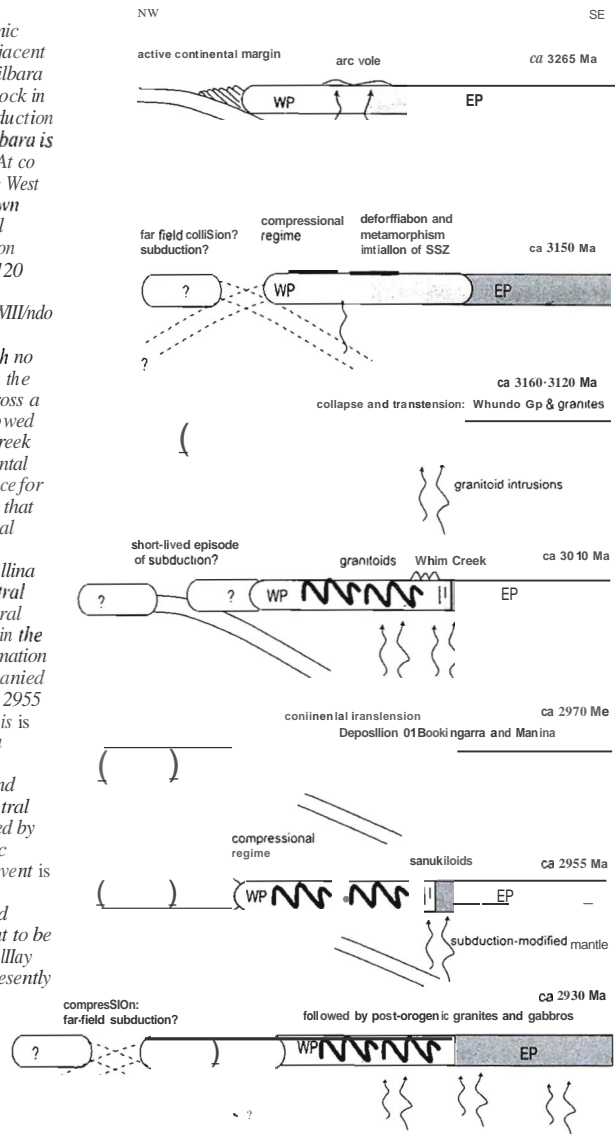
of quiescence across a large area, and on the other hand the area is intruded by granites. This occurred at the onset of a short episode of continental arc activity. According to Pike et al. (2002) the ca 3010 Ma Whim Creek Group may be related to a short-lived episode of compression in a continental arc setting (Figure 5.26).

The ca 2975 Ma Bookingarra Group formed at the onset of intracontinental transtension between the Sholl and Tabba Tabba Shear Zones. Continued continental transtension resulted in the development of the Mallina Basin in the Central Pilbara. During deposition of the ca 2970 Ma Bookingarra Group and Mallina sediments, sinistral-normal displacement occurred on the marginal shears of the Caines Well Batholith and northeast trending structures (Table 5.8). Barley (1987) suggested a sinistral transtensional setting for the Whim Creek Basin, however, at that time the age constraints were very poor and the tectonic setting has been reinterpreted as discussed above (e.g. Smithies, 1997a; Pike et al., 2002).

After deposition of the ca 2970 Ma sediments in the Mallina Basin, the whole of the Central and West Pilbara were affected by northwest-southeast directed compressional events at about between 2955 and 2930 Ma (Figure 5.26). During this event all structures were oversteepened. In the early stages this caused north-side up reverse movement on the Sholl Shear Zone, juxtaposing amphibolite grade units of the Roebourne Domain to low greenschist grade units of the Sholl Belt. In the Whim Creek area there is no evidence for reverse movement on the Sholl Shear Zone. It is interpreted that the Roebourne Domain was slightly tilted such that only the southwestern section was uplifted. This can also explain the decreasing metamorphic grade in the Regal Formation towards the northeast, at the present erosional level. This is illustrated in Figure 5.16.

During the later stages of the same event, at ca 2930 Ma, the now subvertical Sholl Shear Zone became active as a dextral transpressive structure, and a northwest-verging fold and thrust belt

Figure 5.26. Proposed tectonic evolution of the West and adjacent Central Pilbara. The East Pilbara (EP) is drawn in a solid block in the east. At ca 3265 Ma subduction from the northwest: West Pilbara is a continental volcanic arc. At ca 3150 Ma compression in the West Pilbara caused by an unknown event. Emplacement of Regal 'ophiolite' suggests subduction regime. Between ca 3160-3120 Ma collapse and sinistral transtension occur and the Willindoo Group is deposited. This is followed by a period of which no record exists. At ca 3020 Ma the Cleaverville is deposited across a large area, immediately followed by deposition of the Whill Creek Group, possibly in a continental arc. There is no other evidence for compression or subduction at that time. Subsequently continental transtension occurs and the Bookingarra Group and Mallina Fm are deposited in the Central Pilbara at ca 2970 Ma. Several phases of strike-slip activity in the Central Pilbara cause deformation of the Mallina Basin accompanied by granitoid intrusions at ca 2955 Ma. The tectonic cause for this is not known. At ca 2930 Ma a compressional phase cause northwest directed folding and thrusting throughout the Central and Western Pilbara, followed by the intrusion of post-orogenic granites. The cause of this event is unknown. For all of the compressional events far-field plate-interactions are thought to be the cause. Terrane accretion may have occurred outside the presently exposed granite-greenstone terrain, but this is highly speculative.



Details regarding the evolution of the Central Pilbara can be found in Chapters 6, 7 and 8.

developed across the West and Central Pilbara. The tectonic cause for this major and widespread event cannot be reconstructed from field evidence at present. The last intrusions (2925 Ma) in the area are calc-alkaline late to post-orogenic monzogranites and gabbros.

The area was thermally disturbed at approximately 2860 Ma, at which time granites and pegmatites were intruded in the Central Pilbara. The area was cut by northeast trending dextral brittle faults during the initial stages of the opening of the Hamersley Basin. Partly reset $^{40}\text{Ar}/^{39}\text{Ar}$ ages indicate the area remained susceptible to disturbance throughout the late Archaean and even the Proterozoic.

5.7 Summary and conclusions

The magmatic and structural history of the West and Central Pilbara indicate several major horizontal tectonic events affected the area in the mid-to late Archaean. A model is proposed where the West Pilbara represents a continental volcanic arc at 3265 Ma, when the Ruth Well and Nickol River Formations were formed. The undated Regal Formation has MORB-like characteristics. It was emplaced onto the older components of the Roeboume Domain by thrusting. This phase of thrusting took place at about 3150 Ma, as indicated by $^{40}\text{Ar}/^{39}\text{Ar}$ geochronology, and was associated with high amphibolite grade metamorphism. The underlying (tectonic) cause of this major event probably lies outside of the presently exposed granite-greenstone terrain and can not be reconstructed with the data presented in this chapter.

Sinistral displacement occurred along the Sholl Shear Zone prior to 3020 Ma, because granitoids of that age show no evidence for sinistral deformation. It is interpreted that the sinistral displacement occurred possibly during deposition of the Whundo Group at ca 3120 Ma, in an intracontinental transtensional zone in the Central Pilbara. After deposition of the Cleaverville Formation across large areas in the West and Central Pilbara, the Whim Creek Group was deposited south of the Sholl Shear Zone, possibly in a short-lived continental volcanic arc setting (Pike et al., 2002). Then the transtensional continental rifting continued and the Mallina Basin was formed. At ca 2930 Ma a major compressional event affected the whole of the West and Central Pilbara, resulting in the formation of a northwest verging fold and thrust belt, and ending with dextral transpressional deformation of all pre-existing structures. Finally, the area was intruded by calc-alkaline late to post-orogenic monzogranites and gabbros at ca 2925.

Acknowledgements

I would like to thank the Dr. Schtirmann Fund for their financial support of the field work with grant numbers 1998114, 1999114, 2000114a and 2001114a and the Molengraaff Fund for their financial support of the field work in 1998-2001. Dr. R.H. Smithies and Dr. A.H. Hickman are thanked for providing GSWA imagery and air photos. Dr. R.S. Blewett is thanked for providing geophysical imagery in a collaborative program with AGSO. I would like to thank Dr. Herman van Roermund, Diana de Leeuw, Pieter Bruijnen, and Stephanie Veltkamp for their company and assistance in the field.

New constraints on the timing of tectonic events in the Archaean Central Pilbara Craton, Western Australia.

This manuscript has been published as Beintema, K.A., Mason, P.R.D., Nelson, D.R., White, S.H. and Wijbrans, J.R., 2003. New constraints on the timing of tectonic events in the Archaean Central Pilbara Craton, Western Australia, *Journal of the Virtual Explorer*, and is available on line at <http://virtualexplorer.com.au/>
The manuscript is reprinted in this thesis with permission of the publisher.

Abstract

The Archaean Pilbara Craton in Western Australia has a domainal architecture which has been interpreted to reflect a history of accretion. The Tabba Tabba Shear Zone is the major division between the East and West Pilbara blocks: this interpretation is based on significant differences in the tectono-thermal histories of the bordering terranes. New laser ablation ICP-MS and SHRIMP U-Pb zircon geochronological data, coupled with trace element data for the same core parts of the sampled mineral grains, indicate a range of magmatic crystallization ages for representative igneous rocks emplaced before, during or after shearing. Results from both dating techniques agree for two separate homogeneous samples to within analytical error (2σ). Our data indicate that a granodioritic suite intruded the area at about 3250 Ma, followed by gabbroic suite at 3235 Ma. The area was subsequently affected by an early dextral compressive event during which the Tabba Tabba Shear Zone was formed, and the granodiorites and gabbros were incorporated into the Tabba Tabba Shear Zone. A granitoid suite intruded the shear zone at 2940 Ma, with xenocrystic populations of 3115 Ma and 3015 Ma, a possibly West Pilbara association. The East and West Pilbara terranes may thus have been relatively close to each other between 3250 and 3115 Ma.

The Tabba Tabba Shear Zone currently forms the eastern bounding fault of the Mallina Basin. The last major activity in the structure occurred during a major phase of oblique movement, corresponding to closure of the Mallina Basin. Ages of late syn-kinematic granitic intrusions indicate that this occurred at about 2940 Ma.

6.1 Introduction

The Pilbara Craton in the north west of Western Australia (Figure 6.1) comprises a mid-Archaean granite-greenstone terrane and the overlying late-Archaean volcano-sedimentary sequence of the

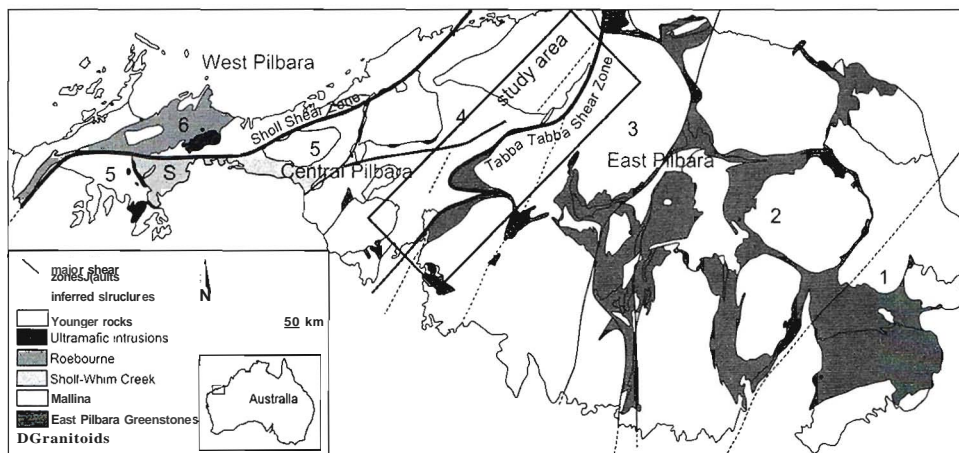


Figure 6.1. The Archaean Pilbara Craton in Western Australia. The study areas are indicated. The six domains of Krapez and Eisenlohr (1998) are also shown: 1 = Nullagine Domain, 2 = Marble Bar Domain, 3 = Pilgangoora Domain, 4 = Mallina Domain, 5 = Sholl-Whim Creek Domain, 6 = Roeboume Domain. Van Kranendonk et al. (2002) include the Sholl Belt (S) in the West Pilbara. Blewett (2002) regards the Sholl Shear Zone as the boundary between the West and Central Pilbara. This is adopted in this study.

Hamersley Basin. This study is concerned only with older tectonic processes during the construction of the granite-greenstone terrane. The Tappa Tappa Shear Zone (Figure 6.2) has historically been interpreted as the major division between the East and West Pilbara because of the different tectono-thermal histories of the bordering terranes. Rocks to the west have no pre- 3.3 Ga history: the 3.5 Ga Coontenmah Group (Buick et al., 1995) and 3.47-3.43 Ga Warwoona Group (Hickman, 1999) do not occur to the west of this shear zone, and the 3.45 and 3.3 Ga tectonic events recorded in the East Pilbara (White et al., 1998) have not been recognized in the West Pilbara.

Barley (1997) suggested that the Tappa Tappa Shear Zone is the boundary along which the West Pilbara Terrane was accreted onto the East Pilbara Terrane at about 2.9 Ga. This interpretation was adopted by Blewett (2002). However, our observations (Beintema et al., 2001) suggest that the East Pilbara granite-greenstone terrane may have been connected with the West Pilbara granite-greenstone terrane prior to 2.9 Ga.

This study aims to better constrain the timing of tectonic activity in the Central Pilbara, by dating major magmatic events related to activity on the shear zone. Laser ablation ICP-MS and SHRIMP U-Pb techniques have been applied to date rocks taken from key locations, previously identified from structural-kinematic analyses (Beintema et al., 2001). Regional and structural relationships based on detailed field mapping in combination with the geochronology provide time-constraints on the tectonic history.

6.2 Geological setting

The Tappa Tappa Shear Zone is a major structural and compositional discontinuity that can be traced from northeast to southwest across the central part of the Pilbara Craton (Figure 6.1). The structure has a maximum width of approximately 2 km (Figure 6.2) and separates sedimentary units

of very low metamorphic grade (the Mallina Basin) at its western margin from migmatitic gneisses (Carlindi Granitoid Complex) at its eastern margin.

Analysis of aerial photographs has revealed a regional foliation rotating into the Tabba Tabba Shear Zone (Figure 6.2). Field data show that the shear zone has experienced an early phase of compressional deformation with a dextral component (Beintema et al., 2001). The structural field data also indicate a major phase of sinistral oblique movement, overprinting most of the pre-existing structures in the shear zone and bringing the southeast block up relative to the northwest. Minor late brittle dextral deformation has overprinted the major sinistral phase. This phase may correspond to closure of the Mallina Basin (Beintema et al., 2001). After deformation had ceased, the central part of the Pilbara Craton was intruded by large volumes of post-tectonic monzogranite, between at ca 2930 Ma (Smithies et al., 2001).

The Tabba Tabba Shear Zone has been intruded by a suite of granodiorites, a suite of primitive mantle-derived gabbros and a later, more voluminous suite of gabbros derived from an enriched mantle source (De Leeuw et al., 2001). This suggests the Tabba Tabba Shear Zone was part of a major crustal scale structure that enabled melts to rise from the subcontinental lithospheric mantle.

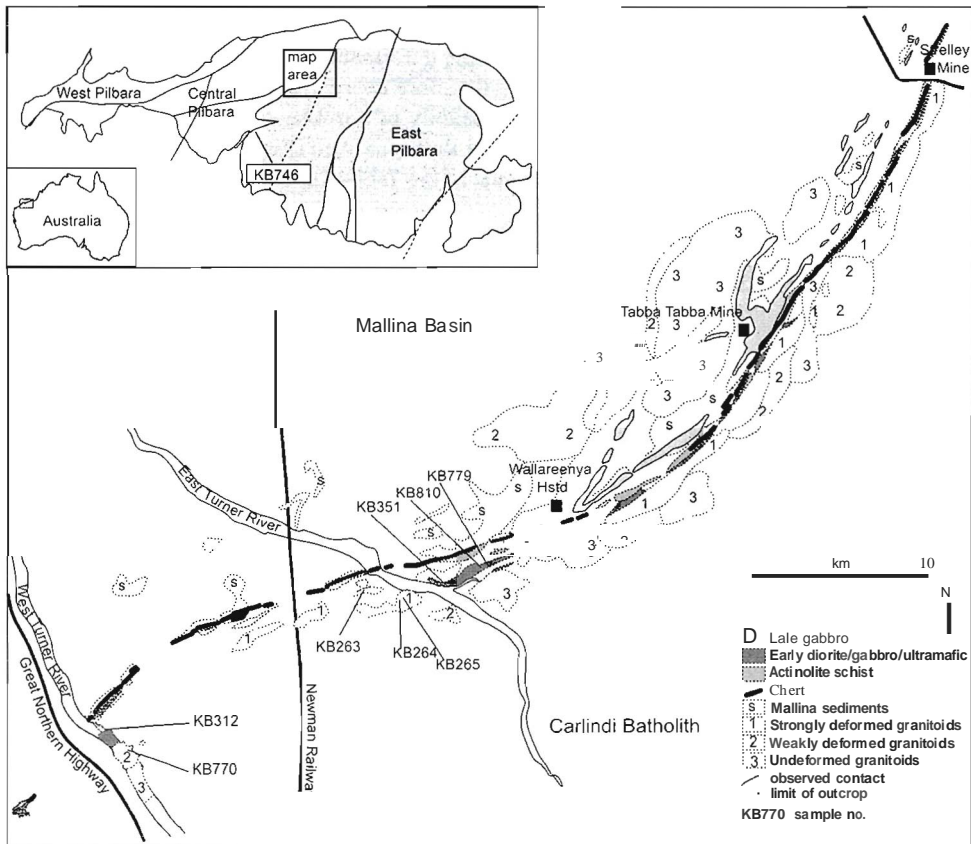


Figure 6.2. Simplified map of the exposed central section of the Tabba Tabba Shear Zone. Lithology based on 1:100,000 geological map (Smithies, 2000) and aerial photograph interpretation. Geochronology sample locations are indicated.

6.3 Sample descriptions

The sampling locations, rock type and mineralogy of the samples are given in Table 6.1 and Figure 6.2. An overview of the zircon morphologies for all samples is given in Table 6.2. Sample KB263 is a quartz-muscovite schist collected from the Tabba Tabba Shear Zone at the East Turner River (Figure 6.2). It is enclosed in quartz-albite-actinolite-chlorite schists. Based on petrology and chemical composition (De Leeuw et al., 2001) these schists are interpreted to be deformed and metamorphosed granites and granodiorites. Sample KB312 is a quartz-muscovite schist from the same suite, collected at the West Turner River. These supracrustal rocks are incorporated in the south eastern side of the Tabba Tabba Shear Zone. They form the footwall and we interpret them to have originated from a crustal block now east of, and possibly also underlying the Mallina Basin.

Samples KB265 and KB264 were collected from the southern part of the Tabba Tabba Shear Zone at the East Turner River (Figure 6.2). They are a metagranodiorite and a metagranite respectively. Both rock types are moderately foliated and lineated. The orientation of their foliation is consistent with an early dextral phase of deformation in the Tabba Tabba Shear Zone, but the lineation in high-strain zones is parallel to that of the major sinistral phase of movement on the Tabba Tabba Shear Zone. Their magmatic ages must therefore predate early deformation of the shear zone. The granite has intrusive contacts with the granodiorite, and is therefore expected to be younger.

Sample KB779 is a metadiorite consisting mainly of hornblende and plagioclase. It was collected from within the Tabba Tabba Shear Zone at Balbryna Well (Figure 6.2). The metadiorite occurs in elongate lenses along the southeastern side of the Tabba Tabba Shear Zone in the section

Table 6.1. Sample locations and descriptions. GPS locations in UTM, zone 50K. Australian geodetic grid /966.

Sample	Location	GPS	Rock type	Mineralogy	Freshness
KB263	East Turner River,	0678504	Muscovite schist	qtz, muse	moderate
	Poonthuna Pool	7699525			
KB264	East Turner River,	0678610	Foliated granite	qtz, pig, muse, bio	very fresh
	Poonthuna Pool	7699349			
KB265	East Turner River,	0678876	Foliated granodiorite	qtz, pig, bio, hbl	very fresh
	Poonthuna Pool	7699316			
KB312	West Turner River,	0663537	Muscovite schist	qtz, muse	moderate
	Red Rock Pool	7691680			
KB351	East Turner River,	0682167	Aplitic vein	qtz, pig, muse, garnet	moderate
	Balbryna Well	7699555			
KB746	Yandeyarra, Black	0642906	Granite	qtz, pig, kfs, muse, bio	very fresh
	Gin Well	7654053			
KB770	West Turner River,	0664812	Granite	qtz, pig, kfs, muse, bio	moderate
	Red Rock Pool	7690743			
KB779	East Turner River.	0684277	Foliated metadiorite	hbl, pig, qtz, garnet	very fresh
	Balbryna Well	7700096			
KB810	East Turner River,	0684259	Gabbro	01, OpX, tic, srp, chi, opq	moderate
	Balbryna Well	7700190			

Table 6.2. Zircon morphology.

sample	size	shape	Internal structure	clearness	color
KB263	60-120 μm	euohedral	Inclusions, zoning	medium	yellow
	60-120 μm	square	Rounded cores, zoning	clear	pink
KB264	90-140 μm	euohedral	Sub rounded cores, zoning	clear	pink
KB265	90-140 μm	euohedral, elongate	Cracks along length, zoning	medium	pink
KB312	60-120 μm	euohedral	Oscillatory zoning	medium	yellow
	60-120 μm	square	Rounded cores, zoning	clear	pink
KB351	60-140 μm	euohedral, elongate	Oscillatory zoning	medium	yellow-brown
	60-140 μm	euohedral, elongate	Oscillatory zoning	medium	pink
	30-90 μm	round, fragments	Oscillatory zoning	medium	orange
	30-90 μm	subhedral	no structure at all	milky	yellow-White
KB746	90-120 μm	euohedral, elongate	Cores, oscillatory zoning	clear	pink
KB770	90-120 μm	rounded	Zoning, cracks, inclusions	milky	yellow
	90-120 μm	euohedral	Cores. oscillatory zoning	clear	pink
	90-120 μm	euohedral (fragments)	Zoning, inclusions	medium	yellow
KB779	60-120 μm	euohedral	Oscillatory zoning	clear	pink
	60-120 μm	euohedral (fragments)	no structure at all	medium	pink
KB810	60-120 μm	round (fragments)	Oscillatory zoning	milky	pink
	60-120 μm	round (fragments)	no structure at all	medium	pink

near the East Turner River. Sample KE810 is a metagabbro with relics of olivine and orthopyroxene. Most of the rock now consists of talc, serpentine, chlorite and opaque minerals. The sample was collected from the Tabba Tabba Shear Zone at Balbryna Well, near sample location *KE9*. The metagabbro occurs in lenses that are up to a few hundred meters long and up to 50 meters wide, and is closely associated with the metadiorite of sample *KB9* as it only occurs inside the lenses of metadiorite. Both rocks are expected to be younger than the quartz-muscovite schists and metagranite-granodiorite, as the metadiorite has been observed to have intruded the metagranite-granodiorite.

Sample *KEO* is a granite from Red Rock Pool, just south east of the Tabba Tabba Shear Zone in the West Turner River (Figure 6.2). This granite is weakly deformed. Pegmatites associated with it intrude the Tabba Tabba Shear Zone at a low angle and are moderately deformed. They do not show evidence for deformation as a result of the early dextral phase of movement on the structure, supporting a younger age. These intrusions do show evidence for deformation related to the major sinistral phase and must therefore have been emplaced between the two tectonic events. This granite is interpreted to have caused the observed contact metamorphism in the schists in the West Turner River.

Sample KB351 is an aplitic vein from the central part of the Tabba Tabba Shear Zone. It is moderately deformed and therefore interpreted to have intruded late syn-kinematically during the major sinistral phase (Beintema et al., 2001). It is expected to provide a minimum age for this major phase of activity of the Tabba Tabba Shear Zone. As it is a thin vein it is expected to have picked up xenocrysts before or during emplacement, and thus may provide information on the ages of the underlying rocks.

Sample KB746 is a weakly foliated K-feldspar porphyritic biotite monzogranite from Yandeyarra. It occurs on the eastern boundary of what has been interpreted to be the southerly

extension of the Tabba Tabba Shear Zone (Figure 6.1). The age of this late syn-kinematic granite constrains the last stages of movement of this part of the structure. This section is not linked in outcrop to the main part of the Tabba Tabba Shear Zone, but it does show a similar structural and tectonic history.

6.4 Analytical procedures

6.4.1 Sample preparation

Sample locations were selected on the basis of structural relations and the availability of suitable rock types. All samples showed evidence for at least low greenschist grade metamorphism. At each locality 20 kg was sampled of the freshest available rock. Mineral separation was done at the Vrije Universiteit, Amsterdam. The process involved crushing, sieving, cleaning, density and magnetic separation, and hand-picking of the final fractions. The selected grains were mounted in epoxy and polished to expose the interiors of the grains.

The SHRIMP mounts were evaporatively coated with high purity gold. The LA-ICP-MS mounts were carbon-coated for electron microscope imaging. Cathodoluminescence (CL) and Scanning Electron Microscope (SEM) images of the grains were made on a Philips XL30 SEM, to identify inclusions, inhomogeneities and zoning.

6.4.2 Laser ablation ICP-MS U-Pb zircon analysis

Laser ablation ICP-MS measurements were performed at Utrecht University, The Netherlands, in February 2002 and November 2002. We used the method of Horn et al. (2000) that employs simultaneous laser ablation and solution nebulization to correct for instrumental mass discrimination and laser related elemental fractionation. A standard solution containing a known concentration and isotopic composition of both Th and U was used to correct for mass bias, eliminating the need for an external (solid) standard. The system hardware is described in detail by Mason and Kraan (2002). It consists of a Microlas Geolas 200Q 193 nm excimer laser ablation system (Gunther et al., 1997) with optics designed to ensure a flat energy density profile across the beam at the point of ablation.

Table 6.3. Mean TIMS V-Pb zircon data for the 91500 zircon standard (from Wiedenbeck et al., 1995).

	$^{201}\text{Pb}/^{238}\text{U}$	$^{206}\text{Pb}/^{238}\text{U}$	$^{207}\text{Pb}/^{206}\text{Pb}$
Ratio	1.8502	0.17917	0.07488
Age (Ma)	discordant	1065.4 ± 0.6	1062.4 ± 0.8

Table 6.4. Mean TIMS V-Pb zircon data for the eZ3 zircon standard (from Nelson, 1997).

	$^{207}\text{Pb}/^{235}\text{U}$	$^{206}\text{Pb}/^{238}\text{U}$	$^{207}\text{Pb}/^{206}\text{Pb}$	U (ppm)
value	0.743	0.0914	0.05892	551
Age (Ma)	563.3 ± 1.0	562.8 ± 1.2	565.5 ± 1.5	

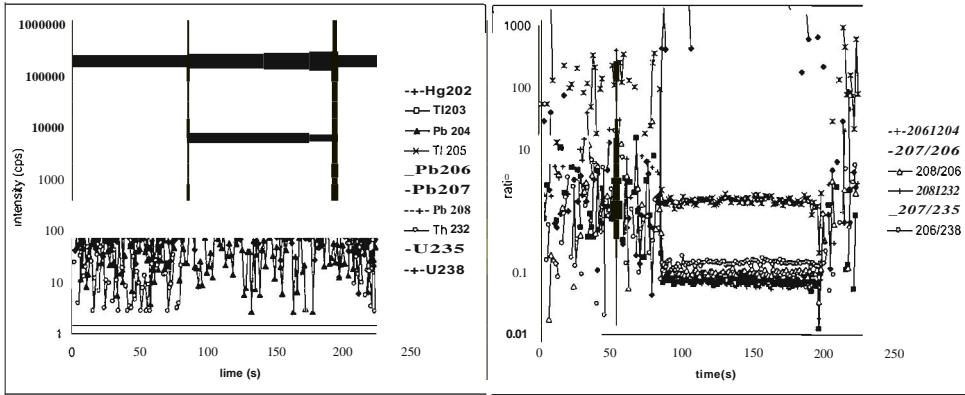


Figure 6.3. Typical example O/O laser ablation signal. the laser was switched on after ca 80 seconds O/O measuring the background signal. The laser was switched off at ca 180 seconds. a) Count rates vs time. b) Isotope ratios vs time.

Energy density at the sample surface was constant during all experiments at 6 mJ/cm^2 per pulse and different apertures produced ablation crater sizes of 20, 30, 40, 60, 80 and $120 \mu\text{m}$. Samples were ablated with a laser pulse repetition rate between 5 and 10Hz. The sample cell was purged with He (0.45 l/min) which was then mixed with Ar (0.65 l/min) carrying the nebulized TI-U standard solution before injection into the rCP-MS (Micromass Platform rCP). This quadrupole-based mass spectrometer has only one ion lens, which reduces the possibility to minimize mass bias but gives a very stable response over time. Typical sensitivity was approximately 9000 cps per ppm at $m/z = 238$ for the 91500 standard zircon at a laser pulse repetition rate of 10Hz and with a $120 \mu\text{m}$ crater. The formation of uranium oxides was kept to a minimum; the ratio of UO^+/U^+ was less than 4% during all analyses.

Each zircon analysis started with 60 seconds of background signal measurement before the laser was switched on. Standard zircon 91500 (Table 6.3) and in-house standard CZ3 (Table 6.4)

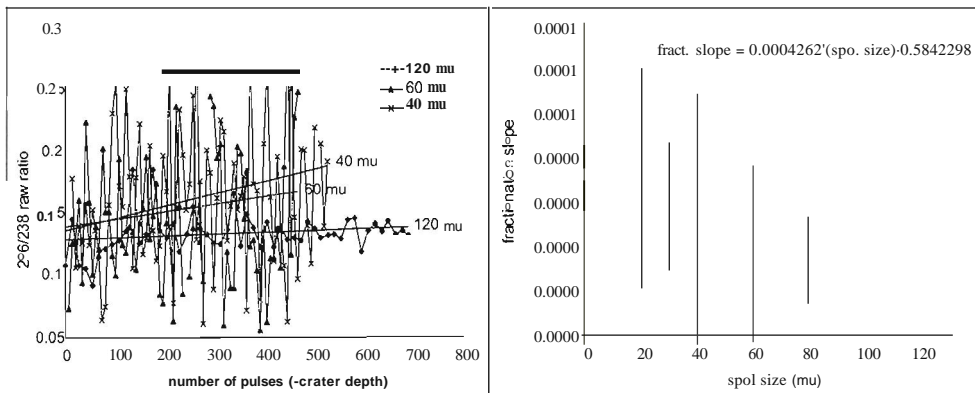


Figure 6.4. The fractionation slope or LA-ICP-MS analyses was determined on the standard, by plotting a) raw isotope ratios vs. crater depth. and b) fractionation slope vs. crater diameter.

were measured for 100 seconds. Sample measurements lasted as long as was allowed by the thickness of the mineral with a maximum analysis time of 200 seconds. A typical example of a laser ablation signal is shown in Figure 6.3. The raw time-intensity laser ablation spectra were processed using a modified version of the LAMTRACE spreadsheet program (Jackson, 1997). Laser induced fractionation can be related to the ablation crater geometry (Mank and Mason, 1999; Hom et al., 2000) and a correction factor was calculated using the standard data and applied as shown in Figure 6.4. A common Pb correction was applied as outlined below using the abundance of ^{204}Pb following a correction for the isobaric overlap of ^{204}Hg using ^{202}Hg and assuming $^{202}\text{Hg}/^{204}\text{Hg}$ to be 4.35. The calibration of Pb-Pb and U-Pb ages was checked against the 91500 zircon.

6.4.3 SHRIMP V-Pb zircon analysis

Sensitive High Resolution Ion Micro Probe (SHRIMP) measurements were performed on the facility at the Department of Applied Physics, at Curtin University of Technology in Perth, Western Australia in February 2001. Analytical procedures and data processing are described in detail by Nelson (1997).

Before every analysis the mount surface was cleaned to reduce the amount of common lead present. This was done by rastering the primary beam across the mount surface for at least two minutes. During the analysis the secondary ion beam was focused into an electron multiplier by switching the magnetic filter and moving the ion collector appropriately for the species of interest. Ten ion species were measured consecutively in seven cycles. During every cycle the following measurements were made: $^{90}\text{Zr}^{16}\text{O}^+$ (2 secs), $^{204}\text{Pb}^+$ (10 secs), background at 204.1 (10 secs), $^{206}\text{Pb}^+$ (10 secs), $^{207}\text{Pb}^+$ (20 secs), $^{208}\text{Pb}^+$ (10 secs), $^{238}\text{U}^+$ (5 secs), $^{232}\text{Th}^{16}\text{O}^+$ (5 secs), $^{235}\text{U}^{16}\text{O}^+$ (2 secs) and $^{238}\text{U}^{16}\text{O}_2^+$ (2 secs). A common Pb correction was applied as described below.

Isobaric interference in SHRIMP analysis arises from the formation of hydrides; e.g. $^{206}\text{Pb}^1\text{H}^+$ interferes with $^{206}\text{Pb}^+$. The occurrence of these species was monitored by comparing the ^{206}Pb corrected ratios on the standard, with the assumed value of 0.0592. It was not necessary to apply a correction to any of the samples in this study.

Analyses that were concordant, or which defined a recent lead-loss trajectory were pooled on the basis of their $^{207}\text{Pb}/^{206}\text{Pb}$ ages. Individual analyses were rejected if they were highly discordant and on the basis of unusual zircon morphology (e.g. shape, zonation, cracks, lattice damage).

The errors reported on individual analyses in this study are based on counting statistics, include the scatter on the $^{206}\text{Pb}/^{238}\text{U}$ versus $^{206}\text{Pb}/^{235}\text{U}$ calibration curve, and include the errors introduced by the common Pb correction. Errors on the pooled ages include the uncertainty in the reproducibility of the Pb/U values in the standard.

6.4.4 V-Pb data processing

Analyses with large errors that can be attributed to the presence of zoning, cracks and inclusions in the analyzed zircon, were rejected from the dataset. All LA-ICP-MS analyses with an integration interval shorter than 20 seconds were rejected because of poor counting statistics. In some cases it was possible to use separate integration intervals in the LA-ICP-MS data to exclude disturbances, but when the intervals were shorter than 20 seconds those analyses were rejected. High uranium content may cause a zircon to become metamict due to destruction of the crystal lattice by radiation. This enhances the mobility of U and especially Pb. As a consequence, high uranium content was also a reason for rejection of some analyses.

A correction was applied for common Pb on the basis of the abundance of ^{204}Pb , which was typically 10 ppm in all standards measured and variable in the samples. This was assumed to be common lead from the mount surface and a correction as described by Compston et al. (1984) was applied, assuming the common Pb component to have the isotopic composition of Broken Hill Pb ($^{204}\text{Pb}/^{206}\text{Pb}=0.0625$, $^{207}\text{Pb}/^{206}\text{Pb}=0.9618$ and $^{208}\text{Pb}/^{206}\text{Pb}=2.2285$). Pooled $^{207}\text{Pb}/^{206}\text{Pb}$ ages and upper intercept U-Pb concordia ages were calculated using Isoplot (Ludwig, 2003). Cumulative probability diagrams were used to identify different populations within samples. Concordia diagrams show the U-Pb upper intercept ages and the degree of discordance. All samples show discordancy trends that are consistent with radiogenic Pb-loss at zero age. A summary of the interpreted ages is given in Table 6.5. All errors are 2σ errors.

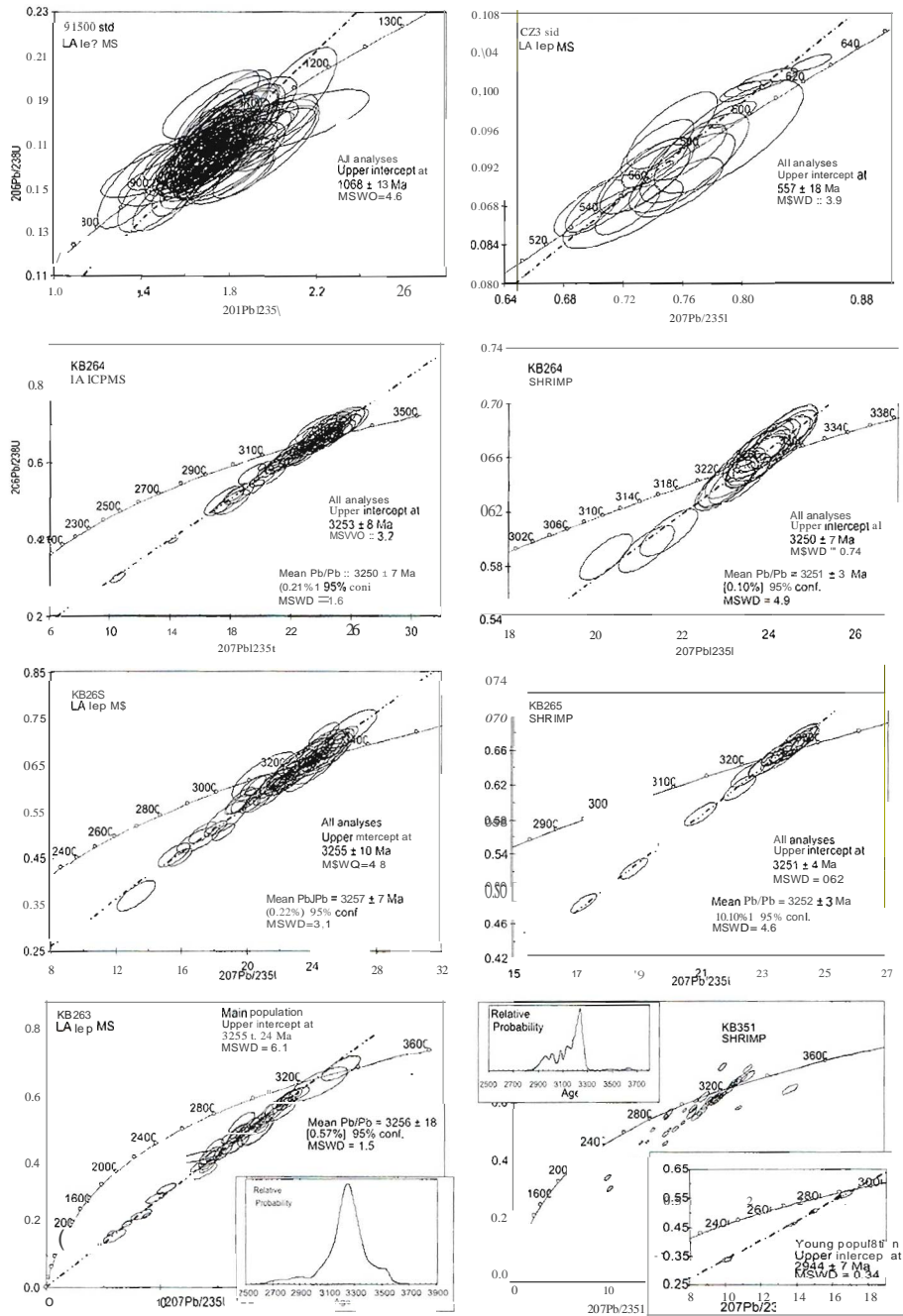
6.4.5 Zircon major and trace element analysis

The chemical composition of selected zircons from samples KB770, KB779 and KB810 was measured by electron microprobe (EMP) and laser ablation ICP-MS analysis. Major elements were determined using a Leol 8600 Superprobe with 5 wavelength dispersive spectrometers. A 15 kV accelerating potential and 10 nA beam current were used to measure $1\ \mu\text{m}$ analysis sites and a correction was applied using the $\phi(\rho z)$ algorithm supplied by Noran.

Trace elements were measured by laser ablation ICP-MS analysis on $20\ \mu\text{m}$ diameter sites within the same growth zones of each zircon and adjacent to the craters measured for the U-Pb dating described above. Zones were identified using optical microscopy and CL techniques, but as an additional check the Pb-Pb ages were determined within the same analytical run as the trace element measurements. Precision on these age measurements (not reported here) was degraded due to poorer counting statistics but was sufficient in most cases to check that the correct zone had been identified. Although we measured a different part of the sample to measure the trace elements the homogeneity of their distribution within a zone (as seen in depth resolved plots and during repeat analyses) supports this approach. Calibration was performed against NIST SRM 610 glass using the compiled concentration data of Pearce et al (1997) and EMP Hf data for internal standardization. Accuracy for trace element results was assessed using zircon 91500 (Wiedenbeck et al., 1995).

6.5 Results

A summary of the U-Pb age dating results is given in Table 6.5. The concordia diagrams are shown in Figure 6.5. The Laser Ablation data tables can be found in Appendix 6.A, the SHRIMP data tables in Appendix 6.B. The inclusion of results in our dataset by both laser ablation ICP-MS and SHRIMP required a careful validation of the agreement of the two techniques for a number of samples. The relatively fast analysis time by laser ablation ICP-MS enabled populations of at least 60 zircons to be routinely measured per sample. However, in some samples heterogeneous populations were measured and a range of U-Pb ages could be determined depending upon the interpretation of the number of different xenocryst populations. To overcome this limitation, trace element data were used to better constrain the origin and extent of xenocryst groups. Full U-Pb and major and trace element concentration data are reported in Appendix 6.C.



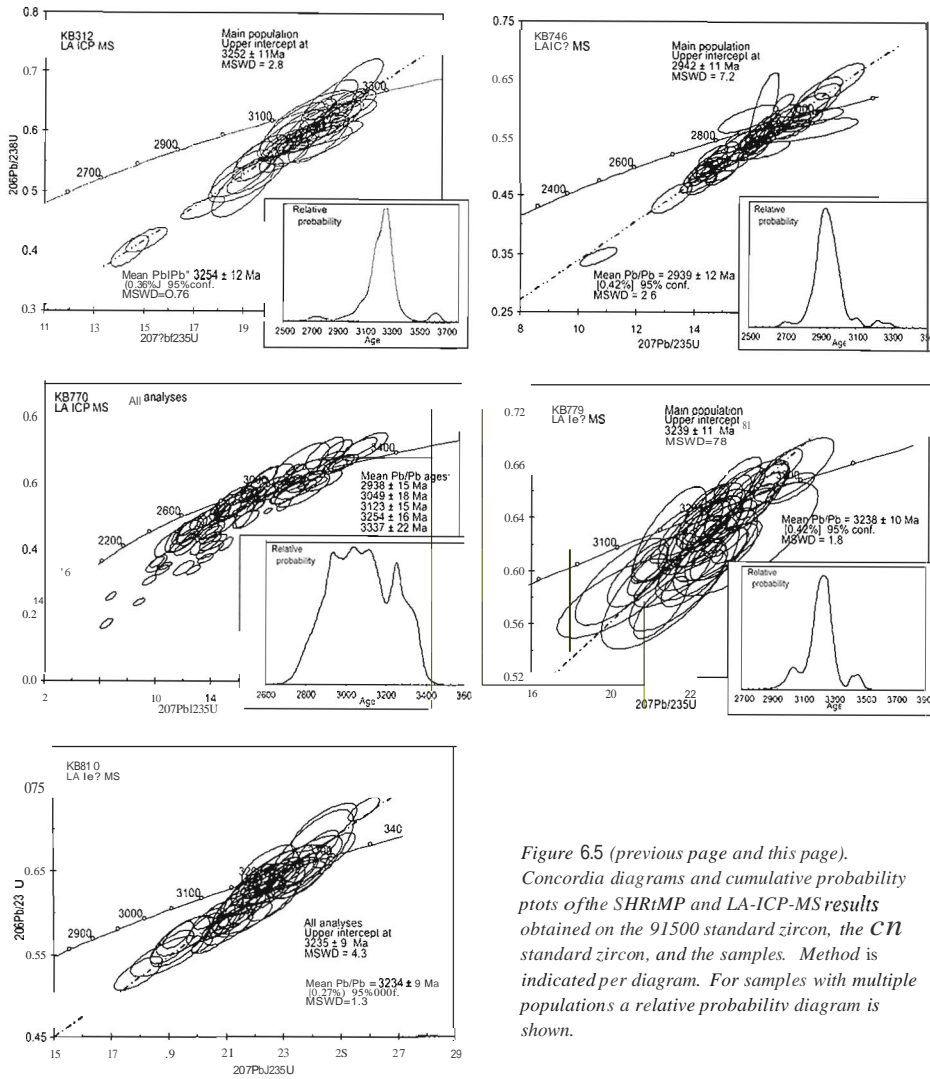


Figure 6.5 (previous page and this page). Concordia diagrams and cumulative probability plots of the SHRIMP and LA-ICP-MS results obtained on the 91500 standard zircon, the CN standard zircon, and the samples. Method is indicated per diagram. For samples with multiple populations a relative probability diagram is shown.

6.5.1 Standard data

The CZ3 in-house standard zircon was used as an internal standard for the SHRIMP analyses and as an external check for the LA-ICP-MS results. Pidgeon et al. (1994) reported that this Sri Lankan gem-quality zircon is free of inclusions and zoning, contains no detectable ^{206}Pb and that its crystal lattice is undamaged. This homogeneous zircon was dated previously by the TIMS method (Nelson, 1997), giving a concordant age of 564 Ma. In this study, LA-ICP-MS gave a mean Pb-Pb age of 559

Table 6.5. *SummQ/Y of age results. All errors are 2s errors. n = number of analyses.*

Sample	Method	Main Population		Xenocrysts	Overprint
		U/Pb concordia upper intercept age	$^{207}\text{Pb}/^{206}\text{Pb}$ (n) date	$^{207}\text{Pb}/^{206}\text{Pb}$ (n) date	$^{207}\text{Pb}/^{206}\text{Pb}$ (n) date
KB263	LA-ICP-MS	3255 ± 24 Ma	3256 ± 18 Ma (43)	3464 ± 44 Ma (5)	2766 ± 52 Ma (2)
KB264	SHRIMP	3250 ± 7 Ma	3251 ± 3 Ma (21)		
KB264	LA-ICP-MS	3253 ± 7 Ma	3250 ± 7 Ma (60)		
KB265	SHRIMP	3251 ± 4 Ma	3252 ± 3 Ma (19)		3069 ± 41 Ma (4)
KB265	LA-ICP-MS	3255 ± 10 Ma	3257 ± 7 Ma (66)		
KB312	LA-ICP-MS	3252 ± 11 Ma	3254 ± 12 Ma (50)	3629 ± 35 Ma (2)	2758 ± 44 Ma (2)
KB351	SHRIMP	2944 ± 8 Ma	2944 ± 7 Ma (9)	3241 ± 9 Ma (19)	
KB746	LA-ICP-MS	2942 ± 11 Ma	2939 ± 12 Ma (55)	3108 ± 38 Ma (1) 3251 ± 32 Ma (2)	2712 ± 51 Ma (1)
KB770	LA-ICP-MS	2931 ± 16 Ma	2938 ± 15 Ma (22)	3049 ± 18 Ma (18) 3123 ± 15 Ma (22) 3254 ± 16 Ma (18) 3337 ± 22 Ma (7)	2851 ± 27 Ma (8) 2789 ± 57 Ma (1)
KB779	LA-ICP-MS	3239 ± 11 Ma	3238 ± 10 Ma (50)	3426 ± 27 Ma (2) 3465 ± 33 Ma (2)	3045 ± 24 Ma (10)
KB810	LA-ICP-MS	3235 ± 9 Ma	3234 ± 9 Ma (54)		

± 20 Ma and an upper intercept U-Pb age of 557 ± 18 Ma (Figure 6.5) showing excellent agreement with the TIMS value.

Accuracy of the LA-ICP-MS was further assessed using the standard 91500 zircon. Wiedenbeck et al. (1995) reported that this very large (293 gr) single grain of zircon is free of inclusions and zoning, contains no significant ^{204}Pb and that its crystal lattice is undamaged. On the basis of data acquired by the TIMS method, Wiedenbeck et al. (1995) assigned standard values and ages to the isotope ratios as shown in Table 6.3. The results are very slightly discordant with a mean $^{207}\text{Pb}/^{206}\text{Pb}$ age of 1062.4 Ma. The 91500 zircon standard was ablated during every analytical session at regular intervals. Furthermore it was ablated during the setting up of the instrument, and it was measured every 20 minutes to monitor drift. The results were stable and consistent over the time period during which all analyses were performed. Agreement with the reference TIMS data was again excellent; the TIMS age is within the error of both LA-ICP-MS Pb-Pb and U-Pb mean ages.

6.5.2 Comparison of laser ablation ICP-MS and SHRIMP results

Laser ablation ICP-MS has been widely used and developed for in situ U-Pb zircon dating over the past decade (e.g. Feng et al., 1993; Fryer et al., 1993; Hirata and Nesbitt, 1995). Recent techniques involving the simultaneous nebulization of a standard solution (as used here) have eliminated the need for an external standard (Hom et al., 2000) and give very similar results to SIMS for zircon dating (Kosler et al., 2002). We have further verified the ability of both techniques to give identical results in this study. Although the results on the 91500 and CZ3 zircon standards have shown that the LA-ICP-MS system returns accurate and reproducible data, it was necessary to show agreement with the SIMS results before further interpreting the ages in a geological context. A comparison was made by measuring two concordant samples with single populations (KE 264 and KB 265) by both

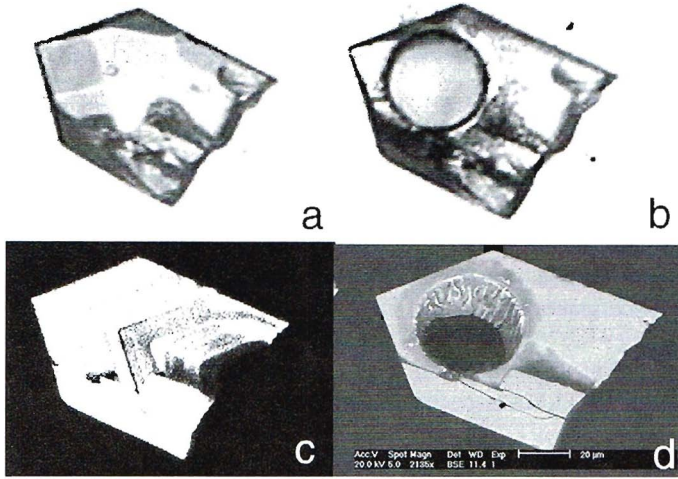


Figure 6.6. Photomicrographs of zircon (a) before and (b) after analysis by LA-ICP-MS. CL image of the same zircon before analysis (c) and SEM image after analysis by LA-ICP-MS (d).

methods. As these samples are significantly older (3250 Ma) than the 91500 standard zircon (1062 Ma) and CZ3 (564 Ma) they contain more radiogenic Pb, and therefore the results are more precise. Agreement was excellent, the laser ablation results being within error of the SHRIMP results and vice versa (Figure 6.5).

The volume of material analyzed was significantly larger in laser ablation than for SHRIMP analyses. The SHRIMP spots were typically 15-20 μm in diameter and no more than 5-10 μm deep (Figure 6.6), whereas the laser ablation craters were typically 40-60 μm in diameter and penetrated all the way through the zircon grain (Figure 6.7). The greater 3D volume component during laser

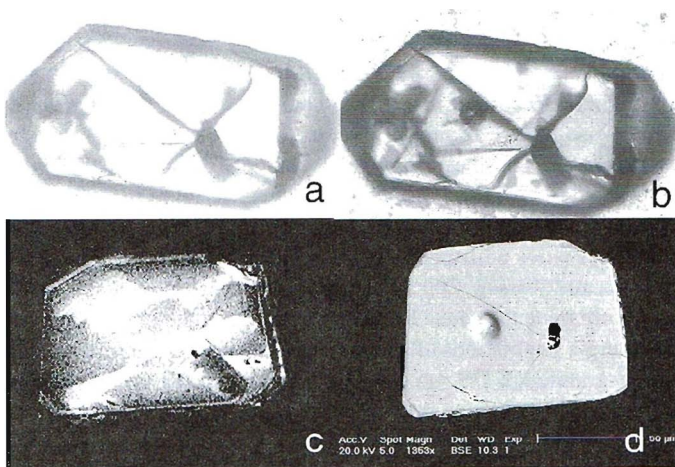


Figure 6.7. Photomicrograph of a zircon before (a) and after (b) analysis with the SHRIMP. CL image before analysis (c) and SEM image after analysis with the SHRIMP (d).

ablation increased the chance of sampling different zones within the zircon during an analysis. The chances of hitting a crack, inclusion or other impurity were therefore much larger during laser ablation and this may account for the generally more discordant nature of the laser ablation results. However, despite this it has been shown here that the pooled $^{207}\text{Pb}/^{206}\text{Pb}$ ages by laser ablation ICP-MS agree to within error to those of the SHRIMP.

6.6 Discussion

The oldest rocks found in the Tabba Tabba area are quartz-muscovite schists interleaved with actinolite schists. On the basis of their geochemistry (De Leeuw et al., 2001) they are interpreted to represent a deformed and metamorphosed granite-granodioritic suite. The obtained $^{207}\text{Pb}/^{206}\text{Pb}$ ages of 3256 ± 18 Ma and 3254 ± 12 Ma from samples KB263 and KB312 are within error of each other and are interpreted to record the time of igneous crystallization. The samples contain apparent zircon populations of 3464 ± 44 Ma and 3629 ± 35 Ma respectively that interpreted to be xenocrystic in origin.

Field relationships show that a granodiorite (sample KB265) has been intruded by granite (sample KB264). The SHRIMP $^{207}\text{Pb}/^{206}\text{Pb}$ ages of 3252 ± 3 Ma and 3251 ± 3 Ma are identical within error to the LA-ICP-MS results, and are interpreted as magmatic crystallization ages of the granodiorite and granite respectively. No other granites of this age are known to occur in this part of the Pilbara. The occurrence of these rocks and the quartz-mica-amphibole schists is confined to a narrow strip within the Tabba Tabba Shear Zone.

Dioritic and gabbroic suites represented by samples KB779 and KB810 intrude the granite-granodiorite suite. The $^{207}\text{Pb}/^{206}\text{Pb}$ ages of 3238 ± 10 Ma and 3234 ± 9 Ma are interpreted as the time of magmatic crystallization (Table 6.5). Their occurrences are confined to lenses within the Tabba Tabba Shear Zone. The diorite contains xenocrystic zircon populations of 3465 ± 33 Ma and 3426 ± 26 Ma. In order to establish the origin of the zircons, trace elements chemistry was determined by laser ablation ICP-MS. Their trace element concentrations and patterns (Figure 6.8) are consistent with dioritic to gabbroic source rocks and the ages of the zircons are therefore interpreted to *correlate* to the magmatic ages of the rocks.

Granite sample KB770 contains a young population at 2939 ± 21 Ma, which is interpreted to represent the magmatic crystallization age of the rock. It also contains apparent xenocrystic populations with $^{207}\text{Pb}/^{206}\text{Pb}$ ages of 3049 ± 18 Ma and 3123 ± 14 Ma, and a group at 3250 Ma which indicates the presence of basement rocks similar in age to the muscovite schists and granite-granodiorite suite (Table 6.5). Primary oscillatory zoning in zircons (as seen most clearly in CL images) is due to unstable chemical gradients. It has been suggested (Connely, 2000) that diffusion associated with metamorphism blurs and destroys the zoning, and this may be an indication of Pb loss and associated discordance. However, diffusion rates of Pb in zircon are probably so slow that under most geologic conditions Pb isotopes ratios will not be altered as the mean closure temperature for zircon is more than 900°C (Cherniak and Watson, 2000). The absence of zoning in many of the zircons sampled here is therefore unlikely to be the cause for the differences in the obtained ages.

In order to identify possible multiple populations of zircons, we investigated the relationship between zircon morphology and age. In granite KB770, which is the sample with the most strikingly different populations (Table 6.5), there was no obvious correlation between age and length-width aspect ratio, CL intensity or discordance as can be seen in Figure 6.9. The type of zoning is the only visual indication of the presence of more than one age population, see Figure 6.10 and Figure 6.11.

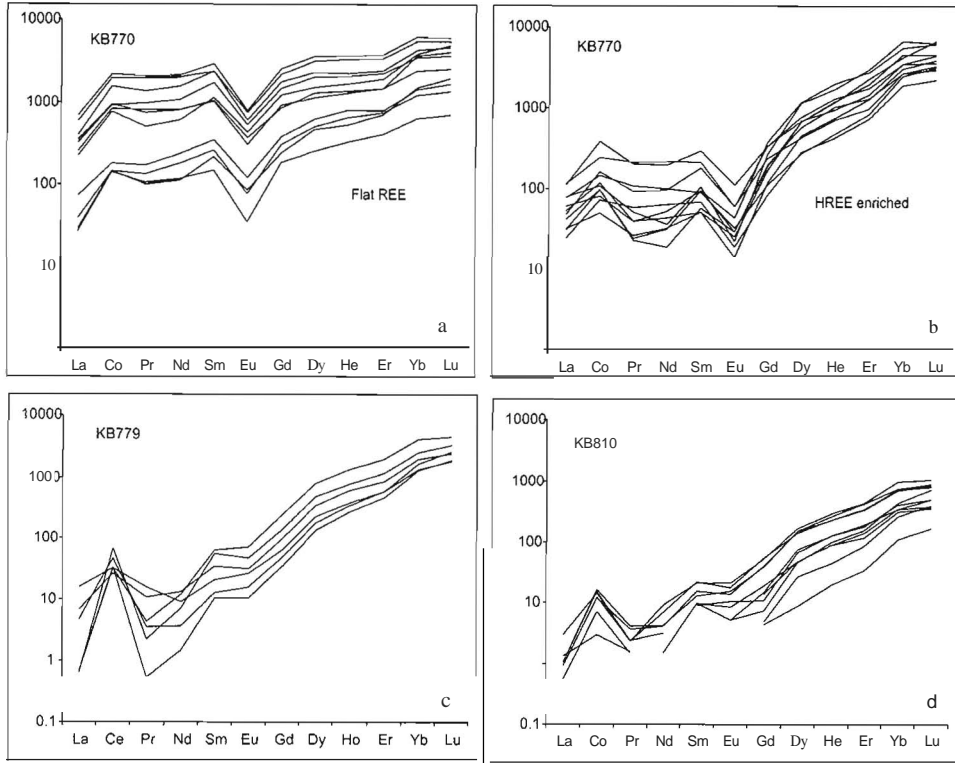


Figure 6.8. Chondrite-normalized REE patterns of zircons from sample KB770 (a, b), KB779 (c) and KB810 (d). Normalizing values from Sun and McDonough (1989). In sample KB770 there are two distinct types of patterns: relatively flat patterns, and a steeper pattern.

Another, potentially more powerful tool for distinguishing populations is to use the trace element chemistry of the zircons (Belousova et al., 2002). The zircons of sample *KBno* can be divided into two groups on the basis of their REE patterns, as shown in Figure 6.8. There is a distinction between flat patterns and those that are enriched in HREE. The group with the flatter REE pattern corresponds to both the cores and rims of zircons from the group with an age of approximately 3250 Ma, confirming that this is most probably xenocrystic in nature. Zircons with this type of flat REE patterns typically originate from highly LREE enriched melts consistent with a granitic origin (Belousova et al., 2002).

The HREE enriched zircons in sample *KBno* are from groups with ages of ca 2940 Ma, 3050 Ma, and 3115 Ma. The magnitude of the HREE enrichment (Figure 6.12) is weakly related to age, being larger in the younger zircons. The Th/U ratio and Y content is lowest for the 3050 Ma group (Figure 6.12) whilst Eu/Eu* is elevated (>0.25 as opposed to <0.25 for the other groups). The whole rock analyses of the host granite provide an opportunity to model the expected REE compositions in zircons that are in equilibrium with this rock. That is, assuming the whole rock is representative of the melt composition, and assuming the zircons were in equilibrium with the melt.

The results for three different models (Nagasawa, 1970; Fujimaki, 1986; Bea et al., 1994) and shown in Figure 6.13.a. When compared with the zircon patterns in Figure 6.13.b it might be concluded that the steepest pattern is most likely to be in equilibrium with the granite. It is concluded that the 2940 Ma age group represents the magmatic age of the rock. However, the differences are very small and it is difficult to convincingly separate the groups on the basis of this small amount of data.

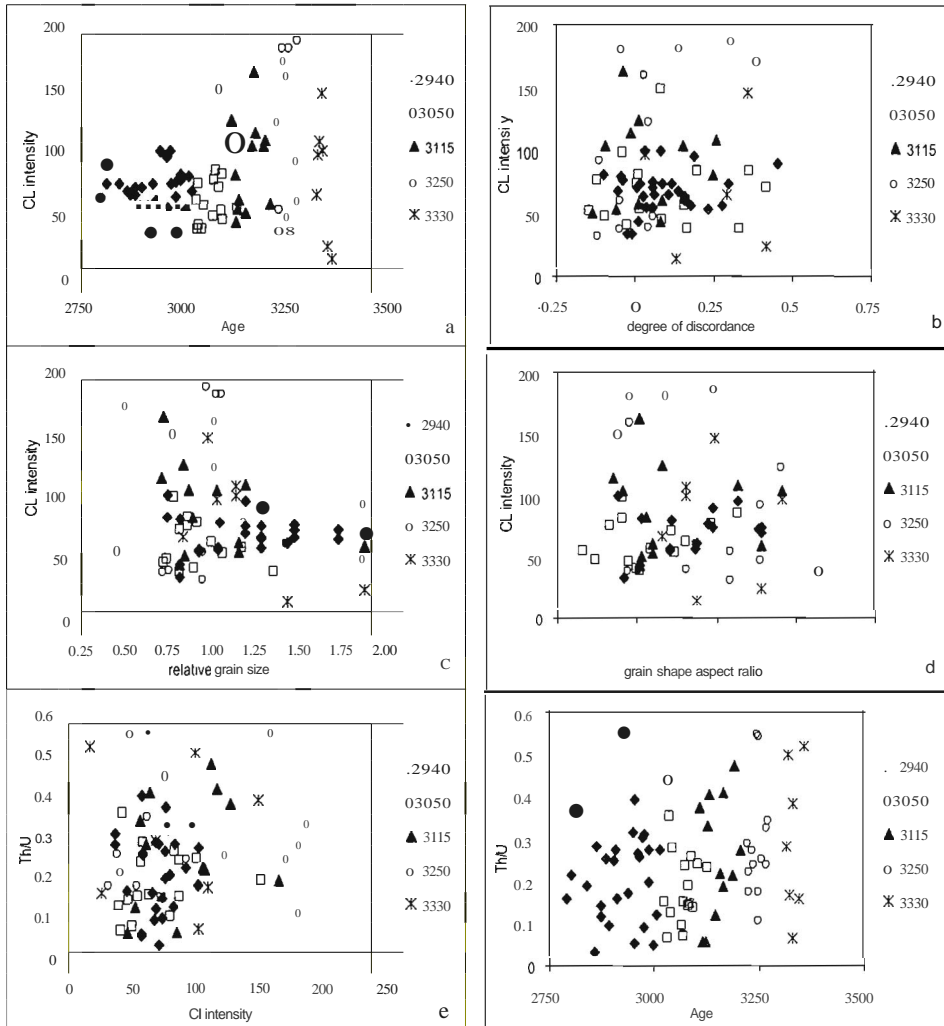


Figure 6.9. Plots of morphological relationship in the zircons of sample KB770. a) CL intensity (0 = dark, 255 = light) versus Age (Ma). b) CL intensity versus the degree of discordance c) CL intensity versus relative grain size (normalized against the average grains size in the sample) d) CL intensity versus grain shape aspect ratio (length/width ratio or complete grains) e) Th/U ratio versus CL intensity. f) Th/U ratio versus age. No clear relations can be observed that allow a distinction between groups on the basis of the plotted characteristics.

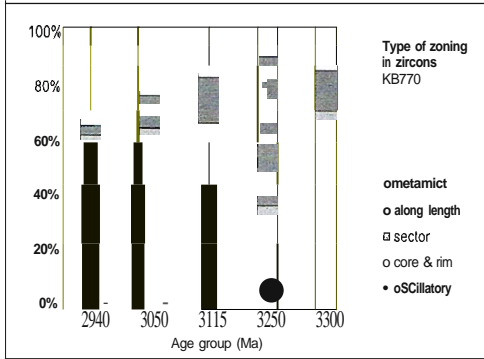
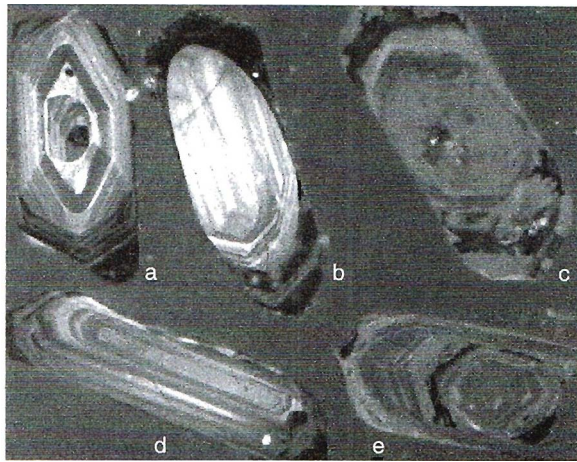


Figure 6.10 Diagram showing the different types of zoning in the five zircon populations in sample KB770. There is no unique type of zoning for any of the different populations.

Figure 6.11. CL images of examples of the different types of zoning in zircons in sample KE770. a) sector zoning, b) core & rim, c) metamict, d) lengthwise zoning, e) oscillatory zoning.



The aplitic vein of sample KB351 is weakly deformed and its youngest zircons, with a $^{207}\text{Pb}/^{206}\text{Pb}$ age of 2944 ± 8 Ma, provide an estimate of the timing of the last stages deformation of the Tappa Tappa Shear Zone. The sample contains many xenocrysts, and the biggest population indicates the presence of rocks of 3250 Ma in this area. This is confirmed by the results of other samples presented here.

The weakly foliated granite of sample KB746 is from the southerly extension of the Tappa Tappa Shear Zone at Yandeyarra (Figure 6.1). The $^{207}\text{Pb}/^{206}\text{Pb}$ magmatic crystallization age of 2939 ± 12 Ma of this granite confines the last stages of movement of this part of the structure. It contains xenocrysts of 3108 ± 38 Ma and 3251 ± 32 Ma. This corresponds to the data obtained from the Turner River locations. This section is not linked in outcrop to the main part of the Tappa Tappa Shear, but it does show a relation in gravity and magnetic images (courtesy AGSO, Blewett pers. comm. 2000) and has a similar tectonic and geochronological history.

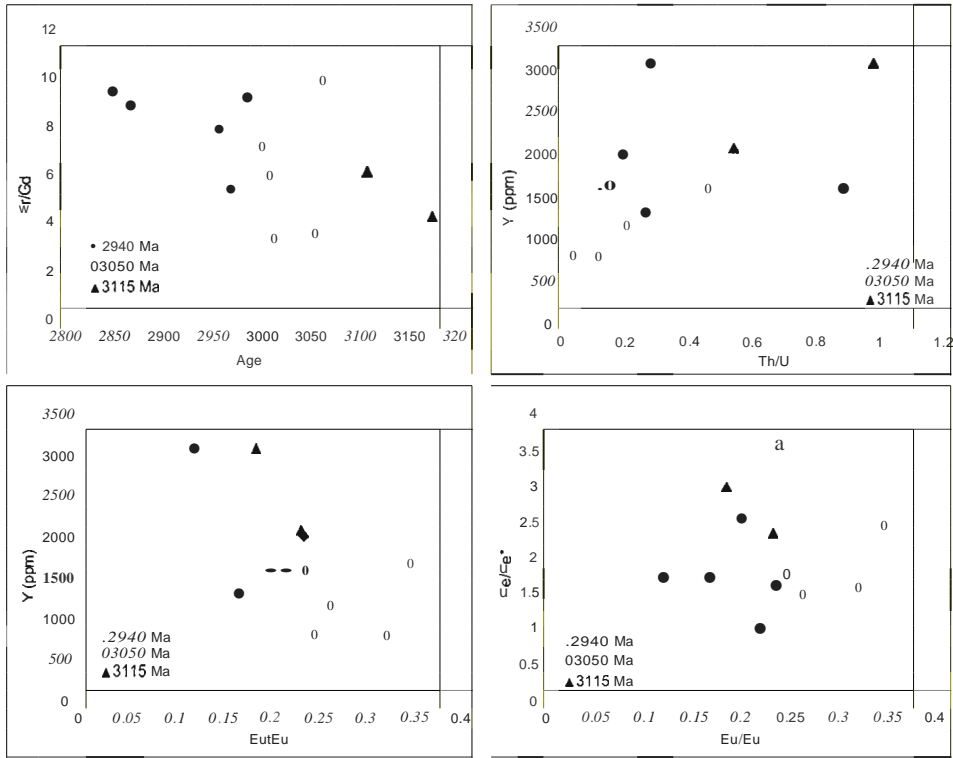


Figure 6.12. Trace element correlations/or zircons from sample KB770 for the 2940 Ma, 3050 Ma and 3115 Ma populations.

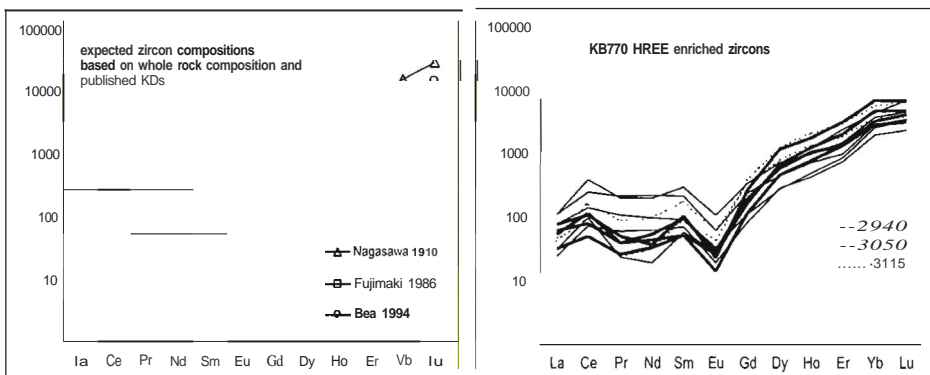


Figure 6.13. a) Expected trace element concentrations in zircons from sample KB770, that are in equilibrium with the melt, modeled on the bulk rock composition of sample K.B770. b) trace element ratios found in zircons of the three populations. On this basis it is interpreted that the steepest pattern is most likely to represent the magmatic zircons. This is the ca 2940 ma population. The other populations are then xenoclysts.

6.7 Tectonic implications

The history of this part of the Pilbara Craton started with the intrusion of a granite-granodiorite suite into unidentified basement at about 3255 Ma. The presence of xenocrysts similar in age to the 3475-3435 Ma Warrawoona Group (Pidgeon, 1978; Williams and Collins, 1990; Thorpe et al., 1992; Bickle et al., 1993; McNaughton et al., 1993; Nelson, 1996; Zegers et al., 1996; Zegers, 1996; Nelson, 1998; Nelson, 1999; Nelson, 2000; Nelson, 2001; Zegers et al., 2001; Buick et al., 2002), indicates a possible basement or precursor rock of that age, and implies a relation to the East Pilbara. The older (ca 3630 Ma) xenocrysts are similar in age to parts of the Warrawagine granite, also in the East Pilbara, and detrital zircons of this age range also occur in the Mallina Basin (Smithies et al., 2001). The granitic and granodioritic schists are similar in age to the Golden Cockatoo Formation in the Abydos Belt, between the Pilgangoora Belt and the Yule Batholith. These rocks are described as metamorphic pelite, quartzite, BIF and rhyolite, must have been deposited on >3312 Ma rocks and are crosscut by 3240 Ma granites (Blewett, 2002; Van Kranendonk et al., 2002). Alternatively the granite and granodiorite may correlate to intrusive components of the Sulphur Springs Group.

A dioritic and gabbroic suite intruded the area at about 3235 Ma, and the occurrence of these rocks restricted to lenses within the Tabba Tabba Shear Zone. This age is similar to the age of the intermediate to felsic volcanic Sulphur Springs Group and Strelley Granite in the East Pilbara (Vearncombe and Kerrich, 1999; Buick et al., 2002), but their age is the only similarity between the two occurrences. These rocks also contain xenocrysts with ages corresponding to the ca 3.45 Ga Warrawoona Group and gneisses in the East Pilbara (Pidgeon, 1978; Nelson, 1998; Nelson, 1999; Nelson, 2000).

The rock types described above are the oldest in the area and they occur only within the Tabba Tabba Shear Zone. They are interpreted to represent an exotic block of possibly East Pilbara crust. A detrital zircon study of the Mallina Basin (Smithies et al., 2001) indicates that sediments containing zircons with ages between 3250 and 3200 Ma were derived from the east. This conforms with the interpretation that the strip of rocks of that age within the Tabba Tabba Shear Zone, represents a crustal block originally east of the Tabba Tabba Shear Zone.

Structures within the Tabba Tabba Shear Zone indicate a dextral compressive event affected the area after the early intrusive events described above. The 3115 Ma age of xenocrystic zircons in younger granites within the Tabba Tabba Shear Zone corresponds to a magmatic and volcanic event in the West Pilbara represented by the Whundo Group and Cheratta Granitoid Complex (Nelson, 1996; Nelson, 1998; Smith et al., 1998; Hickman, 1999; Hickman et al., 2001), and may indicate that the East and the West Pilbara spatially closer associated by that time. The compressive event is interpreted to correspond to that event.

Undeformed to weakly deformed granitoids in the area have an age of 2940 Ma (Smithies et al., 1999). Older samples show a metamorphic overprint at about 2940 Ma. This overprint is interpreted to be due to a major oblique sinistral tectonic event on the Tabba Tabba Shear Zone, and the thermal disturbance associated with late- to post-kinematic granite intrusions. Its age is within error of data from other studies which suggest the main phase of activity of the Tabba Tabba Shear Zone took place between 2955 and 2928 Ma (Smithies et al., 2001). This major sinistral event is interpreted to correspond to closure of the Mallina Basin, which existed between 2970 and 2940 Ma.

Two much weaker and younger overprints possibly correspond to intrusion of tin-bearing monzogranites in the Pilbara at 2850 Ma (Nelson, 1998) and the onset of the Fortescue Group volcanism at 2770 Ma (Arndt et al., 1991; Nelson, 1997; Wingate, 1999). This indicates the structure may have been reactivated at that time.

6.8 Summary and Conclusions

The Tabba Tabba Shear Zone is a structure with a history of more than 300 million years. Early granite and granodiorite intruded between 3255 and 3250 Ma. Subsequently the area was intruded by diorite and gabbro, at about 3235 Ma. Xenocrysts in these rocks indicate the presence of basement rocks similar in age to the Warrawoona Group in the East Pilbara.

A compressive event with a dextral component affected the structure and the surrounding area before 3115 Ma, as indicated by xenocrystic ages in a suite of granites. The Whundo Group and Cheratta Granitoid Complex in the West Pilbara comprise extensive extrusive and intrusive suites of about 3115 Ma. This leads to the interpretation that the East and West Pilbara had coalesced at that time. The observed early dextral compression may be the structural record of that event.

The Tabba Tabba Shear Zone then acted as a bounding fault of the Mallina Basin, before it became reactivated during the major phase of oblique sinistral movement on the Tabba Tabba Shear Zone, that occurred before intrusion of granites at about 2940 Ma. The end of the major sinistral event is interpreted to correspond to closure of the Mallina Basin, which existed between 2970 and 2940 Ma. After deformation had ceased, the central Pilbara was intruded by post-tectonic granite, between 2940 and 2930 Ma. This marked the end of the active tectonics of the Pilbara Granite Greenstone Terrane.

Acknowledgements

We are grateful to the Dr. Schtirmann Fund for the financial support of our field work in the Pilbara with grant numbers 1999/14a, 2000/14a and 2001/14a, and we would like to thank the Molengraaff Fund for their financial support in 1999, 2000 and 2001. The Netherlands Organization for Scientific Research (NWO) is thanked for their financial contribution with grant number R75-386 to the SHRIMP part of this project, and for providing funding for the Utrecht LA-ICP-MS laboratory. We would like to thank R. van Elzas for his assistance with the mineral separation, Dr. H.L.M. van Roermund for his assistance with electron microscope imaging, A. Frew for his assistance with the SHRIMP analyses, and Dr. M. Barth and G. Nobbe for their help with the laser ablation analyses.

The Tabba Tabba Shear Zone: its role in the mid-Archaean tectonic evolution of the Central Pilbara Craton, Western Australia

Abstract

The early- to mid- Archaean Pilbara Craton in Western Australia comprises several domains separated by major shears. The Tabba Tabba Shear Zone forms the reactivated boundary between the East and Central Pilbara Superdomains. This paper reports the results of a combined structural, geochronological and geochemical study of the Tabba Tabba Shear Zone and the Central Pilbara. New structural-kinematic analyses, integrated with geochronology and geochemistry, show that this area has a complex geological history spanning more than 700 million years. Pre-existing basement was intruded by ca 3255 Ma granite and granodiorite and ca 3235 Ma gabbro and diorite with continental arc-affinity, before the Tabba Tabba Shear Zone was deformed during a dextral transpressional deformation phase.

The structure presently forms the western margin of the East Pilbara and the eastern margin of the Mallina Basin in the Central Pilbara. This basin contains components ranging in age between 3020 Ma and 2970 Ma, which were deposited during several phases of transtensional basin formation. The Mallina Basin contains ca 2970 Ma boninites and ca 2955 Ma sanukitoids which both are remarkable in the lack of coeval subduction, although far-field tectonic events may have caused this signature. A final and major northwest-southeast directed compressional event occurred at ca 2930 Ma, followed by the intrusion of post-orogenic granite and gabbro. New $^{40}\text{Ar}/^{39}\text{Ar}$ analyses indicate the area was thermally disturbed at about 2860 Ma and 2760 Ma, and during the mid- and late-Proterozoic.

7.1 Introduction

The Pilbara Craton in the northwest of Western Australia comprises two components. The first is the early to mid-Archaean North Pilbara Granite-Greenstone Terrain, which is the subject of this paper, and for convenience, will be called Pilbara Craton from here on (Figure 7.1). The second component is the overlying late-Archaean volcano-sedimentary sequence of the Hamersley Basin.

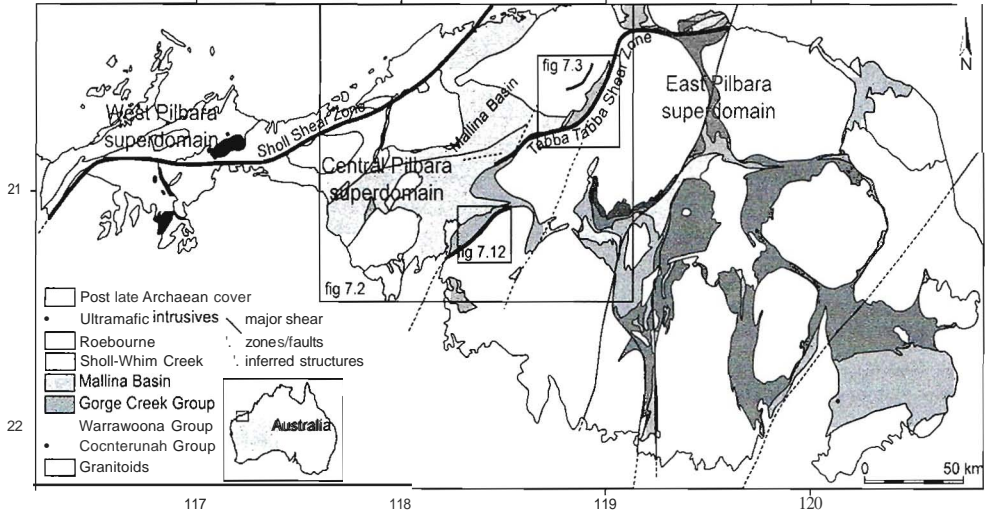


Figure 7.1. The Pilbara Craton in North Western Australia. The study areas in the Central Pilbara are indicated and details can be found in the respective figures.

Major structures separating domains have been found to be typical features of continental crust of all ages, including the Archaean (De Wit, 1998). The Pilbara Craton has such a domainal architecture which is interpreted to reflect a history of accretion (e.g. Krapez and Barley, 1987; Barley, 1997; Smith et al., 1998), because it bears similarity to the geometry of accreted terranes in Phanerozoic continents (e.g. Coney, 1989). Major shears with a long history of reactivation mark the domain boundaries in the Pilbara Craton. The timing and kinematics of these structures may contain important clues to the tectonic history of the Archaean Earth.

The West, Central and East Pilbara are shown in Figure 7.1. A number of publications have presented domainal subdivisions of the Pilbara Craton. The division proposed by Blewett (2002) has been adopted in this paper, on the basis of lithology and deformation history. In this paper the terms West, Central and East Pilbara will refer to the respective superdomains.

The Tappa Tappa Shear Zone is regarded as the western boundary of the East Pilbara, because the domains to the west of it have no pre- 3.3 Ga history. The 3.51 Ga Coonterunah Group (Buick et al., 1995) and the 3.47-3.42 Ga Warrawoona Group (Hickman, 1983; 1999) do not occur to the west of this shear zone, and the 3.45 and 3.3 Ga tectonic events recognized in the East Pilbara (e.g. Barley, 1997; White et al., 1998) are not recognized to the west of this structure. The Tappa Tappa Shear Zone now forms the eastern margin of the Mallina Basin (Figure 7.2) and its complex reactivation and intrusive history suggest it is a major crustal scale structure with a long history of activity. This structural and geochronological study was undertaken to investigate the tectonothermal evolution of the eastern part of the Central Pilbara, and the role of the Tappa Tappa Shear Zone in the mid to late Archaean tectonic evolution of the area.

7.2 Regional Geology

A tabular stratigraphy for the greenstone successions in the entire Pilbara Craton was originally proposed (Hickman, 1983; Horwitz, 1990), but with the recognition of domains and their boundary

structures this stratigraphy has been revised (e.g. Hickman, 1999). The greenstone successions of the different domains can not or only partially be correlated across domain boundaries. Recently published stratigraphy and distribution of the East Pilbara greenstone successions are summarized in Table 7.1. The East Pilbara comprises the ca 3.51 Ga Coonterunah Group, the ca 3.47-3.43 Ga Warrawoona Group, the ca 3.23 Ga Sulphur Springs Group, the un-dated Gorge Creek Group and the ca 2.95 Ga De Grey Group. The West and Central Pilbara lithology has been summarized in Table 7.2. The West Pilbara comprises a ca 3.265 Ga succession in the Roeboume Domain, and an undated mafic sequence of possibly oceanic origin. The Central Pilbara comprises the 3.12 Ga volcanics in the Sholl Belt, a ca 3.01-2.97 Ga volcano-sedimentary succession in the Whim Creek Belt, and 2.97 Ga continental sediments in the Mallina Basin. An overprinting strike-slip event and

Table 7.1. Supracrustal sequences in the East Pilbara Granite-Greenstone Terrain. Compiled from Van Kranendonk et al. (2002) and references therein. Numbers in the left column refer to the domains shown in Figure 7.1.

Group	Formation	Lithology	age (Ma)	thickness (km)
De Grey (1,2,3,(4))	Lalla Sandstone	Rookh Sandstone, conglomerate, shale	ca 2950	
Gorge Creek (1,2,3)	Pyramid Hill Honeyeater Basalt Paddy Market Corboy Pincunah Hill	Banded iron formation (BIF) Basalt shale, chert sandstone, mudstone, conglomerate shale, BIF, sandstone, felsic volcanics	<3235	max 3.5
Sulphur Springs (2,3)	Kangaroo Caves Kunagunarrina Leilira	tholeiitic mafic to felsic volcanics, chert, BIF pillow basalt, high-Mg basalt, chert wacke, rhyolite, sandstone, mudstone, chert	3238-3235	max 1.5 max 2.4
(3)	Golden Cockatoo	BIF, rhyolite, quartzite, metapelite	>3238	
(2)	Budjan Creek	conglomerate, sandstone, siltstone, felsic vole	3308	max 1.2
W Kelly A Subgroup R (1,2,3)	Charteris Basalt Wyman Euro	komatiite, basalt felsic volcanics tholeiitic and komatiitic pillow basalt and chert	3325	max 1.1 max 9.4
R Salgash A Subgroup W (1,2,3)	Strelley Pool Chert Panorama Apex Towers	quartzite, chert, stromatolites felsic volcanics, tuffaceous sandstones altered basalts, chert blue, black, white layered chert	3459-3434	1.5 max 4
O O Tatga Taiga N Subgroup A (1,2,3)	Duffer MIA da Dresser McPhee North Star Basalt	dacitic tuff, agglomerate basalt and chert stromatolitic barite-chert felsic schist basalt	3471-3463 ca 3490 3477	max 5 2 0.5
Coonterunah (3)	Double Bar Coucal Table Top	Basalt, volcanogenic seds Mafic and felsic volcanics, chert, BIF basalt, komatiite	3508 3515	max 6

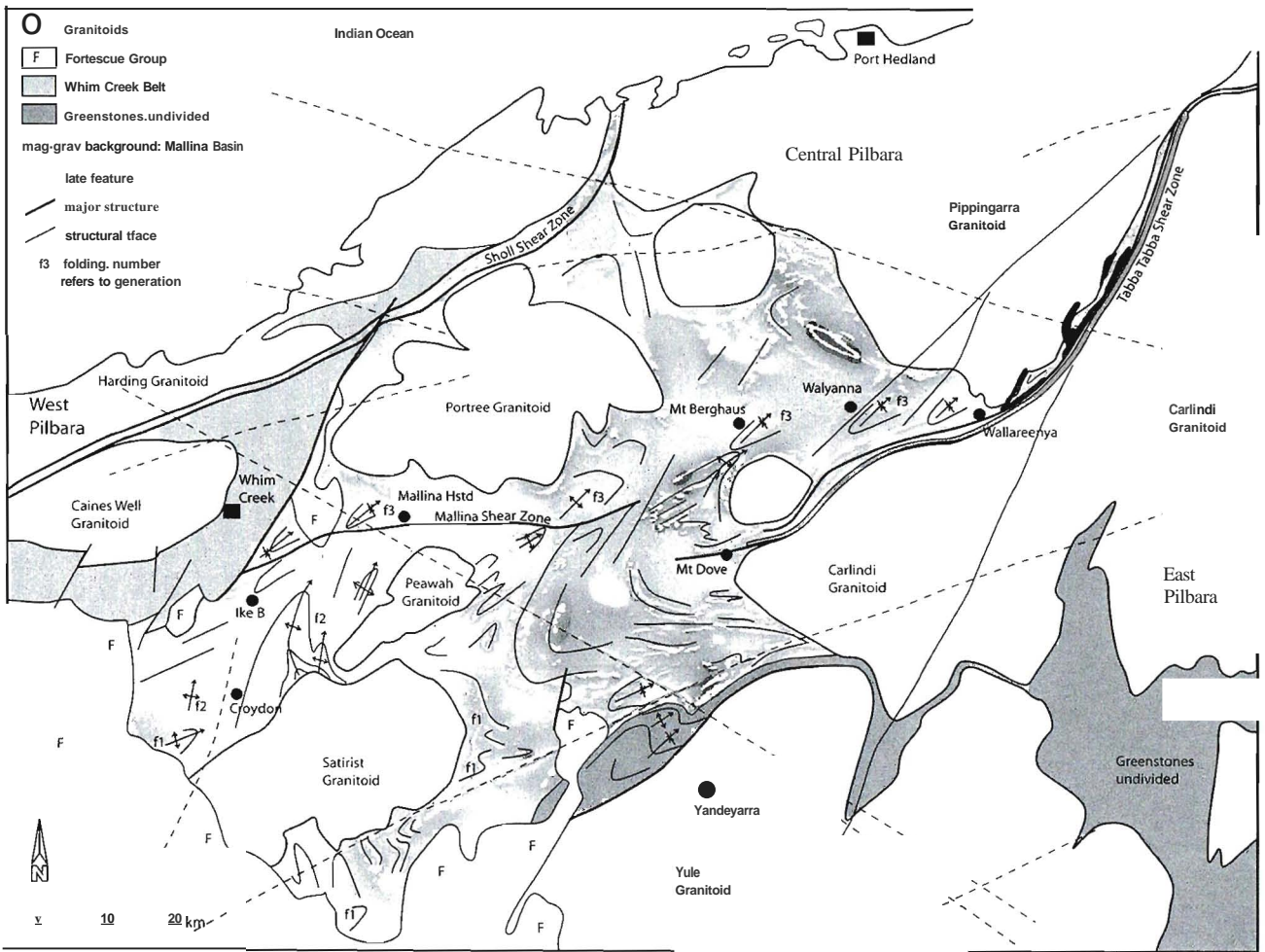


Figure 7.2. The Malina Basin with its bounding structures: the Sholl Shear Zone and the Tabba Tabba Shear Zone. Short-wavelength magnetic anomaly image is shown for the Mallina Basin and traces of structures are shown.

Table 7.2. Supracrustal sequences in the West and Central Pilbara Granite Greenstone Terrains. the Roebourne Group in the Roebourne Domain (West Pilbara), the Whundo Group in the Sholl Belt (Central Pilbara), Cleaverville Formation which occurs both north and south of the Sholl Shear Zone, the Whim Creek and Bookingarra Groups in the Whim Creek Belt (Central Pilbara), and the Mallina Basin (Central Pilbara). Compiled from Hickman et al. (2001) and references therein. Numbers in the left column refer to the domains shown in Figure 7.1. In domain 5: WC = Whim Creek Belt, S = Sholl Belt

Group (Occurrence)	Formation	Lithology	age (Ma)	Thickness (km)
Mallina (4)	Mallina Fm	sandstone, slate	ca 2975	
	Constantine Sandstone	conglomerate, sandstone	ca 2975	
Bookingarra (5WC)	Kialrah Rhyolite	rhyolite	ca 2975	
	Negri + Loudon Volcanics	mainly mafic volcanics		
	Cistern Fm + Rushall Slate	clastic sediments	ca 2978	
Whim Creek (5WC)	Mons Cupri Dacite	dacitic intrusions	ca 3010	0.2
	Red Hill Volcanics	andesite, rhyodacite, sandstone, breccia	ca 3010	0.3
	Warambie Basalt	basalt, minor seds		0.2
	(4,5,6)	Cleaverville Fm	chert, BIF, basalt and felsic volcanics	ca 3020-3015
Whundo (5-S)	Woodbrook Fm	basalt and felsic volcanics	ca 3115	1
	Bradley Basalt	basalt, minor felsic volcanics	ca 3115	>4
	Tozer Fm	basalt, rhyolite, sediments and chert	ca 3120	2.5
	Nallana Fm	basalt, minor ultramafics, pyroclastics	ca 3125	2
Roebourne (6)	Regal Fm	komatiites, basalt	not known	2
	Nickol River Fm	volcanogenic sediments, chert	ca 3270-3250	0.1-0.5
	RulhWell Fm	basalt, talc schist, chert	ca 3270	1-2

associated igneous activity records a craton-wide event at about 2.92 Ga (Barley, 1997; White et al., 1998).

Because there are significant changes in lithology, structure and geochronology across the Tabba Tabba Shear Zone (Barley, 1997; White et al., 1998), it has been interpreted to represent a tectonic boundary *sensu stricto* (Sengor and Dewey, 1990). In the present configuration, the shear zone forms the eastern margin of the Mallina Basin, and the western margin of the Carlindi and Yule Batholiths (Figure 7.2). Because the Mallina Basin (as a part of the Central Pilbara) forms the link between the East and West Pilbara, the structural evolution of the basin is as important in the evaluation of the tectonic history of the Central Pilbara as the Tabba Tabba Shear Zone itself.

The Cleaverville Formation, with an age of 3020-3015 Ma possibly forms the base of the Mallina Basin (Smithies et al., 1999). The Mallina Basin fill consists of the dominantly volcanic Whim Creek and Bookingarra Groups (Pike and Cas, 2002; Pike et al., 2002), and complete submarine flat-ramp-fan systems including turbidites, breccias, sandstones, and mudstones of the Mallina Formation (Krapez, 1993; Krapez and Eisenlohr, 1998). The main accumulation in the Mallina Basin occurred between 2990 and 2970 Ma, as the basin developed in an intracontinental setting (Smithies et al., 1999; Huston et al., 2000). SHRIMP U-Pb zircon ages of detrital grains in turbidites of the Mallina Basin have a major population of 3250-3150 Ma (Nelson, 1997; Smithies et al., 2001), reflecting the age of the source regions. The ca 3250 Ma age group is likely to be derived from granitoids in the East Pilbara (Beintema et al., in press), the ca 3150 Ma age group is likely to

be derived from granitoids in the West Pilbara (Smith, in press). This indicates both the East and West Pilbara were in close proximity at that time.

Smithies (1999) reported that the Mallina Basin experienced folding at approximately 2955 Ma, immediately followed by intrusion of a suite of High-Mg diorites (sanukitoids) along a linear belt parallel to the basin axis. Large volumes of alkaline granites intruded in the northern part of the basin between 2950 and 2940 Ma (Smithies and Champion, 1999). The entire area was intruded by monzogranites at approximately 2935 Ma (Smithies et al., 1999).

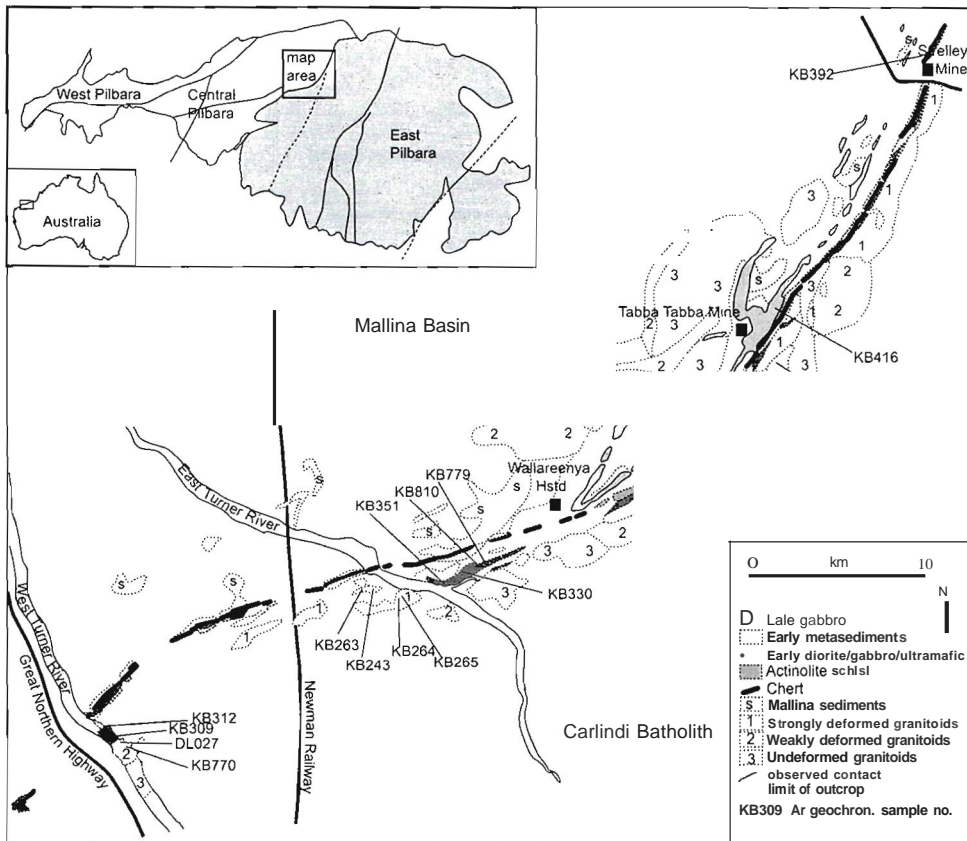


Figure 7.3. Simplified map of the exposed central section of the Tabba Tabba Shear Zone. Lithology based on 1:100,000 geological map (Smithies, 2000) and aerial photograph interpretation. Geochronology sample locations are indicated. For structural and kinematic data see Figure 7.5.

7.3 Lithology and Structural Geology

7.3.1 Introduction

On aeromagnetic and gravity images, the Tabba Tabba Shear Zone can be traced from northeast to southwest across the middle of Pilbara Craton (Blewett et al., 2000). The central section is locally exposed and has been subjected to field studies and sampling (Figure 7.3). The northern section of the structure curves to the northeast; the southern section branches to the southwest beneath the Mallina Basin. A structure with similar orientation occurs on the western margin of the Yule Batholith, and forms the extension of the Tabba Tabba Shear Zone in a southwesterly direction (Figure 7.1).

Although outcrop in the Central Pilbara is generally poor, parts of the Tabba Tabba Shear Zone itself are locally well exposed as it contains erosion-resistant lithologies such as chert and gabbro that provide some topography and outcrop along the structure (Figure 7.7.a). The field studies were concentrated on a number of traverses across the Tabba Tabba Shear Zone and included mapping based on aerial photographs (courtesy GSWA, R.H. Smithies pers. comm. 1999-2001), detailed structural-kinematic analyses, metamorphic studies, and sampling for $^{40}\text{Ar}/^{39}\text{Ar}$ and U-Pb geochronology (Beintema et al., in press) and major and trace element geochemical analyses. Although there is very little outcrop in the Mallina Basin, several traverses and locations were visited for structural studies.

7.3.2 Lithology and metamorphism

The lithologies and their relative and absolute age relations discussed below, are illustrated in Figure 7.4. The metasediments of the Mallina Basin consist of folded shales and wackes metamorphosed to low greenschist grade as indicated by the limited presence of chlorite and sericite. In contact metamorphic zones around granitoids and gabbroic intrusions in the Mallina Basin, the metamorphic grade is locally higher as indicated by the observation of minor cordierite and andalusite as mm-sized spots in slate.

A unit of chert occurs in outcrop along most of the eastern boundary of the Mallina Basin. This chert is thought to be of (volcano-) sedimentary origin and in the south of the Mallina Basin it has an age of 3020–3015 Ma (Nelson, 1998). It is interpreted to be equivalent to the Cleaverville Formation in the West Pilbara because it has an identical age and lithological characteristics, and it may underlie the entire Mallina Basin (Smithies et al., 2001).

On the eastern side of the chert, tremolite-actinolite-carbonate schists can be found, which are interleaved with lenses of massive mafic and ultramafic rocks and finely laminated cherts (Figure 7.4). This second type of chert is interpreted to be tectonized and silicified mafic to ultramafic rock, as it is locally observed to grade into actinolite-chlorite-serpentine-carbonate schist. In the East and West Turner River sections (for location see Figure 7.3) quartz-muscovite and quartz-actinolite schists occur to the southeast of the chert ridge, which are interpreted to be a deformed and metamorphosed granites and granodiorites on the basis of their composition and field relations. Their mineralogy comprises variable amounts of hornblende, actinolite, quartz, biotite, chlorite, epidote. In the Turner River sections, granite, granodiorite, diorite and gabbro occur to the southeast of these schists, as illustrated in Figure 7.4.

The Tabba Tabba Shear is lined by granites on the east and southeast along its entire length. Early granites are strongly foliated, with tectonized sheared contacts with the v[granite have irregular intrusive contacts, locally destroying the shear zone as illustrated in Figure 7.4, and undisturbed contact metamorphic aureoles. On the western side of the structure a suite of

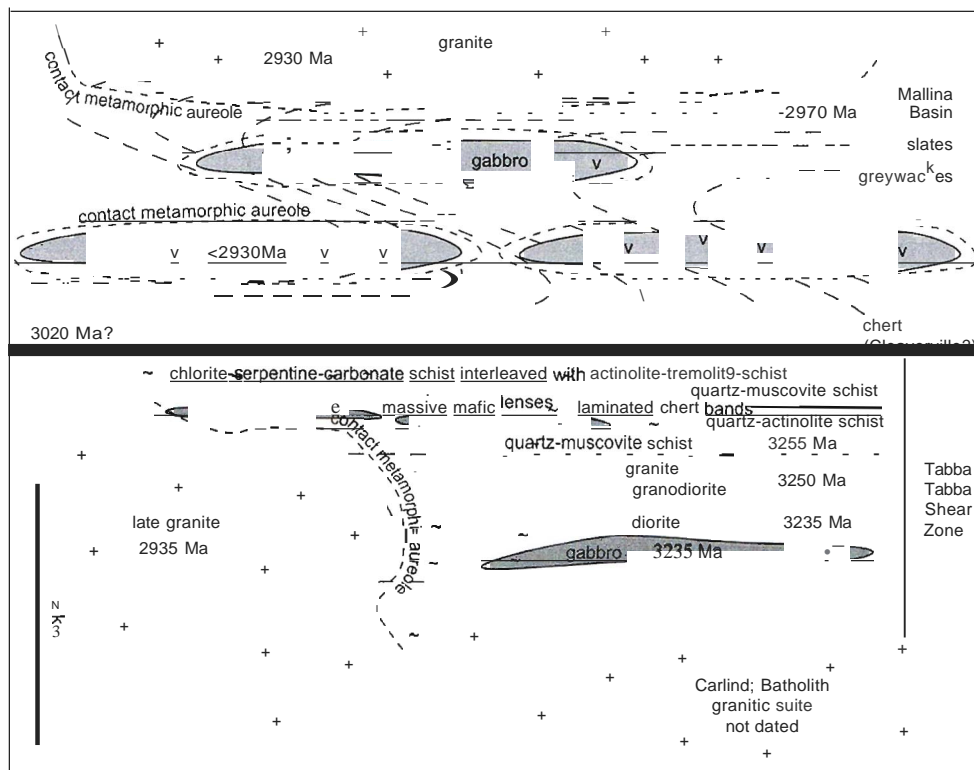


Figure 7.4. Sketch map illustrating the relative and absolute timing relations of the different lithologies inside and outside the Tabba Tabba Shear Zone. This sketch is representative of the exposed central section of the Tabba Tabba Shear Zone as shown in Figure 7.3. ~ indicates mylonitic foliation.

late granites and gabbros has been emplaced into the already deformed sediments of the Mallina Basin. This late gabbro occurs as a series of lenses with slightly sheared margins and undeformed centers. These lenses can be observed clearly on the maps based on aerial photograph interpretations (Appendix 7.A).

7.3.3 Structural geology of the Tabba Tabba Shear Zone

7.3.3.1 J Strelley Mine, Tabba Tabba Mine, Boundary Well

At the Strelley Mining Center, the northern-most exposure of the Tabba Tabba Shear Zone (Figure 7.5), a subvertical foliation and subvertical actinolite-hornblende mineral lineations were observed in tremolite-actinolite schist (Figure 7.6.a). South of the Strelley Mining Center, the Tabba Tabba Shear Zone has almost continuous outcrop (Figure 7.5). On the western side, foliated chlorite-bearing metasediments of the Mallina Basin occur. Bedding and a bedding-parallel foliation in the sediments are subvertical and north-northeast trending. Locally cm-scale folds occur, with subvertical axes and a steeply west-dipping axial planar cleavage. The sediments have been intruded by granite, which has scattered outcrop and is undeformed.

A prominent ridge of massive ultramafics, chert and actinolite schist marks the eastern margin of the Mallina Basin. Actinolite schist has weak subvertical actinolite lineations overprinted by random actinolite, indicating a late thermal overprint. East of the ridge, strongly flattened granite and pegmatites (Figure 7.7.e) are in sheeted tectonized contact with the actinolite schist. A mylonitic foliation in the granite is subvertical and quartz stretching lineations are subvertical to steeply south plunging (Figure 7.6.a, b and c). Towards the east the deformation becomes less intense and the tectonic foliation and lineation in the granite stop about two kilometers east of the contact. A weak northeast striking subvertical magmatic foliation defined by feldspar alignment continues in the granite, giving way to a weak sub horizontal magmatic foliation approximately eight kilometers east of the contact.

On traverses between the Strelley Mining Center and Wallareenya Station (Figure 7.5) it has been established that the lithological and structural profiles are very consistent in the northern section of the structure. Dominant and pervasive fabrics are a north-northeast trending subvertical foliation and steeply south-plunging mineral and stretching lineations, associated with sinistral and west-

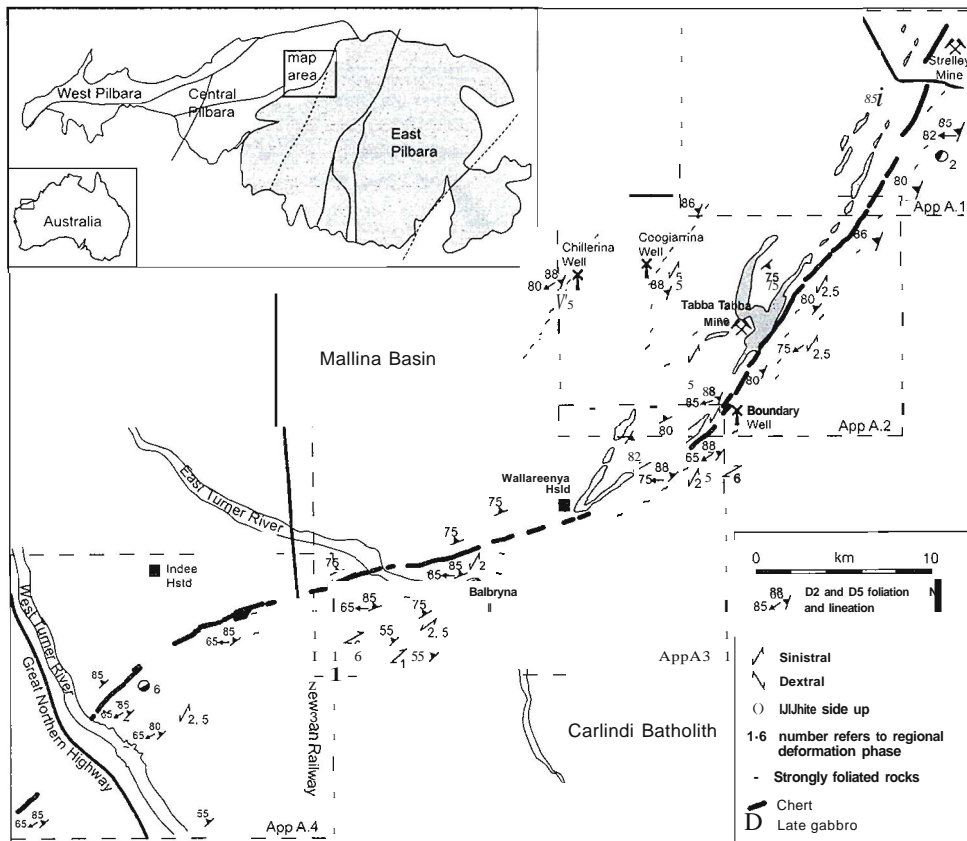


Figure 7.5 Summary structural-kinematic map of the exposed central section of the Tabba Tabba Shear Zone. The chert ridge and late gabbro are shown for reference of location: a/lithologies are shown in Figure 5.3. This map is based on the more detailed maps in Appendix A. Dashed outlines indicate the areas covered by

side-down kinematic indicators such as rotated K-feldspar clasts in granite (Figure 7.7.h) and oblique sinistral shear bands. These structures are locally overprinted by (semi-) brittle crenulations and kinks with subvertical northwest trending axial planes, northeast trending dextral shear bands, and dextral brittle faults (Figure 7.7.b). In granites in the eastern, high grade side of the Tabba Tabba Shear Zone, migmatitic textures were observed (Figure 7.7.i). Their age and the magmatic age of the precursor rocks are unknown.

In Figure 7.6 stereoplots of the mylonitic foliation and lineation associated with oblique sinistral deformation in the Tabba Tabba Shear Zone are shown. It can be observed that the lineations show two consistent trends: the plunge of the lineation becomes gradually more shallow, when going towards the southwest along the shear zone. This is related to the curved geometry of the Tabba Tabba Shear Zone: in order to accommodate a sinistral component of slip, the movement direction must be more vertical towards the northern section of the structure. A second trend shows that the higher grade lineations (hornblende) plunge at a steeper angle than the lower grade lineations (chlorite streaks) by which they are overprinted. This reflects a second episode of oblique sinistral activity on the Tabba Tabba Shear Zone, with roughly similar kinematics but at lower metamorphic grade, when the area was being exhumed. This will be discussed further in section 7.3.3.4.

Southwest of Wallarenya Station, the Tabba Tabba Shear Zone is poorly exposed except for two sections in the East and West Turner Rivers respectively (Figure 7.5). At these locations detailed traverses were made.

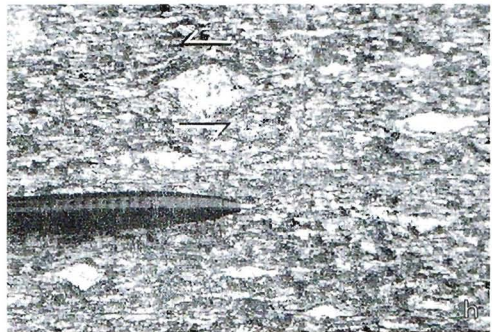
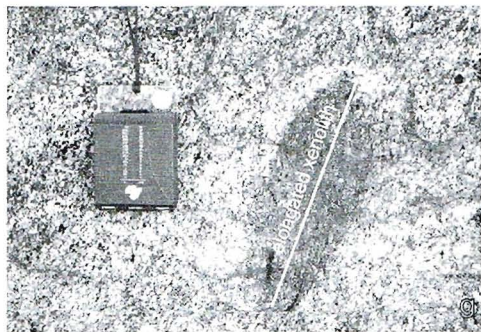
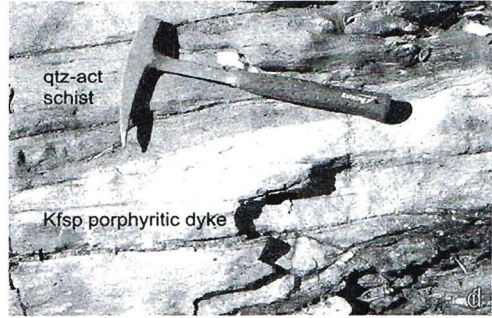
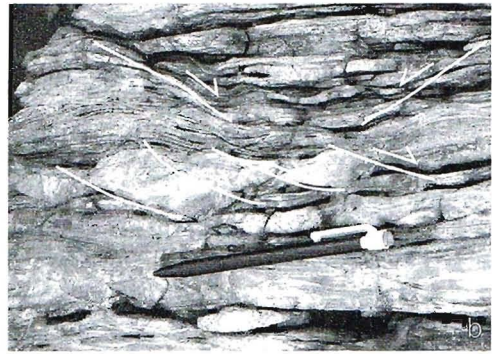
7.3.3.2 East Turner River

Near the East Turner River, the Tabba Tabba Shear Zone runs roughly east west (Figure 7.5). A detailed traverse map is shown in Figure 7.8. A chert ridge marks the northern margin of the shear: north of the chert strongly altered metasediments of the Mallina Formation occur. The ridge itself contains **1-10m** thick beds of banded chert. The northern part of the ridge might be of sedimentary origin, as it contains dm-scale folds that are interpreted to be slump folds because they are randomly orientated. On the south side of the ridge, schistose and silicified ultramafic rocks and finely laminated chert bands grade into talc-chlorite-actinolite-tremolite schist. This chert displays a moderately west-plunging ribbing lineation parallel to the axes of em-scale folds (Figure 7.6.d). This is interpreted to indicate that this chert is of tectonic origin. Geochemical analysis and dating of both types of chert might provide a conclusive answer to this unresolved question.

South of the cherts, actinolite-chlorite-serpentine-tourmaline schists occur, alternating with schistose gabbro. These schists show evidence for three phases of deformation (Figure 7.9). On 100 meter-scale, the strike of the foliation in the granites to the south of the chert ridge, changes in an anticlockwise fashion. This can be seen on aerial photograph interpretations (Figure 7.5 and Appendix 7.A.3, on CD) and is sketched in Figure 7.9.a. This geometry is interpreted to reflect a dextral sense of shear on the Tabba Tabba Shear Zone. Since it is overprinted by the sinistral and dextral events described below (see also Figure 7.9), and occurs exclusively in early granitoid phases, it is interpreted as the earliest deformation phase.

A mylonitic foliation and sinistral shear bands represent a major deformation phase with a large sinistral component (Figure 7.9.c). Those are refolded by a phase with a dextral component represented by crenulations and dm- to m-scale folds with a northeast striking vertical axial plane and sub vertical fold axes (Figure 7.9.b). Tourmaline overprints all generations of structures indicating a late thermal and (fluid-) alteration event.

From 500 meters south of the chert, an alteration of quartz-muscovite schist, quartz-actinolite schist, and deformed and locally mylonitized granites and gabbros occur. Within the schists isoclinal intrafolial folds with subvertical fold axes were observed (Figure 7.7.c). The relative timing of these structures is not known. Zircons from this muscovite schist were dated at 3256 ± 18 Ma



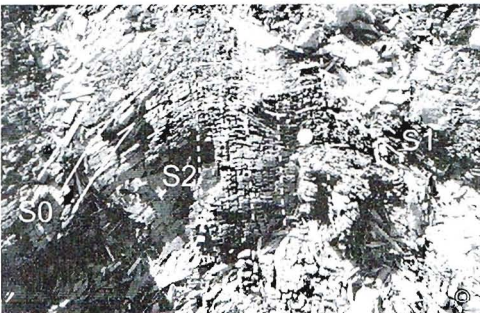
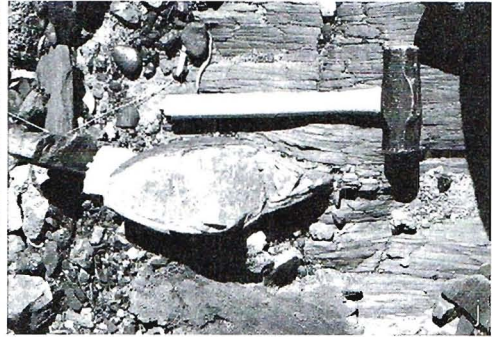


Figure 7.7. (previous pages). Field photographs of structural elements in the Tabba Tabba Shear Zone (TTSZ). Location names refer to Figure 7.5. a) Landscape with the chert ridge marking the western margin of the TTSZ. Looking southwest towards the east and West Turner Rivers. b) Conjugate shears indicating flattening, with a dominant dextral component, in finely laminated chert near Balbajna Well. c) Isoclinal folds in quartz-muscovite schist near the East Turner River. d) K-feldspar porphyritic dyke cutting quartz-acinolite schist, West Turner River. e) Strongly flattened granite and pegmatite of the Carlindi Batholith, east of the Strelley Mining Centre. GPS for scale. f) Migmatitic lexture in granite of the Carlindi batholith, near the TaMa TaMa Mining Centre. g) Flattened and elongated dioritic xenolith in granite, looking horizontally onto the vertical foliation plane: the lineation plunges 70 degrees to the west, East Turner River. h) Sinistral sigma-type clasts in granite near Boundary Well. i) Sinistral kink bands in chlorite schist, cutting dominant D foliation, TTSZ, West Turner River. j) Epidote-albite grade boudin in quartz-mica-amphibole schist, TTSZ, West Turner River. k) Amphibolite grade boudins in quartz-mica-amphibole schist, TTSZ, West Turner River. l) Near migmatite grade boudins in quartz-mica-amphibole schist, TTSZ, West Turner River. In pictures j, k, the lineation makes a high angle with the plane of the photographs, so no kinematics can be interpreted. m) muscovite schist with dextrally folded and flattened pegmatite, West Turner River. n) Muscovite schist with kink fold indicating NW side (right side) up, TTSZ, West Turner River. o) F2 folds in Mallina Fm near the Bore. p) F310 folds in Mallina Formation near Wallareenya Hill.

(sample KB263, see section 7.4). The schists consistently show oblique sinistral shear bands and steeply west plunging stretching lineations and hornblende lineations (Figure 7.6.d).

Between 400 and 700 meters south of the chert ridge subvertical zones of chlorite-bearing schist occur (Figure 7.8). They consistently display sinistral shear bands and moderately west-plunging chlorite-streak lineations (Figure 7.6.d). These schists are interpreted to be overprinting shear zones that were active at a later time (but before late dextral deformation), when the zone was exhumed to greenschist metamorphic grade and there was more of a strike-slip component in the movement direction. Similar observations were described above for the northern section of the structure.

Foliated and lineated granite occurs 1.2 kilometers south of the chert ridge. It contains flattened and elongated granodioritic xenoliths (Figure 7.7.g). A veined intrusive contact with granodiorite to the south has been observed. These two rock types have been the objective of zircon dating and have ages of 3251 ± 3 Ma and 3252 ± 3 Ma (samples KB264 and KB265, respectively, see section 7.4). The granodiorite has variable compositions ranging between dioritic and more granitic end-members. The granodiorite continues until 1.7 kilometers south of the chert, where it is intruded by large quantities of pegmatite.

Pegmatite forms the northern contact of a later suite of granite that occurs 1.8 km south of the chert ridge. It is only slightly deformed, has a foliation dipping moderately to the northwest, and an age of 2944 ± 7 Ma (zircon sample KB351). The intensity of this foliation decreases towards the south, and 3 kilometers south of the chert the granite is undeformed.

East of the East Turner River (Balbajna Well, see Figure 7.5), a series of lenses of very coarse mafic rocks occurs (relict pyroxene crystals of 1-10 cm). These rocks now consist of talc, serpentine, tremolite, chlorite and opaque minerals, with relics of olivine and orthopyroxene. They have an age of 3238 ± 10 Ma (zircon sample KB810). This rock type occurs exclusively within a unit of diorite with an age of 3234 ± 9 Ma (zircon sample KB779), which in turn has intrusive contacts with the granite-granodiorite suite.

In summary, the deformation history of this area shows an early dextral deformation phase post-dating the ca 3250 Ma granites. A major sinistral transtensional phase affected the area during amphibolite grade metamorphism in the foot wall, bringing the northwest-side down. This was followed by a second event with roughly similar kinematics at greenschist grade conditions. All of this is overprinted by a semi-brittle dextral transpressive event.

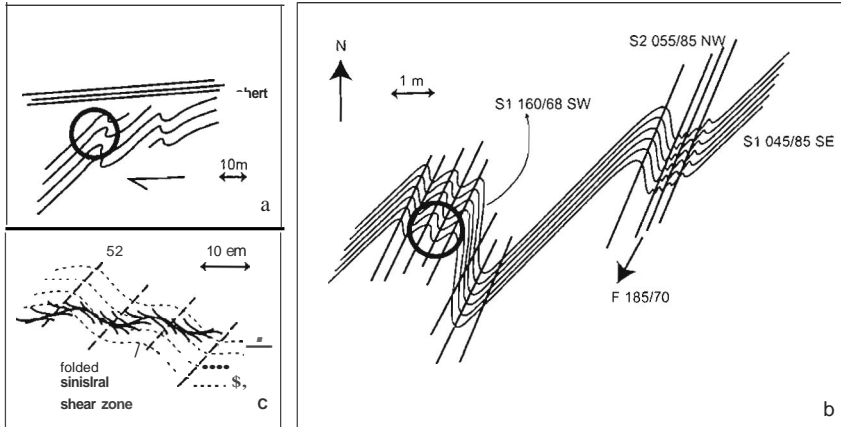


Figure 7.9. Overprinting relations in multiply deformed schists south of the chert in the Tabba Tabba Shear Zone, East Turner River: Location indicated in Figure 7.9. a) 100m-scale trend of foliation in granites south of the chert indicating a dextral shear sense. b) Detail from a: the pre-existing foliation forms crenulations and folds associated with dextral deformation. c) Detail from b: sinistral shear bands cut the pre-existing foliation, but are themselves folded by the dextral crenulations.

7.3.3.3 West Turner River

In the West Turner River (Figure 7.5) a complete traverse of the Tabba Tabba Shear Zone is exposed; a detailed traverse map is shown in Figure 7.10. To the north of the chert, the metasediments of the Mallina Formation are locally exposed, showing folding and a steeply northwest dipping axial planar foliation. Chlorite, sericite, and locally sub-mm sized garnet occur within the metasediments. The main chert ridge has a sedimentary appearance with small-scale chaotic folds, and west-plunging ribbing lineations on bedding planes. The origin of this lineation is unclear. It could be a stretching lineation or an intersection lineation of bedding and a weak tectonic fabric.

Serpentine-chlorite-carbonate schists are exposed until 750 meters south of the chert. Chlorite streak lineations plunge towards the west (Figure 7.6.e), and a large number of cm-scale sinistral shears and kinks was observed (Figure 7.7.i). 850 meters south of the chert ridge, a unit of diorite occurs within serpentine-carbonate schist. From about 900 meters, quartz-muscovite schists (zircon sample KB312, 3254 ± 12 Ma) alternate with coarse gabbroic units and schists with a highly variable composition.

Chlorite is abundant on foliation planes and streaks form a west plunging lineation overprinting earlier hornblende and actinolite. Some bands are more chloritized than others, and they are interpreted to be parts of the shear that were active at lower metamorphic grade. The chlorite streaks generally plunge less steeply than the amphiboles (Figure 7.6.e and Figure 7.11). The quartz-muscovite schist alternates with quartz-albite-actinolite schist. Thin felsic units occur at a small angle to the schistose foliation, they contain K-fsp clasts, and could possibly be rhyolitic dykes or sills (Figure 7.7.d). The sequence is also intruded by a set of very dark mafic dykes (e.g. at 1350 m and 1450 m in Figure 7.10). These dykes show a west-plunging hornblende lineation.

The majority of the schists is interpreted to represent deformed and metamorphosed granite and granodiorite. In these schists, oblique sinistral shears (Figure 7.10) are overprinted by semi-brittle dextral kinks. In quartz-mica schist asymmetrical, semi-brittle folds with a northwest-side-

up geometry were observed (Figure 7.7.n), which are interpreted to be late features in the deformation history. They occur between 900 and 1250 meters southeast of the chert ridge.

Starting one kilometer southeast of the chert in the West Turner River, pegmatite intrusions occur at a small angle to the main foliation (Figure 7.1 D). They intrude all lithological components in the section, and are slightly foliated. Their geometry and angle with the foliation is interpreted to reflect that they were intruded during dextral shearing into the extensional (R) direction, and locally they are folded (Figure 7.7.m).

Towards the southeast, the quartz-mica-amphibole schists described above become of higher metamorphic grade; they no longer contain chlorite, albite and epidote, and larger amphiboles and K-feldspars appear. The metamorphic grade increases towards the southeast from epidote-albite through amphibolite, to near-migmatite, which can be most clearly observed within the quartz-mica-amphibole schists (Figure 7.7.j, k and I respectively). Locally the rock shows true migmatitic textures as it has segregated into melanocratic and leucocratic components. This migmatitic zone is about 250 meters wide and shows a consistent hornblende mineral lineation plunging to the southwest. Oblique sinistral shears are abundant and consistent with kinematics in the lower grade parts of the shear. At its southeastern edge the migmatite zone is swamped with pegmatite and a 25D-meter wide zone consists entirely of weakly foliated pegmatite. The pegmatites form the contact with a granite of 2938 ± 15 Ma (geochronology sample *KBnO*), similar to the granite at the south side of the East Turner River traverse. The tectonic foliation within the granite dips moderately to the northwest.

In Figure 7.11 the orientations of foliation and lineation, related to the major sinistral oblique deformation phase in the Tappa Tappa Shear Zone in the West Turner River traverse, are shown. The general trend of the foliation is that it dips to the northwest in the northeast, goes through vertical in the center, and is dips to the northwest in the southeast. This km-scale geometry is

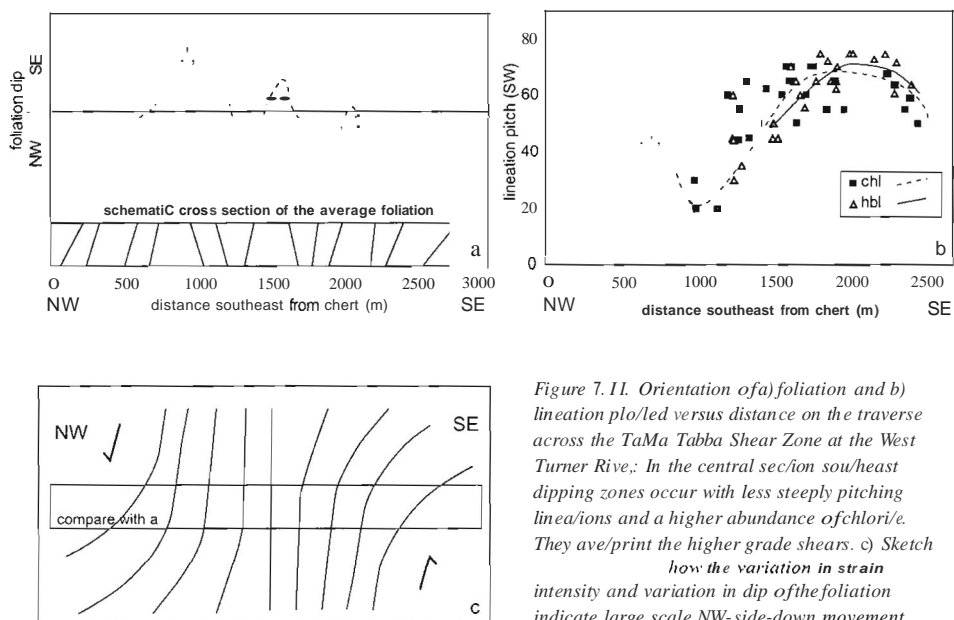


Figure 7.11. Orientation of a) foliation and b) lineation plotted versus distance on the traverse across the Tappa Tappa Shear Zone at the West Turner River. In the central section southeast dipping zones occur with less steeply pitching lineations and a higher abundance of chlorite. They overprint the higher grade shears. c) Sketch how the variation in strain intensity and variation in dip of the foliation indicate large scale NW-side-down movement.

interpreted to indicate large scale normal movement and a strain gradient going from low to high, to low strain again through the Tabba Tabba Shear Zone, as explained in Figure 7.II.c.

In the northwest chlorite is more abundant, indicating overall lower metamorphic grades. In the center, there is a zone with more shallowly plunging lineations i.e. more of a strike-slip component in the movement direction. The chlorite streak lineations occur only on foliation planes, and they overprint the pervasive hornblende lineations at a slightly shallower angle. This is interpreted to reflect renewed oblique sinistral deformation, with a larger strike-slip component and at lower metamorphic grade.

In summary, the deformation history of this area shows a major sinistral oblique phase affected the area during amphibolite grade metamorphism, bringing the northwest-side down. This was followed by a second event with roughly similar kinematics at greenschist grade conditions and is overprinted by a semi-brittle oblique dextral event with northwest-side up movement.

7.3.3.4 Chillerina Well

A set of shear zones runs parallel and to the northwest of the Tabba Tabba Shear Zone, within the Pippingarra granitoid, east of Coogiarinna Well and west of ChilJerina Well (Figure 7.5). The orientation of the tectonic fabrics is shown in Figure 7.6. Sinistral oblique shear bands occur within strongly foliated zones, and stretching lineations plunge to the southwest. There is no indication that this area experienced an early dextral phase of deformation as observed within the Carlindi Batholith on the eastern side of the Tabba Tabba Shear Zone.

Because the granitoid in which the shears were formed intruded into the already deformed Mallina Basin, there must have been two separate oblique sinistral events with roughly similar kinematics affecting the Tabba Tabba area. The first was related to the subsidence of the Mallina Basin, and hornblende mineral lineations formed in the Tabba Tabba Shear Zone during this event. The second occurred later, at lower metamorphic grade, and affected both the Tabba Tabba Shear Zone and the Chillerina granitoids. Smithies and Champion (2001) proposed that these granitoids were intruded syn-kinematically into a releasing bend of the sinistrally deforming Tabba Tabba Shear Zone at about 2940 Ma.

7.3.3.5 Yandeyarra

In the southern extension of the Tabba Tabba Shear Zone, on the western margin of the Yule Batholith (Figure 7.I, Figure 7.12), a brief field study was conducted. Structures within the Pilbara Well Greenstone Belt, on the western side of the contact, have a complex deformation history. Moderately southwest plunging mineral and stretching lineations L1 were observed (Figure 7.12.c). Sinistral shear bands and sinistrally rotated K-fsp clasts occur within the Cheearra Granite, however, the kinematics are locally inconclusive and symmetrical clasts indicate there was a large component of flattening.

In a 2939 ± 12 Ma granite near Black Gin Well (geochronology sample KB746) weakly developed dextral shear bands and associated northeast plunging mineral and stretching lineations L2 have been observed (Figure 7.12.c). The overprinting relations indicate that the dextral event is later than the sinistral event. This sequence is only partly similar to that observed in the northern extension of the Tabba Tabba Shear Zone. An early dextral event has not been observed, nor two separate sinistral events. It may indicate that this part of the shear participated only in the later events.

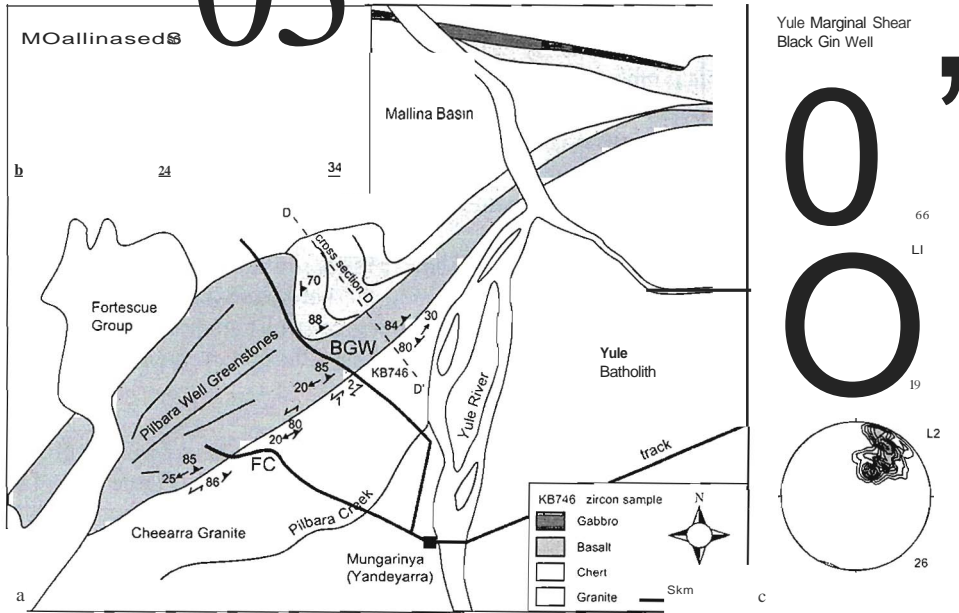


Figure 7.12. a) Simplified geological map of the southern extension of the rabba rabba Shear Zone, in the Yandeyarra Reserve. b) Lower hemisphere equal area stereoplots of structural data in the Mallina Basin. c) Lower hemisphere equal area stereoplots of structural data in the margin of the Yule Batholith. Lithology based on 1:100,000 geological map (Smithies and Farrell, 2000). BGW = Black Gin Well. FC = Friendly Creek. Location of the map area is indicated in Fig 7.1.

7.3.4 Structural geology of the Mallina Basin

Outcrop in the Mallina Basin is generally very poor, however, several locations were visited for structural studies. The regional gravity and magnetic anomaly images provide some information about the sub-surface; an interpretation is shown in Figure 7.2. As the maximum age of the basin fill is 2970 Ma (Smithies et al., 2001), the deformation history will only provide information about the latest tectonic history of the Central Pilbara. In the studied area no unconformities have been observed or reported, so the deformation history applies to the complete observed stratigraphy.

The oldest structures recognized in the Mallina Basin were observed in the southwestern part of the basin near Croydon outstation. Meter-scale tight folds have been observed in the shales (Figure 7.13.a). The FJ fold axes plunge to the east-northeast (Figure 7.14.d). These folds are refolded by a set of north-northeast trending open folds (Figure 7.13.b). This north-northeast trending fabric is only developed in the western half of the Mallina Basin (Figure 7.7.0). Throughout the basin a third, dominant fabric (S3) is present (Figure 7.13.c and Figure 7.14). It is the axial planar cleavage to a set of northeast-trending folds (Figure 7.7.p) and is most strongly developed in the northern and eastern part of the basin. In Figure 7.2 and Figure 7.14 is shown that the different sets of folds do not occur basin-wide. Therefore they are interpreted to be fault-controlled on a local to regional scale. This is in agreement with the distribution of faults and folds on the regional gravity and magnetic anomaly image (Figure 7.2).

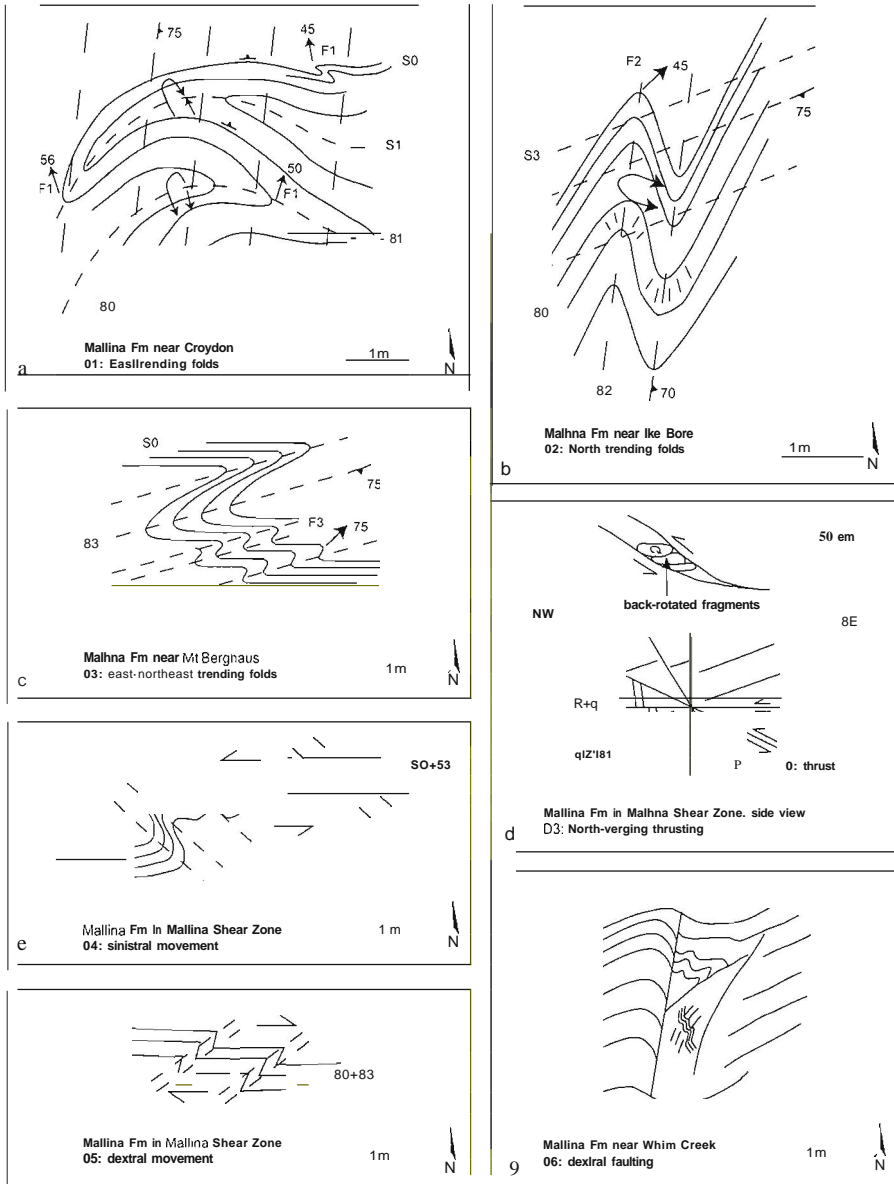


Figure 7.13. Field sketches of the deformation phases observed in the Malina Basin: for location names see Figure 7.2. a) F1 folds refolded by F2, north of Croydon Outstation. b) F2 folds and S2 cleavage observed west of Ike Bore. c) F3 folds, low-scale as well as 10-m scale, observed at Mount Berghaus. d) D3 north-verging thrust structures, observed in the Malina Shear Zone north of Ike Bore. The geometry of minor structures and quartz veins are also consistent with thrusting. e) D4 sinistral movement in the Malina Shear Zone southwest of Malina Homestead. f) D5 dextral brittle asymmetrical kinks/aids observed in the Malina Shear Zone southwest of Malina Homestead. g) North and north-east-trending dextral brittle faults observed near Whim Creek.

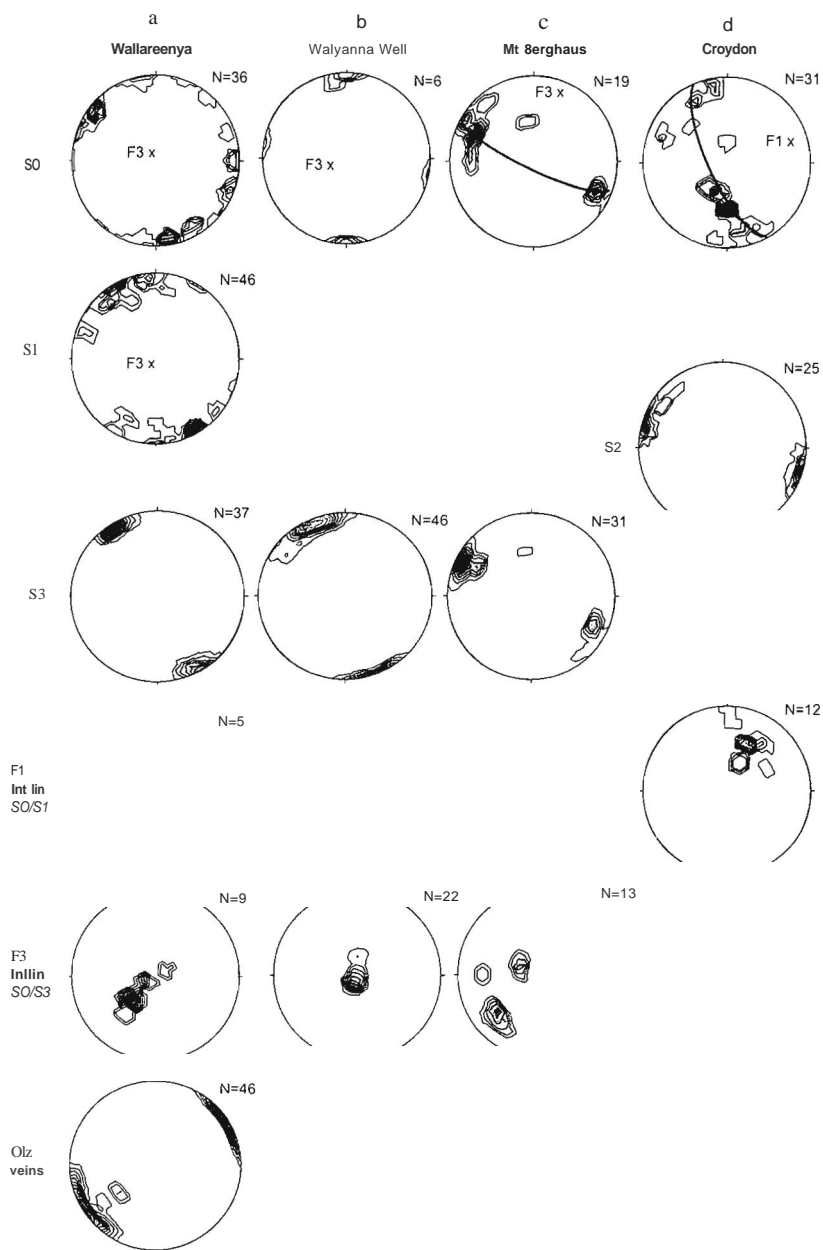


Figure 7.14. StrUCIUr data for the Mollino Basin, represented in lower hemisphere equal area stereoplots. Bin-size adjusted/or $\Delta\lambda$ & contour levels. Location names are indicated in Figure 7.2. The 'x' indicates reconstructed/old axes.

On regional gravity and magnetic anomaly image it can be observed that the Mallina Basin is transected by an east-west trending structure, the Mallina Shear Zone (Figure 7.2). Because it is so prominent in these images, it is interpreted to be the surface expression of a major basement structure. At the surface it now consists of strongly sheared, folded, altered and calcitized metasediments. North-northwest-verging thrust structures were observed in quartzite, north of Ike Bore (Figure 7.13.d). They are interpreted to have formed during the same event as the F3 folds. Locally, sinistrally verging asymmetrical folds were observed within the Mallina Shear Zone (Figure 7.13.e). The dominant fabric within the Mallina Shear Zone is formed by dextral folds and kinks (Figure 7.13.f).

At Wallareenya, just northwest of the Tabba Tabba Shear Zone, a set of very large (1 m wide, 100 m long) quartz veins occurs. They are subvertical and northwest-trending (Figure 7.14.a) and are related to dextral brittle movement on the Tabba Tabba Shear Zone as well as the Mallina Shear Zone. The youngest structures in the Mallina Basin are northeast trending dextral brittle faults, which cross cut all previous structures (Figure 7.13.g).

7.3.5 Summary of deformation history

The regional deformation history can be constructed by combining the data for the Tabba Tabba Shear Zone and the Mallina Basin. The result is summarized in Table 7.5 and will be discussed below. The oldest deformation event within the Tabba Tabba Shear Zone is represented by a regional foliation in the oldest granites on the southeastern side of the structure, seen at the East Turner River and Boundary Well. It is interpreted to be related to a compressional event with a component of dextral shear (D1). Its timing is poorly constrained between the early intrusives in the area and the next event. The second event is a major sinistral transtensional phase of movement on the Tabba Tabba Shear Zone, which is interpreted to be related to the formation of the Mallina Basin (02). This occurred at about 2970 Ma (Smithies et al., 2001). During this event amphibolite grade rocks on the eastern side of the structure were juxtaposed to the sediments in the subsiding Mallina Basin.

Subsequently, the Mallina Basin experienced inversion and folding. The associated structures are not regional, but appear to be mainly fault-controlled. This is confirmed by the regional geophysical images (Figure 7.2). The first phase of inversion (regional 03) produced east-west trending F1 folds and axial planar cleavage, the second north-south trending F2 folds and cleavage (04). During renewed sinistral transtension on the Tabba Tabba Shear Zone, granites and granodiorites intruded the already deformed Mallina Basin (05). Smithies et al. (2001) report a short phase of renewed sedimentation in the northern part of the basin. The last major phase of folding resulted in northeast trending F3 folds and axial planar cleavage, and the Tabba Tabba Shear Zone experienced dextral (brittle) deformation (06). The last deformation event recognized in the area involved dextral normal movement of northeast trending brittle faults and is interpreted to be related to the formation of the Hamersley Basin (07).

7.4 Geochronology

7.4.1 Introduction - geochronology

In this project, geochronological techniques were applied to obtain temporal constraints on the observed tectonic evolution of key areas identified from structural-kinematic analysis. U-Pb zircon dating was applied to obtain information on the primary crystallization history of the area. The results are described in detail in Beintema et al. (in press, or see chapter 6 of this thesis). $^{40}\text{Ar}/^{39}\text{Ar}$ single mineral geochronology was applied to obtain constraints on the (late) thermotectonic evolution of the area and these new data will be presented here.

7.4.2 Analytical techniques - $^{40}\text{Ar}/^{39}\text{Ar}$ geochronology

Samples for $^{40}\text{Ar}/^{39}\text{Ar}$ laser probe geochronology were selected on the basis of suitability of location, structural relations and mineralogy. Sample descriptions can be found in Table 7.3, locations are indicated in Figure 7.3. The selected samples were crushed, sieved and washed before mineral separation. Sieve fractions of 250-500 μm and 125-250 μm were selected. A Carpco roll magnet was used for hornblende separation, sheet silicates were separated with a Faul-table separator. The remaining fractions were cleaned ultrasonically in demineralized water. Between one and fifteen clean single crystals of hornblende, biotite, or muscovite were selected per sample by handpicking under a microscope. Aluminium trays were loaded with 4 flux monitor standards and 16 samples. Several trays were stacked in an aluminium can and irradiated with high-energy neutrons for 75 hours in a rotating cadmium shielded setup (RODEO) in the ECN/EU high flux research nuclear facility in Petten, The Netherlands. The step-heating degassing experiments were carried out at the VU geochronology laboratory in Amsterdam, with an argon laserprobe as described by Wijbrans et al. (1995).

7.4.3 Results - geochronology

The results of all $^{40}\text{Ar}/^{39}\text{Ar}$ analyses are summarized in Table 7.3, age spectra are shown in Figure 7.15. All data of the individual step-heating experiments can be found in Appendix 7.C (on CD). The identification of a plateau age is done according to the following criteria: a minimum of three contiguous steps of ages within 2σ error is required; these steps should yield a well-defined isochron; and a significant portion of the ^{39}Ar release must be during these steps (McDougall and Harrison, 1999). It can be observed that very few samples have yielded good age plateaux. The cumulative probability trend of all step heating analyses from the Tabba Tabba Shear Zone and the Mallina Basin shows maxima at 2870 Ma and 2750 Ma (Figure 7.16), confirming an Archaean history of the area. Significantly several samples have escaped nlll overprinting in the late Archaean or Proterozoic. Samples KB243, KB286, and KB52 yielded more or less disturbed ages >3000 Ma.

Detailed discussion of SHRIMP and LA-ICP-MS U-Pb zircon dating can be found in Beintema et al. (in press, see chapter 6). The results are summarized in Table 7.4; locations are indicated in Figure 7.3.

7.4.4 Discussion - geochronology

The zircon geochronology shows that the Tabba Tabba Shear Zone contains rocks of roughly similar age as the Roebourne Domain in the West Pilbara: 3265 Ma (Nelson, 1998; Smith et al., 1998;

Table 7.3. Sample description and summary of the results of $^{40}\text{Ar}/^{39}\text{Ar}$ analyses (2s errors). CPS locations in UTM zone 50K, AC66. t_f = total fusion.

Sample	GPS	Location	expected result	min	semiplateau (Ma)	% ^{39}Ar	t.f.	(Ma)	
KB134A	0709548	Strelley Mine: mafic	hbl cooling age of	hbl			2670	9	
	7727061	band in muscovite schist	high grade side						
KB134B	0709548	Strelley Mine: muscovite	musc cooling age	musc			1634	13	
	7727061	schist	of high grade event						
KB392	0709541	Strelley Mine: muscovite	musc cooling age	muse	2734	15	95	2693	47
	7727862	schist	of high grade event						
KB416-1	0700130	TT Mine, gabbro	hbl cooling age of	act	2767	15	82	2828	42
	7718044		undef (late) gabbro						
KB416-2 duplo	0700130	TT Mine, gabbro	hbl cooling age of	act	2860	23	93	2925	41
	7718044		undef (late) gabbro						
KB421A	0701552	6 mile W: weakly foliated	musc cooling age	musc			2615	17	
	7709364	monzogranite	of undef (late) gran.						
KB421B	0701552	6 mile W: weakly foliated	bio cooling age of	bio			1907	1710	
	7709364	monzogranite	undef (late) granite						
KB330	0683669	Balbryna W: diorite	hbl cooling age of	hbl	2838	10	85	2837	32
	7700353		diorite intr (early)						
KB351	0682167	Balbryna W pegm vein	musc cooling age	musc	2750	40	78	2727	18
	7699555		of late pegm intr						
KB264A	0678610	ETR, deformed granite	musc cooling age	muse			2721	24	
	7699349		of high grade event						
KB243	0678328	ETR. gabbro	hbl cooling age of	hbl			2817	25	
	7699969		high grade event						
KB265	0678876	ETR: granodiorite	hbl cooling age of	hbl	2825	21	95	2820	20
	7699316		high grade event						
KB286	0663537	WTR gabbro dyke in	hbl cooling age of	hbl			3265	43	
	7691680	muscovite schist	gabbro dyke						
DL27	0664066	WTR. pegmatite	musc cooling age	mu	2865	11	55	2833	17
	7691059		of late pegm intr						
KB309	0663976	WTR: granite patch in	musc cooling age	hbl			2783	24	
	7691118	diorite	of high grade even						
KB52	0589435	Mallina Basin: silly	muse formation	muse	3048	10	73	2964	25
	7685312	horizon in Mallina Shear	age of Mallina Shear						

Smith, in press) and the Sulphur Springs Group in the East Pilbara: 3235 Ma (Buick et al., 2002). Quartz-muscovite and quartz-actinolite schists have been dated at ca 3255 \pm 15 Ma. A granite and granodiorite of ca 3252 \pm 3 Ma could either have been intruded into the ancestral Tabba Tabba Shear Zone, or they represent slices of a previously unknown suite of the Carlindi Batholith of this age. In any case, their known occurrence is restricted to a narrow strip within the Shear Zone. Detrital zircons in the Mallina Basin have a large population of this age, indicating the existence of a significant source area exposing such granites (Smithies et al., 2001).

The center of the Mallina Basin was intruded by high-Mg diorites at 2955 Ma (Smithies and Champion, 1999). Granites directly adjacent to the Tabba Tabba Shear Zone (on both sides), are dominated by a suite with an age of 2940-2930 Ma (Nelson, 2001; Smithies and Champion, 2001; 8eintema et al., in press). A number of granite lithologies have not been dated, such as the strongly deformed banded granite-pegmatite east of the Strelley Mining Center (Figure 7.7.e) and migmatitic gneisses east of the Tabba Tabba Mining Center (Figure 7.7.f). The ages of these rocks are expected to be useful in putting temporal constraints on the early history of the structure.

The $^{40}\text{Ar}/^{39}\text{Ar}$ analyses have mostly yielded post- 2900 Ma ages. However, the total fusion age of an early mafic dyke sample in the West Turner River had a value of 3265 ± 43 Ma. If this represents the cooling age of the hornblende in the dyke (and not excess radiogenic argon acquired from the surrounding rocks) it indicates the dyke is approximately the same age as the quartz-muscovite-actinolite schists and the early granites (~3250 Ma, see Table 7.4 or Chapter 6). The anomalously old step with an age of 3390 Ma suggests that excess argon is present.

The 3050 Ma plateau age of muscovite from the Mallina Shear Zone possibly indicates that the muscovite is of detrital origin. There was no detrital muscovite found in the thin section of this rock, however, it may be present in low abundance. Detrital zircons of similar age have been reported (Nelson, 1997; Smithies et al., 2001). Alternatively, it represents excess radiogenic argon.

Table 7.4 Sample descriptions and SHRIMP and LA-ICP-MS V-Pb zircon results (2s errors). For details see chapter 6. ETR = East Turner River. WTR = West Turner River, (n) = number of analyses.

Sample	GPS	Rock type	Method	Main Population $^{20}\text{Pb}/^{208}\text{Pb}$ (n) date	Xenocrysts $^{20}\text{Pb}/^{208}\text{Pb}$ (n) date	Disturbance $^{20}\text{Pb}/^{208}\text{Pb}$ (n) date
KB263	0678504	Muscovite schist	LA-ICP-MS	3256 ± 18 Ma (43)	3464 ± 44 Ma (5)	2766 ± 52 Ma (2)
	7699525	ETR				
KB264	0678610	Foliated granite	SHRIMP	3251 ± 3 Ma (21)		
	7699349	ETR				
KB265	0678876	Foliated	SHRIMP	3252 ± 3 Ma (19)		3069 ± 41 Ma (4)
	7699316	granodiorite ETR				
KB312	0663537	Muscovite schist	LA-ICP-MS	3254 ± 12 Ma (50)	3629 ± 35 Ma (2)	2758 ± 44 Ma (2)
	7691680	WTR				
KB351	0682167	Aplitic vein ETR	SHRIMP	2944 ± 7 Ma (9)	3241 ± 9 Ma (19)	
	7699555					
KB746	0642906	Granite	LA-ICP-MS	2939 ± 12 Ma (55)	3108 ± 38 Ma (1)	2712 ± 51 Ma (1)
	7654053	Yandeyarra			3251 ± 32 Ma (2)	
KB770	0664812	Granite WTR	LA-ICP-MS	2938 ± 15 Ma (22)	3049 ± 18 Ma (18)	2851 ± 27 Ma (8)
	7690743				3123 ± 15 Ma (22)	2789 ± 57 Ma (1)
					3254 ± 16 Ma (18)	
					3337 ± 22 Ma (7)	
KB779	0684277	Foliated	LA-ICP-MS	3238 ± 10 Ma (50)	3426 ± 27 Ma (2)	3045 ± 24 Ma (10)
	7700096	metadiorite ETR			3465 ± 33 Ma (2)	
KB810	0684259	Metagabbro ETR	LA-ICP-MS	3234 ± 9 Ma (54)		
	7700190					

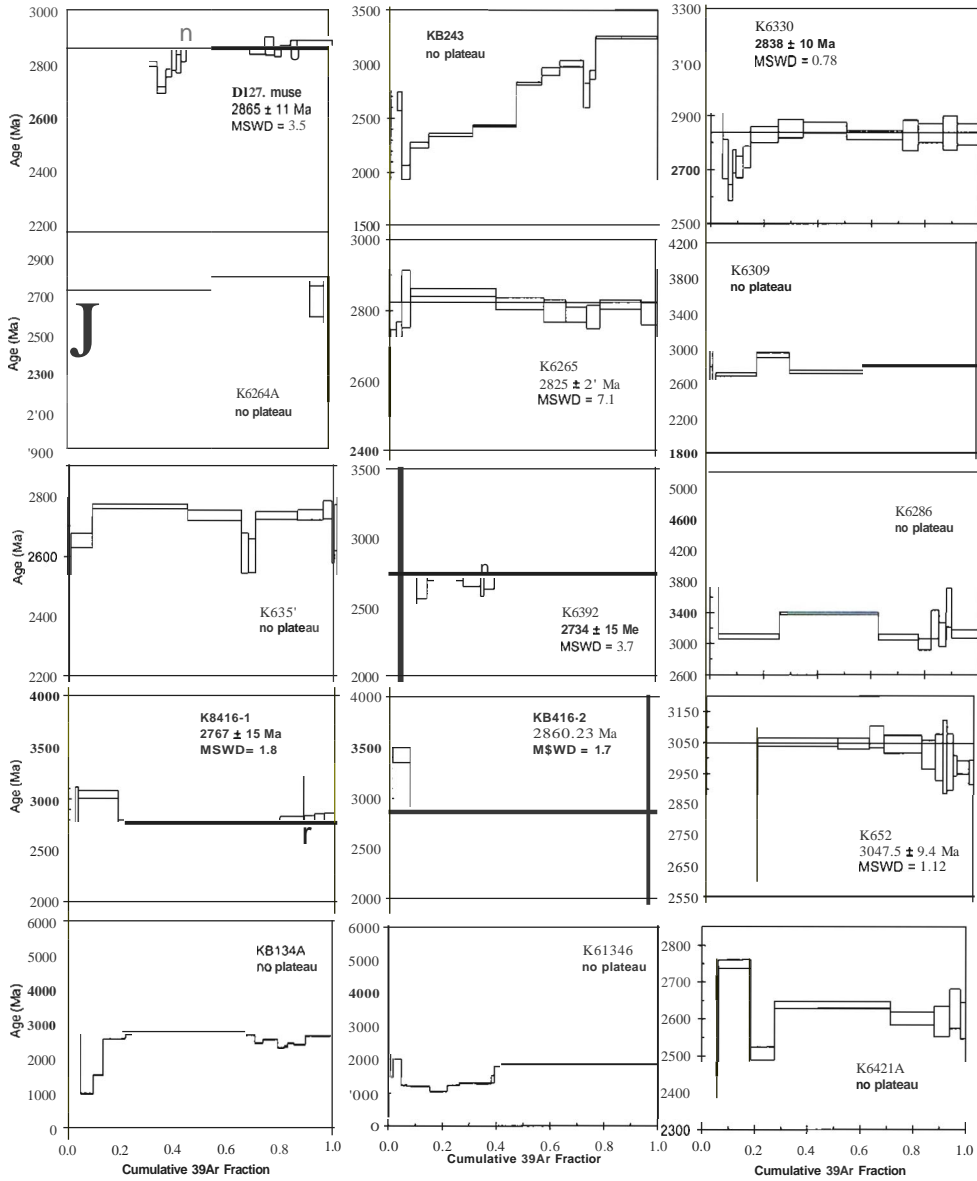


Figure 7.15. Age spectra for $^{40}\text{Ar}/^{39}\text{Ar}$ laser step-heating analyses of 15 samples.

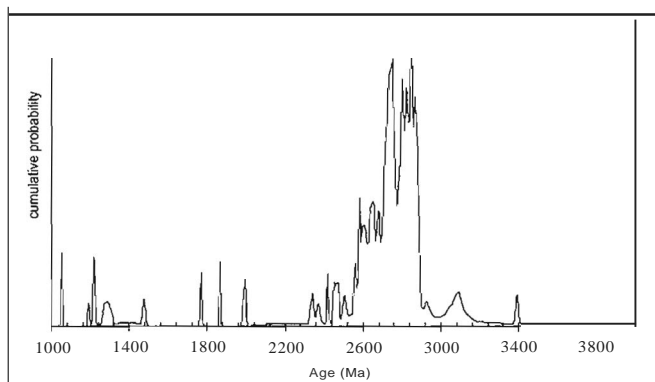


Figure 7.16. Cumulative probability diagram for $a//^{40}\text{Ar}/^{39}\text{Ar}$ data from step-heating experiments, obtained from samples of the Central Pilbara.

Metamorphic muscovite from this area cannot be older than 2970 Ma, because this is the maximum deposition age of the sediments as indicated by the youngest detrital zircons (Smithies et al., 2001). The last three steps of the experiment on this sample have an age of approximately 2960 Ma, which is a realistic age for metamorphic muscovite from the Mallina Shear Zone.

The combined results of all $^{40}\text{Ar}/^{39}\text{Ar}$ analyses (Figure 7.16) indicate two thermal events occurred at ca 2860 Ma and ca 2760 Ma. The first disturbance is interpreted to be due to intrusion of tin-bearing granites and pegmatites of this age, in the Central Pilbara (Blewett, 2002). As the volume of these granites in the Yule Batholith is large, it may have been associated with a significant thermal disturbance of the surrounding rocks. The second event can be correlated to initiation of the overlying Hamersley Basin (Blake, 1993), and intrusion of the Black Range Dykes.

Figure 7.16 reveals that there are Proterozoic disturbances at approximately 1900, 1200 and 900 Ma. The first may correspond to the Capricorn Orogeny which involved deformation, metamorphism and magmatism due to collision of the Pilbara Craton with the Yilgarn Craton to the south (Tyler, 2000). The ca 1200 Ma disturbance corresponds to Grenville age activity which is seen throughout Rodinia, and 900 Ma may be the result of early Pan-African activity in East Gondwana (Rogers et al., 1995). When compared to the results from earlier work in the East Pilbara (e.g. Wijbrans and McDougall, 1987; Davids et al., 1996; Zegers, 1996), more often severely disturbed spectra have been observed, showing evidence for Proterozoic overprinting. However, this effect seems to be much stronger in the West and Central Pilbara.

7.5 Geochemistry

7.5.1 Introduction - geochemistry

The West and Central Pilbara consist of three domains which have been reported to have formed by accretionary and subduction processes (e.g. Krapez and Eisenlohr, 1998; Smith et al., 1998; Kiyokawa et al., 2002). This geochemical study was undertaken to investigate the possible role of subduction, accretion, or intracontinental rifting in the formation and deformation history of the Central Pilbara and its characteristic mafic rock suites. The mafic rocks in the Roeboume Domain and Sholl Belt have been discussed in Chapter 5. The Whim Creek Belt has recently been described in detail by

Pike and Cas (2002) and Pike et al. (2002). This study focuses on the Mallina Basin and the Tabba Tabba Shear Zone.

Mafic and intermediate intrusions in the Mallina Basin have been analyzed in order to characterize the condition of the mantle beneath the Mallina Basin during different stages of the basin development and basin closure. In addition, mafic intrusions from within the Tabba Tabba Shear Zone were sampled, as this structure forms the margin of the Mallina Basin. Within the Tabba Tabba Shear Zone older lithologies occur that may provide information on the earlier history of the Central Pilbara.

It should be noted that the discrimination fields in the presented diagrams are based on modern tectonic regimes. Their relevance for Archaean studies may be limited. Firstly, the samples have experienced alteration and metamorphism, although it will be shown that the effects are limited. Furthermore, tectonic and crustal conditions and processes may have been different in the Archaean, such as the geothermal gradient, source rock chemistry, and the type and angle of subduction, if this occurred at all. The geochemical signature of a rock records the physical-chemical condition of the source region and migration path, i.e. the composition of the source and the temperature, depth and degree of melting at which the melt was formed. This does not necessarily imply a similar tectonic regime as is the modern case.

7.5.2 Analytical methods

Sampling focused on mafic and ultramafic rock types. The least deformed rocks were selected and 2-4 kg of the freshest appearing rock was sampled with a sledge hammer. The sample powders were prepared in a rock splitter and jaw crusher, and ground in a Tungsten-Carbide ring mill. The XRF major element analyses of the KB-numbered samples were carried out with a Siemens SRS 3440 spectrometer, at Utrecht University, the Netherlands. The DL-numbered samples were analyzed by a Philips PW 140411 0 spectrometer at the Vrije Universiteit, Amsterdam, the Netherlands.

For trace element analysis by ICP-MS, 0.1 g of sample powder was dissolved in 4 ml HNO_3 , 3 ml HClO_4 , and 5 ml HF acid, in Teflon bombs. They were heated to 180 degrees for 5 hours, followed by a check for un-dissolved minerals such as zircon. None of the samples needed secondary

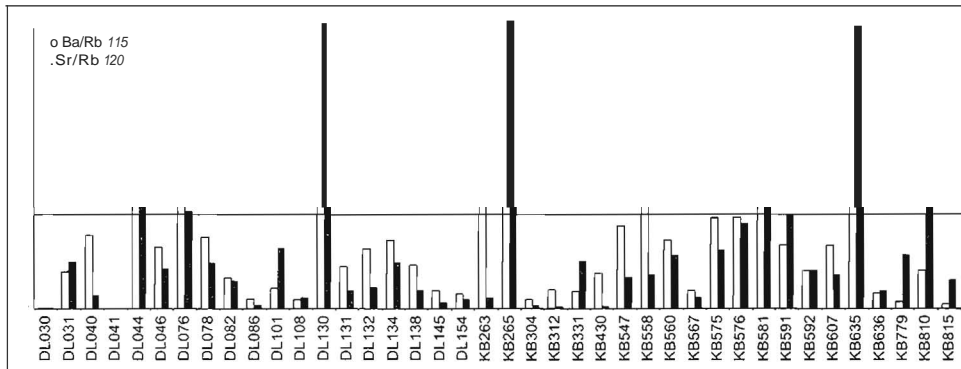


Figure 7. 17. Normalized Ba/Rb and Sr/Rb ratios/or all o/the samples. These ratios can be used as an indication of the degree a/alteration. Normalized values > 1 are all indication O/serious alteration (Hermann and White, /983).

treatment. Trace elements of batch 1 of the KB-numbered samples were measured at Utrecht University, on an Agilent 7500a ICP-MS instrument. KB-batch 2 was measured on an Agilent 4500 ICP-MS instrument with MCN-100 nebulizer, at the Yrije Universiteit, Amsterdam. The DL-numbered samples were analyzed by ICP-MS at Actlabs in Ontario, Canada.

7.5.3 Results of geochemical analyses

At all locations the least deformed samples were selected. Most samples show evidence for at least low greenschist grade metamorphism. However, in some rocks the original igneous textures could still be observed. Sample descriptions and locations have been summarized in Appendix 7.B.1 (on CD), petrographic descriptions in Appendix 7.B.2 (on CD). The results of the major element analyses are given in Appendix 7.B.3 (on CD), the trace elements can be found in Appendix 7.B.4 (on CD).

The major element data are given in weight %, recalculated to a total dry sum of 100% and with total Fe represented as Fe_2O_3 . The uncorrected total sum including the volatiles, deviated no more than 2% from 100% for any of the analyses. To check the accuracy and reproducibility of the major and trace element analyses, in-house and internationally certified standards (BAS-I, OU4, BN02, BR, BHYO-2) were measured as well as sample duplicates. All agreed within standard deviation.

Alteration and metamorphism may have affected the geochemistry of the analyzed rocks. All samples have seen at least low greenschist metamorphism. The samples in the Mallina Basin are expected to have been affected by alteration due to fluids and metamorphism associated with the several phases of folding and cleavage formation in the basin. The samples in the Tabba Tabba Shear zone are all sheared with the exception of the late gabbros, and this is expected to have made them more vulnerable to alteration. In addition, some of these samples unavoidably come from within the contact metamorphic aureole of major granitic intrusions.

Of the major elements Al, Ti, Mn and P have been regarded as relatively immobile (Mullen, 1983). The LILE elements (Rb, Ba, K, U, Sr) are expected to have been most affected by metamorphism and alteration; the other trace elements (HFSE and REE) are expected to have remained immobile (Rollinson, 1993). Certain trace element ratios can be used to check for alteration. Sr and Ba are less mobile than Rb, which is extremely mobile. Alteration commonly results in anomalously high Ba/Rb ratios and low Rb/Sr ratios. In general Ba/Rb ratios > 15 and Rb/Sr ratios < 0.05 are an indication of severe alteration (Hofmann and White, 1983). In Figure 7.17 these normalized ratios are plotted and it can be observed that some of the samples show signs of loss of mobile elements (values > 1 indicate moderate to severe alteration). The most strongly altered samples are from thin dykes (DL044, KB558) or sills (DL076, KB575, KB576, KB581, KB591, KBB635), or strongly foliated schists (DL130, KB263, KB265).

7.5.4 Interpretation of geochemistry

7.5.4.1 Tabba Tabba Shear Zone

The samples of the Tabba Tabba Shear Zone represent a great variety of rock types, which is not surprising because geochronology has shown that the area comprises rock suites that span more than 300 million years, ranging in age between ca 3255 and 2930 Ma (Chapter 6). The major element AFM compositions are very variable (Figure 7.18.a) and this is ascribed to the metamorphism and alteration these rocks experienced because of their occurrence within the shear zone.

On the basis of REE pattern a number of groups has been distinguished (Figure 7.19). One suite of early mafic rocks (early mafics 'A', ca 3235 Ma) forms a tholeiitic to komatiitic series

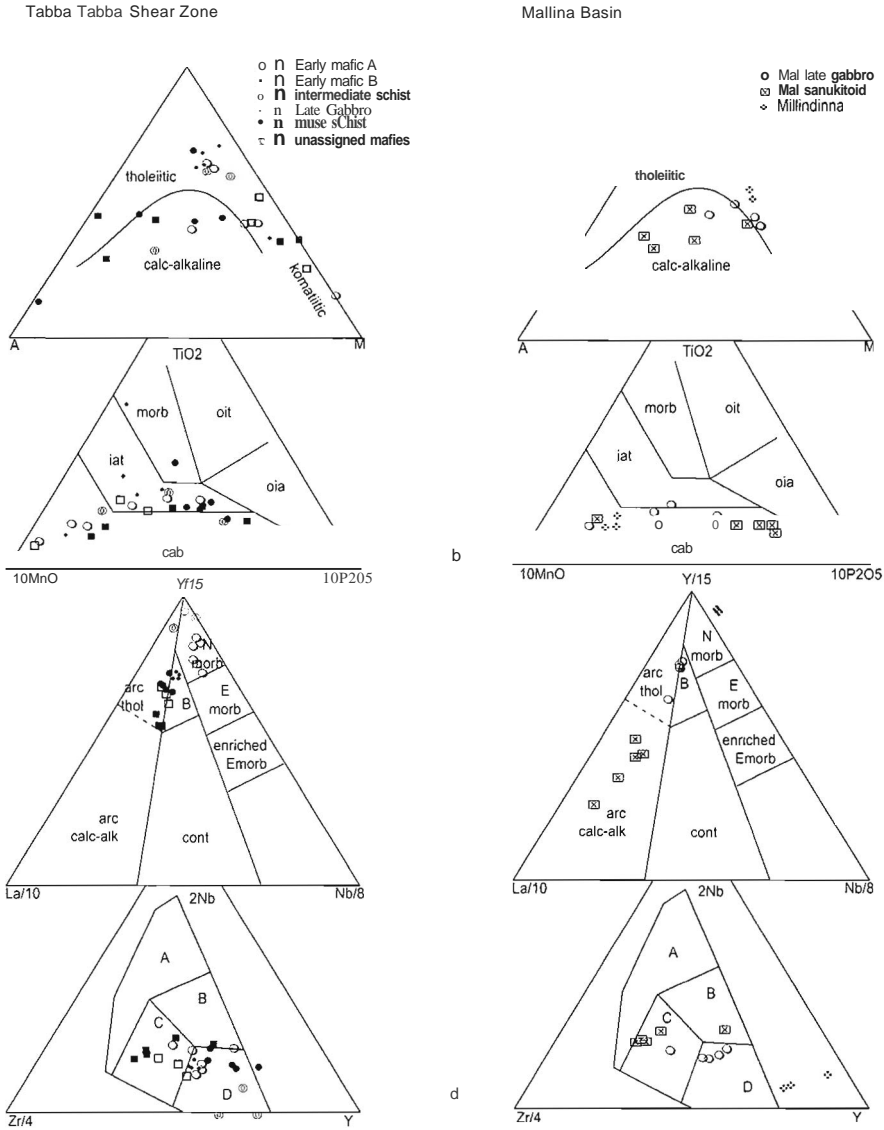


Figure 7.18. Triplots. a) AFM diagram (Irvine and Baragw; 1971). b) MnO-TiO₂-P₂O₅ diagram: cab = calc-alkaline basalt, oia = oceanic island alkaline basalt, oit = oceanic island tholeiitic basalt. morb = mid ocean ridge basalt. iat = island arc tholeiite (Mullen, 1983). c) La/10-Y/15-Nb/8 diagram. B = back arc basalts (Cabanis and Lecoq, 1989) d) Zr/4-2Nb-Y diagram. A = Intraplate alkali basalts. B = plume and E-type MORB, C = Intraplate tholeiites, D = normal MORB. Volcanic arc basalts plot in areas C and D. (Meschede, 1986)

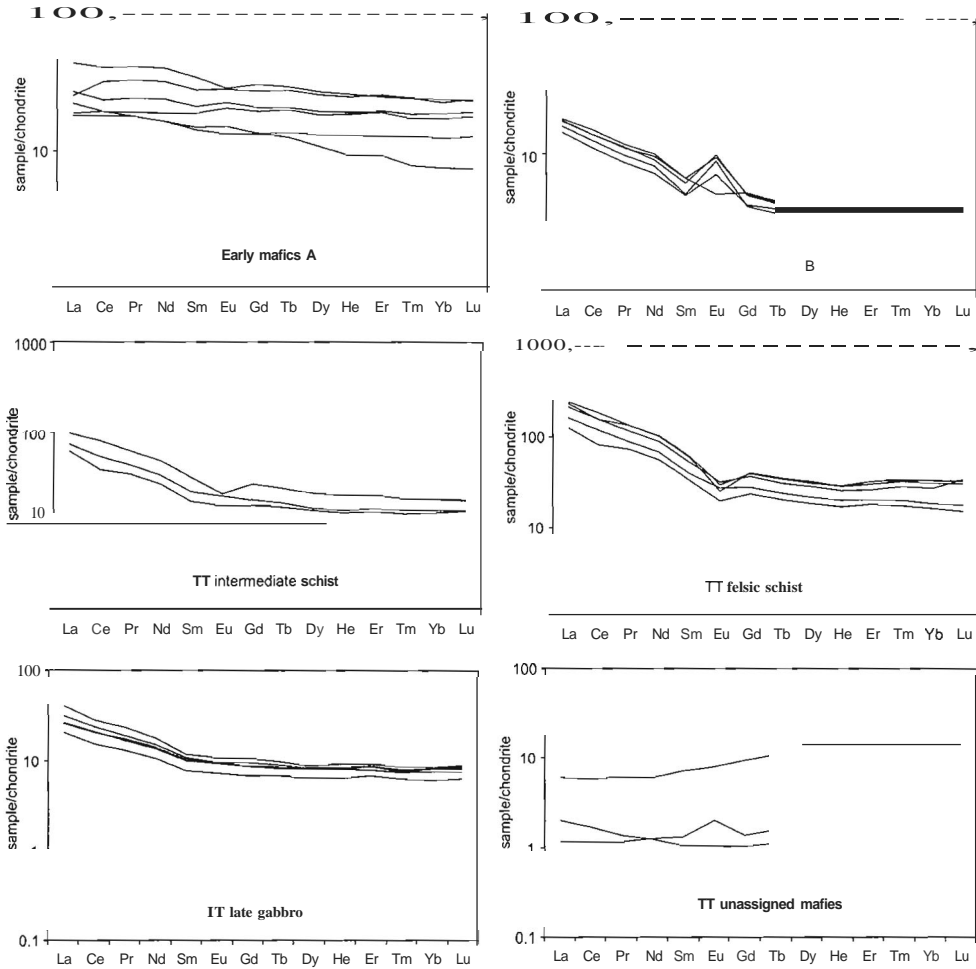


Figure 7.19. Chondrite normalized REE patterns of the samples from the Tabba Tabba Shear Zone, normalizing values from Sun and McDonough (1989).

(Figure 7.18.a). In the Mullen (1983) plot they form a series between island arc tholeiites and calc alkaline basalts (Figure 7.18.b). In the diagram of Cabanis and Lecolle (1989) the samples plot in the N-MORB field (Figure 7.18.c). In the diagram by Meschede (1986) they are classified as arc basalts (Figure 7.18.d). The samples have relatively flat, but overall enriched REE patterns and no Eu anomaly (Figure 7.19.a). The arc-tholeiitic signature of early mafics 'A' and their flat REE patterns suggest an intraplate or back-arc setting, however, in the EMORB-normalized trace element diagram there is no negative Nb anomaly (Figure 7.20). A slight depletion in MREE may indicate the presence of some amphibole or garnet in the residue. These rocks have not been dated, and they are distinctly different from early mafics 'B' by which they are intruded.

Early mafics 'B' plot in the calc-alkaline field in Figure 7.18.a, and are classified as arc tholeiites in Figure 7.18.b and c. In Figure 7.18.d they are very clearly arc-related. The rocks are

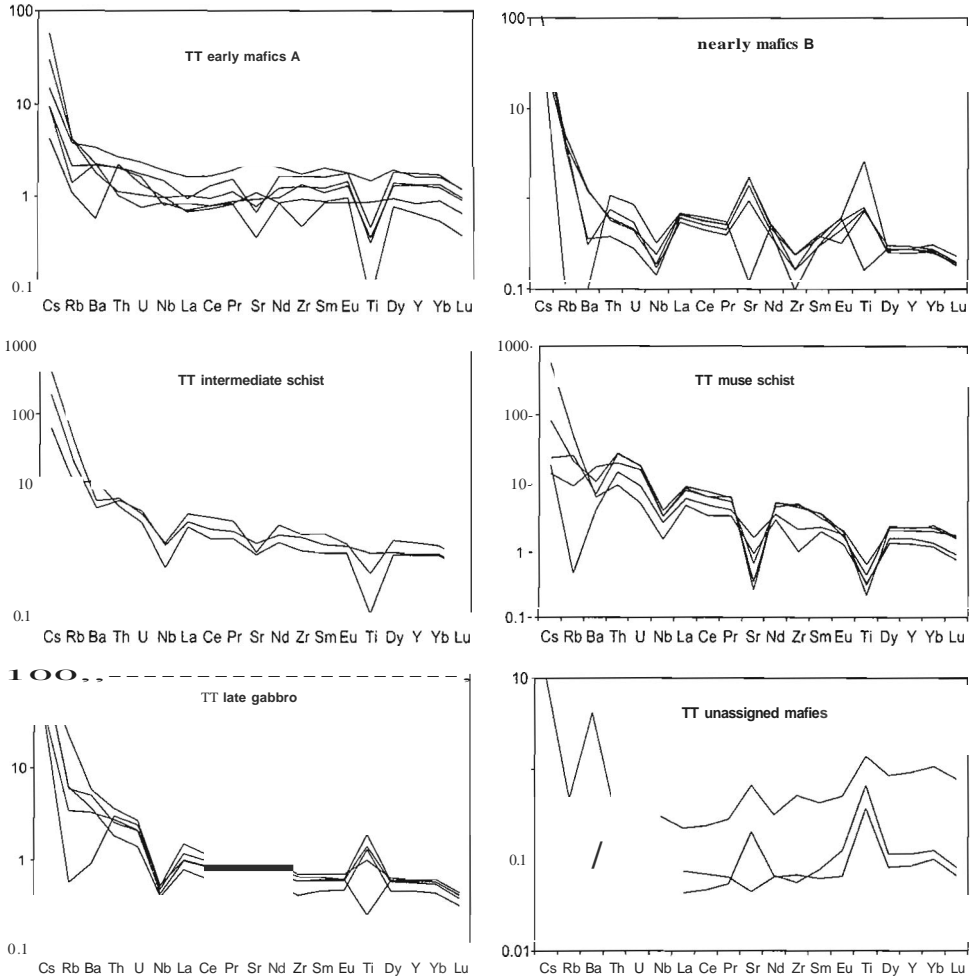


Figure 7.20. EMORB normalized REE patterns of the samples from the Tabba Tabba Shear Zone. normalizing values from Sun and McDonough (1989).

LILE and LREE enriched, and have strong positive Eu anomalies (Figure 7.19.b) interpreted to reflect plagioclase accumulation. The EMORB-normalized pattern of early mafics 'B' shows a very pronounced negative Nb anomaly (Figure 7.20). This might be expected to be accompanied by a negative Ti anomaly, however, in these rocks titanite may occur as a cumulate phase causing the positive anomaly. These rocks have been dated at 3235 ± 15 Ma (Chapter 6). They are interpreted to have originated in a subduction-related environment. This could possibly correlate to the ca 3265 Ma subduction event found in the West Pilbara (Chapter 5).

The oldest rocks that were analysed are a distinct group of intermediate and felsic schists which are interpreted to be of gabbroic origin, and belong to one suite. This is supported by their zircon geochronology: all of these rocks have ages between 3255 and 3250 Ma (Chapter 6). Their major element compositions are quite variable but indicate a high-Mg tholeiitic affinity (Figure

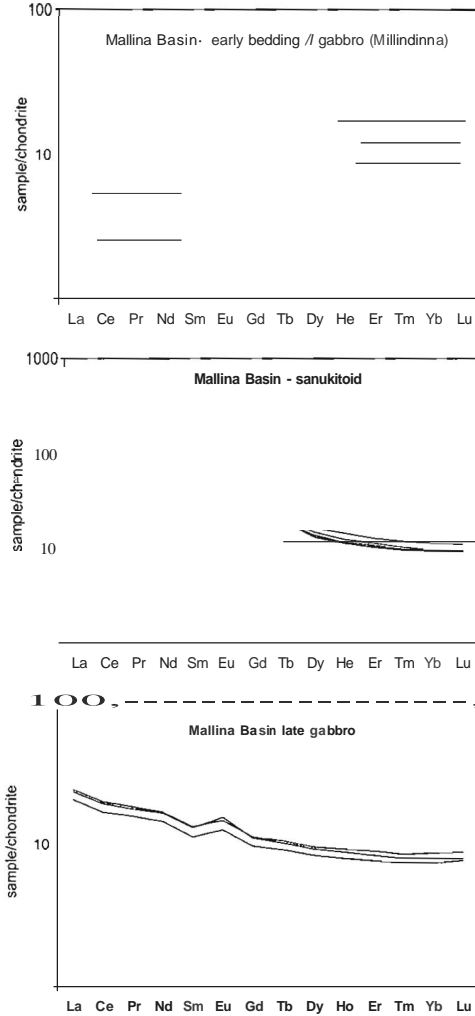


Figure 7.21. Chondrite normalized REE patterns of the samples from the Mallina Basin, normalizing values from Stin and McDonough (1989).

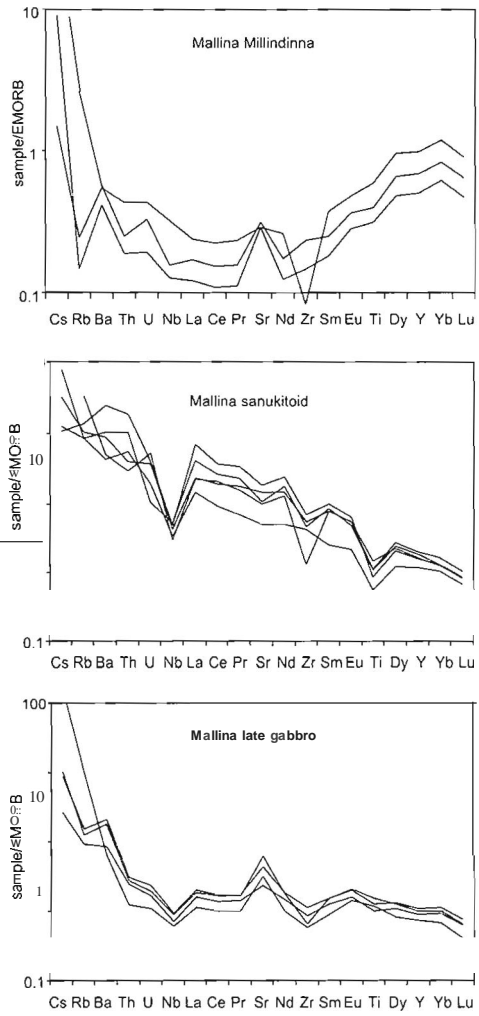


Figure 7.22. E-MORB normalized trace element patterns of the samples from the Mallina Basin, normalizing values from Sun and McDonough (1989).

7.18.a), although some of them have high Al_2O_3 contents up to 18%. In Figure 7.18.b the schists plot in the calc-alkaline to arc-tholeiitic field. In Figure 7.18.c they are classified as arc tholeiites and in Figure 7.18.d as intraplate tholeiites. The pure quartz-muscovite schists are overall more enriched than the intermediate schists, and have more strongly developed negative Eu and Sr anomalies reflecting increasing degrees of plagioclase fractionation (Figure 7.19, Figure 7.20). The rocks have very strongly developed negative Nb and Ti anomalies suggesting a crustal component. Possibly they were formed in the same continental arc setting as early mafics '8' and the ca 3265 Ma West Pilbara arc-related rocks.

Late gabbros (ca 2930 Ma) occur at the western side of the Tabba Tabba Shear Zone (see Figure 7.4). They plot in Fe-tholeiitic field in Figure 7.18.a, and are arc tholeiites and back-arc gabbros in Figure 7.18.b and c. In Figure 7.18.d they are volcanic arc gabbros. They are LREE enriched and have no Eu anomalies (Figure 7.19.c), reflecting an enriched source region below the stability field of plagioclase (Drake and Weill, 1975). The negative Nb anomaly indicates a crustal component, possibly indicating volcanic-arc affinity.

Finally, unassigned mafic rocks are reported, associated with the early schists and mafics in the Tabba Tabba Shear Zone, amongst which peridotitic komatiites. They are tholeiitic with a possible N-MORB affinity (Figure 7.18). However, they are very depleted and the REE and EMORB normalized trace element patterns are slightly U-shaped. Especially the least depleted sample (DL 130) resembles the boninite-like rocks in the Mallina Basin (see next section). Unfortunately, their structural and geochronological relations are unclear.

7.5.4.2 Mallina Basin

Three samples were taken of the ca 2970 Ma Millindinna mafic intrusive suite in the Mallina Basin. Two samples come from the core of the Croydon Anticline; one sample was taken at Walyanna Well (see Figure 7.2). These rocks are tholeiitic in the AFM-diagram (Figure 7.18.a), and have high MgO contents (7-9%). However, they are calc-alkaline on the basis of MnO, TiO₁ and P₂O₅ (Figure 7.18.b), and MORB-like in the trace-element triplots (Figure 7.18.c and d). Smithies (2002) reported these rocks in the Croydon Anticline and has described them in detail. They have V-shaped trace element patterns characteristic of boninitic rocks (Figure 7.21, Figure 7.22). Smithies (2002) found these rocks remarkable in their apparent lack of association with a subduction setting, as would be expected from modern analogues (Crawford, 1989), and interpreted that they may have been derived from a mantle source that was enriched during an earlier subduction event.

Five samples of the ca 2955 Ma granodiorite intrusions (sanukitoids) from the Mallina Basin plot in the calc-alkaline field (Figure 7.18.b). They contain up to 11% MgO, and have high Ni and Cr contents (up to 600 ppm and 300 ppm respectively). In Figure 7.18.a the rocks also plot in the calc-alkaline field, and in Figure 7.18.b they form an calc-alkaline series. In Figure 7.18 they are also classified as arc-cal-alkaline, but in Figure 7.18.d they are intraplate tholeiites. They are strongly enriched in LREE and have no, to very weak, Eu anomalies (Figure 7.21). The EMORB-normalised trace element patterns show strongly developed negative Nb and Ti anomalies (Figure 7.22). Smithies and Champion (1999) reported similar rocks (sanukitoids), and explained this combination of properties by melting of a metasomatized mantle. They suggested that the diorites were derived from an enriched mantle source, but they noted the absence of evidence for coeval subduction at the time of their emplacement, approximately 2955 Ma (Nelson, 2000). However, this study has shown that between 2955 Ma and 2930 Ma the Mallina Basin was in the process of being deformed by several phases of folding between transcurrent crustal scale structures, and speculation about the far-field causes for this deformation does not exclude the possibility of subduction. Alternatively, the enrichment OCCURRED during an earlier subduction event.

The third group of rocks sampled in the Mallina Basin are ca 2930 Ma undeformed late gabbros from the central part of the basin. The plot on the borderline of calc-alkaline and tholeiitic fields (Figure 7.18.a and b) and show a possible back-arc or even MORB relation in Figure 7.18.c and d respectively. They have a weak positive Eu anomaly and LREE enrichment Figure 7.21. A negative Nb anomaly in Figure 7.22 suggest the involvement of a crustal component.

7.5.5 Summary of geochemistry

The granite-granodiorite suite within the Tabba Tabba Shear Zone, and schists that were derived from them, are quite high in Mg and have arc-tholeiite affinity with distinctly negative Nb and Ti anomalies. Early mafics 'A' have many characteristics of intraplate tholeiites, however, they lack a negative Nb anomaly to support this. Early mafics 'B' are a more calc-alkaline association of continental arc rocks. All of these ca 3255-3235 Ma arc-related rocks possibly coITelate to the ca 3265 Ma arc-related rocks in the West Pilbara.

The ca 2970 Ma Millindinna suite are boninite-like rocks, even though they occur in a continental basin without evidence for coeval subduction (see also Smithies, 2002). Their OCCUTence is not limited to the southern part of the basin as they have now been identified in the central part as well. The slightly younger (ca 2955 Ma) sanukitoids in the Mallina Basin are high-Mg calc-alkaline arc-related rocks derived from a subduction-modified mantle (see also Smithies and Champion, 1999), but also at this time there was no evidence for coeval subduction. However, their intrusion coincides with a regional northwest-southeast compressive regime and the far-field cause for this is now known.

Ca 2930 Ma gabbros that line the Tabba Tabba Shear Zone on the western side (Figure 7.3) are arc-tholeiitic gabbros with a crustal component as indicated by their negative Nb anomalies. They are quite similar to the late gabbros from the center of the Mallina Basin, but those show evidence for plagioclase accumulation and are richer in Mg. They are interpreted to be post-orogenic continental gabbros.

A small number of mafic rocks from the Tabba Tabba Shear Zone does not belong to any of the groups described above. They are associated with the early schists and mafics in the Tabba Tabba Shear Zone but their precise structural and geochronological relations are unclear. They vaguely resemble the Millindinna boninite-Iike rocks, but are much more depleted. Clearly these rocks represent an interesting and challenging target for further research if their relation to the sUITounding rocks can be unraveled.

7.6 Synthesis

Based on field observations, geochemistry, and relative and absolute geochronology, a consistent sequence of events can be described for the Tabba Tabba Shear Zone and adjacent Mallina Basin in the Central Pilbara. This has been summarized in Table 7.5. The area was intruded by a granite-granodioritic suite at about 3251 ± 3 Ma and by a diorite-gabbro suite at about 3235 ± 15 Ma (Beintema et al., in press). Xenocrysts in these rocks indicate the presence of precursor or basement rocks similar in age to the WalTawoona Group in the East Pilbara (3.42-3.46 Ga). Mafic schists with tholeiitic characteristics are intercalated with these felsic and intermediate schists. There is no conclusive evidence that indicates whether the intrusive suites were emplaced into the ancestral Tabba Tabba Shear Zone, or were incorporated into the shear zone as crustal slices, at a later stage. However, their occurrence and that of the felsic, intermediate and mafic schists is currently confined to a narrow strip within the Tabba Tabba Shear Zone. Geochemistry indicates these rocks have arc-affinity and they possibly correlate to the ca 3265 Ma arc-related rocks in the West Pilbara.

Local dextral and compressive structures and the dextral geometry of a regional foliation on the eastern side of the structure indicate that the Tabba Tabba Shear Zone experienced an early deformation phase with a dextral component (D 1), but the exact timing of this event remains uncertain (Table 7.5). These structures only occur in the ~ 3255 to ~3235 Ma rocks and they are overprinted

Deformation phase Timing (Ma)	Regional stress regime	Mallina Basin										Mallina Basin	Tabba Tabba Shear Zone		Tectonic regime					
		Mallina Sz	Croydon	Ike Bere	Mt Beaufort	West Turne R	East Turne R	Boundary Wel	Streley Mine	Chierria Wel	Yandeyama									
2770 07																	breakup of continental plate containing the Pilbara Craton end of active tectonics			
2930 06				F3	F3												post-orogenic granitoids and continental gabbros dextral transpression, low greenschist metamorphic grade	major regional nw-se compressional event far field cause unknown		
2940 05																	ca 2930 Ma Intrusion (d) granite/continental gabbro regional northwest-verging folding and thrusting: inversion	2940 Ma Intrusion (a) granite/pegm sinistral transtension greenschist metamorphic grade	brief local episode of intracontinental transtension	
pre 2955 04			F2	F2													ca 2940 Ma Intrusion (d) granite/pegm minor sedimentation (d) ca 2955 Ma Intrusion (c) high Mg granodiorite fault-controlled local folding/inversion	intracontinental compression far-field tectonic cause not known subduction-modified mantle		
pre 2955 03			F1														ca 2955 Ma Intrusion (c) high Mg granodiorite fault-controlled local folding/inversion	intracontinental compression far-field tectonic cause not known subduction-modified mantle		
2970 02																	major sedimentation (b)	sinistral transtension, amphibolite metamorphic grade in footwall	sedimentation 'boninites?' intracontinental transtensional basin	
post 3235 01																		dextral shear		
																		pre- 01	3235 Ma Intrusion (a) gabbro/diorite 3252 Ma Intrusion (a) granite/grDnodiiorite	continental volcanic arc? or intraplate magmatism

Table 7.5. Summary of deformation events in the Mallina Basin and Tabba Tabba Shear Zone. It shows a consistent deformation history affected only by the curved geometry of the Tabba Tabba Shear Zone, and by intrusive events. See text for discussion in regional context. References for absolute ages: a: Beitema et al (in press), b: Smithes, R.H., Nelson, D.R. and Pike, G., (2001), c: Smithes and Champion (1999), d: Smithes and Champion (2001).

by all following events. It must have occurred early in the history of the area and at least before 2970 Ma, when the next deformation phase occurred. Geochemical analyses reveal that some of the earlier mafic intrusions into the Tabba Tabba Shear Zone have very high Mg contents, indicating that the Tabba Tabba Shear Zone is a structure that might extend into the mantle (also reported by Smithies and Champion, 1999; De Leeuw et al., 2001). From geochemical analysis it is clear that within the Tabba Tabba Shear Zone there is no evidence for the preservation of MORB-like slices of lithosphere, as may be expected in a true suture zone. There is also no evidence for the presence of a large accretionary complex. However, they may be hidden beneath the Mallina Basin or removed by erosion.

The Tabba Tabba Shear Zone experienced a major phase of sinistral transtensional movement, bringing the northwest block down relative to the southeast: the structure acted as a bounding fault of the Mallina Basin (O2). During the early stages of basin development, mafic rocks with boninite-like characteristics were emplaced into the lower part of the basin. However, there is no direct evidence for a subduction-related event at that time, but it can not be ruled out as a possible mechanism (Table 7.5). This was followed by a few local, fault controlled deformation (inversion) events in the Mallina Basin (D3, D4), followed by large-scale intrusion of dioritic to granitic calc-alkaline material into the Mallina Basin at approximately 2955 Ma. These rocks have been described as sanukitoids (Nelson, 1998; Smithies and Champion, 1998) and they too are remarkable in their lack of a subduction setting. As a renewed phase of sinistral transtension affected the Tabba Tabba Shear Zone (O5), sedimentation occurred in the northern part of the Mallina Basin (Smithies et al., 2001), and granites were intruded along the Tabba Tabba Shear Zone at approximately 2940 Ma (Smithies and Champion, 2001).

The Tabba Tabba Shear Zone and Mallina Basin were intruded by a suite of calc-alkaline intracontinental granites and gabbros between 2940 and 2930 Ma (Nelson, 1998-2001). Xenocrysts in these rocks indicate the presence of precursor or basement rocks similar in age to the Whundo Group in the Sholl Belt (3120 Ma, Beintema et al., in press, see chapter 6). This is interpreted to indicate that not only the western part, but also the eastern part of the Central Pilbara was affected by a magmatic event at about 3120 Ma, and consequently, that the East and West Pilbara Craton were probably geographically close at that time.

A major northwest-southeast-directed compressional event (D6) resulted in the formation of the main regional northeast trending folds and associated axial planar foliation in the Mallina Basin, and the observed late brittle dextral event on the Tabba Tabba Shear Zone is interpreted to correspond to this event (Table 7.5). The far-field cause for this event is not known, and probably lies outside the presently exposed granite-greenstone terrain.

The combined results of all $^{40}\text{Ar}/^{39}\text{Ar}$ analyses, and the weak overprints found in all in zircon samples, indicate two thermal overprints occurred. The first disturbance at ca 2860 Ma is interpreted to be due to intrusion of tin-bearing granites and pegmatites in the area (Blewett, 2002). As the volume of these granites in the Yule Batholith is large, it may have been associated with a significant thermal disturbance of the surrounding rocks. The second event, at ca 2760 Ma, can be correlated to initiation of the overlying Hamersley Basin (Blake, 1993), and intrusion of the Black Range Dykes. Proterozoic disturbances occurred at approximately 1900, 1200 and 900 Ma. The first may correspond to the Capricorn Orogeny (Tyler, 2000). The ca 1200 Ma disturbance corresponds to Grenville age activity which is seen throughout Rodinia, and 900 Ma may be the result of early Pan-African activity in East Gondwana (Rogers et al., 1995). This overprinting effect seems to be much stronger in the WeSL and Central Pilbara than in the East Pilbara.

7.7 Summary & Conclusions

The central part of the exposed Pilbara Craton has a complex geological history spanning more than 700 million years. The - 3.47-3.43 Ga Warrawoona Group and granites of similar age are the oldest components of the rock record in the East Pilbara, adjacent to the Tabba Tabba Shear Zone. A granite-granodiorite suite with arc-affinity intruded between 3255 and 3250 Ma, and a tholeiitic gabbro-diorite suite with arc-affinity intruded at ca 3235 Ma. These rocks are possibly *related* to the slightly older arc-rocks in the West Pilbara (ca 3265 Ma) and the Sulphur Springs Group in the East Pilbara (Buick et al., 2002). There is no evidence for the presence of an accretionary wedge or crustal slices with oceanic affinity, as would be expected if the Tabba Tabba Shear Zone were a true suture zone along which continental blocks were assembled that were once separated by an ocean.

The area experienced an early dextral transpressional deformation phase before the Tabba Tabba Shear Zone became active as a sinistral transtensional structure. The western margin of the East Pilbara, now formed by the Tabba Tabba Shear Zone, is also the eastern margin of the Mallina Basin. This basin contains the ca 3020 Ma Cleaverville Formation, the 30JO Ma Whim Creek group, and the 2990-2970 Ma Mallina and Bookingarra Groups, which were deposited during several phases of transtensional basin formation. Inversion and folding within the Mallina Basin between ca 2970 and 2940 Ma was mostly local and fault-controlled.

The Mallina Basin and Tabba Tabba Shear Zone were intruded by sanukitoids at ca 2955 Ma (Smithies and Champion, 1999). There is no evidence for coeval subduction but the regional compression at that time may be the result of an unknown far-field tectonic event. Post orogenic granite and continental gabbro intruded between 2940 and 2930 Ma. A final northwest-southeast directed compressional event occurred at about 2930 Ma.

The area was thermally disturbed by granites and pegmatites at about 2860 Ma, and subjected to several kilometers of erosion, before it was disturbed by the opening of the Hamersley Basin at about 2760 Ma. Major Proterozoic orogenic events along the western margin of the craton caused a prolonged history of disturbance.

Acknowledgements

I would like to thank the Dr. Schürmann Fund for their financial support of the field work with grant numbers 1998/14, 1999/14, 2000/14a and 2001/14a, and the Molengraaff Fund for their financial support of the field work in 1998-2001. Dr. R.H. Smithies is thanked for providing GSWA imagery and air photos, and geological discussions and feedback. Dr. R.S. Blewett is thanked for providing geophysical imagery in a collaborative program with AGSO. Diana de Leeuw analyzed a portion of the geochemistry samples discussed in this chapter, as part of her M.Sc. project at the Vrije Universiteit Amsterdam in 1999. She is thanked for making her data available. Helen de Waard is thanked for performing the second batch of ICP-MS analyses at Utrecht University in 2001, and Bas van der Wagt for performing the third batch of ICP-MS analyses in 2003, at the Vrije Universiteit Amsterdam. I would like to thank Dr. Herman van Roermund, Dr. Kim Hein, Dr. Hugh Smithies, Diana de Leeuw, Pieter Bruijnen, and Stephanie Velkamp for their assistance and company in the field.

The West and Central Pilbara Craton, Australia: a mid-Archaean active continental margin

Abstract

The mid-Archaean granite-greenstone terrain in the Pilbara Craton in Western Australia consists of several elongate domains. It has been previously suggested that this 'domainal' architecture reflects a history of accretion. Models have been proposed in which the western margin of the Pilbara was interpreted to be an accreted island arc. However, no evidence for island arc accretion in the presently exposed granite-greenstone terrain was found. In this paper an alternative model is proposed, where the West and Central Pilbara represent a small part of an Andean type active continental margin associated with at least two episodes of subduction beneath the West Pilbara from the northwest. The continental margin was subsequently affected by several phases of transpression and transtension involving major crustal scale structures, resulting in the formation and deformation of the intracontinental Mallina Basin.

The components of the West Pilbara were formed over a history spanning more than 300 million years between ca 3270 Ma and 2930 Ma. The 'island-arc' components of the West Pilbara are at least 100 million years older than the 'extensional back-arc' components of the Central Pilbara, making a genetic link unlikely. Further more, extensional back arc basins form only when the subducting plate goes down at a sufficiently high angle to cause extension in the overriding plate. This can only occur when the downgoing plate has a negative buoyancy, which was believed to be unlikely in the early Archaean because of the higher mantle temperatures and associated thicker and more buoyant basaltic oceanic crust. However, geochemical data confirm that subduction may have occurred in the mid to late Archaean. It is proposed that this occurred at a low angle, beneath an convergent continental margin.

8.1 Introduction

The aim of this chapter is to summarize and integrate the data collected in the Pilbara and presented in the previous chapters in this thesis, and to place them in an Archaean geodynamic context. It has been argued that geodynamic processes may have been significantly different in the Archaean than

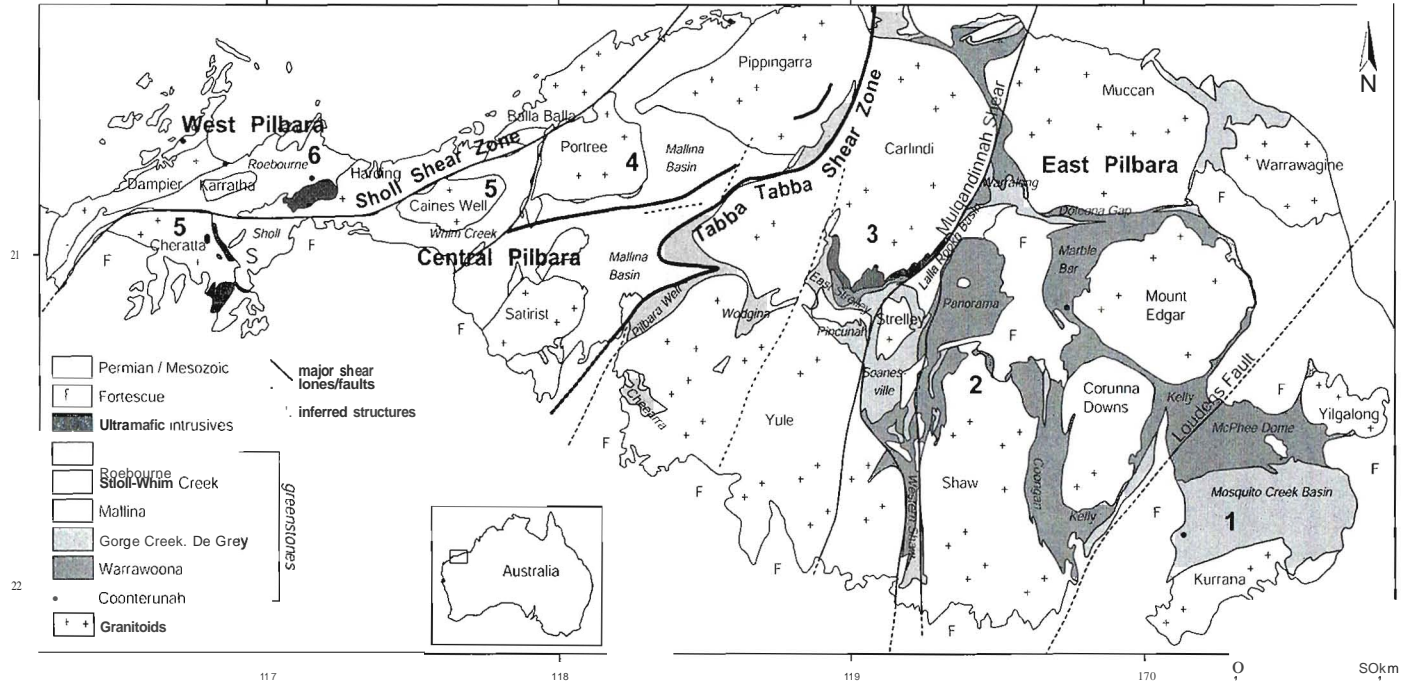


Figure 8.1. The Pilbara Cratoll in North Western Australia. The main supracrustal groups, granitoid complexes and major structures are shown. The six domains of Krupar and Eisler (1998) are also indicated: 1 = Nullagine Domain, 2 = Marble Bar Domain, 3 = Pilgangoora Domain, 4 = Mallina Domain, 5 = Sholl-Whim Creek Domain, 6 = Roebourne Domain. Van Kranendonk et al. (2002) include the Sholl Belt (S) in the West Pilbara. Blewett (2002) and this study consider the Sholl Shear Zone to be the boundary between the West and Central Pilbara. The Tabba Tabba Shear Zone is the boundary between the Central and East Pilbara. Names in small regular font are granitoid complexes. Names in small italic font are greenstone belts.

in the Phanerozoic, due to a higher potential mantle temperature and possibly different modes of heat loss for the cooling Earth. There is still controversy on whether Phanerozoic-style plate tectonics, characterized by spreading and subduction of the ocean floor, and continental growth by lateral accretion of terranes (Rudnick, 1995), operated in the early Archaean. However, recently much geological data have been collected, and will be discussed below, indicating that this possibly was an active process in the mid and late Archaean.

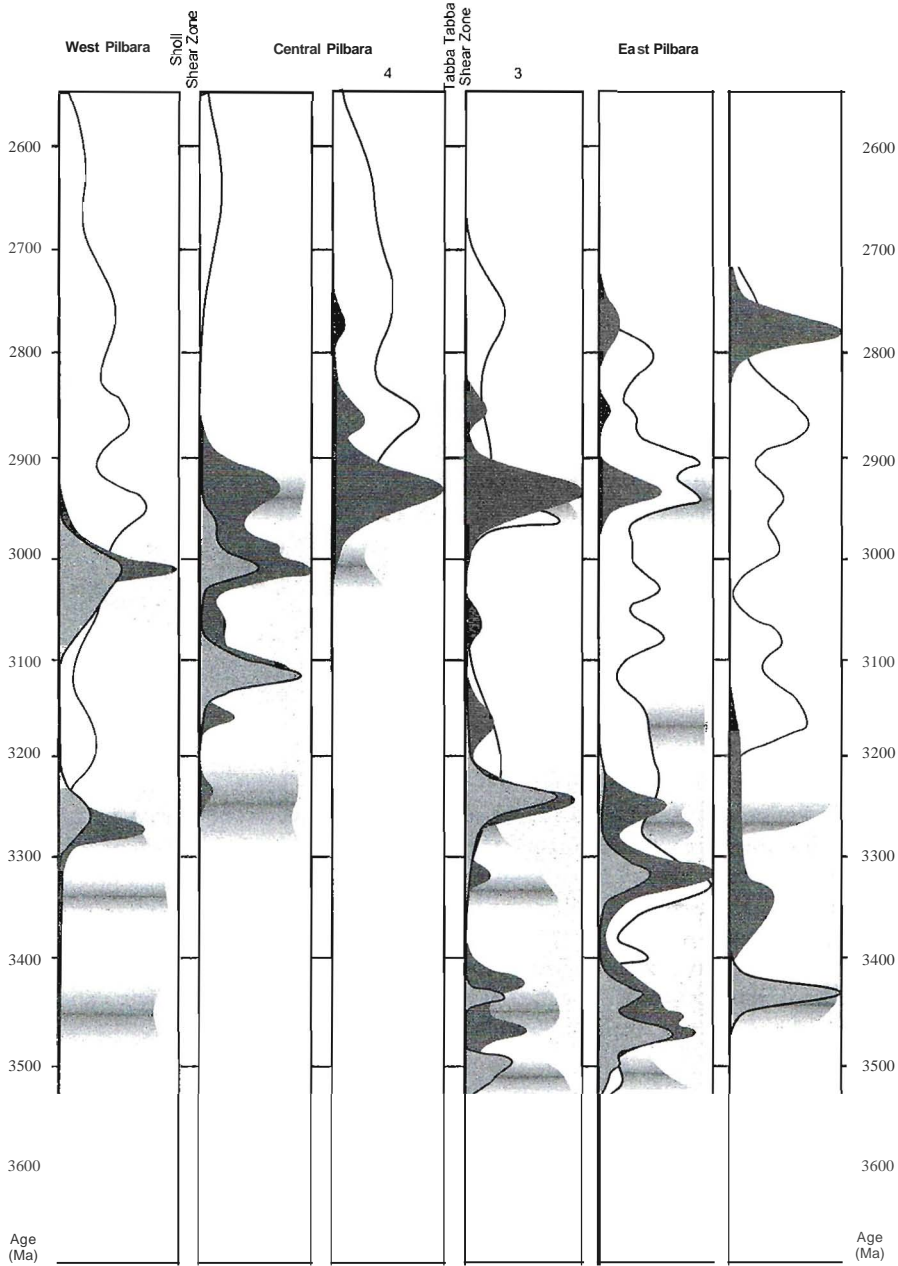
It has long been thought that the differences between Phanerozoic orogens and Archaean terrains are the lack of high pressure metamorphism, ophiolite complexes, molasse basins, large accretionary wedges and subduction-related magmatism (e.g. summary by Hamilton, 1998). However, most of these features have now been identified in Archaean terrains (e.g. summary by De Wit, 1998; Kusky and Polat, 1999).

Greenstone belts, which are an important component of Archaean terrains, commonly contain voluminous mafic volcanic rocks that were erupted in a marine environment. Consequently some greenstone belts have been interpreted to represent Archaean oceanic crust (De Wit and Ashwal, 1995). However, geochemical evidence points to interaction of the magmas with continental crust on their way to the surface, indicating that the lavas possibly were erupted onto submerged continents (Barley, 1986; Bickle et al., 1994; Arndt, 1999; Green et al., 2000, and chapter 4 of this thesis). Recent models for the formation and deformation sequences of greenstone belts tend towards a comparison with Phanerozoic tectonic settings, as the genetic order of the greenstone packages suggests a relation to the opening and closure of ocean basins (e.g. Barley, 1997; Krapez and Eisenlohr, 1998). Recycled hydrated basaltic crust probably was the source of the earliest continental crust in the form of TTG's (e.g. De Wit and Hart, 1993; De Wit, 1998). The recycling may have occurred through subduction or alternatively through stacking of obducted oceanic slices (De Wit et al., 1992).

Major structures separating domains have been found to be typical features of continental crust of all ages, including the Archaean (De Wit, 1998). Kusky and Polat (1999) suggested that lateral accretion of terranes may have been a dominant process of growth of cratons in the mid and late Archaean, resulting in a 'domainal architecture' of continents. The granite-greenstone terrain in the Archaean Pilbara Craton (Figure 8.1) has such a domainal architecture. Mainly on the basis of different geochronology (Figure 8.2) these domains were interpreted to reflect a history of accretion (e.g. Barley, 1997; Kiyokawa and Taira, 1998; Krapez and Eisenlohr, 1998; Smith et al., 1998). These accretionary models have been further investigated in this study, by structural-kinematic analysis of the crustal scale structures, geochemical analysis of the mafic volcanic components within the domains, and U-Pb and $^{40}\text{Ar}/^{39}\text{Ar}$ geochronology.

8.2 Plate tectonics and subduction in the Archaean

When describing Phanerozoic plate tectonics there are several characteristic features. Most diagnostic are those that are directly related to subduction, such as ophiolites, accretionary tectonic melanges, and the occurrence of high pressure-low temperature metamorphic rocks at the surface. Other characteristic features are the occurrence of magmatic products from the subducting plate or the subduction-enriched mantle, intermediate magmatism, and compression-strike-slip-extension tectonic cycles. In order to establish whether Phanerozoic-style plate tectonics may have operated in the Mid-Archaean, these features have been researched in the Pilbara in [this thesis].



- O** Argon cooling ages (left to right)
- Volcanic rocks, SHRIMP (left to right)
- Intrusive rocks, SHRIMP (left to right)
- Inherited zircons (detrital in domain 4) SHRIMP (right to left)
- Sm-Nd model ages (shaded error margins)

Figure 8.2. Cumulative probability diagrams of age occurrences in the North Pilbara Granite-Greenstone Terrain. One column per domain (domain numbers refer to Figure 8.1) Based on 282 published SHRIMP ages, 103 mostly unpublished Argon ages and 36 published Sm-Nd model ages. Peak height merely indicates the number of samples (which is neither the number of analyses, nor a measure of the volume of rock).

8.2.1 Subduction - or not?

8.2.1.1 Ophiolites

It has been suggested that greenstone belts represent Archaean oceanic crust, however, many of the mafic volcanic assemblages in early Archaean greenstone belts bear very little resemblance to Phanerozoic oceanic crust (Arndt et al., 1997). Studies in the North Pilbara Granite-Greenstone Terrain suggest that most of the early and mid-Archaean mafic volcanic sequences were probably deposited on a sialic basement (Barley, 1986; Bickle et al., 1994; Green et al., 2000, Chapter 4 in this thesis). However, there are reports of a ca 3.25 Ga mafic succession with MORB-like geochemistry in the West Pilbara (Ohta et al., 1996, and chapter 5 of this thesis).

8.2.1.2 High pressure-low temperature metamorphism

High pressure-low temperature metamorphic terrains are rare in the Archaean, but eclogitic xenoliths have been found in kimberlites and basalts in Archaean cratons (e.g. Abbott et al., 2000; Carlson et al., 2000). Such xenoliths indicate that it was possible to bring basaltic material down to great depths, however, this does not provide information on the mechanism. Eclogite may form in a subducting slab, but also at the base of an over-thickened crust (e.g. Kroner, 1980).

In the Pilbara kyanite is locally present in greenstone belts. It has been suggested that it is related to partial convective overturn of the granite-greenstone terrain (Collins et al., 1998; Collins and Van Kranendonk, 1999). However, Kloppenburg et al. (2000) dispute this. In accordance with Bickle et al. (1980) they interpreted these assemblages to have formed during crustal thickening due to horizontal tectonics.

8.2.1.3 Accretionary wedges

Phanerozoic accretionary wedges form at the leading edge of the overriding plate in a subduction setting. They consist of oceanic sediments and fragments of basaltic oceanic crust, as well as fragments of the continental crust. In a Phanerozoic subduction zone geometry (as well as lower angle geometries Figure 8.3), depending on the dip of the slab, this accretionary prism is several hundred kilometers away from the volcanic arc. As the West Pilbara has been interpreted as a volcanic arc, the absence of an accretionary wedge in the presently exposed granite-greenstone terrain can be explained by this larger scale geometry, although the presence of a possibly oceanic slice may indicate that an accretionary wedge may have been nearby. In larger Archaean cratons such as the Superior Province in Canada, tectonic assemblages resembling accretionary wedges have been reported (e.g. Kusky and Polat, 1999).

8.2.1.4 Extensional back-arcs

Due to higher mantle temperatures in the Archaean the thicker oceanic plates may not have become 'subductable' (Davies, 1992, see chapter 2). Instead, obduction may have dominated the tectonic process; the thick thrust stacks of oceanic lithosphere may have started to differentiate internally to generate TTG magmatism (De Wit et al., 1992). In this scenario certainly no steep subduction would have occurred, and no extensional back arcs would have formed. However, flat subduction under an actively overriding plate may have been possible (Van Hunen et al., 2000), and towards the late Archaean flat or 'low-angle' subduction may have taken place (Smithies, 2000; Foley et al., 2003). This is further investigated in this chapter in the context of the tectonic framework developed for the West and Central Pilbara.

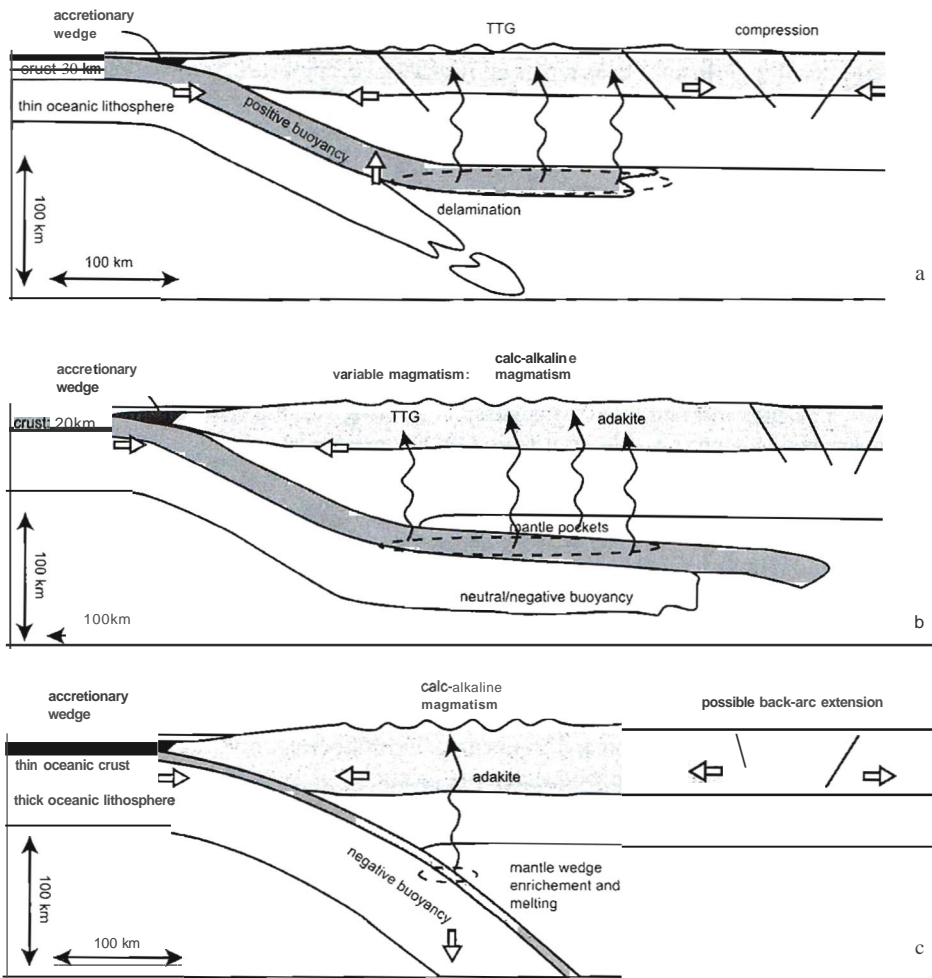


Figure 8.3. Arc/arc and modern subduction zone geometries. a) Early Archaean. Flat subduction: thick oceanic crust and relatively thin lithosphere (e.g. Davies 1992). Ultramafic lower crust and lithosphere may have delaminated (e.g. Foley & 2003). TTG magmatism was generated by the recycling of the delaminated material (e.g. Smithies, 2000). Because of the flat geometry slab melting occurred over a large area (dashed outline) and the subduction-related magmatism occurred in a wide zone. The buoyant underplating causes compression in the overriding plate. b) Mid-Late Archaean. Transition stage: medium thickness ocean crust and lithosphere. Low angle subduction, with possible entrapment of mantle material above subducted slab. TTG as well as 'normal' arc-magmatism may have occurred. Because of the flat geometry slab melting occurred over a large area (dashed outline) and the subduction-related magmatism occurred in a wide zone. c) Phanerozoic. Steep subduction, thin oceanic crust, thick lithosphere, negative buoyancy. Typical arc magmatism and adakite, are produced by interaction of slab-derived fluids with a thick mantle wedge (e.g. Smithies, 2000). Subduction zone roll-back and consequently back-arc extension may occur if the convergence cannot keep up with the sinking slab. Because of the steep geometry slab melting occurs in a small area (dashed outline) and the subduction-related magmatism occurs in a narrow zone.

8.2.1.5 *Subduction-related magmatism*

There are numerous geological observations in Archaean terrains that can be explained in the context of Phanerozoic-style plate tectonics and subduction (see summaries by De Wit, 1998; Kusky and Polat, 1999). Many of these arguments are based on geochemical observations. The relations between geochemical signatures and tectonic regimes are largely observational in Phanerozoic magmatic systems. However, there are some basic principles that apply to all igneous rocks, Phanerozoic and Archaean: the composition of the source material, the pressure and temperature at the time of partial melting and fractional crystallization, and interaction with the host rock determine the final composition of the melt and therefore geochemistry does provide useful information.

The occurrence of boninite-like rocks and sanukitoids (high-Mg diorite) indicate that a (subduction-) enriched mantle source existed at some time in the geological history of the Pilbara (Smithies and Champion, 1999). Other studies indicate that igneous rock suites bear resemblance to fore arcs, island arcs, and back arcs (Smith et al., 1998). And finally, structural studies have shown that the Pilbara experienced compression-extension tectonics followed by collapse and major strike-slip events (see Chapters 5 and 7), and recent papers by Kloppenburg et al., 2001, Blewett, 2002), similar to those observed in modern orogenic cycles (Dewey, 1988).

8.2.2 **Shallow subduction**

Subduction in Phanerozoic tectonic settings occurs in many different varieties. Firstly, the types of plates involved in the collision (oceanic or continental) determine the type of subduction. Secondly, the relative plate velocities and the buoyancy of the downgoing plate determine the angle of subduction. As has been discussed before (Chapter 2), the Archaean oceanic crust is expected to be more buoyant than modern oceanic crust, and steep subduction of early and mid-Archaean oceanic plates is unlikely. A complication lies in spreading rates, which also determine the thickness and composition of the crust, but this has not been quantified in detail for the Archaean.

Even though the early and mid-Archaean oceanic crust was probably much thicker and more buoyant than the average modern oceanic crust (Vlaar, 1986), it may still have been subducted involving a 'flat' geometry (Van Hunen et al., 2000). This can be compared to modern very fast subduction zones, subduction of young and buoyant oceanic lithosphere (Drummond and Defant, 1990), or subduction of oceanic plateaus and seamounts (Gutscher et al., 2000). An example of modern flat subduction occurs below Peru and Chile in the Central Andes. It has been shown that the subducted slab is forced down as deep as the mechanical root of the continent at about 100 kilometers depth (Gutscher et al., 2000), and then continues horizontally for several hundreds of kilometers. It is thought that the cause for flat subduction in this area is the presence of an oceanic plateau in the subducting plate, making it more buoyant.

Due to the positive buoyancy of the Archaean ocean floor, this 'flat' geometry might apply to subduction in the Archaean Earth (e.g. Smithies, 2000; Foley et al., 2003), as shown in Figure 8.3.a. It implies that after the initiation of subduction, there is no mantle wedge as in a 'normal' subduction setting, and melt and fluids derived from the subducting plate will not interact with mantle material. The geochemical characteristics of the volcanic arc of the upper plate contain important clues to these processes (see also Chapter 2). It is proposed that during the Mid-Archaean there may have been an intermediate stage, during which both types of subduction were possible, or pockets of mantle existed between the two crustal slices, and a large variety of magmatic suites ranging between TTG and arc-magmatism, was created; similar ideas were developed by Smithies and Champion (2000). Foley et al. (2002; 2003) presented more polarized models and suggested

that subduction is a necessary mechanism to generate continental crust and that it must have occurred at least from the mid-Archaeon.

8.2.3 Subduction-related magmatism

In a 'nonnal' Phanerozoic subduction regime (Figure 8.3.c), fluids are produced as a result of slab dehydration. Depending on the geometry, the fluids are mostly generated where the slab reaches a depth of about 110 kilometers (Tatsumi and Eggins, 1995). Interaction of these slab fluids with the overlying mantle wedge results in calc-alkaline basaltic and andesitic volcanism (Selundt and Poli, 1998) which occurs in a relatively narrow zone (Figure 8.3.c). Subduction of young and hot oceanic lithosphere results in dehydration of the downgoing slab at much shallower levels. Because magma genesis occurs at deeper levels, the melt generation in the then dry slab will involve lower degrees of partial melting and there will be less metasomatism in the mantle wedge (Harry and Green, 1999). This shows that even in Phanerozoic subduction systems many variables are present which hamper a simple and conclusive interpretation of the geochemistry of subduction-related magmatism.

During flat subduction, which may have occurred in the Archaeon, there exists no material between the subducting slab and the bottom of the overriding lithospheric plate (Figure 8.3.a). As a consequence, the slab melts do not interact with mantle material. The hydrated mafic crust may still contain amphibole and the melting occurs below the plagioclase stability depth and in the presence of garnet. The resulting magmas are adakitic (Drummond and Defant, 1990). Smithies (2000) found that TTG's are distinct from adakites, as they show no evidence for interaction with mantle material. Martin and Moyen (2002) noticed that the composition of TTG from the early Archaeon through to the Proterozoic reflected a gradual change towards higher Mg, reflecting more interaction with a mantle wedge. These data may suggest that during the early Archaeon only flat subduction occurred.

During the mid and late Archaeon the mantle temperature became progressively lower, consequently a thinner oceanic crust would have been produced (Davies, 1992). General consensus in the recent literature is that subduction at a small to medium angle may have become possible in the Late Archaeon. This is also illustrated in Figure 8.3.b.

8.3 Regional geology of the Archaeon Pilbara Craton

8.3.1 Domains and domain boundaries

The Archaeon Pilbara Craton in the north west of Western Australia (Figure 8.1) comprises two major components: the ca 3650-2850 Ma North Pilbara Granite-Greenstone Terrain (e.g. Hickman, 1983; Hickman, 1999) and the unconformably overlying volcano-sedimentary sequence of the ca 2775 to 2450 Ma Hamersley Basin (Blake, 1993). This study is concerned with the ca 3265-2925 Ga history of the West and Central parts of the North Pilbara Granite-Greenstone-Terrain.

Previous studies (e.g. Krapez and Barley, 1987; Krapez, 1993; Krapez and Eisenlohr, 1998) have shown that the North Pilbara Granite-Greenstone Terrain consists of several elongate domains (Figure 8.1) and it has been suggested that this domainal structure reflects a history of terrane accretion (Krapez, 1993; e.g. Barley, 1997; Smith et al., 1998; Kiyokawa et al., 2002). The terrane accretion concept was first developed for the Phanerozoic margin of Western North America (Coney, 1989). It has since then been applied extensively in other areas such as the Iutic Archaeon Superior Province in Canada, and other late Archaeon Cratons (e.g. Kusky and Polat, 1999). Krapez and Eisenlohr (1998) attempted to apply the terrane-concept to the Pilbara Craton. They recognized six

Table 8.1. Supracrustal sequences in the East Pilbara Granite-Greenstone Terrain. Compiled from Van Kranendonk et al. (2002) and references therein. The timing and occurrence of granitoid intrusions can be seen in Figure 8.2. Numbers in the left column refer to the domains shown in Figure 8.1.

Group	Formation	Lithology	age (Ma)	thickness (km)
De Grey (1,2,3,(4))	Lalla Rookh Sandstone	Sandstone, conglomerate, shale	ca 2950	
Gorge Creek (1,2,3)	Pyramid Hill Honeyeater Basalt Paddy Market Corboy Pincunah Hill	Banded iron formation (BIF) Basalt shale, chert sandstone, mudstone, conglomerate shale, BIF, sandstone, felsic volcanics	<3235	max 3.5
Sulphur Springs (2,3)	Kangaroo Caves Kunagunarrina Leilira	tholeiitic mafic to felsic volcanics, chert, BIF pillow basalt, high-Mg basalt, chert wacke, rhyolite, sandstone, mudstone, chert	3238-3235	max 1.5 max 2.4
(3)	Golden Cockatoo	BIF, rhyolite, quartzite, metapelite	>3238	
(2)	Budjan Creek	conglomerate, sandstone, siltstone, felsic volc	3308	max 1.2
W Kelly A Subgroup R (1,2,3)	Charteris Basalt Wyman Euro	komatiite, basalt felsic volcanics tholeiitic and komatiitic pillow basalt and chert	3325 3369-3343	max 1.1 max 9.4
R Salgash A Subgroup W (1,2,3)	Strelley Pool Chert Panorama Apex	quartzite, chert, stromatolites felsic volcanics, tuffaceous sandstones altered basalts, chert	3459-3434	1.5 max 4
a a Taiga Taiga N Subgroup A (1,2,3)	Towers Duffer MtAda Dresser McPhee North Star Basalt	blue, black, white layered chert dacitic tuff, agglomerate basalt and chert stromatolitic barite-chert felsic schist basalt	<3463 3471-3463 ca 3464 ca 3490 3477	max 5 2 0.5
Coonterunah (3)	Double Bar Coulac Table Top	Basalt, volcanogenic seds Mafic and felsic volcanics, chert, BIF basalt, komatiite	3508 3515	max 6

tectonostratigraphic domains, which they claimed were consistently younging towards the west. Recent U-Pb geochronology (Nelson, 1998a; Smith et al., 1998; Nelson, 1999; Nelson, 2000) has disproved this younging sequence. However, the terrane-accretion concept has been developed as a working hypothesis for the tectonic assembly of the Pilbara Craton (e.g. Barley, 1997; Smith et al., 1998; Blewett, 2002; Kiyokawa et al., 2002; Van Kranendonk et al., 2002), and was further investigated in this thesis,

Recently the North Pilbara Granite-Greenstone-Terrain has been considered to be divided in three parts: 'East Pilbara', 'Central Pilbara' and 'West Pilbara' (Hickman, 1999; Smithies et al., 1999; Blewett, 2002; Van Kranendonk et al., 2002). Different boundaries have been proposed: Van Kranendonk et al. (2002) included the Sholl Belt in the West Pilbara, however, they do not describe a structure separating the West Pilbara from the Central Pilbara in this scenario. In this paper the Sholl Shear Zone will be regarded as the boundary between the Central and West Pilbara, because it is a major crustal scale structure separating significantly different domains, in accordance with

Chapter 8

Table 8.2. Supracrustal sequences in the West and Central Pilbara Granite Greenstone Terrains. The Roebourne Group in the Roebourne Domain (West Pilbara), the Whundo Group in the Sholl Belt (Central Pilbara). Cleaverville Formation which occurs both north and south of the Sholl Shear Zone. (the Whim Creek and Bookingarra Groups in the Whim Creek Belt (Central Pilbara), and the Mallina Basin (Central Pilbara). Compiled from Hickman et al. (2001) and references therein. The timing and occurrence of granitoid intrusions can be seen in Figure 8.2. Numbers in the left column refer to the domains shown in Figure 8.1. In domain 5: WC = Whim Creek Belt. S = Sholl Belt.

Group (Occurrence)	Formation	Lithology	age (Ma)	Thickness (km)
Mallina	Mallina Fm	sandstone, slate	ca 2975	
(4)	Constantine Sandstone	conglomerate, sandstone	ca 2975	
Bookingarra	Kialrah Rhyolite	rhyolite	ca 2975	
(5-WC)	Negri + Loudon Volcanics	mainly mafic volcanics		2
	Cistern Fm + Rushall Slate	clastic sediments	ca 2978	
Whim Creek	Mons Cupri Dacite	dacitic intrusions	ca 3010	0.2
(5-WC)	Red Hill Volcanics	andesite, rhyodacite, sandstone, breccia	ca 3010	0.3
	Warambie Basalt	basalt, minor sed		0.2
(4.5.6)	Cleaverville Fm	chert, BIF, basalt and felsic volcanics	ca 3020-3015	1.5
Whundo	Woodbrook Fm	basalt and felsic volcanics	ca 3115	
(5-S)	Bradley Basalt	basalt, minor felsic volcanics	ca 3115	>4
	Tozer Fm	basalt, rhyolite, sediments and chert	ca 3120	2.5
	Nallana Fm	basalt, minor ultramafics, pyroclastics	ca 3125	2
Roebourne	Regal Fm	komatiites, basalt	not known	2
(6)	Nickol River Fm	volcanogenic sediments, chert	ca 3270-3250	0.1-0.5
	Ruth Well Fm	basalt, talc schist, chert	ca 3270	1-2

Blewett (2002). The Tabba Tabba Shear Zone will be regarded as the boundary between the East and Central Pilbara (Figure 8.1).

8.3.2 Lithology and stratigraphy

A tabular stratigraphy for the greenstone successions in the Pilbara was originally proposed (Hickman, 1983; Horwitz, 1990), but with the recognition of the domain boundary structures and new precise geochronological constraints, this interpretation has been revised (e.g. Van Kranendonk et al., 2002). The greenstone successions of the different domains cannot or only partially be correlated across domain boundaries.

The East Pilbara is characterized by the 'typical' ovoid granitoid complexes surrounded by greenstone belts. The greenstone succession comprises the ca 3.51 Ga Coonterunah Group, the ca 3.47-3.43 Ga Warrawoona Group, the ca 3.23 Ga Sulphur Springs Group, the un-dated Gorge Creek Group and the ca 2.95 Ga De Grey Group. A detailed overview of the most recently published East Pilbara stratigraphy is given in Table 8.1. The Central Pilbara is made up of the 3.12 Ga volcanics in the Sholl Belt, a ca 3.01-2.97 Ga volcano-sedimentary succession in the Whim Creek Belt, ca 2.97 Ga continental sediments in the Mallina Basin and several granitoid complexes. The West Pilbara is an elongate domain on the western margin of the Pilbara Craton, comprising a ca 3.265 Ga supracrustal succession and granitoids, and an undated mafic sequence of possibly oceanic origin. A detailed overview of the most recently published West and Central Pilbara stratigraphy is given in Table 8.2. The distribution and timing of granitoids and also volcanic rocks can be seen in Figure 8.2. This thesis is mainly concerned with the post 3.25 Ga history of the West- and Central Pilbara.

After stabilization of the Pilbara Craton and slow uplift and erosion, the ca 2.77 - 2.45 Ga volcano-sedimentary succession of the Hamersley Basin was deposited over a large part of the craton. This was the result of a complex event that involved breakup through rifting of a continental plate which contained the Pilbara Craton (Blake and Barley, 1992; Blake, 2001).

The deep structure of the Pilbara has remained enigmatic. Drummond (1979; 1981) found that the crustal thickness in the Pilbara is 28-33 kilometers. The base of the greenstone belts is inferred to occur at 14 kilometers, and a similar average thickness was modeled for the granitoid complexes with an inferred shape of a vertical cylinder (Drummond, 1979; Wellman, 1999).

8.3.3 Geochronology

The rocks of the Pilbara Craton have been the subject of numerous geochronological studies. Most of these dates have been discussed in previous chapters in their regional context. In a joint effort with A. Kloppenburg, a large number of published and unpublished dates have been collected in a database. The database has been analyzed statistically, on age distribution and geographical distribution. A diagram showing the spatial and temporal distribution of zircons in intrusive and volcanics rocks and zircon xenocrysts (SHRIMP ages), Argon cooling ages, and limited Sm-Nd model ages, can be found in Figure 8.2.

It is clear that the age distribution is unique for every domain, and this has been used as evidence for terrane accretion models in the past. However, there are also distinct similarities. The three East Pilbara domains have common peaks around 3450 Ma, 3300 Ma, 3240 Ma and 3100 Ma (Figure 8.2). Because they only occur to the east of the Tappa Tappa Shear Zone, this structure is interpreted as an important boundary. The oldest peak in the West Pilbara lies at ca 3260 Ma, followed by ca 3150 Ma and 3020 Ma. From about 2950 all domains have a similar history.

As the ca 3260 peak only occurs to the north of the Sholl Shear Zone, this structure represents a major break and was interpreted as an important boundary. Alternatively, the 3260 Ma peak in the West Pilbara and the 3230 Ma peak in the East Pilbara could represent a diachronous event affecting the whole craton.

The striking age 'gap' in the Central Pilbara (it contains no rocks older than ca 2970 Ma, see Figure 8.2) occurs due to the development of the Whim Creek-Mallina Basin, covering older basement. In this scenario the Pilbara may have been a single unit throughout the Archaean. These ideas will be discussed below in the context of newly acquired geochronological, geochemical and structural data.

8.3.4 Previous tectonic models for the Pilbara

Most tectonic interpretations concerning the Archaean can be placed in either of two end-member models. The first is a 'vertical' tectonic regime dominated by diapirism, the second is a 'horizontal' tectonic regime dominated by plate interactions. General arguments for and against Phanerozoic-style plate tectonics in the Archaean have been discussed elaborately by De Wit (1998) and Hamilton (1998) respectively. These arguments have also been discussed in the context of the North Pilbara Granite-Greenstone Terrain (e.g. Bickle et al., 1980; Hickman, 1984; Krapez and Eisenlohr, 1998; Collins and Van Kranendonk, 1999; Kloppenburg et al., 2001; Zegers et al., 2001; Blewett, 2002; Van Kranendonk et al., 2002). However, most of these studies have been concerned with local or regional problems, and do not provide craton-wide tectonic scenarios.

Hickman (1983) was the first to publish a Pilbara-wide model. It was based on a deformation history consisting of major events (Table 8.3). This involved magmatism, volcanism, metamorphism

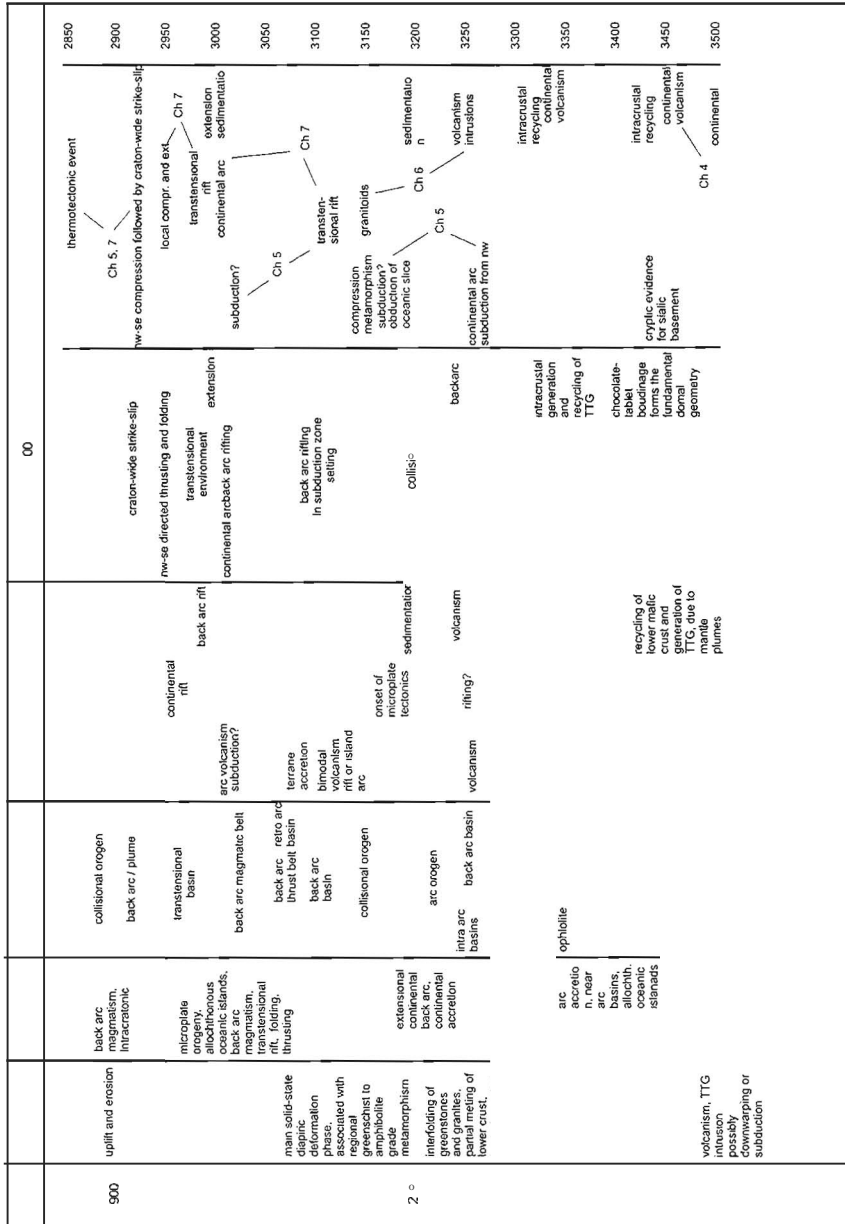


Table 8.3. Comparison of different models of the tectonic evolution of the North Pilbara Granite Greenstone Terrain from the Early to Late Archaean. Gray/black indicate times of tectonic and/or rock-forming activity. Hickman (1983) did not divide the Pilbara into domains, and noted that absolute geochronology was scarce. Krapez (1993) described an evolution starting in the East Pilbara and progressing towards the West. Krapez and Eisenlohr (1998) used a division of six domains, as shown in Figure 8.1. Their model only describes domains 4, 5 and 6 in detail. The domains are also indicated at the bottom of the models of Van Kranendonk (2002), Blewett (2002) and this study.

and deformation between 3600 Ma and 2950 Ma and focused on diapiric processes. Krapez (1993) presented a model that divided the Pilbara greenstone successions into first and second-order sequence stratigraphic units (Table 8.3). He recognized four first-order cycles which he interpreted in terms of fore-arc, arc, and back-arc tectonic evolution in settings that he directly related to convergent margins in Wilson and Supercontinent cycles. Krapez and Eisenlohr (1998) refined this model for the West Pilbara (Table 8.3).

Blewett (2002) presented structural data that he interpreted to indicate that the dome and basin geometry (characteristic of the East Pilbara, and used by many as evidence for diapirism) was established as a result of far-field horizontal stresses related to plate interactions. Blewett (2002) proposed a chocolate-table style of deformation, rather than early diapirism. He interpreted the entire structural history of the Pilbara in terms of extensional and compressive events (Table 8.3), and suggested that granite-driven diapirism is, at best, a modifying factor. He reinterpreted the vertical lineations in a 'zone of sinking' (see Collins and Kranendonk, 1998) as intersection lineations. Van Kranendonk et al. (2002) presented structural data (Table 8.3) that they interpreted to contradict the 'horizontal' structural models published for the Marble Bar area and further support Hickman's (1983, 1984) diapiric model. However, Van Kranendonk et al. (2002) interpret that the Roeboume Domain may be an accreted terrane as proposed by Smith et al (1998) and Krapez and Eisenlohr (1998), and thus suggest that after 3.25 Ga 'microplate tectonics' may have taken over from diapirism as the most significant tectonic process. This paper focuses on the post 3.25 Ga history of the West- and Central Pilbara and therefore will not elaborate further on the 'vertical vs. horizontal tectonics' discussion.

8.4 Tectonic framework for the West and Central Pilbara

The structural, geochronological and geochemical data presented in the previous chapters of this thesis will now be summarized and placed in a common context. The three domains of the West and Central Pilbara will be discussed, as well as the major structures that separate them. This tectonic framework forms the basis for the geodynamic model presented in the next section.

8.4.1 The Roeboume Domain, West Pilbara

The evolution of the Roeboume Domain is discussed in detail in Chapter 5. The oldest rocks in the West Pilbara are represented by the meta-basalt, talc schist and minor cherts of the Ruth Well Formation. The mafic rocks in this formation are high-Mg arc volcanics that share characteristics of calc-alkaline basalts and tholeiites. They are interpreted to have formed at a continental margin above a subduction zone (chapter 5). The Ruth Well Formation is overlain by the metasediments, felsic volcanics and chert of the ca 3265 Ma Nickol River Formation (Nelson, 1998a). The Nickol River Formation is coeval with intrusion of the Karratha Granodiorite, which also has a subduction signature (Nelson, 1998b; Smith et al., 1998) and Sm-Nd model ages of 3480-3420 Ma (Sun and Hickman, 1998). Blewett (2002) reported south verging folds and thrusts indicating a deformation phase predating emplacement of a ca 3260 Ma suite of the Harding Granitoid in the West Pilbara, however, in this study these structures were not observed.

The major and trace element geochemistry of the pre-3150 Ma Regal Formation in the Roeboume Group suggest it may represent Archaean ocean floor; however, it differs from Phanerozoic MORB in its higher Fe and REE content, and lower Ti. This might be explained by a higher fertility of the mantle, and a higher degree of partial melting which started at greater depth than at present

suggested a sinistral transtensional setting for the Whim Creek Basin, however, at that time the age constraints were very poor and the tectonic setting has been reinterpreted as discussed above (e.g. Smithies, 1997a; Pike et al., 2002).

The subsidence of the intracontinental transtensional basin continued during deposition of the 2970 Ma Bookingarra Group (Pike et al., 2002) (W-d2, Table 8.4). Extension stopped prior to 2950 Ma, at which time the sediments in the Whim Creek Group were locally folded along north trending axes (W-d3, Table 8.4). North-west verging folds and thrusts developed at ca 2930 Ma during a major northwest-southeast directed compressional event (W-d4, Table 8.4). Finally, the area was cut by northeast trending dextral brittle faults during the initial stages of the opening of the Hamersley Basin (W-d5, Table 8.4).

8.4.5 The MaJlina Basin, Central Pilbara

The structural evolution of the Tabba Tabba Shear Zone and Mallina Basin is discussed in detail in Chapter 7. The Cleaverville Formation is interpreted to form the lowermost succession in large parts of the Mallina Basin (Smithies et al., 1999; Van Kranendonk et al., 2002). During the early stages of basin development, mafic rocks with boninite-like characteristics were emplaced into the lower part of the basin (Smithies, 2002, chapter 7 of this thesis). There is no direct evidence for a subduction-related event at that time. Possibly the source region was enriched during an earlier subduction event (e.g. the ca 3010 Ma event). The Mallina Basin was inverted by mostly local, fault controlled deformation (M-d1, M-d2, Table 8.4). These folds were also reported by e.g. Krapez and Eisenlohr (1998), Smithies et al. (1999), Huston et al. (2000) and Blewett (2002). The local folding was followed by large-scale intrusion of high-Mg granites and granodiorites into the Mallina Basin at approximately 2955 Ma. These rocks have been described as sanukitoids and have been reported to be derived from a subduction-modified mantle (Nelson, 1998a; Smithies and Champion, 1998). A short episode of renewed extension along some faults resulted in the local deposition of some more sediments in the northern part of the Mallina Basin (Smithies et al., 2001).

At ca 2930 Ma a dominant northeast trending fabric and regional folds were formed in the Mallina Basin (M-d3, Table 8.4). A major structure in the MaJlina Basin, the east-trending Mallina Shear Zone, contains north-verging thrust structures correlated to M-d3, which mainly resulted in northeast trending folds and cleavage. Locally sinistrally verging asymmetrical folds were observed within the Mallina Shear (M-d4, Table 8.4). The dominant fabric within the Mallina Shear are dextral folds and kinks, overprinting all other structures (M-d5, Table 8.4). Throughout the Mallina Basin, northeast trending faults occur, with small dextral displacement on them (M-d6). After ca 2930 Ma, post-orogenic granites and continental gabbros were intruded in the Mallina Basin.

8.4.6 The Tabba Tabba Shear Zone: boundary between Central and East Pilbara

The western margin of the East Pilbara Craton has a complex geological history spanning more than 700 million years (see Table 8.3). The granitoids of the Carlindi Batholith with Warrawoona age (ca 3.42-3.46 Ga) are the oldest components of the rock record in the area adjacent to the Tabba Tabba Shear Zone. The structural evolution of the Tabba Tabba Shear Zone has been discussed in detail in Chapter 7, and its V-Pb geochronology is discussed in Chapter 6 (Beintema et al., in press). A granite-granodioritic suite with arc-affinity within the Tabba Tabba Shear Zone has been dated at 3251 ± 3 Ma and a diorite-gabbro suite with arc-affinity at 3235 ± 15 Ma (Beintema et al., in press). Xenocrysts in these rocks indicate the presence of precursor or basement rocks similar in age to the Warrawoona Group in the East Pilbara (ca 3.42-3.46 Ga). These arc-related rocks possibly correlate

to the slightly older arc-rocks in the West Pilbara (ca 3265 Ma) and the Sulphur Springs Group in the East Pilbara (Buick et al., 2002). There is no evidence for the presence of an accretionary wedge or crustal slices with oceanic affinity, as would be expected if the Tabba Tabba Shear Zone were a true suture zone along which continental blocks were assembled that were once separated by an ocean.

Mafic schists with tholeiitic characteristics are intercalated with these felsic and intermediate schists. There is no conclusive evidence that indicates whether the intrusive suites were emplaced into the ancestral Tabba Tabba Shear Zone, or were incorporated into the shear zone as crustal slices, at a later stage. However, their occurrence and that of the felsic, intermediate and mafic schists is currently confined to a narrow strip within the Tabba Tabba Shear Zone. These rocks may be correlated to the 3270-3230 Ma Sulphur Springs Group in the East Pilbara (Table 8.1) or the 3270-3250 Ma Roebourne Group in the West Pilbara (Table 8.2), as can be seen in Figure 8.2.

Locally dextral transpressional were observed within the oldest rock suites in the Tabba Tabba Shear Zone. This, and the dextral geometry of an early regional foliation on the eastern side of the structure (e.g. map in Appendix 7.AJ) indicate that the Tabba Tabba Shear Zone experienced an early deformation phase with a dextral component (TTSZ-d1, Table 8.4). This occurred due to northwest-southeast compression, but the exact timing of this event remains uncertain. These structures only occur in the ~3255 to ~3235 Ma rocks and they are overprinted by all following events. It must have occurred early in the history of the structure and at least before 2970 Ma, when the next deformation phase occurred. It has been tentatively correlated to the early northwest-southeast directed compressional event in the Roebourne Domain at ca 3150 Ma (R-d1, Table 8.4).

Geochemical analyses reveal that some of the older components in the Tabba Tabba Shear Zone have very high Mg contents, indicating that the Tabba Tabba Shear Zone is a structure that might extend into the mantle (also reported by Smithies and Champion, 1999; De Leeuw et al., 2001). From the geochemical analyses it is clear that within the Tabba Tabba Shear Zone there is no evidence for the preservation of oceanic-like slices of lithosphere, as may be expected in a true suture zone when two continental fragments are docked, and an ocean is destroyed in the middle.

The Tabba Tabba Shear Zone experienced a major phase of sinistral transtensional movement, bringing the northwest block down relative to the southeast: the structure acted as a bounding fault during subsidence of the Central Pilbara and formation of the Mallina Basin at ca 2970 Ma (TTSZ-d2, Table 8.4). In Chapter 5 it was suggested that at ca 3150-3120 Ma a major phase of sinistral transtension affected both the Sholl and Tabba Tabba Shear Zones. In the field no evidence was found to confirm the timing, but possibly major sinistral transtensional deformation took place in the Tabba Tabba Shear Zone at ca 3150 Ma-3120 Ma. It is likely that due to similar kinematics, it can not be distinguished from the ca 2970 Ma sinistral transtensional event. In addition, xenocrysts of ca 3150-3120 Ma were found in a ca 2940 Ma granite in the Tabba Tabba Shear Zone, indicating the presence of a basement or precursor rock of that age (similar to the age of the Sholl Belt).

During a renewed phase of sinistral transtension on the Tabba Tabba Shear Zone (TTSZ-d3, Table 8.4), sedimentation occurred in the northern part of the Mallina Basin (Smithies et al., 2001), and granites were intruded in an extensional jog adjacent to the Tabba Tabba Shear Zone at approximately 2940 Ma (Smithies and Champion, 2001).

The Tabba Tabba Shear Zone and Mallina Basin were intruded by a suite of calc-alkaline granites and continental gabbros between 2940 and 2930 Ma (Nelson, 1998a-2001). A suite of monzogranites and gabbros intruded in a sinistral extensional bend in the Tabba Tabba Shear Zone at about 2940 Ma (Smithies and Champion, 2001). Xenocrysts in these rocks indicate the presence of precursor or basement rocks in the eastern part of the Central Pilbara, similar in age to the Whundo Group in the Sholl Belt, in the western part of the Central Pilbara (3120 Ma, Beintema et

al., in press, see chapter 6). This is interpreted to indicate that not only the western part, but also the eastern part of the Central Pilbara was affected by a magmatic event at about 3120 Ma, and consequently, that the East and West Pilbara Craton may have been geographically close at that time.

A major northwest-southeast-directed compressional event resulted in the formation of the main regional northeast trending folds and associated axial planar foliation in the Mallina Basin, and the observed late brittle dextral event on the Tabba Tabba Shear Zone is interpreted to correspond to this event (TTSZ-d4, Table 8.4).

The combined results of all $^{40}\text{Ar}/^{39}\text{Ar}$ analyses in the West and Central Pilbara, and the weak overprints found in all in zircon samples, indicate two major thermal overprints occurred. The first disturbance at ca 2860 Ma is interpreted to be due to intrusion of tin-bearing granites and pegmatites in the Central Pilbara and adjoining regions (Blewett, 2002; Sweetapple and Collins, 2002). As the volume of these granites in the Yule Batholith is large, it may have been associated with a significant thermal disturbance of the surrounding rocks. The second event, at ca 2760 Ma, can be correlated to initiation of the overlying Hamersley Basin (Blake, 1993), and intrusion of the Black Range Dykes.

The $^{40}\text{Ar}/^{39}\text{Ar}$ analyses indicate that between 2500 and 1900 Ma partial resetting occurred. This is possibly associated with the Capricorn Orogeny which involved deformation, metamorphism and magmatism due to collision of the Pilbara Craton with the Yilgarn Craton to the south (Tyler, 2000). Furthermore, there are mid- and late-Proterozoic disturbances at approximately 1200 and 900 Ma. The ca 1200 Ma disturbance may correspond to Grenville age activity which is also seen throughout Rodinia, and the ca 900 Ma disturbance may correspond to very early Pan-African activity in East Gondwana (Rogers et al., 1995).

8.4.7 The role of the East Pilbara

The long term stability of the East Pilbara has implications for the evolution of the West and Central Pilbara and is important to the central theme of this thesis. Throughout this thesis, the East Pilbara was assumed to be a stable block after at least ca 3265 Ma, relative to the West and Central Pilbara. Blewett (2002) and Baker et al. (2002) have shown that parts of the East Pilbara, adjacent to the Central Pilbara, have a complex structural history, also post-dating ca 3265 Ma. However, this is interpreted to have limited effect on the described evolution for the Central and West Pilbara, and detailed structural studies in those areas lie outside of the scope of this thesis.

The North Star Basalt in the Marble Bar Belt was subject to a detailed study which has confirmed that the East Pilbara has been a continental block since at least 3470 Ma. It was thought to be a potential ophiolitic sequence (see comment in De Wit (1998)) and in this light it was studied in this thesis, in the search for evidence for Phanerozoic-style plate tectonics. The North Star Basalt is the lowermost formation of the Warrawoona Group and one of the oldest greenstones sequences in the Archaean Pilbara Craton in Western Australia (Figure 8.1). It consists mainly of pillowed and massive basalts, minor gabbro, and comprises a large number of mafic and ultramafic dykes. This study (chapter 4) has shown that lithologically and geochemically the North Star Basalt does not resemble a modern ophiolite, however, the rocks were erupted in water as recorded by the pillowed basalts. The majority of the dykes in the area were emplaced during distinct regional events (Kloppenborg et al., 2001), few are genetically related to the basaltic stratigraphy.

Zegers (1996) suggested the North Star Basalt was part of the Coonterunah Group. Whether it belongs to the Coonterunah or Warrawoona Group, correlation with the work of Green et al. (2000) suggests that the sequence cannot be oceanic. Green et al. (2000) indicated that the basalts of

Table 8.4. Summary of the post 3265 Ma structural evolution (D= regional event) of the West and Central Pilbara. Roebourne Domain (R), Sholl Shear Zone (SSZ) Sholl Belt (S) Whim Creek Belt (W), Mallina Basin (M), and Tabba Tabba Shear Zone (TTSZ). 'i' indicates intrusion event, 'dep' indicates volcanic or depositional event. Data presented in chapters 5, 6, 7. A hypothetical geodynamic/tectonic model is shown in Figure 8.4.

time (Ma)	D	R	SSZ	S	W	M	TTSZ	short description of local geology
ca 2770	D7	d5		d3	d5	d6	d5	sinistral transtension on NE trending brittle faults: Hamersley Basin
	D6	d4	d4				d5 d4	dextral deformation on SSZ, Mallina Shear sinistral deformation on Mallina Shear
ca 2930	D5	d3	d3	d2	d4	d3	d4	regional northeast trending, north-northwest verging folding and thrusting, dextral transpression on northeast trending structures
ca 2940	D4.c						d3	sinistral component on TTSZ, intrusion of granites and gabbros
ca 2955								sanukitoids: subduction enriched mantle
	D4.b				d3	d2		north-trending folds, E-W compression
	D4.a					d1		east trending folds, N-S compression
ca 2970	D3.b		d2		dep d2	dep	d2	Bookingarra Group and Mallina Sediments: Centr Pilb subsides in sinistral continental transtension (mainly on TTSZ).
3020-3110	D3.a				dep d1			Whim Creek Group: continental arc (Pike et al., 2002). Sinistral transtension on NE trending structures
ca 3020		dep		dep	dep	dep		Extension, deposition of Cleaverville, intrusion of granitoids
3150-3115	D2	d2	d1	d1 dep				Granites in Sholl Domain, Whundo Group: rift/island arc, sinistral transtension on SSZ and possibly NSZ
ca 3150	D1	d1					d1	northwest-southeast directed compression
ca 3265		dep					dep	Roebourne: island arc (Smith et al., 1998), Tabba Tabba: (Beintema et al., in press) Strelley: back arc? slightly younger at ca 3235 Ma (Vearncombe and Kerrich, 1999)

the Coonterunah and upper Warrawoona groups were deposited in a continental environment, and this was confirmed by the research in chapter 4. This may indicate that the East Pilbara has been a stable continental block since at least the deposition of the ca 3515 Ma Coonterunah Group,

8.4.8 Tectonic synthesis

Some of the deformation events in the West and Central Pilbara described above, are of regional significance, others are recognized only locally. All events have been summarized in Table 8.4. A regional compilation and correlation has resulted in the definition of seven significant deformation events. A granite-grauodiorite suite with arc-affinity intruded the Tabba Tabba Shear Zone between 3255 and 3250 Ma, and a tholeiitic gabbro-diorite suite with arc-affinity intruded at ca 3235 Ma. These rocks are possibly related to the slightly older arc-rocks in the West Pilbara (ca 3265 Ma) and

the Sulphur Springs Group in the East Pilbara (Buick et al., 2002). There is no evidence for the presence of an accretionary wedge or crustal slices with oceanic affinity, as would be expected if the Tabba Tabba Shear Zone were a true suture zone along which continental blocks were assembled that were once separated by an ocean.

The first regional deformation event (D1) is recognized in the Roebourne Domain, Sholl Shear Zone, as well as the Tabba Tabba Shear Zone, and involved northwest-southeast directed compression, folding and thrusting at ca 3150 Ma. During this event an oceanic slice was emplaced as a thrust sheet in the Roebourne Domain. This is not considered 'terrane accretion' as described by Coney (1989), but it may indicate the presence of an accretionary wedge, from which the oceanic slice was then derived. However, the preferred interpretation is that the oceanic slice was emplaced during the subduction event at ca 3265 Ma.

During the second event (D2) the Sholl Shear Zone and Tabba Tabba Shear Zone acted as a coupled system of sinistral strike-slips, bounding an intracontinental transtensional basin. This extension may have occurred in response to the earlier compressional event at ca 3150 Ma. The Whundo Group was deposited within this intracontinental transtensional setting in the Central Pilbara at ca 3130-3115 Ma. In a similar stress regime (D3), but over 100 Ma later, the Whim Creek, Bookingarra and Mallina Groups were deposited in a basin with a depositional center located more to the east, closer to the Tabba Tabba Shear Zone. The early stages of this event may have occurred in a continental arc setting as recorded by the geochemistry of the Whim Creek Group (Pike et al., 2002).

The Mallina Basin was closed in a series of transpressional events (D4) involving the Tabba Tabba and Sholl Shear Zones as transpressional structures, resulting in local fault-related folding in the basin, accompanied by sanukitoid, granite and gabbro intrusions, between 2950 and 2930 Ma. A major compressional event (D5) occurred during which a northwest verging fold and thrust belt developed throughout the Central and Western Pilbara at ca 2930 Ma. This was immediately followed by dextral strike-slip activity on all east and northeast trending structures (D6). Finally, the area was affected by faulting related to the initiation of the Hamersley Basin rift at ca 2770 Ma (D7).

8.5 Geodynamic model

8.5.1 Introduction

Historically the ideas about the early tectonic evolution of the Pilbara have been strongly polarized between the end-members of dominantly 'vertical tectonics' and dominantly 'horizontal tectonics' (e.g. Zegers et al., 1996; Collins et al., 1998; Kloppenburg et al., 2001; Blewett, 2002; Van Kranendonk et al., 2002). These disputes continue until the present day, although the advocates of diapirism have restricted their diapiric models to the pre-3.2 Ga history of the East Pilbara. There seems to be consensus about the occurrence of at least some form of (micro-) plate tectonics after about 3.25 Ga. Because this thesis is mostly concerned with the post- ca 3.26 Ga history of the West and Central Pilbara, this discussion will not be elaborated on.

As can be seen in Figure 8.2, there are significant differences in the geochronological architecture of the different domains recognized in the Pilbara. This, in addition to geochemical data, has led to the proposition of accretionary models, in which domains were accreted onto a cratonic core. Some of these models (e.g. Barley, 1997; White et al., 1998) stated that a commonly recognized event in all domains occurred at ca 2.9 Ga, and therefore proposed that the West Pilbara was accreted onto the East Pilbara at about that time. Others have proposed that only

domain 6 was accreted and that this occurred at ca 2.9 Ga (e.g. Kiyokawa and Taira, 1998; Krapez and Eisenlohr, 1998; Smith et al., 1998).

More recent models have defined a Central Pilbara (logically situated between the East and the West Pilbara) which possibly developed over an older suture (e.g. Smithies et al., 1999). In these recent models the actual accretion event is interpreted to have taken place at ca 3250 Ma (e.g. Blewett, 2002; Van Kranendonk et al., 2002), and was associated with a common to slightly diachronous peak in volcanism and intrusions at ca 3250 Ma (Figure 8.2). In this thesis, it is proposed that no accretion of terranes (as defined by Coney, 1989) occurred in the presently exposed North Pilbara Granite Greenstone Terrain. Instead, it may have been an active continental margin affected by at least two episodes of subduction followed by collapse, intracontinental transtensional basin formation and igneous activity associated with those events (Chapters 5, 6 and 7). Accretion outside of the currently exposed North Pilbara Granite Greenstone Terrain, and the emplacement of allochthonous thrust sheets, may have accompanied some of the compressional events. However, there is no evidence for accretion of large terranes such as island arcs.

In the previous section, the structural kinematic data, geochronology and geochemistry collected in the West and Central Pilbara have been placed in an internally consistent framework for the period between ca 3265 Ma and 2925 Ma. A hypothetical geodynamic model based on the data will be presented below. Schematic lithospheric-scale sections and sketch-maps for the different time-slices are shown in Figure 8.4.

8.5.2 ca 3265 Ma

At ca 3265 Ma arc-related volcanism and associated calc-alkaline granitoid intrusions occurred in the West Pilbara (chapter 5). Possibly, the Roebourne Group correlates to the ca 3270-3230 Ma Sulphur Springs Group (Buick et al., 2002) in the East Pilbara, and the unnamed intrusive complex described by Beintema et al. (in press/chapter 6 this thesis) within the Tappa Tappa Shear Zone, at the western margin of the East Pilbara. This slightly diachronous event can also be seen in Figure 8.2. Detrital zircons and Nd isotopic evidence suggest that there are precursor or basement rocks present in the West Pilbara of the same age as the ~3.45 Ga Warrawoona Group and associated granitoids in the East Pilbara (Nelson, 1998a; Sun and Hickman, 1998). A possible scenario is that subduction occurred at a low angle beneath the West Pilbara as shown in Figure 8.4.a, causing the observed igneous activity at ca 3265 Ma (Smith, 2003).

Accretion of the West Pilbara onto the East Pilbara (as previously proposed) implies that an ocean basin was destructed in the middle. In the case of southeast-directed subduction this would have resulted in widespread ca 3265 Ma arc-like rocks and possibly ophiolites in the East Pilbara (which is not the case). In the case of north-west directed subduction beneath the West Pilbara ophiolites and arc rocks would be in the West Pilbara (which is correct). In both scenarios there should be an accretionary wedge between the West and East Pilbara (which is not there). Figures supporting these arguments can be found in Chapter 5.

The in this thesis preferred interpretation is that that the Pilbara Craton was a single unit throughout the early and mid-Archaeon. The Central Pilbara represents a transtensional-transpressional intracontinental zone separating the East and West Pilbara. It consists of a younger basin covering the older basement. The Central Pilbara was developed in situ at a later time; it was not accreted at some stage in the geological history. The West Pilbara was part of an active continental margin, rather than an accreted terrane, although it does contain minor allochthonous components.

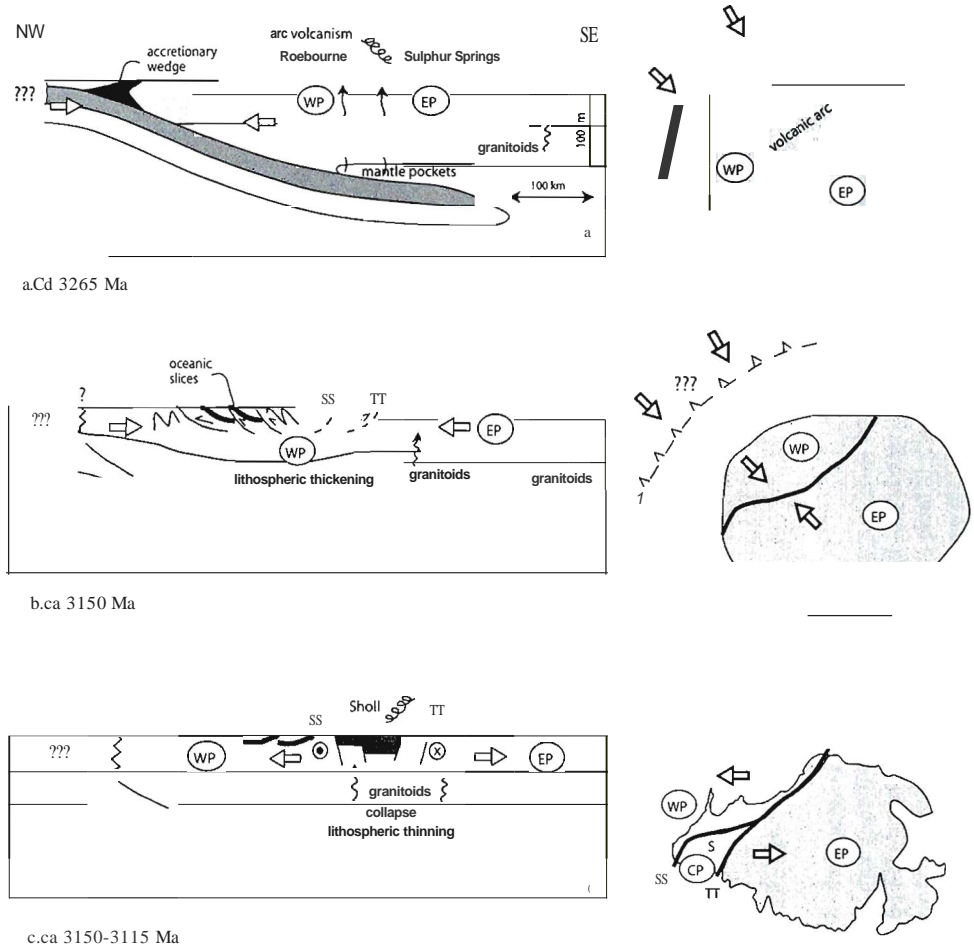
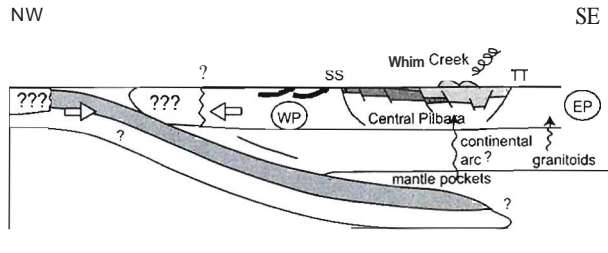


Figure 8.4. Sketch geodynamic model for the evolution of the West (WP) and Central Pilbara (CP) relative to the East Pilbara (EP) as an active continental margin between 3265 Ma and 2925 Ma. SS = Sholl Shear Zone. TT = Tabba Shear Zone.

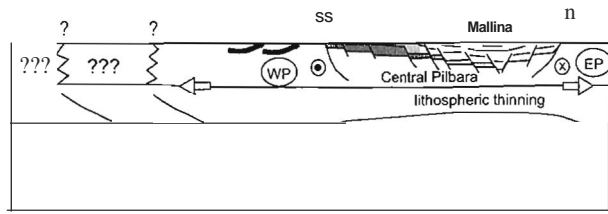
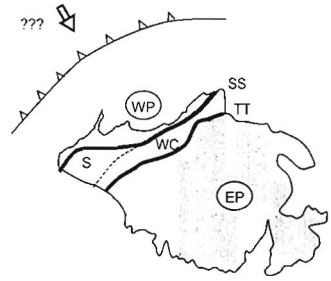
a) At ca 1265 Ma subduction-related magmatism occurred in the West Pilbara. It may have been related to (shallow) subduction from the northwest. If any terrane accretion occurred, it was outside the presently exposed granite-greenstone terrain. The fate of the subducted slab, after subduction ceased, is not known.

b) At ca 1150 Ma a thrusting and metamorphic event affected the West Pilbara (D/). The SS and possibly the TT were formed at this time. An oceanic slice (Regal Fm) was emplaced as a thrust sheet in the West Pilbara (thick black lines). There is no other evidence for a subduction-event at this time, but emplacement of the ophiolite requires subduction in the NW. Possibly the ophiolite was emplaced in the previous time slice. If any terrane accretion occurred, it was outside the presently exposed granite-greenstone terrain.

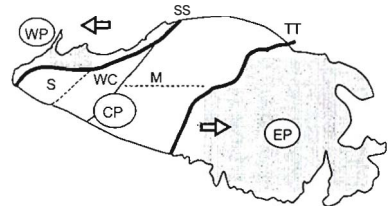
c) Between ca 1150 - 3130 Ma the Sholl Domain (S) was intruded by several phases of granitoids, possibly in response to the ca 3150 Ma compressional event. Between ca 3130 - 1115 Ma the TT and SS (thick lines) were active as sinistral transensional structures (D2). The CP began to form as it subsided, and the Whundo Group was deposited in the Sholl Basin (S).



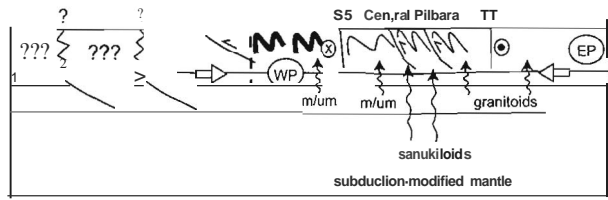
d. ca 3020-3010 Ma



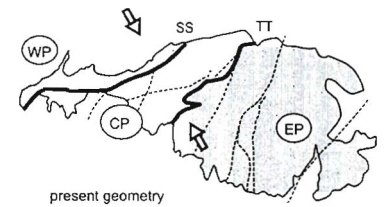
e. ca 2970 Ma



presently exposed



f. ca 2955-2925 Ma



present geometry

c) After a long period of quiescence, the end of which was marked by the intrusion of granitoids and the deposition of the ca 3020 Ma Cleaveland Fm over a large area in the West and Central Pilbara, continental arc volcanism occurred in the ca 30/0 Ma Whim Creek Belt (WC, possibly related to subduction in the NW (D3a). If any terrane accretion occurred, it was outside the presently exposed granite-greenstone terrain. The fate of the subducted slab is unclear; however, it did cause metasomatism of the Central Pilbara mantle.

d) Sinistral transtension on TT and SS (D3b), and subsidence of the Central Pilbara region; the ca 2970 Ma Bookingarra Group is deposited in the Whim Creek Belt and the ca 2970 Ma Mallina Basin is filled with bOllinite-like rocks, conglomerate and turbidites. A major structure underlies the axis of the Mallina Basin. The surface expression is the Mallina Shear Zone (M).

j) Compression occurred at ca 2955 Ma and the Mallina Basin was inverted (D4). Sanukitoids intruded in fault-bounded local extensional areas in an overall compressional regime. Folding in the basin was mostly local and fault-bounded. After a short episode of renewed extension at ca 2940 Ma, a major NW-SE directed fold and thrust belt developed over the whole of the West and Central Pilbara, and the TT and SS were oversteepened and reactivated as dextral transpressive structures (D5). At ca 2930-2925 Ma the IVP and CP were intruded by post-orogenic granites and mafic-ultramafic complexes (m/um), possibly in response to the preceding compressional episode. If any terrane accretion occurred, it was outside the presently exposed granite-greenstone terrain.

West and Central Pilbara Synthesis: Geodynamic Model

8.5.3 ca 3150 Ma

A phase of thrusting (D1) took place in the West Pilbara at about 3150 Ma (Kiyokawa and Taira, 1998; Hickman et al., 2001; Blewett, 2002) and a thermal event is indicated by Ar geochronology (chapter 5). It was associated with upper amphibolite grade metamorphism. This event post-dates the ca 3265 Ma arc magmatism in the Roeboume Domain by more than 100 million years and is therefore interpreted to represent a separate event. It is interpreted that the ancestral Sholl and Tabba Tabba Shear Zones were formed at this time (Chapter 5). The observed early northwest-southeast directed compressional event in the Tabba Tabba shear Zone between 3235 and 3115 Ma may correspond to the northwest-directed thrusting event in the Roebourne Domain dated at approximately 3150 Ma (Figure 8.4.b).

Sun and Hickman (1999) suggested that the Regal Formation in the Roeboume Domain could represent a slice of oceanic crust, which was obducted and emplaced during the observed metamorphic and deformation event at 3150 Ma. This is supported by the structural and geochemical data presented in Chapter 5. However, the exact age and circumstances of formation, and the timing of emplacement of the Regal Formation are uncertain. It may have occurred during an episode of subduction at ca 3150 Ma (Figure 8.4.b), however, no arc-volcanism of this age is known.

Alternatively, continuous subduction may have occurred between ca 3265 Ma and ca 3150 Ma. This lifetime is not uncommon for Phanerozoic subduction systems. However, no associated voluminous igneous rocks of the intermediate period (between ca 3265 and 3150 Ma) occur in the West or Central Pilbara (or at least they have not been found to date). This hypothesis is not supported by the data and is therefore rejected. The third and preferred alternative is that the oceanic Regal Formation was emplaced much earlier, during the ca 3265 Ma subduction-related event described above. Possibly the deformation associated with the emplacement correlates to the early ('*kD1*') structures observed by Blewett (2002).

Some of the ca 3150-3130 Ma granitoids in the Sholl Domain (Smith, 2003) may be related to the ca 3150 Ma tectono-thermal event in the West Pilbara. Nelson (2000) dated ca 3165 Ma granitoids in the Yule Granitoid Complex in the western margin of the East Pilbara (Figure 8.1), which may also correlate to the same event. This time period remains an important missing link in the tectonic history of the West and Central Pilbara and presents a target for future research.

8.5.4 ca 3150 - 3115 Ma

Smith (2003) reported granitoid intrusions in the Sholl Domain between ca 3150 and 3130 Ma, and her geochemical data suggest a continental setting. At ca 3130 - 3115 Ma a phase of continental extension occurred (Chapter 5) by sinistral transtension along major, presently subvertical, structures such as the Sholl Shear Zone and the Tabba Tabba Shear Zone (D2), and possibly on structures that are now concealed in the Central Pilbara. As a consequence, the Sholl Basin formed between the West and the East Pilbara, in which the Whundo Group was deposited, forming the oldest component of the Central Pilbara (Figure 8.4.c). The Whundo Group has characteristics of crustal contamination, interpreted to indicate an intracontinental setting (Chapter 5). This transtensional phase is interpreted to have occurred due to collapse following the earlier compressional event, similar to the evolution seen in Phanerozoic orogens (Dewey, 1988).

8.5.5 ca 3020 - 3010 Ma

100 million years later and after a period of quiescence, large areas of the West and Central Pilbara were covered by the cherts and minor basalts of the ca 3020 Ma Cleaverville Formation (Chapters 5 and 7). The West Pilbara and Sholl Shear Zone were intruded by minor granitoids immediately after, interpreted to record the onset of a short-lived compressional event (D3a). The ca 3010 Ma Whim Creek Group (Figure 8A.d) contains calc-alkaline components, which are interpreted to record a brief episode of continental arc formation and possibly subduction (Pike et al., 2002).

8.5.6 ca 2970 Ma

Subsequently, the central portion of the basin subsided further during renewed continental transtension (D3b) and was filled by the Bookingarra Group in the western part and the turbidites of the Mallina Formation in the central part of the basin (Figure 8A.e) at ca 2970 Ma (Smithies et al., 2001). The Sholl Shear Zone shows no evidence for shearing during this phase, and is thought to have been locked at this time. Major sinistral transtensional activity did occur on the Tabba Tabba Shear Zone resulting in a shift of the depositional center towards the Tabba Tabba Shear Zone (Chapter 7). This transtensional collapse possibly occurred in response to the earlier compressional event at ca 3010 Ma, a sequence commonly seen in modern orogens (Dewey, 1988).

8.5.7 ca 2955 - 2925 Ma

At 2955 Ma the transtensional phase ended abruptly and the Mallina Basin was inverted (Chapter 7). Shortly after, the area was intruded by high-Mg diorites, derived from a subduction-modified mantle (Smithies and Champion, 1999). Possibly this enrichment occurred during the ca 3020 Ma short-lived (inferred - Pike et al., 2002) episode of subduction. The high-Mg diorites intruded in local fault-controlled extensional areas in an overall compressional regime (D4). Folding in the basin was mostly local and fault-controlled (Chapter 7). After a short episode of renewed transtension on the Tabba Tabba Shear Zone, and sedimentation in the Mallina Basin, a major northwest-southeast directed fold and thrust belt developed over the whole of the West and Central Pilbara (D5) at ca 2930 Ma, and the Tabba Tabba Shear Zone and Sholl Shear Zone were reactivated as dextral transpressive structures (Figure 8A.f). This event is recognized throughout the West and Central Pilbara (Chapters 5 and 7), and it is accompanied by a major tectonothermal and magmatic signature throughout all domains in the Pilbara (Figure 8.2).

This major compressional event was followed by intrusion of post-orogenic monzogranites and gabbros at ca 2925 Ma, interpreted to occur during collapse following the earlier compressional event. The cause of this compressional episode may be a collision (with a continent or island arc) to the northwest, outside of the presently exposed area of the North Pilbara Granite-Greenstone Terrain, but this is highly speculative.

8.5.8 Discussion and summary

Firstly it should be noted that the North Pilbara Granite Greenstone Terrain is in fact a very small fragment of continental crust. When the outline of the craton is projected onto a modern active continental margin (Figure 8.5), this becomes especially clear. The Central Andes were chosen for this comparison, because this is an example of shallow subduction of an unusually thick oceanic crust. Because the North Pilbara Granite-Greenstone Terrain is so small, we may only expect to find

Table 8.5. Summary of the geodynamic evolution of the West and

Timing	Event	Kinematics	Tectonics	Geodynamics
ca 2930	05	STR-SL	regional fold and thrust belt regional strike slip activity, post-orogenic granites	end of orogeny
ca 2955	04a,b,c	NW-SE COMPR	high Mg intermediate intr	collision or slab drop-off
ca 2970	03b	E-W EXT	subsidence of central Pilbara	intracontinental transtensional rift, mainly activity of TTSZ
3020-3010	03a	NW-SE COMPR	brief compressional episode	continental magm arc (Whim Ck Belt)
3150-3115	02	E-W EXT	subsidence of central Pilbara	intracontinental transtensional rift between coupled SSZ and NSZ
ca 3150	01	NW-SE COMPR	thrusting and metamorphism	collision in NW? obduction of oceanic slice
ca 3265		NW-SE COMPR	shallow subduction from NW	continental magmatic arc

limited geological evidence of the inferred geodynamic processes. It is not expected that a complete geological record for the Pilbara Craton, spanning the roughly 700 million years between 3.6 and 2.9 Ga, can be reconstructed in detail. However, the preferred reconstruction for the period between 3.3 and 2.9 Ga has been presented for the West and Central Pilbara.

In Table 8.3 the data presented in this thesis are compared with previously published models, which have been discussed in section 8.3.4. There are common features in all models. However, the interpreted geodynamic causes of these events are different. Recent publications indicate the existence of a sialic basement since at least ca 3600 Ma (Blewett, 2002; Van Kranendonk et al., 2002). The oldest greenstone sequences were deposited onto this basement (Barley, 1986; Green et al., 2000, chapter 4 of this thesis). The style of deformation and the tectonic regime that dominated in the period before ca 3250 Ma are still a matter of debate (e.g. Zegers et al., 1996; Collins et al., 1998; Kloppenburg et al., 2001; Blewett, 2002; Van Kranendonk et al., 2002). This is also indicated in Table 8.3.

All previous models included an episode of terrane accretion, either at 3.2 Ga or at 2.9 Ga. In the model presented here, no 'terrane accretion' took place in the presently exposed area of the Pilbara. However, the West Pilbara does contain a minor allochthonous oceanic slice. Terrane accretion or collision may have occurred beyond the limits of the current exposure of the craton, but this remains speculative. The presently exposed granite-greenstone terrain is interpreted to form part of an active continental margin between ca 3.265 Ga and 2.930 Ga, with the interior of the continent lying to the southeast. Therefore the West and Central Pilbara have been most affected by the inferred collision and rifting events.

The interpreted episodes of subduction are relatively short-lived (ca 10-20 Ma) compared to most Phanerozoic convergent settings, as indicated by the limited age-ranges of arc-related rocks. Subduction may have ceased quickly as the still elevated mantle temperatures in the mid-Archaeon would have resulted in a thicker and weaker downgoing plate. This may have led to jamming of the subduction zone, ending the subduction process. Alternatively, the eclogitic part of the subducted slab may have delaminated as soon as it formed, taking away any slab pull. The associated thermal

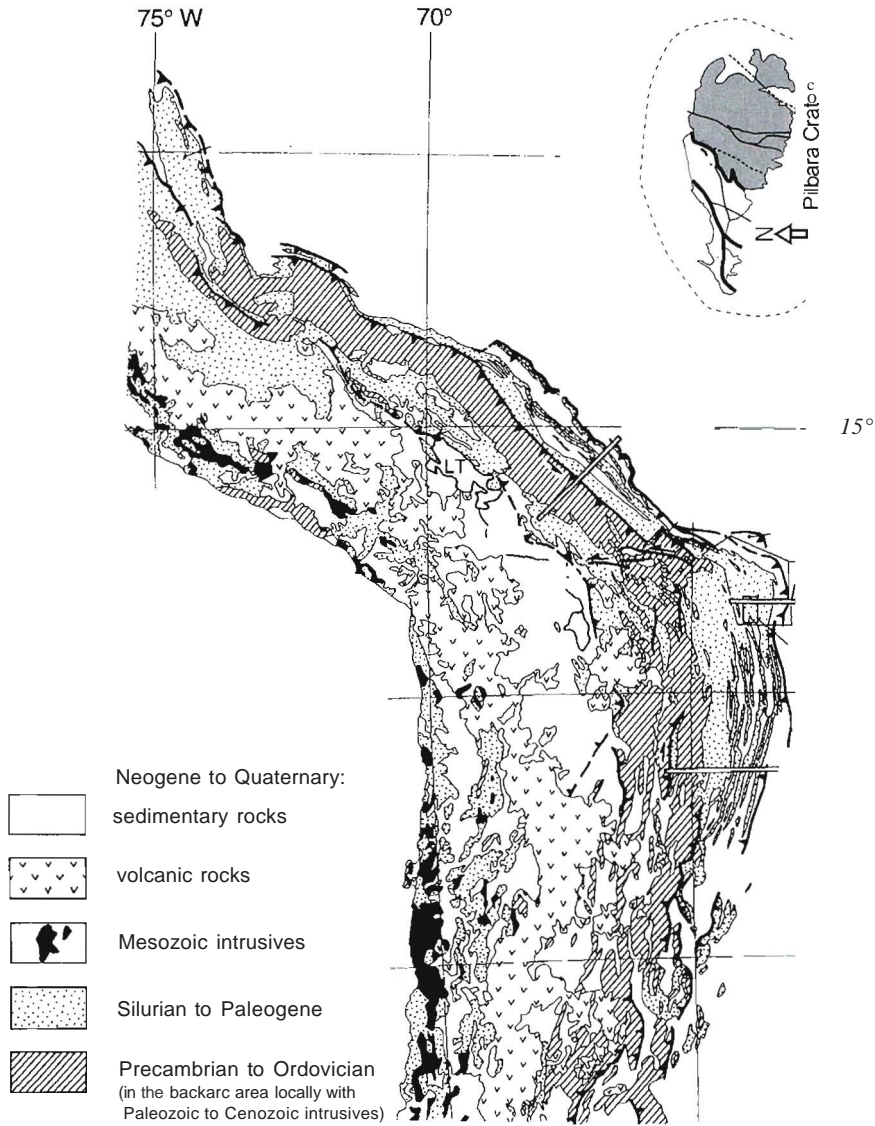


Figure 8.5. The scale of the Pilbara Craton in comparison with a modern active continental margin: the Bolivian section of the Andes. Map of Andes from Kley (1999). This active continental margin is taken as an example of a modern shallow subduction: in this area an oceanic plateau is subducting beneath the South American Continent.

pulse would then explain the observed post-tectonic thermal and extensional events and post-collisional intrusion of granites and gabbros, and relatively transient nature of the magmatic events (Van de Zedde and Wortel, 2001). However, this scenario is purely hypothetical.

Short-lived episodes of subduction from the northwest would also explain why there are no post 3.25 Ga arc-related rocks in the East Pilbara. If a convergence rate of 5 centimeters per year is assumed (for the sake of this simple calculation), subduction would have led to the formation of 50 kilometers of subducted slab per million years. With a trench situated to the northwest (e.g. Figure 8.4.a), at least 500 kilometers of under-plated slab (i.e. 10 million years after the initiation of subduction) are needed to generate arc magmatism in the core of the East Pilbara. Such arc magmatism is not present and is therefore interpreted not to have occurred, except possibly at ca 3265 Ma. At that time the trench may have been located closer to the core of the Craton (Figure 8.4.a) and the Sulphur Springs volcanism occurred in domain 3. This may explain why it is slightly younger than the Roeboume arc volcanism (see Figure 8.2). However, the time scales and rates of tectonic processes in the Archaean are not well constrained and this interpretation is highly speculative.

8.6 Conclusions

A ca 3.47 Ga possible ophiolitic sequence in the East Pilbara was investigated. However, it was determined that the basaltic rocks were deposited in a continental environment. This supports the assumption that the East Pilbara acted as a rigid block relative to the Central and West Pilbara, at least after ca 3.25 Ga when that area was tectonically active. On the basis of the observations, it can be concluded that plate tectonic processes including subduction cannot be ruled out for the mid-Archaean. The compression-extension-strike-slip cycles that were reconstructed for the Central and West Pilbara, in combination with the geochemical and petrological characteristics of igneous rocks, can be explained in the context of Phanerozoic tectonic settings. It is concluded that at least after ca 3.27 Ga, Phanerozoic tectonic processes such as subduction (although with a low angle geometry) and transtensional rifting, occurred in the Archaean Pilbara Craton. It is proposed that the West and Central Pilbara Craton were part of an active continental margin between ca 3.27 Ga and 2.92 Ga. The area experienced at least two short-lived episodes of subduction from the northwest followed by transpression and transtension cycles involving the coupled pair of the crustal scale Tabba Tabba and Sholl Shear Zones. This resulted in the formation and deformation of the intracontinental Mallina Basin.

Acknowledgements

I would like to thank the Dr. SchUnnann Fund for their financial support of the field work with grant numbers 1997/14, 1998/14, 1999/14, 2000/14a and 2001/14a, and the Molengraaff Fund for their financial support of the field work in 1998-2001. The Netherlands Organization for Scientific Research (NWO) is thanked for their financial contribution with grant number R75-386. Dr. R.H. Smithies and Dr. R.S. Blewett are thanked for providing air photos and geophysical imagery, and geological discussions and feedback. Dr. Hennis van Roennund, Dr. Kim Hein, Marije van Koolwijk, Diana de Leeuw, Pieter Bruijnen, and Stephanie Veltkamp were good company and provided assistance in the field.

References

- Abbott, D. et al., 2000. Quantifying Precambrian crustal extraction: the root is the answer. *Tectonophysics*, 322: 163-190.
- Abe, Y., 1993. Physical state of the very early Earth. *Lithos*, 30: 223-235.
- Anderson, D.L., 2001. Top-down tectonics? *Science*, 293: 2016-2018.
- Anonymous, 1972. Ophiolites. *Geotimes*, 17: 24-25.
- Armstrong, R.L., 1968. A model for the evolution of strontium and lead isotopes in a dynamic earth. *Rev. Geophysics*, 6: 175-199.
- Armstrong, R.L., 1981. Radiogenic isotopes: the case for crustal recycling on a near steady state, no continent growth. *Earth.Phil.Trans.Royal Soc.London*, 301: 443-472.
- Armstrong, R.L., 1991. The persistent myth of crustal growth. *Australian Journal of Earth Sciences*, 38: 613-630.
- Arndt, N., 1999. Why was flood volcanism on submerged continental platforms so common in the Precambrian. *Precambrian Research*, 97: 155-164.
- Arndt, N. and Brooks, C., 1980. Komatiites. *Geology*, 8: 155-156.
- Arndt, NT, 1983. Role of a thin, komatiite-rich oceanic crust in the Archaean plate-tectonic process. *Geology*, **11**: 372-375.
- Arndt, NT, Albarede, F. and Nisbet, E.G., 1997. Mafic and ultramafic magmatism. In: L.D.Ashwal (Editor), *Greenstone Belts*. Oxford University Press, pp. 233-254.
- Arndt, NT, Nelson, D.R., Compston, W., Trendall, A.F. and Thome, A.M., 1991. The age of the Fortescue Group, Hamersley basin, Western Australia, from ion microprobe zircon U-Pb results. *Aus! J.Earth Sci.*, 38: 261-281.
- Bailey, R.C., 1999. Gravity-driven continental overflow and Archaean tectonics. *Nature*, 398: 413-415.
- Baker, D.E.L., Seccombe, P.K. and Collins, W.J., 2002a. Structural history and timing of gold mineralisation in the northern East Strelley Belt, Pilbara Craton, Western Australia. *Economic Geology*, 98: 775-785.
- Baker, D.E.L., Seccombe, P.K. and Collins, W.J., 2002b. Structural history and timing of gold mineralization in the northern East Strelley Belt, Pilbara Craton, Western Australia. *Economic Geology*, 98: 775-785.
- Barley, M.E., 1986. Incompatible-element enrichment in Archean basalts: a consequence of contamination by older sialic crust rather than mantle heterogeneity. *Geology*, 14: 947-950.
- Barley, M.E., 1987. The Archean Whim Creek Basin, an ensialic fault-bounded basin in the Pilbara Block, Australia. *Precambrian Research*, 37: 199-215.
- Barley, M.E., 1993. Volcanic, sedimentary and tectonostratigraphic environments of the ~3.46 Ga Warrawoona Megasequence: a review. *Precambrian Research*, 60: 47-67.
- Barley, M.E., 1997. The Pilbara Craton. In: M.D. Wit and LD. Ashwal (Editors), *Greenstone Belts*. Clarendon, Oxford, pp. 657-664.
- Barley, M.E. and Groves, D., 1992. Supercontinent cycles *Geology*, 20(291-294).
- Barley, M.E., Loader, S.E. and McNaughton, N.J., 1998. 3430 to 3417 Ma calc-alkaline volcanism in the McPhee dome and Kelly Belt, and growth of the eastern Pilbara Craton. *Precambrian Res.*, 88: 3-24.
- Barley, M.E. and Pickard, A.L., 1999. An extensive, crustally derived, 3325 to 3310 Ma silicic volcanoplutonic suite in the eastern Pilbara Craton: evidence from the Kelly Belt, McPhee Dome and Corunna Downs Batholith. *Precambrian Research*, 96: 41-62.
- Bea, F., Pereira, M.D. and Stroh, A., 1994. Mineral/leucosome trace-element partitioning in a peraluminous migmatite (a laser ablation-ICP-MS study). *Chemical Geology*, 117: 219-312.
- Beintema, K.A., De Leeuw, G.A.M., White, S.H. and Hein, K.A.A., 2001. The Tabba Tabba Shear; a crustal scale structure in the Archaean Pilbara Craton, WA, 41AS. AGSO, Record 2001/37, Perth, WA, pp. 285-287.

- Beintema, K.A., Mason, P.R.D., Nelson, D.R., White, S.H. and Wijbrans, J.R., in press. New constraints on the timing of tectonic activity in the Archaean Central Pilbara Craton, Western Australia, *Journal of the Virtual Explorer*.
- Belousova, E.A., Griffin, W.L., O'Reilly, S.Y. and Fisher, N.I., 2002. Igneous zircon: trace element composition as an indicator of source rock. *Contrib Mineral Petrol*, 143: 602-622.
- Bickle, M.I., 1978. Heat loss from the Earth: constraints on Archaean tectonics from the relation between geothermal gradients and the rate of plate production. *EPSL*, 40: 301-315.
- Bickle, M.I., Bellenay, L.F., Boulter, C.A., Groves, O.I. and Morant, P., 1980. Horizontal tectonic interaction of an Archaean gneiss belt and greenstones, Pilbara block, Western Australia. *Geology*, 8: 525-529.
- Bickle, M.I. et al., 1993. Origin of the 3500-3300 Ma calc-alkaline in the Pilbara Archaean; Isotopic and geochemical constraints from the Shaw Batholith. *Precambrian Research*, 60: 117-149.
- Bickle, M.I., Nisbet, E.G. and Martin, A., 1994. Archaean Greenstone Belts Are Not Oceanic Crust. *Journal of Geology*, 102: 121-138.
- Blake, T.S., 1993. Late Archaean crustal extension, sedimentary basin formation, flood basalt volcanism and continental rifting: The Nullagine and Mt Jope Supersequences, Western Australia. *Precambrian Research*, 60: 185-242.
- Blake, T.S., 2001. Cyclic continental mafic tuff and flood basalt volcanism in the Late Archaean Nullagine and Mount Jope Supersequences in the eastern Pilbara, Western Australia. *Precambrian Research*, 107: 139-177.
- Blake, T.S. and Barley, M.E., 1992. Tectonic evolution of the Late Archaean to Early Proterozoic Mount Bruce Megasequence Set, Western Australia. *Tectonics*, 11: 1415-1425.
- Blewett, R., 2002. Archaean tectonic processes: a case for horizontal shortening in the North Pilbara Granite-Greenstone Terrane, Western Australia. *Precambrian Research*, 113: 87-120.
- Blewett, R.S., Huston, D.L., Mernagh, T.P. and Kamprad, J., 2002. The diverse structure of Archaean lode gold deposits of the southwest Mosquito Creek Belt, East Pilbara Craton, Western Australia. *Economic Geology*, 97: 787-800.
- Blewett, R.S., Wehman, P., Ratajkoski, M. and Huston, D.L., 2000. Atlas of North Pilbara Geology and Geophysics. AGSO Record, 2000/04: 36 pp.
- Bolhar, B., Woodhead, J.D. and Hergt, J.M., 2002. Comment on: 'Growth and recycling of early Archaean continental crust: geochemical evidence from the Coonterunah and Warrawoona groups, Pilbara Craton, Australia' by Green, M.G. et al. (*Tectonophysics* 322, 69-88). *Tectonophysics*, 344: 289-292.
- Boulter, C.A., Bickle, M.I., Gibson, B. and Wright, R.K., 1987. Horizontal tectonics pre-dating upper Gorge Creek Group sedimentation Pilbara block, Western Australia. *Precambrian Research*, 36: 241-258.
- Bowring, S.A. and Housh, T., 1995. The Earth's early evolution. *Science*, 269: 1535-1540.
- Brauns, C.M., Hergt, J.M., Woodhead, J.D. and Maas, R., 2000. Os Isotopes and the Origin of the Tasmanian Dolerites. *Journal of Petrology*, 41 (7): 905-918.
- Buick, R. et al., 2002. Geochronology and stratigraphic relationships of the Sulphur Springs Group and Strelley Granite: a temporally distinct igneous province in the Archaean Pilbara Craton, Australia. *Precambrian Research*, 114: 87-120.
- Buick, R. et al., 1995. Record of emergent continental crust ~3.5 billion years ago in the Pilbara craton of Australia. *Nature*, 375: 574-577.
- Cabanis, B. and Lecolle, F., 1989. Le Diagramme La10 - Y/15 - Nb/8: un outil pour la discrimination des series volcaniques et la mise en evidence des processus de melange et de contamination crustale. *C.R. Acad. Sci. Ser. II*, 309: 2023-2029.
- Campbell, I.H. and Griffiths, R.W., 1992. The changing nature of mantle hotspots through time: implications for the chemical evolution of the mantle. *Journal of Geology*, 100: 497-523.
- Carlson, R.W. et al., 2000. Continental growth, preservation and modification in Southern Africa. *GSA Today*, 10(2): 1-6.
- Champion, D.C. and Smithies, H., 1998. Archaean granites of the Yilgarn and Pilbara Cratons. AGSO Record, 1998/33: 24-25.
- Cherniak, D. and Watson, E.B., 2000. Pb diffusion in zircon. *Chemical Geology*, 172: 5-24.
- Clark, R.M. and Cox, S.I.D., 1996. A modern regression approach to determining fault displacement-length scaling relationship. *Journal of Structural Geology*, 18(2/3): 147-152.
- Collerson and McCulloch, 1983. Field and Sr-Nd isotopic constraints on Archaean crust and mantle evolution in the Eastern Pilbara Block, Western Australia. *Geol Soc Austr Abstr*, pp. 167-168.
- Collins, W.J., 1989. Polydiapirism in the Archaean Mount Edgar Batholith, Pilbara Block, Western Australia. Precambrian Research, 36: 41-62.**
- Collins, W.J., 1993. Melting of Archaean sialic crust under high $a_{\text{H}_2\text{O}}$ conditions: genesis of 3300 Ma Na-rich granitoids in the Mount Edgar Batholith, Pilbara Block, Western Australia. *Precambrian Research*, 60: 151-174.

- Collins, W.J. and Gray, C.M., 1990. Rb-Sr isotopic systematics of an Archaean granite-gneiss terrain: The Mount Edgar Batholith, Pilbara Block, Western Australia. *Australian Journal of Earth Sciences*, 37: 9-22.
- Collins, W.J. and Kranendonk, M.J.V., 1998. Partial convective overturn of Archaean crust in the east Pilbara Craton, Western Australia: driving mechanisms and tectonic implications. *J Struct Geology*, 20(9/10): 1405-1424.
- Collins, W.J. and Van Kranendonk, M.J., 1999. Model for the development of kyanite during partial convective overturn of Archaean granite-greenstone terrains: the Pilbara Craton, Australia. *J. Metamorphic Geol.*, 17: 145-156.
- Collins, W.J., Van Kranendonk, M.J. and Teyssier, C., 1998. Partial convective overturn of Archaean crust in the east Pilbara Craton, Western Australia: driving mechanisms and tectonic implications. *Journal of Structural Geology*, 20(9/10): 1405-1424.
- Compston, W., Williams, I.R. and Meyer, C., 1984. U-Pb geochronology of zircons from lunar braccia 73217 using a sensitive high mass-resolution ion microprobe. *Journal of Geophysical Research*, B 89: 525-534.
- Condie, K.C., 1981. *Archaean Greenstone Belts*. Elsevier, Amsterdam, 434 pp.
- Condie, K.C., 1994. *Archaean Crustal evolution*. *Developments in Precambrian Geology*, 11. Elsevier, Amsterdam, 528 pp.
- Condie, K.C., 1998. Episodic continental growth and supercontinent formation: a mantle avalanche connection? *EPSL*, 163: 97-108.
- Condie, K.C., 2000. Episodic continental growth models: afterthoughts and extensions. *Tectonophysics*, 322: 153-162.
- Coney, P.J., 1989. Structural aspects of suspect terranes and accretionary tectonics in western North America. *Journal of Structural Geology*, 11(1/2): 107-125.
- Connely, J.N., 2000. Degree of preservation of igneous zonation in zircon as a signpost for concordancy in U/Pb geochronology. *Chemical Geology*, 172: 25-39.
- Cooper, J.A., James, P.R. and Rutland, R.W.R., 1982. Isotopic dating and structural relationships of granitoids and greenstones in the East Pilbara, Western Australia. *Precambrian Research*, 18: 199-236.
- Coward, M.P. and Ries, A.C., 1995. *Early Precambrian Processes*. Geological Society Special Publications, 95. The Geological Society, London, 295 pp.
- Crawford, A.J., 1989. *Boninites*. Unwin-Hyman, London, UK.
- Dann, J.e. and Bowring, S.A., 1997. The Payson ophiolite and the Yavapai-Mazatzal Orogenic Belt of Central Arizona. In: M.D. Wit and L.D. Ashwal (Editors), *Greenstone Belts*. Clarendon, Oxford.
- Davids, C., Wijbrans, J.R. and White, S.H., 1996. $^{40}\text{Ar}/^{39}\text{Ar}$ laser probe ages of metamorphic hornblendes from the Coongan Belt, Pilbara, Western Australia. *Precambrian Res.*, 83: 221-242.
- Davies, G.P., 1992. On the Emergence of plate tectonics. *Geology*, 20: 963-966.
- Davies, G.F., 1995. Punctuated tectonic evolution of the earth. *Earth and Planetary Science Letters*, 136: 363-379.
- Davies, G.F., 1998. The mantle dynamical repertoire: plates, plumes, overturns and tectonic evolution. *AGSO J Aus Geol. Geoph.*, 17(1): 93-99.
- Davies, G.P. and Richards, M.A., 1992. Mantle convection. *Journal of Geology*, 100: 151-206.
- De Leeuw, G.A.M., Beintema, K.A., Wijbrans, J.R. and White, S.H., 2001. Chemistry of Archaean gabbros intruding the Tappa Tappa Shear Zone, Pilbara, WA, 4IAS. AGSO, Record 2001/37, Perth, WA, pp. 143-145.
- De Smet, J., Van den Berg, A.P. and Vlaar, N.J., 2000. Early formation and long-term stability of continents resulting from decompression melting in a convecting mantle. *Tectonophysics*, 322: 19-33.
- De Smet, J.H., Van den Berg, A.P. and Vlaar, N.J., 1998. Stability and growth of continental shields in mantle convection models including recurrent melt production. *Tectonophysics*, 296: 15-29.
- De Smet, J.H., Van den Berg, A.P. and Vlaar, N.J., 1999. The evolution of continental roots in numerical thermo-mechanical mantle convection models. *Lithos*, 48: 153-170.
- De Wit, M.J., 1998. On Archaean granites, greenstones, cratons and tectonics: does the evidence demand a verdict? *Precambrian Research*, 91: 181-226.
- De Wit, M.J., Armstrong, R., Hart, R. and Wilson, A., 1987a. Felsic igneous rocks within the 3.3-3.5 Ga Barberton Greenstone Belt: high level crustal equivalents of the sulfidated tonalite-trondhjemite terrain, emplaced during thrusting. *Tectonics*, 6: 529-549.
- De Wit, M.J. and Ashwal, L.D., 1995. Greenstone belts; what are they? *South African Journal of Geology*, 98(4): 505-520.
- De Wit, M.J. and Ashwal, L.D., 1997. *Greenstone Belts*. Oxford Monographs on Geology and Geophysics, 35. Oxford University Press, Oxford, 809 pp.
- De Wit, M.J. and Hart, R.A., 1993. Earth's earliest continental lithosphere, hydrothermal flux and crustal recycling.** *Lithos*, 30: 309-335.
- De Wit, M.J., Hart, R.A. and Hart, R.J., 1987b. The Jamestown ophiolite complex, Barberton Mountain Belt: a section through 3.5 Ga oceanic crust. *J.Afr. Earth Sci.*, 6: 681-730.

- De Wit, M.J. and Hynes, A., 1995. The onset of interaction between the hydrosphere and oceanic crust, and the origin of the first continental lithosphere. In: M.P. Coward and A.C. Ries (Editors), *Early Precambrian Processes*. *Geol. Soc. Spec. Publ.*, pp. 1-9.
- De Wit, M.J. et al., 1992. Formation of an Archaean Continent. *Nature*, 357: 553-562.
- Dewey, J.F., 1988. Extensional collapse of orogens. *Tectonics*, 7(6): 1123-1139.
- Dewey, J.F. and Windley, B.F., 1981. Growth and differentiation of the continental crust. *Phil. Trans. Royal Soc. London*, A301: 189-206.
- Dirks, P.H.G.M., Jelsma, B.A. and Hofmann, A., 2002. Thrust-related accretion of an Archaean greenstone belt in the Midlands of Zimbabwe. *Journal of Structural Geology*, 24(11): 1707-1727.
- Drake, M.J. and Weill, D.P., 1975. Partition of Sr, Ba, Ca, Y, Eu²⁺, Eu³⁺ and other REE between plagioclase feldspar and magmatic liquid: an experimental study. *Geochimica et Cosmochimica Acta*, 39: 689-712.
- Drummond, B.L., 1979. A crustal profile across the Archaean Pilbara and northern Yilgarn Cratons, northwest Australia. *BMR Journal of Australian Geology & Geophysics*, 4: 171-180.
- Drummond, B.L., 1981. Crustal structure of the Precambrian terrains of northwest Australia from seismic refraction data. *BMR Journal of Australian Geology & Geophysics*, 6: 123-135.
- Drummond, M.S. and Defant, M.J., 1990. A model for Trondhjemite-Tonalite-Dacite genesis and crustal growth via slab melting: Archaean to Modern comparisons. *Journal of Geophysical Research*, 95(B13): 503-521.
- England, P. and Bickle, M., 1984. Continental thermal and tectonic regimes during the Archaean. *Journal of Geology*, 92(4): 353-365.
- Eriksson, K.A., 1981. Archaean platform-to-trough sedimentation, East Pilbara Block, Australia. *Spec. Pubis geol Soc. Aust.*, 7: 235-244.
- Eriksson, K.A., Krapez, B. and Fralick, P.W., 1994. Sedimentology of Archaean greenstone Belts: signatures of tectonic evolution. *Earth-Sc. Rev.*, 37: 1-88.
- Feng, R., Machado, N. and Ludden, J., 1993. Lead geochronology of zircon by laserprobe ICP MS. *Geochimica et Cosmochimica Acta*, 57: 3479-3486.
- Foley, S., Tiepolo, M. and Vannucci, R., 2002. Growth of early continental crust controlled by melting of amphibolite in subduction zones. *Nature*, 417: 837-840.
- Foley, S.F., BOore, S. and Jacob, D.E., 2003. Evolution of the Archaean crust by delamination and shallow subduction. *Nature*, 421: 249-252.
- Fripp, R.E.P. and Jones, M.G., 1997. Sheeted Intrusions and Peridotite-Gabbro Assemblages in the Yilgarn Craton, Western Australia: Elements of Archaean Ophiolites. In: M.J.D.W.a. Ashwall (Editor), *Greenstone Belts*, pp. 423-436.
- Froude, D.O. et al., 1983. Ion microprobe identification of 4100-4200 Myr-old zircons. *Nature*, 304: 616-618.
- Fryer, B.L., Jackson, S.E. and Longerieh, H.P., 1993. The application of LAM-ICP-MS to in situ (D)-Pb geochronology. *Chemical Geology*, 109: 1-8.
- Fujimaki, H., 1986. Partition coefficients of Hf, Zr, and REE between zircon, apatite, and liquid. *Contrib Mineral Petrol*, 94: 42-45.
- Galer, S.J.G. and Metzger, K., 1998. Metamorphism, denudation and sea level in the Archaean and cooling of the Earth. *Precambrian Research*, 92: 389-412.
- Glikson, A. Y., 1993. Asteroids and early Precambrian crustal evolution. *Earth-Science Reviews*, 35: 285-319.
- Glikson, A. Y., 1995. Asteroid/comet mega-impacts may have triggered major episodes of crustal evolution. *Eos*, 76: 54-55.
- Glikson, A. Y., 1996. Mega-impacts and mantle-melting episodes: test of possible correlations. *AGSO Journal of Australian Geology and Geophysics*, 16(4): 587-607.
- Glikson, A. Y., 2001. The astronomical connection of terrestrial evolution: crustal effects of post-3.8 Ga mega-impact clusters and evidence for major 3.2 +/- 0.1 Ga bombardment of the Earth-Moon system. *Journal of Geodynamics*, 32: 205-229.
- Green, M.G., Sylvester, P.J. and Buick, R., 2000. Growth and recycling of early Archaean continental crust: geochemical evidence from the Coonterunah and Warrawoona Groups, Pilbara Craton, Australia. *Tectonophysics*, 322: 69-88.
- Green, M.G., Sylvester, P.J. and Buick, R., in press. Reply to the comment by Bolhar et al. on 'Growth and recycling of early Archaean continental crust: geochemical evidence from the Coonterunah and Warrawoona Groups, Pilbara Craton, Australia'. *Tectonophysics*, 6565.
- Grieve, R.A.F., 1980. Impact bombardment and its role in proto-continental growth of the early Earth. *Precambrian Research*, 10: 217-248.
- Gruau, G. et al., 1987. Age of the Archaean Taiga-Taiga Subgroup, Pilbara Block, Western Australia, and early evolution of the mantle: new Sm-Nd isotope evidence. *EPSL*, 85: 105-116.

- Gunther, D., Frischknecht, R., Heinrich, C.A and Kahlert, H.J., 1997. Capabilities of an argon fluoride 193 nm excimer laser for laser ablation inductively coupled plasma mass spectrometry microanalysis of geological materials. *Journal of Analytical Atomic Spectrometry*, 12: 939-944.
- Gutscher, M. A, Spakman, W., Bijwaard, H. and Engdahl, E.R, 2000. Geodynamics of flat subduction: seismicity and tomographic constraints from the Andean margin. *Tectonics*, 19: 814-833.
- Hamilton, P.J., Evensen, N.M., Nions, R.K.O., Glikson, A.Y. and Hickman, A.H., 1981. Sm-Nd dating of the North Star Basalt, Warrawoona Group, Pilbara Block, Western Australia. *Special Publications Geol. Soc. Australia*, 7: 187-191.
- Hamilton, W.B., 1998. Archaean magmatism and deformation were not products of plate tectonics. *Precambrian Research*, 91: 143-179.
- Harry, D.L. and Green, N.L., 1999. Slab dehydration and basalt petrogenesis in subduction systems involving very young lithosphere. *Chemical Geology*, 160: 309-333.
- Herzberg, C., 1999. Phase equilibrium constraints on the formation of cratonic mantle. In: Y. Fei, C.M. Bertka and B.O. Mysen (Editors), *Mantle Petrology: Field observations and high pressure experiments: A tribute to Francis R. (Joe) Boyd*. Geochemical Society Special Publication, pp. 241-257.
- Hickman, A.H., 1977. New and revised definitions of rock units in the Warrawoona Group, Pilbara Block. GSWA Ann Rep, 1976: 53.
- Hickman, A.H., 1983. Geology of the Pilbara Block and its environs. GSWA Bulletin, 127, 268 pp.
- Hickman, A.H., 1984. Archaean diapirism in the Pilbara Block, Western Australia. In: A. Kroner and R. Greiling (Editors), *Precambrian Tectonics Illustrated*, pp. 113-127.
- Hickman, A.H., 1997. Dampier, WA Sheet 2256. GSWA, 1:100,000 Geological Map Series.
- Hickman, A.H., 1999. New tectono-stratigraphic interpretations of the Pilbara Craton, Western Australia. GSWA Record, 1999/6: 4-6.
- Hickman, A.H., 2000. Roebourne, WA Sheet 2356. GSWA, 1:100,000 Geological Map Series.
- Hickman, A.H., Smithies, R.H. and Huston, D.L., 2000. Archaean Geology of the West Pilbara Granite Greenstone Terrane and Mallina Basin - A field guide. GSWA Record, 2000/9: 61p.
- Hickman, A.H., Smithies, R.H., Pike, G, Farrell, T.R. and Beintema, K.A., 2001. Evolution of the West Pilbara Granite-Greenstone Terrane and Mallina Basin, Western Australia - a field guide. GSWA Record, 2001/16: 65p.
- Hill, R.I., Campbell, G.F., Davies, G.F. and Griffiths, R. W., 1992. Mantle plumes and continental tectonics. *Science*, 256: 186-193.
- Hirata, T. and Nesbitt, R.W., 1995. *V-Pb* isotope geochronology of zircon: Evaluation of the laser probe ICP MS technique. *Geochimica et Cosmochimica Acta*, 59(12): 2491-2500.
- Hoatson, D.M. and Sun, S.-S., 2002. Archaean layered mafic-ultramafic intrusions in the West Pilbara Craton, Western Australia: a synthesis of some of the oldest orthomagmatic mineralizing systems in the world. *Economic Geology*, 97: 847-872.
- Hofmann, A.W. and White, W.M., 1983. Ba, Rb and Cs in the Earth's Mantle. *Z. Naturforsch. Sect. A-J. Phys. Sci.*, 38: 256-266.
- Holttä, P., Hubma, H., Manttari, I. and Paavola, J., 2000. P-T-t development of Archaean granulites in Varpaisjärvi, central Finland; II, Dating of high-grade metamorphism with the *V-Pb* and Sm-Nd methods. *Lithos*, 50(1-3): 121-136.
- Hom, I., Rudnick, R.L. and McDonough, W.P., 2000. Precise elemental and isotope ratio determination by simultaneous solution nebulization and laser ablation ICP-MS: application to *V-Pb* geochronology. *Chemical Geology*, 167: 405-425.
- Horwitz, R.C., 1990. Paleogeographic and tectonic evolution of the Pilbara Craton, Northwestern Australia. *Precambrian Research*, 48: 327-340.
- Horwitz, R.C. and Pidgeon, R.T., 1993.3.1 Ga tuff from the Sholl belt in the West Pilbara: further evidence for diachronous volcanism in the Pilbara Craton of Western Australia. *Prec. Res.*, 60: 175-183.
- Hurley, P.M., 1968. Absolute abundance and distribution of Rb, K and Sr in the Earth. *GCA*, 32: 273.
- Huston, D.L., Smithies, R.H. and Sun, S.S., 2000. Correlation of the Archaean Mallina-Creek Basin: implications for base-metal potential of the central part of the Pilbara granite-greenstone terrane. *Australian Journal of Earth Sciences*, 47: 217-230.
- Irvine, T.N. and Baragar, W.R.A., 1971. A guide to the chemical classification of common volcanic rocks. *Canadian Journal of Earth Sciences*, 8: 523-548.
- Jackson, M.I. and Pollack, H.N., 1984. On the sensitivity of parameterized convection to the rate of decay of internal heat sources. *Journal of Geophysical Research*, 89: 10103-10108.

- Jackson, S.E., 1997. LAMTRACE v 1.73, LAM-ICP-MS data reduction spreadsheet. Department of Earth Sciences, Memorial University of Newfoundland, St John's, Canada.
- Kiyokawa, S. and Taira, A., 1998. The Cleaverville Group in the West Pilbara Coastal Granitoid -Greenstone Terrain of Western Australia: an example of a Mid-Archaean immature oceanic island-arc succession. *Precambrian Research*, 88: 109-142.
- Kiyokawa, S., Taira, A., Byrne, T., Bowring, S.A. and Sano, Y., 2002. Structural evolution of the middle Archaean Coastal Pilbara Terrane, Western Australia. *Tectonics*, 21(5): 1044.
- Kley, J., 1999. Geologic and geometric constraints on a kinematic model of the Bolivian orocline. *Journal of South American Earth Sciences*, 12: 221-235.
- Kloppenburg, A., White, S.H. and Zegers, T.E., 2001. Structural evolution of the Warrawoona Greenstone Belt and adjoining granitoid complexes, Pilbara Craton, Western Australia: implications for Archaean tectonic processes. *Precambrian Research*, 112: 107-147.
- Kosier, J., Fonneland, H., Sylvester, P., Tubrelt, M. and Pedersen, R.-B., 2002. U-Pb dating of detrital zircons for sediment provenance studies - a comparison of laser ablation ICPMS and SIMS techniques. *Chemical Geology*, 182: 605-618.
- Krapez, B., 1993. Sequence stratigraphy of the Archaean supracrustal belts of the Pilbara Block, Western Australia. *Precambrian Res.*, 60: 1-45.
- Krapez, B. and Barley, M.E., 1987. Archaean strike-slip faulting and related ensialic basins: evidence from the Pilbara Block, Australia. *Geol. Mag.*, 124(6): 555-567.
- Krapez, B. and Eisenlohr, B., 1998. Tectonic settings of Archaean (3325-2775 Ma) crustal-supracrustal belts in the West Pilbara Block. *Precambrian Res.*, 88: 173-205.
- Kroner, A., 1979. Precambrian crustal evolution in the light of plate tectonics and the undation theory. *Geologie en Mijnbouw*, 58(2): 231-240.
- Kroner, A., 1980. *Precambrian Plate Tectonics*. Elsevier, Amsterdam.
- Kroner, A., 1983. Proterozoic mobile belts compatible with the plate tectonic concept. *Geological Society of America Memoir*, 161: 59-72.
- Kriener, A., 1984. Evolution, growth and stabilization of the Precambrian lithosphere. *Phys. Chem. Earth*, 15: 69-106.
- Kroner, A., 1985. Evolution of the Archaean continental crust. *Ann. Rev. Earth Planet. Sci.*, 13: 49-74.
- Kroner, A., 1991. Tectonic evolution in the Archaean and Proterozoic. *Tectonophysics*, 187: 393-410.
- Kroner, A. and Layer, P.W., 1992. Crust Formation and Plate Motion in the Early Archaean. *Science*, 256: 1405-1411.
- Kusky, T.M. and Polat, A., 1999. Growth of granite-greenstone terranes at convergent margins, and stabilization of Archaean cratons. *Tectonophysics*, 305: 43-73.
- Lambert, L.B., 1976. Archaean Geothenn. In: B.F. Windley (Editor), *The Early History of the Earth*. Wiley, London, pp.619.
- Ludwig, K.R., 2001. *Isoplot*, v 2.49. Berkeley Geochronology Center Special Pub/. 1a.
- Mank, A.J.G. and Mason, P.R.D., 1999. A critical assessment of laser ablation ICP-MS as an analytical tool for depth analysis in silica-based glass samples. *Journal of Analytical Atomic Spectrometry*, 14: 1143-1153.
- Marshall, S., 1999. Deformation style way back then: thoughts on the contrasts between Archaean/Palaeoproterozoic and contemporary orogens. *J. Struct. Geol.*, 21: 1175-1182.
- Martin, H., 1994. Archaean grey gneisses and the genesis of continental crust. In: K.C. Condie (Editor), *Archaean Crustal Evolution: Developments in Precambrian Geology*. Elsevier, pp. 505-525.
- Martin, H. and Moyen, J.P., 2002. Secular compositional changes in tonalite-trondhjemite-granodiorite composition as markers for the progressive cooling of the Earth. *Geology*, 30: 319-322.
- Mason, P.R.D. and Kraan, W.T., 2002. Attenuation of spectral interferences during laser ablation inductively coupled plasma mass spectrometry (LA-ICP-MS) using an rf only collision and reaction cell. *Journal of Analytical Atomic Spectrometry*, 17: 858-867.
- McCulloch, M.T. and Bennett, V.C., 1994. Progressive growth of the Earth's continental crust and depleted mantle: geochemical constraints. *Geoch. Cosmoch. Acta*, 58: 4717-4738.
- McDonough, W.F. and Sun, S.-S., 1995. The composition of the Earth. *Chemical Geology*, 120: 223-253.
- McDougall, I. and Harrison, T.M., 1999. *Geochronology and thermochronology by the ⁴⁰Ar/³⁹Ar method*. Oxford University Press, New York, 270 pp.
- McKenzie, D. and Bickle, M.J., 1988. The volume and composition of melt generated by extension of the lithosphere. *Journal of Petrology*, 29: 625-679.
- McNaughton, N.J., Compston, W. and Barley, M.E., 1993. Constraints on the age of the Warrawoona Group, eastern Pilbara Block, Western Australia. *Precambrian Res.*, 60: 69-98.

- McNaughton, N.J. and Dahl, N., 1987. A geochronological framework for gold mineralization in the Yilgarn Block, Western Australia. In: S.E. Ho and D.I. Groves (Editors), *Advances in understanding Precambrian Gold deposits*, Volume II. Geol. Dept & Univ. Extension, Univ. West. Aust., pp. 29-50.
- Meschede, M., 1986. A method of discriminating between different types of mid-ocean ridge basalts and continental tholeiites with the Nb-Zr-Y diagram. *Chemical Geology*, 56: 207-218.
- Miyashiro, A., 1994. *Metamorphic Petrology*. VCL Press, London, 404 pp.
- Mojzsis, S.J., Harrison, T.M. and Pidgeon, R.T., 2001. Oxygen-isotope evidence from ancient zircons for liquid water at the Earth's surface 4,300 Myr ago. *Nature*, 409: 178-181.
- Morgan, J.P., 1998. Thermal and rare gas evolution of the mantle. *Chemical Geology*, 145: 431-445.
- Morgan, P., 1984. The thermal structure and evolution of the continental lithosphere. *Phys. Chem. Earth*, 15: 107-193.
- Mullen, E.D., 1983. MnO/TiO₂/P₂O₅: a minor element discriminant for basaltic rocks of oceanic environments and its implications for petrogenesis. *Earth and Planetary Science Letters*, 62: 53-62.
- Myers, J.S., 1995. The generation and assembly of an Archean super continent: evidence from the Yilgarn Craton, Western Australia. In: M.P. Coward and A.C. Ries (Editors), *Early Precambrian Processes*. Geol. Soc. Lond. Spec. Publ.
- Myers, J.S. and Kroner, A., 1994. Archean tectonics. In: P.L. Hancock (Editor), *Continental Deformation*. Pergamon Press, Oxford, pp. 355-369.
- Nagasawa, 1970. zircon trace element partition coefficients.
- Nelson, D.R., 1996. Compilation of SHRIMP U-Pb zircon geochronology data, 1995. 1996/5, Geological Survey of Western Australia.
- Nelson, D.R., 1997. Compilation of SHRIMP U-Pb zircon geochronology data, 1996. 1997/2, Geological Survey of Western Australia.
- Nelson, D.R., 1998a. Compilation of SHRIMP *V-Pb* zircon geochronology data, 1997. 1998/2, Geological Survey of Western Australia.
- Nelson, D.R., 1998b. Granite-greenstone crust formation on the Archean Earth: a consequence of two superimposed processes. *EPSL*, 158(3-4): 109-119.
- Nelson, D.R., 1999. Compilation of SHRIMP U-Pb zircon geochronology data, 1998. 1999/2, Geological Survey of Western Australia.
- Nelson, D.R., 2000. Compilation of SHRIMP U-Pb zircon geochronology data, 1999. 2000/2, Geological Survey of Western Australia.
- Nelson, D.R., 2001. Compilation of SHRIMP U-Pb zircon geochronology data, 2000. 2001/2, Geological Survey of Western Australia.
- Nesbitt, R.W. and Sun, S.-S., 1976. Geochemistry of Archean spinifex-textured peridotites and magnesian and low-magnesian tholeiites. *Earth and Planetary Science Letters*, 31: 433-453.
- Neumayr, P. et al., 1998. Timing of gold mineralization in the Mt York district, Pilgangoora Greenstone Belt, and implications for the tectonic and metamorphic evolution of an area linking the eastern and western Pilbara Craton. *Precambrian Research*, 88: 249-265.
- Nijman, W., Willigers, B.J.A. and Krikke, A., 1998. Tensile and compressive growth structures: the relation between sedimentation, deformation and granite intrusion in the Archean Coppin Gap Greenstone Belt, East Pilbara, W. Australia. *Precambrian Research*, 88: 83-108.
- Nisbet, E.G., 1987. *The Young Earth: an introduction to Archean geology*. Allen & Unwin, Boston.
- Nisbet, E.G., Cheadle, M.J., Bickle, M.J. and Arndt, N.T., 1993. Constraining the potential temperature of the Archean mantle: A review of the evidence from komatiites. *Lithos*, 30: 291-308.
- Nisbet, E.G. and Fowler, C.M.R., 1983. Model for Archean plate tectonics. *Geology*, II: 376-379.
- Nutman, A.P., 2001. On the scarcity of >3900 Ma detrital zircons in >3500 Ma metasediments. *Precambrian Research*, 105: 93-114.
- Nutman, A.P. and Collerson, K.D., 1991. Very early Archean crustal-accretion complexes preserved in the North Atlantic Craton. *Geology*, 19: 791-794.
- Ohta, H., Maruyama, S., Takahashi, E., Watanabe, Y. and Kato, Y., 1996a. Field occurrence, geochemistry and petrogenesis of the Archean Mid Oceanic Ridge Basalts (AMORBs) of the Cleaverville area, Pilbara Craton, Western Australia. *Lithos*, 37: 199 - 221.
- Ohta, H., Maruyama, S., Takahashi, E., Watanabe, Y. and Kato, Y., 1996b. Field occurrence, geochemistry and petrogenesis of the Archean Mid Oceanic Ridge Basalts (AMORBs) of the Cleaverville area, Pilbara Craton, Western Australia. *Litho.*, 37: 199 - 221.
- O'Nions, R.K. and Pankhurst, R.J., 1978. Early Archean rocks and geochemical evolution of the earth's crust. *EPSL*, 38: 211-236.

- Oversby, V.M., 1976. Isotope ages and geochemistry of Archean acid igneous rocks from the Pilbara, Western Australia. *Geochimica et Cosmochimica Acta*, 40: 817-829.
- Park, R.G., 1981. Origin of horizontal structure in high-grade Archean terrains. In: D.L. Groves (Editor), *Archean Geology*. *Geol. Soc. Austr. Spec. Publ.* 7, pp. 481-490.
- Pearce, N.J.G. et al., 1997. A compilation of new and published major and trace element data for NIST SRM 610 and NIST SRM 612 glass reference materials. *Geostandards Newsletter*, 21: 115-144.
- Peltier, W.R., Butler, S. and Solheim, L.P., 1997. The influence of phase transformations on mantle mixing and plate tectonics. In: D.J. Crossley (Editor), *Earth's Deep Interior*. Gordon & Breach, Amsterdam, pp. 405-430.
- Pidgeon, R.T., 1978. 3450-m.y.-old volcanics in the Archean layered greenstone succession of the Pilbara Block, western Australia. 37: 421-.
- Pidgeon, R.T., 1984. Geochronological constraints on early volcanic evolution of the Pilbara Block, Western Australia. *Australian Journal of Earth Sciences*, 31: 237-242.
- Pidgeon, R.T., Furfaro, D., Kennedy, A.K., Nemchin, A.A. and Van Bronswijk, W., 1994. Calibration of zircon standards for the Curtin SHRIMP II, 8th International Conference on Geochronology, Berkeley, USA. USGS Circular, 1107, pp. 251.
- Pike, O. and Cas, R., 2002. Stratigraphic evolution of Archean volcanic rock-dominated rift basins from the Whim Creek Belt, west Pilbara Craton, Western Australia. *Special Pubs. of the Int. Ass. Sediment.*, 33: 213-234.
- Pike, O., Cas, R. and Smithies, R.H., 2002. Geologic constraints on base metal mineralization of the Whim Creek Greenstone Belt, Pilbara Craton, Western Australia. *Economic Geology*, 97: 827-845.
- Platt, J.P., 1980. Archean greenstone belts: a structural test of tectonic hypotheses. *Tectonophysics*, 65: 127 - 150.
- Polat, A. and Kerrich, R., 2001. Geodynamic processes, continental growth, and mantle evolution recorded in late Archean greenstone belts of the southern Superior Province, Canada. *Precambrian Research*, 112: 5-25.
- Pollack, H.N., 1997. Thermal characteristics of the Archean. In: L.D. Ashwal (Editor), *Greenstone Belts*. Clarendon Press, Oxford.
- Ramsey, J.o. and Hubert, M.I., 1983. *The techniques of modern structural geology - Volume I: Strain Analysis*. Academic Press Limited, London, p.303 pp.
- Reymer, A. and Schubert, O., 1984. Phanerozoic addition rates to the continental crust and crustal growth. *Tectonics*, 3: 63-78.
- Richards, I.R. and Blockley, J.G., 1984. The base of the Fortescue Group, Western Australia- further galena lead isotope evidence on its age. *Australian Journal of Earth Sciences*, 31: 257-268.
- Richards, J.R., Fletcher, L.R. and Blockley, J.o., 1981. Pilbara galenas: precise isotope assay of the oldest Australian leads; model ages and growth curve implications. *Mineralium Deposita*, 16: 7-30.
- Rogers, J.J.W., Unrug, R. and Sultan, M., 1995. Tectonic assembly of Gondwana. *Journal of Geodynamics*, 19(I): 1-34.
- Rollinson, H., 1993. *Using geochemical data: evaluation, presentation, interpretation*. Longman, Essex, England, 352 pp.
- Rudnick, R.L., 1995. Making continental crust. *Nature*, 378: 571-578.
- Schmidt, M.W. and Poli, S., 1998. Experimentally based water budgets for dehydrating slabs and consequences for arc magma generation. *Earth and Planetary Science Letters*, 163: 361-379.
- Sengor, A.M.C. and Dewey, J.F., 1990. *Terranology: vice or virtue?* *Philosophical Transactions of the Royal Society of London*, A331: 457-477.
- Shirey, S.B. et al., 2002. Diamond genesis, seismic structure and evolution of the Kaapvaal-Zimbabwe Craton. *Science*, 297: 1683-1686.
- Simonson, B.M., Hassler, S.W. and Beukes, N.J., 1999. Late Archean impact spherule layer in South Africa that may correlate with a Western Australian layer. In: B.O. Dressler and v.L. Sharpton (Editors), *Large meteorite impacts and planetary evolution; II. Special Paper - Geological Society of America (GSA)*, Boulder.
- Sleep, N.H. and Windley, B.P., 1986. Archean plate tectonics: constraints and inferences. *Journal of Geology*, 90: 367-379.
- Smith, J.B., 2003. The episodic development of intermediate to silicic volcano-plutonic suites in the Archean West Pilbara, Australia. *Chemical Geology*, 194: 275-295.
- Smith, J.B., in press. The episodic development of intermediate to silicic volcano-plutonic suites in the Archean West Pilbara, Australia. *Chemical Geology*.
- Smith, J.B., Barley, M.E., Groves, D.L., Krapez, B. and McNaughton, N.J., 1998. The Sholl Shear Zone, Western Pilbara: Evidence for a domain boundary structure from integrated tectonostratigraphic analyses, SHRIMP U-Pb dating and isotopic and geochemical data of granitoids. *Precambrian Res.*, 88: 143-171.
- Smithies, R.H., 1996. Refinement of the stratigraphy of the Whim Creek Belt, Pilbara granite-greenstone terrain: new field evidence from Sherlock 1:100,000 sheet. *GSWA Annual review(1995-96)*: 118-123.

- Smithies, R.H., 1997a. The Mallina Formation, Constantine Sandstone and Whim Creek Group; a new stratigraphic and tectonic interpretation – part of the western Pilbara Craton. *GSWA Annual Review, 1996-1997*; 83-88.
- Smithies, R.H., 1997b. Sherlock, WA Sheet 2456. GSWA, 1:100,000 Geological Map Series.
- Smithies, R.H., 2000a. The Archaean tonalite-trondhjemite-granodiorite (TTG) series is not an analogue of Cenozoic adakite. *EPSL*, 182; 115-125.
- Smithies, R.H., 2000b. Wallaringa, WA Sheet 2656. GSWA, 1:100,000 Geological Map Series.
- Smithies, R.H., 2002. Archaean boninite-like rocks in an intracratonic setting. *Earth and Planetary Science Letters*, 197: 19-34.
- Smithies, R.H. and Champion, D.C., 1998. Secular compositional changes in Archaean granites of the West Pilbara. *GSWA Annual Review, 1997-98*; 71-76.
- Smithies, R.H. and Champion, D.C., 1999. High-Mg diorite from the Archaean Pilbara Craton: anorogenic magmas derived from a subduction-modified mantle. *GSWA Annual Review, 1998-99*; 45-49.
- Smithies, R.H. and Champion, D.C., 2000. The Archaean high-Mg diorite suite; links to tonalite-trondhjemite-granodiorite magmatism and implications for early Archaean crustal growth. *Journal of Petrology*, 41 (12); 1653-1671.
- Smithies, R.H. and Champion, D.C., 2001. Assembly of a composite intrusion at a releasing bend in an active Archaean shear zone - temporal and spatial evolution of the Wallareena Jog, northwestern Australia. *GSWA Annual Review, 2000*: 63-68.
- Smithies, R.H. and Farrell, T.R., 2000. Satirist, WA Sheet 2555. GSWA, 1:100,000 Geological Map Series.
- Smithies, R.H., Hickman, A.H. and Nelson, D.R., 1999. New constraints on the evolution of the Mallina Basin, and their bearing on relationships between the contrasting eastern and western granite-greenstone terranes of the Archaean Pilbara Craton Western Australia. *Precambrian Research*, 94: 11-28.
- Smithies, R.H., Nelson, D.R. and Pike, G., 2001. Development of the Archaean Mallina Basin, Pilbara Craton, northwestern Australia: a study of detrital and inherited zircon ages. *Sedimentary Geology*, 141-142; 79-94.
- Stein, M. and Hofmann, A.W., 1994. Mantle plumes and episodic crustal growth. *Nature*, 372: 63-68.
- Stem, C.R. and De Wit, M.J., 1997. Geophysics and deep structure of greenstone belts. In: M.J.D. Wit and L.D. Ashwal (Editors), *Greenstone Belts*. Clarendon, Oxford.
- Stem, R.A., Hanson, G.N. and Shirey, S.B., 1989. Petrogenesis of mantle-derived, LILE-enriched Archaean monzodiorites and trachyandesites (sanukitoids) in the Southwestern Superior Province. *Canadian Journal of Earth Sciences*, 26: 1688-1712.
- Stettler, E., De Beer, J.H., Eberle, D., Ludden, J. and Mareshal, M., 1997. Geophysics and deep structure of greenstone belts. In: M.D. Wit and L.D. Ashwal (Editors), *Greenstone Belts*. Clarendon, Oxford.
- St-Onge, M.R., Lucas, S.B. and Scott, D.J., 1997. The Ungava Orogen and the Cape Smith Thrust Belt. In: M.D. Wit and L.D. Ashwal (Editors), *Greenstone Belts*. Clarendon, Oxford.
- Sun, S.-S. and Hickman, A.H., 1998. New Nd-isotopic and geochemical data from the West Pilbara: implications for Archaean crustal accretion and shear zone movement. *Australian Geological Research Newsletter*, May 1998: 25-29.
- Sun, S.-S. and Hickman, A.H., 1999. Geochemical characteristics of ca. 3.0-Ga Cleaverville greenstones and later mafic dykes, west Pilbara; implication for Archaean crustal accretion. *AGSO Res. Newsletter*, 31.
- Sun, S.-S. and McDonough, W.F., 1989. Chemical and isotopic systematics of oceanic basalts: implications for mantle composition and processes. In: A.D. Saunders and M.J. Norry (Editors), *Magmatism in the ocean basins*. Geological Society Special Publications No. 42, pp. 313-345.
- Sweetapple, M.T. and Collins, P.L.F., 2002. Genetic framework for the classification and distribution of Archaean rare metal pegmatites in the North Pilbara Craton, Western Australia. *Economic Geology*, 97: 873-895.
- Sylvester, P.J., 1994. Archaean granite plutons. In: K.C. Condie (Editor), *Archean Crustal Evolution*. Developments in Precambrian Geology. Elsevier, Amsterdam, pp. 261-314.
- Tatsumi, Y. and Eggins, S., 1995. *Subduction Zone Magmatism*. Blackwell Science.
- Taylor, S.R., 1989. Growth of planetary crusts. *Tectonophysics*, 161: 147-156.
- Taylor, S.R. and McLennan, S.M., 1985. *The Continental Crust: Its Composition and Evolution*. Blackwell, Oxford.
- Thompson, R.N., Morrison, M.A., Hendry, G.L. and Parry, S.J., 1984. An assessment of the relative roles of crust and mantle in magma genesis: an elemental approach. *Phil. Trans. R. Soc. Lond.*, A310: 549-590.
- Thorpe, R.I., Hickman, A.H., Davis, D.W., Mortensen, J.K. and Trendall, A.F., 1992. U-Pb zircon geochronology of Archaean felsic units in the Marble Bar region, Pilbara Craton, Western Australia. *Precambrian Res.*, 56: 169-189.
- Trendall, A.F., 1995. Paradigms for the Pilbara, Early Precambrian Processes, pp. 127 - 142.
- Tyler, I.M., 2000. Palaeoproterozoic Orogeny in Western Australia. *AGSO J Aus Geol. Geoph.*: 7-8.

- Tyler, I.M., Fletcher, **IR.**, Laeter, I.R.d., Williams, I.R. and Libby, W.o., 1992. Isotope and rare earth element evidence for a late Archaean terrane boundary in the southeastern Pilbara Craton, Western Australia. 54: 211-229.
- Van de Zedde, D.M.A. and Wortel, M.J.R., 2001. Shallow slab detachment as a transient source of heat at midlithospheric depths. *Tectonics*, 20(6): 868-882.
- Van Haafte, W.M. and White, S.H., 1998. Evidence for multiphase deformation in the Archean basal Warrawoona Group in the Marble Bar area, east Pilbara, Western Australia. *Precambrian Res.*, 88: 53-66.
- Van Hunen, I., Van den Berg, A.P. and Vlaar, N.J., 2000. A thermo-mechanical model of horizontal subduction below an overriding plate. *EPSL*, 182: 157-169.
- Van Kranendonk, M.J. and Collins, W.J., 1998. Timing and tectonic significance of Late Archaean, sinistral strike-slip deformation in the Central Pilbara Structural Corridor, Pilbara Craton, Western Australia. *Precambrian Res.*, 88: 207-232.
- Van Kranendonk, M.J., Hickman, A.H. and Collins, W.J., 2001. Comment on "Van Haafte, W.M. and White, S.H., 1998. Evidence for multiphase deformation in the Archean basal Warrawoona Group in the Marble Bar area, east Pilbara, Western Australia. *Precambrian Res.*, 88: 53-66". *Precambrian Research*, 105: 73-78.
- Van Kranendonk, M.J., Hickman, A.H., Smithies, R.H., Nelson, D.R. and Pike, G., 2002. Geology and tectonic evolution of the Archaean North Pilbara terrain, Pilbara Craton, Western Australia. *Economic Geology*, 97: 695-732.
- Veamcombe, S. and Kerrich, R., 1999. Geochemistry and geodynamic setting of volcanic and plutonic rocks associated with early Archaean volcanic massive sulphide mineralization, Pilbara Craton. *Precambrian Research*, 98: 243-270.
- Vlaar, N.J., 1986. Archaean global dynamics. *Geologie en Mijnbouw*, 65: 91-101.
- Vlaar, N.J., 2000. Continental emergence and growth on a cooling earth. *Tectonophysics*, 322: 191-202.
- Vlaar, N.J., van Keken, P.E. and van den Berg, A.P., 1994. Cooling of the Earth in the Archaean: consequences of pressure-release melting in a hotter mantle. *Earth and Planetary Science Letters*, 121: 1-18.
- Warren, P.H., 1984. Effect of impacts on early Earth crust. *Tectonophysics*, 161: 165-.
- Wellman, P., 1999. Granitoid complexes and greenstone belts in the Pilbara Craton interpreted to extend down to the mid-crustal boundary at 14 km. *AGSO Research Newsletter*, 30: 15-17.
- White, S.H., Zegers, T.E., Van Haafte, W.M., Kloppenburg, A. and Wijbrans, J.R., 1998. Tectonic evolution of the eastern Pilbara, Australia. *Geol. Mijnb.*, 76(4): 343-347.
- Wiedenbeck, M. et al., 1995. Three natural zircon standards for U-Th-Pb, Lu-Hf, trace element and REE analyses. *Geostandards Newsletter*, 19: 1-23.
- Wijbrans, I.R. and McDougall, I., 1987. On the metamorphic history of an Archaean granitoid greenstone terrane, East Pilbara, Western Australia, using the $^{40}\text{Ar}/^{39}\text{Ar}$ age spectrum technique. 84: 226-242.
- Wijbrans, J.R., Pringle, M.S., Koppers, A.A.P. and Scheevers, R., 1995. Argon geochronology of small samples using the Vulkana argon laserprobe. *Proc. Kon. Ned. Akad. Wetensch.*, 98(2): 185-218.
- Wilde, S.A., Middleton, M.F. and Evans, B.J., 1996. Terrane accretion in the southwestern Yilgarn Craton: evidence from a deep seismic crustal profile. *Precambrian Research*, 78: 179-196.
- Wilde, S.A., Valley, I.W., Peck, W.H. and Graham, C.M., 2001. Evidence from detrital zircons for the existence of continental crust and oceans on the Earth 4.4 Gyr ago. *Nature*, 409: 175-178.
- Williams, I.S. and Collins, W.J., 1990. Granite-greenstone terranes in the Pilbara Block, Australia, as coeval volcano-plutonic complexes; evidence from U-Pb zircon dating of the Mount Edgar Batholith. *EPSL*, 97: 41-53.
- Williams, I.S., Page, R.W., Froude, D.O., Fosters, J.J. and Compston, W., 1983. Early crustal components in the western Australian Archaean: zircon U-Pb ages by ion microprobe analysis from the Shaw Batholith and Narryer metamorphic belt. *Geol. Soc. Austr. Abstr.*, 9: 169.
- Windley, B.F., 1998. Tectonic models for the geological evolution of crust, cratons and continents in the Archaean. *Revista Brasileira de Geociencias*, 28(2): 183-188.
- Wingate, M.T.D., 1999. Ion microprobe baddeleyite and zircon ages for Late Archaean mafic dykes of the Pilbara Craton, Western Australia. *Australian Journal of Earth Sciences*, 46: 493-500.
- Yardley, B.W.D., 1989. *An Introduction to Metamorphic Petrology*. Longman Scientific and Technical, UK.
- Zegers, T., Keijzer, M.d., Dirks, P. and White, S.W., 1996a. Extensional structures during deposition of the 3460 Ma Warrawoona Group in the eastern Pilbara Craton, Western Australia. *Precambrian Res.*, 80: 89-105.
- Zegers, T.E., 1996. Structural, kinematic and metallogenic evolution of selected domains of the Pilbara granitoid-greenstone terrain. *Geologica Ultraiectina*, 146, 208 pp.
- Zegers, T.E., De Keijzer, M., Dirks, P. and White, S.H., 1996b. Extensional structures during deposition of the 3460 Ma Warrawoona Group in the eastern Pilbara Craton, Western Australia. *Precambrian Res.*, 80: 89-105.
- Zegers, T.E., Keijzer, M.d., Passchier, C.W. and White, S.H., 1998. The Mulgandinnah Shear Zone Complex; an Archean crustal scale shear zone, eastern Pilbara, Western Australia. *Precambrian Research*, 88: 233-248.

References

- Zegers, T.E., Nelson, D.R., Wijbrans, *I.R.* and White, S.H., 2001. SHRIMP U-Pb zircon dating of Archaean core complex formation and pancratonic strike-slip deformation in the East Pilbara Granite-Greenstone Terrain. *Tectonics*, 20(6): 883-908.
- Zegers, T.E. and Van Keken, P.E., 2001. Middle Archaean continent formation by crustal delamination. *Geology*, 29(12): 1083-1086.
- Zegers, T.E., Wijbrans, *I.R.* and White, S.H., 1999. $^{40}\text{Ar}/^{39}\text{Ar}$ age constraints on tectonothermal events in the Shaw area of the eastern Pilbara granite-greenstone terrain (W. Australia): 700 Ma of Archaean tectonic evolution. *Tectonophysics*, 311: 45-81.

Samenvatting in het Nederlands

Het Archaicum

De Aarde is ongeveer 4,5 miljard jaar geleden ontstaan. Het Archaicum is een periode uit de vroege Aardse geschiedenis die duurde van ongeveer 4 tot 2,5 miljard jaar geleden. Omdat het Archaicum zo'n lange tijd beslaat, is kennis over deze periode onmisbaar bij het bestuderen en interpreteren van oude en moderne geologische processen, en voor het begrip van de evolutie van de Aarde tot aan het heden. Het bestuderen van processen die zich zo lang geleden afspeelden is echter niet eenvoudig.

Rutten zei ooit "Het heden is de sleutel tot het verleden". Dit is misschien waar op een algemene schaal: in het Archaicum had de Aarde waarschijnlijk ook al een kern, een mantel, een korst en een atmosfeer, maar er zijn ook grote verschillen met de moderne Aarde. Tijdens het Archaicum ontwikkelde zich bijvoorbeeld het eerste leven, de atmosfeer kreeg plotseling een andere samenstelling, en de grootste bekende goud- en diamant-voorkomens dateren uit het Archaicum. Geodynamische processen kunnen er ook heel anders uitgezien hebben, en die vormen het onderwerp van dit proefschrift.

Plaattektoniek

Er bestaan grote meningsverschillen over de vraag of moderne plaattektoniek wel of niet plaatsvond in het Archaicum. Moderne plaattektoniek wordt gekarakteriseerd door stugge korst-platen die langs het aardoppervlak bewegen; deze bewegingen zijn alleen mogelijk door de productie van oceanische korst bij spreidingsruggen midden in de oceanen, en recycling van oceanische korst in subductiezones. Thermische en geodynamische modellen hebben geen uitsluitsel kunnen geven over de vraag of plaattektoniek ook plaatsvond in het Archaicum. Het grootste probleem dat deze modellen hebben, is dat de temperatuur van het binnenste van de Aarde in die tijd eigenlijk niet goed bekend is. Het is aannemelijk dat deze temperatuur enkele tientallen tot honderden graden hoger was dan tegenwoordig, maar de precieze waarden zijn niet bekend. Geologische veldgegevens kunnen een potentiële bijdrage leveren door randgegevens vast te stellen, zoals de fossiele geothermische gradient, en de snelheden van processen en plaatbewegingen.

De meeste tectonische modellen voor het Archaicum zijn gebaseerd op het idee dat plaattektoniek in het Archaicum niet mogelijk was, vanwege de hogere manteltemperatuur. Door die hogere temperatuur werd meer smelt geproduceerd bij spreidingscentra waardoor de oceanische lithosfeer dikker was. Een dikkere lithosfeer heeft meer drijfvermogen en de modellen suggereren dat subductie van oceanische korst daardoor onmogelijk was. De meeste modellen die werden ontwikkeld gingen dan ook uit van een ander soort tektoniek, gebaseerd op verticale 'diapier'-in plaats van horizontale plaatbewegingen.

De kenmerken van moderne plaattektoniek (spreiding en subductie zoals hierboven beschreven), zijn erg moeilijk te identificeren in oude gesteenten. Het grootste probleem is dat

oceanische karst de hoofdrol speelt in het plaattectonische proces, en dat juist deze oceaankorst continu wordt gerecycled door subductie. Daardoor valt er in de oceanen weinig te bestuderen aan oude plaattectoniek. We kunnen beter op zoek gaan naar kenmerken van plaattectoniek die bewaard zijn gebleven op de continenten. De beste voorbeelden daarvan zijn direct gerelateerd aan subductie, zoals ofiolieten (stukken oceaankorst die op het continent zijn terechtgekomen), tectonische accretiewiggen (gevormd door 'bulldozeren' aan de rand van de overschuivende plaat), en het voorkomen van hoge druk-lage temperatuur metamorfe gesteenten (die laten zien dat kost-materiaal is meegenomen naar grote diepte en weer aan het oppervlak terug is gekomen). Andere verschijnselen die het bestaan van plaattectoniek verraden zijn magmatische producten die van de gesubduceerde plaat afkomstig zijn. Verder wordt plaattectoniek aan de continentranden gekarakteriseerd door tectonische cycli van extensie, compressie en activiteit van grootschalige strike-slip breuken.

Tijdens dit promotieonderzoek zijn de bovengenoemde kenmerken onderzocht in het Archaïsche Pilbara Craton in West Australië, een stuk continentale karst van 3.5 tot 2.5 miljard jaar oud. Op basis van structureel-kinematische gegevens is een tectonisch raamwerk geformuleerd. Dat raamwerk wordt ondersteund door geochronologie (absolute ouderdomsbepalingen), petrologie en geochemie (de chemische samenstelling van magmatische gesteenten). Op basis van dit raamwerk wordt een nieuw geodynamisch model voor de mid- tot laat ontwikkeling van de Westelijke en Centrale Pilbara gepresenteerd.

Het Pilbara Craton

Het Archaïsche Pilbara Craton ligt in het noordwesten van West Australië. Het bestaat uit twee belangrijke componenten: het ca 3650-2850 miljoen jaar oude (Ma) Noord-Pilbara Graniet-Groensteen Terrein, waaroverheen de ca 2775-2459 Ma afzettingen van het Hamersley Bekken zijn afgezet. In het noordelijke deel zijn deze jongere gesteenten verwijderd door erosie, in het zuidelijke deel niet, en daar is de oude Pilbara 'fundering' dus niet te bestuderen. Het vroeg tot mid-Archaïsche graniet-groensteen terrein in de Pilbara bestaat uit graniet-gneis-complexen, groensteengordels (voornamelijk basalt), en sedimentaire bekkens. Dit terrein is het onderwerp van dit proefschrift en zal hierna 'de Pilbara' worden genoemd. De Pilbara is een van de best-bewaarde Archaïsche Cratons ter wereld, met name doordat het is ontsnapt aan de latere deformatie en metamorfose die andere oude terreinen wel hebben meegemaakt. De Pilbara is ook redelijk goed ontsloten vanwege het semi-aride klimaat.

De Pilbara bestaat uit een aantal langwerpige terreinen die worden gescheiden door grote breuken. Zulke breuken komen voor in continentale korst van alle leeftijden (Zie Figuur 1.1). In jonge continenten wordt zo'n architectuur gevormd door terrein-accretie aan actieve plaatranden, als gevolg van plaattectoniek. Er is gesuggereerd dat de domein-architectuur van de Pilbara het resultaat zou kunnen zijn van terrein-accretie en dat er dus ook plaattectoniek was. Deze modellen spreken de eerste modellen die voor de Pilbara werden ontwikkeld tegen. Die gingen nog uit van de eerdergenoemde verticale 'diapier'-bewegingen in plaats van horizontale plaatbewegingen. Echter, in de loop van de tijd werden steeds meer geologische gegevens verzameld over het Archaïcum in het algemeen, en over de Pilbara. Het blijkt dat de meeste van deze gegevens, en met name de magmatische geochemie, alleen te verklaren zijn met behulp van 'moderne' plaattectonische processen. De meeste onderzoekers zijn er nu van overtuigd dat, tenminste na ongeveer 3250 Ma, 'horizontale' tectoniek een dominant proces was.

Dit proefschrift

In dit proefschrift zijn nieuwe structureel-kinematische, geochronologische en geochemische data verzameld. Deze data zijn gebruikt om een reconstructie te maken van de tectoniek van de Westelijke en Centrale Pilbara tussen ca 3265 Ma en 2900 Ma. Op basis van deze reconstructie worden de volgende vragen beantwoord: Zijn er aanwijzingen voor modeme plaattectoniek in de Pilbara? Kan de domein-structuur van de Pilbara zijn gevormd door plaattectoniek? Zijn de eerder voorgestelde accretie-modellen voor met name de Westelijke Pilbara juist? Zijn er alternatieve geodynamische modellen die de geologie van de Pilbara kunnen verklaren? Kunnen die alternatieven worden geplaatst in een modeme plaattectonische context?

Het onderzoek bestond uit drie veldseizoenen van twee maanden in de Pilbara in 1999-2001, en laboratoriumwerk aan de Universiteit Utrecht, de Vrije Universiteit van Amsterdam en Curtin University of Technology in Perth, West Australië. De resultaten zijn opgeschreven in dit proefschrift. De hoofdstukken 4 t/m 7 zijn geschreven als publiceerbare artikelen waardoor een zekere herhaling in de introducties van de hoofdstukken onvermijdelijk is.

In de hoofdstukken 2 en 3 wordt een overzicht gegeven van bestaande ideeën over tectoniek in het Archaëcum, en het Pilbara Craton. In hoofdstuk 4 wordt een deel van een groensteengordel in de Oostelijke Pilbara onderzocht omdat werd gesuggereerd dat het een stuk oceanische korst zou kunnen zijn. In hoofdstuk 5 wordt een nieuw structureel-geochronologisch en geochemisch raamwerk gepresenteerd voor de Westelijke Pilbara. In hoofdstuk 6 worden geochronologische data gepresenteerd voor de Centrale Pilbara, welke zijn verkregen door de ontwikkeling van een nieuwe techniek. In hoofdstuk 7 zijn deze geochronologische gegevens geïntegreerd met structurele en geochemische gegevens en wordt een nieuw model voor de ontwikkeling van de Centrale Pilbara gepresenteerd. Hoofdstuk 8 is de geïntegreerde geodynamische interpretatie voor de gehele Westelijke en Centrale Pilbara.

Het bestaan van de domein-structuur in de Pilbara is bevestigd, echter, de ontstaansgeschiedenis hiervan is mogelijk anders dan tot nu toe werd gedacht. Voor de eerder gepresenteerde accretie-modellen zijn tijdens dit promotieonderzoek geen bewijzen gevonden. De domein-structuur wordt beter verklaard door grootschalige activiteit van breuken in een al bestaand continent.

Het terrein van de Westelijke Pilbara, dat eerder werd aangemerkt als exotisch blok, maakt deel uit van dit al bestaande continent. De huidige architectuur en samenstelling is wel ontstaan als gevolg van subductie; de Westelijke Pilbara vormde een actieve continent-rand waaronder een oceanische plaat wegdook onder een kleine hoek, omstreeks 3265 Ma. Daarna heeft wellicht nog een aantal maal subductie plaatsgevonden onder de Westelijke Pilbara, maar de aanwijzingen hiervoor zijn cryptisch. Tussen twee grote breuken heeft zich omstreeks 2970 Ma een langwerpige sedimentaire bekken gevormd, in wat nu de Centrale Pilbara is.

Dankwoord

Ondanks dat wetenschap nooit af is heb ik er dan toch een punt achter weten te zetten. Zonder iedereen persoonlijk te noemen of te vergeten, wil ik graag al diegenen bedanken die me hebben gesteund tijdens mijn promotietijd. Ik wil met name mijn promotor Stan White en copromotor Jan Wijbrans bedanken. De veldwerken in de Pilbara waren toch echt geen vakanties zoals mijn omgeving vaak grapte, maar ik heb er tijdens het veldwerk wei fantastische dingen meegemaakt. Het uitgraven van auto's, mega-barbeques, illegale activiteiten in mijnen en natuurlijk de kangaroes had ik voor geen goud willen missen. Verder hebben mijn collega's van de vakgroepen structurele geologie, HPT en petrologie vaak een motiverende bijdrage geleverd tijdens het werk op de Uithof. De vele borrels en barbeques waren altijd een goede afsluiting van de week; het gesjouw met bier op vrijdag zal ik erg missen. Mijn collega-promovendi hebben voor (te) veel vertier en afleiding gezorgd tijdens de soms toch wellange sessies op de Uithof. Uitreikingen van vergulde stoelpoten en andere onnozele activiteiten waren een onmisbare toevoeging aan mijn promotietijd. Vanuit het thuisfront had Bernard altijd op het juiste moment positieve feedback, waarbij ik en passant ook nog wat over het Arabisch Nubische Schild geleerd heb. Bovendien wil ik mijn ouders bedanken voor de genetische belasting met een natuurwetenschappelijke interesse, en de vele vakanties in de bergen, want daar is het tenslotte allemaal mee begonnen.

Curriculum Vitae

Ik werd geboren op 23 juli 1975. Het grootste deel van mijn jeugd heb ik doorgebracht in Doornik, waar ik in 1993 mijn VWO diploma behaalde op het Reclus Lyceum. Na een jaar op een universiteit in Pennsylvania te hebben 'gestudeerd', begon ik in 1994 met geologie in Utrecht. Een expeditie met UNESCO naar Antarctica in 1997 was een erg leuk intermezzo. Direct na het behalen van het doctoraal diploma in de structurele geologie begon ik in 1999 aan mijn promotieonderzoek, eveneens aan de Faculteit Aardwetenschappen in Utrecht. Per 1 oktober 2003 werk ik als Exploratory Researcher bij Shell in Rijswijk.

Appendices

Chapter 4. North Star Basalt structures and geochemistry

Appendix 4.A. Geochem data tables North Star Basalt
Appendix 4.B. Argon data tables (on CD-ROM only)

Chapter 5. West Pilbara structures, geochemistry and geochronology

Appendix S.A. Detailed structural map Sholl Shear Zone at Balla Balla
(large version on CD-ROM)
Appendix S.B. Geochem data tables
Appendix S.c. Argon data tables (on CD-ROM only)
Appendix S.D. V-Pb data table (on CD-ROM only)

Chapter 6. Central Pilbara V-Pb geochronology

Appendix 6.A. LA-ICP-MS U-Pb data tables (on CD-ROM only)
Appendix 6.B. SHRIMP U-Pb data tables (on CD-ROM only)
Appendix 6.C. LA-ICP-MS trace element data tables (on CD-ROM only)

Chapter 7. Central Pilbara structures and geochem

Appendix 7.A. Aerial photograph interpretations Tabba Tabba Shear Zone
(compilation on CD-ROM)
Appendix 7.B. Geochem data tables
Appendix 7.C. Argon data tables (on CD-ROM only)

CD-ROM available on request: please e-mail theauthoratbeinrema@geo.uu.nl

Taiga Taiga Sample Description

Sample	East	North	Unit	description	Group	Act	Ep	Czo	Chi	Srp	Ms	Kfsp	PlOtz	Cal	001	Mgs	Tic	Tin	Zrn	Ap	OP9	
96JW11	07965/0	7673290	Lower ultramafic	gabbro	Gabbro	60	5		5				10 10					5 rim			5	
96JW12	0796431	7673612	Lower ultramafic	basalt	ultramafic				15+30				5		20	10	10					10
96JW13	0796312	7673632	Lower ultramafic	basalt	ultramafic				20+20						30	10	10					10
96JW14	0796127	1673390	Lower ultramafic	dolerite	Dolerite	5			30			10		25								10
96JW15	0796121	7673390	Lower ultramafic	pyroxenite	Pyroxenite		5		35bl		10				20		10					10
96JW16	0796260	7673318	Lower ultramafic	dorente	Gabbro	70						10						10				
96JW17	0796306	7673430	Lower ultramafic	gabbro	Gabbro	4.5	5		10				10 10					10 r+s	ace			
96JW18	0795981	7673909	Main Basalt	ren from pyr	Basalt	25		to	10				15					5				
96JW19	0795985	7673686	Gabbroic	gabbro	Gabbro	30	15		5		ser		15 25									
96JW20	0796090	7673554	Gabbroic	gabbro	Gabbro	30	15		10				10 20					10rim				
96JW21	0196068	7673497	Lower ultramafic	pyroxenite	Pyroxenite		5		20		10		5 20									
96JW22	0195935	7673414	Lower ultramafic	pyroxenite	Pyroxenite	60							10 15									
96JW2S	0793425	7674347	Upper extrusive	basall	Basall	20				10			10 20									ace
96JW26	0793425	7674347	Upper extrusive	basall	Basall	10			15				5 10 25									2
VK05	0796298	7672990	Lower ultramafic	gabbro	Gabbro	45		10	10		ser		20 10						ace	ace		5
VK09	0791925	7674086	Green diorite	diorite	Diorite	2.5			15				35 5									5
VK16	0794340	7674565	Green diorite	diorite	Diorite	30					20		5 5									5
VK20	0793650	7673695	Dykes	dotonle dyke	Dykes		10		15		5		5 10 25									10
VK27	0193110	7613335	Main Basalt	mafic contact um schist	Basalt		5		25		5		5 15 35									5
VK28	0793422	7673643	Green diorite	diorite	Diorite	1.5	5		15				15 5									5
VK31	0793900	7673950	Green diorite	diorite	Diorite	5	25		15													B
VK32	0794328	7673554	Gabbroic	gabbro	Gabbro	50	10		15													ace
VK33	0794097	7673533	Dykes	ultramafic dyke	ultramafic				10				10					38				2
VK34	0793921	7673506	Green diorite	feeder diorite	Diorite		2.5		10				15 5 10									5
VK35	0793900	7673405	Main Basalt	basall	Basall	30			20		2		10 20 1									ace 1
VK37	0793324	7672950	Dykes	dyke	Dykes		10		15		5		15 20									ace 5
VK39	0791802	7673582	Dykes	dyke	Dykes				30		10		15 7 20		10							ace 8
VK40	0791845	7673315	Felsic	felsic Sill	Felsic		10				30		10									ace 5
VK41	0791894	7673330	Green diorite	diorite	Diorite	2.5	10		15		5		15 5 5									5
VK43	0792223	7673107	Dykes	dyke dolerite	Dykes		10		5				10 20									5
VK44	0792292	7673116	Green diorite	coarse diorite	Diorite	20	15		10		5		20 5									5
VK46	0792655	7673368	Gabbroic	sill of gabbro	Gabbro	10	25		25	10			15 10									ace 5
VK47	0792679	7673082	Main Basalt	massive basalt	Basalt				30		2		20 35									ace 4
VK49	0794955	7672905	Lower ultramafic	pyroxenite	Pyroxenite				30		10		15									10
VK51	0794923	7672854	Gabbroic	gabbro	Gabbro	20			2.5		10		12					10				
VK52	0794925	7672113	Gabbroic	pegmatoid	Pegmatoid	1.5		15	20				30									
VK54	0795209	7671722	Lower ultramafic	ol/chi dolerite	Dolerite	40		10	5				20 1									10
VK55	0795655	7673317	Main Basalt	basalt with veins	Basalt				30				25									10
VK56	0795671	7673330	Gabbroic	pegmatoid	Pegmatoid	45							10									5
VK58	0795724	7673239	Gabbroic	ren from pyr	Gabbro	40	15		10				20									5
VK59	0795255	7673237	Felsic	felsic	Felsic	40	10		15				25									5
VK60	0795128	7673534	Main Basalt	basalt	Basalt		10		5				50 30									ace 5
VK61	0794933	7673515	Dykes	ultramafic dyke	ultramafic	45							20 10									
VK64	0795427	7673032	Gabbroic	coarse gabbro	Gabbro				2.5				5									20
VK66	0795038	7672928	Dykes	ironized dolerite dyke	Dykes	30	20		5				25									8 r+s
VK71	0794594	7673620	Main Basalt	massive basalt	Basalt	10	10		2.5				10 15									10
VK72	0794625	7673494	Gabbroic	gabbro	Gabbro	40		10	5				15 5									
VK73	0195326	7672437	Lower ultramafic	vesicle rich basalt	Basalt	50			5				30									
VK77	0794684	7674605	Chert	chert	Chert							30	15									
VK78	0794545	7674428	Middle ultramafic	massive ultramafic	ultramafic				35				10		25	10	10					2
VK79	0794005	7674857	Chert	big chert, fault zone	Chert							10	90									1
VK80	0793744	7674673	Upper extrusive	massive basalt	Basalt				20			10	10	35								ace
VK81	0794040	7674765	Upper extrusive	massive ultramafic branched	ultramafic	20			10						25	10	30					
VK83	0795486	7673079	Upper extrusive	ultramafic carb schist	ultramafic				20				10		5	5	50					ace

Taiga Taiga Major Elements

Sample	SiO ₂	Al ₂ O ₃	Fe ₂ O ₃	MnO	MgO	CaO	Na ₂ O	K ₂ O	TiO ₂	P ₂ O ₅	Sum	LOI
96JW11	50.2318	13.3564	15.9897	0.2283	6.9886	9.1212	2.19270.3144	1.4217	0.1552	0.0234	101	1.1
96JW12	43.0207	3.0520	13.8452	0.1672	37.3259	2.2686	0.0000	0.0000	0.2970	0.0234	97.4	11.9
96JW13	43.6026	4.2556	14.9760	0.1872	33.2543	3.2673	0.00000.00470.4104	0.0419	0.0419	0.0419	97.7	11.7
96JW14	43.3776	4.0455	15.3111	0.2040	33.8769	2.7390	0.0000	0.0023	0.4057	0.0378	97.5	10.3
96JW15	43.7767	3.0790	15.0012	0.1458	36.5770	1.0996	0.0000	0.0012	0.3021	0.0174	97.3	10.9
96JW16	46.5395	13.8802	16.0273	0.3054	4.1631	14.5757	2.0261	0.1724	2.0835	0.2268	100.3	1.1
96JW17	48.5012	14.6646	15.7662	0.3093	51442	10.1368	3.0926	0.3750	1.8121	0.1981	99.7	0.8
96JW18	52.147013.9417	14.11410.2058	6.5196	9.3080	1.9062	0.2778	1.4246	0.1551	100.4	1.8		
96JW19	65.4549	12.4928	11.5954	0.1934	0.4985	4.3072	4.3072	0.2463	0.7218	0.1825	100.9	0.6
96JW20	49.2475	16.3248	11.0417	0.1771	6.8214	13.1671	2.23670.1518	0.7783	0.0536	0.0536	100.5	1.7
96JW21	44.3416	4.2843	16.84870.186530.8005	3.1411	0.0000	0.0022	0.3695	0.0255	98.7	8.6		
95JW22	51.4256	4.7641	11.2091	0.2011	16.9425	14.3542	0.4228	0.1557	0.5043	0.0206	99.8	2.8
96JW25	51.7813	14.8709	10.4290	0.2761	8.8499	12.4739	0.6362	0.0670	0.5680	0.0477	98.8	10.8
96JW26	57.1738	13.7663	11.2206	0.1934	4.4577	10.1499	1.7590	0.0776	1.0849	0.1169	98.4	6.9
VK16	51.2031	12.9768	11.3673	0.2012	15.0693	7.2429	0.9054	0.5332	0.4426	0.0382	99.4	
VK05	50.8970	13.5467	16.2561	0.1935	5.0316	8.5151	3.3867	0.5806	1.3643	0.2284	103.4	
VK09	52.1372	14.5663	11.4521	0.1808	9.6439	1.9361	3.1142	0.3215	0.5827	0.0653	99.7	
VK20	49.3509	11.1795	16.2153	0.2115	9.4673	9.9709	1.1079	1.2388	1.1683	0.0896	99.3	
VK27	50.3930	14.3544	16.0850	0.2341	7.0245	9.3660	0.0000	1.4660	0.9773	0.0998	98.3	
VK28	53.7965	14.3655	10.8980	0.1684	7.8267	8.5203	3.5666	0.2279	0.5647	0.0654	100.9	
VK31	53.7965	14.3655	10.8980	0.1684	7.8267	8.5203	3.5666	0.2279	0.5647	0.0654	100.1	
VK32	51.7871	13.2967	11.5971	0.1800	11.4971	8.9978	1.7996	0.1900	0.6098	0.0450	101	
VK33	50.0613	14.4446	13.1584	0.1979	8.4095	10.1904	2.3745	0.3957	0.7222	0.0455	92.7	
VK34	39.9288	9.4966	16.0794	0.3022	5.5037	26.5472	0.0000	1.0792	1.0036	0.0594	99.7	
VK35	55.1887	14.6501	12.6432	0.3311	5.0172	8.5292	2.4082	0.1204	1.0034	0.1084	100.6	
VK37	52.4164	14.4220	14.7204	0.1591	8.3548	6.5645	2.1882	0.1094	0.9548	0.1104	99.5	
VK39	56.2441	14.2619	14.9649	0.1507	8.4366	4.0174	0.0000	0.9843	0.8437	0.0964	96.8	
VK40	45.9290	12.4132	19.0336	0.2690	5.6894	13.9649	1.24130.0000	1.3448	0.1148	100.3		
VK41	65.1391	20.6490	1.5961	0.0200	0.9975	3.2919	3.8904	3.6310	0.7182	0.0668	99.6	
VK43	51.9061	12.2486	10.84300.2008	17.1682	6.1243	8.032	0.3213	0.3514	0.0331	100.3		
VK44	52.0350	11.9621	12.3608	0.1994	10.7659	10.9652	0.8972	0.2392	0.5483	0.0269	100.6	
VK46	52.7933	15.3110	10.9365	0.1690	7.9538	8.4509	3.3804	0.3380	0.6065	0.0606	102.7	
VK47	52.3519	13.1611	17.45060.2437	6.0444	7.3117	1.7548	0.0390	1.4916	0.1511	97.6		
VK49	53.3440	13.4128	14.43670.1638	8.3958	7.4743	1.6382008190.9624	0.0901	100.2				
VK51	46.2834	3.2917	12.0696	0.1596	34.9120	2.9925	0.0000	0.0000	0.2693	0.0219	101.3	
VK52	50.6677	13.9262	16.9880	0.2272	6.4199	7.2100	3.06180.3358	1.0568	0.1067	100.1		
VK54	50.1554	14.5870	13.48800.1998	6.3943	11.0901	2.7975	0.3297	0.8792	0.0789	99.6		
VK55	47.3720	3.2117	11.9434	0.1305	36.9341	0.1004	0.0000	0.0000	0.2810	0.0271	99.2	
VK56	51.1439	10.7937	13.61820.2522	8.8771	11.7016	2.7236	0.1211	0.6960	0.0726	99.7		
VK58	50.9241	7.7340	14.7650	0.2511	10.9482	12.9570	1.3057	0.2411	0.7935	0.0804	103.4	
VK59	48.2354	13.2430	20.9761	0.2610	4.7365	7.6365	2.9966	0.2513	1.5080	0.1556	100.5	
VK60	67.7464	16.0164	3.9792	0.0597	1.2932	4.1782	5.1730	1.0346	0.3979	0.1214	100.9	
VK61	52.9630	12.7705	14.1565	0.2079	5.5438	10.5926	2.1779	0.2970	1.1682	0.1228	90.7	
VK64	43.4265	9.5891	17.0840	0.2976	14.7694	13.9979	0.0000	0.0000	0.7826	0.0529	99.4	
VK66	50.6316	14.2936	13.58900.2215	6.2409	1.1732	2.6171	0.2516	0.8757	0.1057	98.5		
VK71	48.5028	10.9588	16.0323	0.2334	9.3353	11.8720	1.6235	0.2131	1.1365	0.0923	100.4	
VK72	52.9351	12.9822	15.3975	0.2516	5.1325	11.5733	1.40890.1107	0.1037	0.1047	100.4		
VK73	52.0297	14.1098	13.5219	0.2646	4.7033	9.5045	4.21330.2940	1.2346	0.1244	102		
VK77	57.5889	0.8414	36.0866	0.9349	1.1219	3.3656	0.0000	0.0000	0.0000	0.0608	107	
VK78	49.372311.2401	13.1309	0.1786	19.1187	6.3029	0.0000	0.0735	0.5462	0.0368	95.1		
VK79	98.9095	0.4362	0.6543	0.0000	0.0000	0.0000	0.0000	0.0000	0.0000	0.0000	91.9	
VK80	52.9440	13.5727	12.1222	0.2590	10.3609	10.1537	0.0000	0.0000	0.5491	0.0383	96.8	
VK81	49.7694	13.8770	12.5206	0.2713	8.5557	12.7293	1.5651	0.0626	0.6052	0.0438	95.9	
VK83	49.1474	3.7964	10.87600.2155	16.6219	18.8792	0.0000	0.0000	0.4412	0.0226	97.5		
avg 25 error	0.1307	0.0514	0.0136	0.0020	0.0379	0.0193	0.0371	0.0011	0.0057	0.0049		
st. dev.	0.0400	0.0103	0.0050	0.0000	0.0112	0.0092	0.0073	0.0004	0.0016	0.0009		

Talga 1ak

Sample	C.	Pr	Nd	Sm	Eu	Gd	Tb	Dy	Ho	E.	Tm	Yb	Lu	HI	T.	W	TI	Pb	B.	Th	U	
96JW11	22.5	3.267	16	4.23	1.382	4.62	0.91	5.36	1.17	3.33	0.51	31	0.463	3.1	0.38	0.8	0.15	-5	-0.05	1.3	0.31	
96JW12	1.02	0.164	0.92	0.36	0.138	0.61	0.11	0.69	0.14	0.4	0.062	0.35	0.055	0.4	0.02	1.1	-0.05	21	-0.05	0.06	-0.05	
96JW13	2.18	0.325	1.78	0.69	0.243	1.06	0.21	1.18	0.25	0.71	0.102	0.6	0.089	0.6	0.04	0.2	-0.05	-5	0.28	0.12	-0.05	
96JW14	1.78	0.286	1.55	0.54	0.195	0.94	0.18	1.07	0.23	0.61	0.092	0.53	0.08	0.6	0.08	-0.2	-0.05	-5	-0.05	0.1	-0.05	
96JW15	0.83	0.145	0.8	0.32	0.103	0.51	0.1	0.62	0.13	0.38	0.059	0.33	0.051	0.4	0.04	0.4	-0.05	-5	0.61	0.07	-0.05	
96JW16	31.4	4.479	22.5	6.23	2.299	7.52	1.37	8	1.67	4.73	0.725	4.52	0.656	4.5	0.56	0.9	-0.05	5	0.93	1.93	0.48	
96JW17	26.5	4.01	19	5.15	1.61	5.68	1.06	6.46	1.36	3.89	0.597	3.67	0.554	3.5	0.43	1.4	-0.05	-5	0.06	1.57	0.33	
96JW18	20.5	2.998	14.9	4.01	1.348	4.92	0.94	5.66	1.22	3.55	0.534	3.41	0.504	3	0.37	0.9	0.07	-5	0.08	1.3	0.29	
96JW19	29.5	4.393	23.2	7.65	2.595	10.5	1.99	11.7	2.43	6.88	1.065	6.56	0.935	6.8	0.58	1.8	0.07	-5	0.11	1.96	0.39	
96JW20	5.23	0.798	4.48	1.57	0.638	2.34	0.45	2.72	0.54	1.54	0.221	1.4	0.199	1.3	0.1	0.8	-0.05	-5	-0.05	0.28	0.07	
96JW21	1.42	0.222	1.31	0.49	0.077	0.78	0.16	0.98	0.2	0.56	0.089	0.48	0.071	as	0.03	-0.2	-0.05	-5	0.84	0.09	-0.05	
96JW22	1.78	0.324	1.89	0.86	0.342	1.48	0.3	1.76	0.36	1	0.143	0.86	0.121	0.6	0.03	0.7	-0.05	-5	0.75	0.08	-0.05	
96JW25	11.5	1.56	7.38	1.96	0.585	2.56	0.51	3.08	0.69	2.15	0.348	2.13	0.323	1.6	0.19	0.4	-0.05	-5	-0.05	0.85	0.21	
96JW25	16.1	2.28	11.1	3.19	1.313	4.03	0.78	4.8	1.06	3.14	0.488	3.04	0.45	2.2	0.26	1.7	-0.05	-5	0.16	0.89	0.34	
VK16	8.61	1.204	5.79	1.66	0.483	2.07	0.41	2.6	0.59	1.77	0.277	1.8	0.271	1.4	0.2	0.7	0.1	-5	-0.05	0.74	0.13	
VK05	23.7	3.225	16.7	5.08	1.648	6.12	1.14	6.66	1.42	4.12	0.636	4.04	0.595	3.8	0.5	0.8	0.17	-5	0.14	1.68	0.32	
VK09	9.5	1.306	6.5	1.9	0.674	2.41	0.48	2.99	0.65	1.96	0.323	2.08	0.311	1.5	0.17	0.8	0.08	-5	0.07	0.73	0.17	
VK20	12.3	1.93	10.5	2.98	1.149	3.46	0.62	3.81	0.77	2.28	0.338	2.12	0.3	1.7	0.24	1.8	3.25	-5	0.29	0.29	0.07	
VK27	14	1.952	9.86	2.88	0.906	3.65	0.71	4.44	0.97	2.79	0.436	2.72	0.406	2.1	0.24	8.7	0.64	-5	0.19	0.85	0.21	
VK25	7.74	1.14	5.93	2.03	0.647	2.61	0.53	3.44	0.77	2.33	0.375	2.48	0.363	1.7	0.15	0.7	0.1	6	0.18	0.75	0.16	
VK31	8.77	1.213	5.98	1.76	0.566	2.28	0.45	2.86	0.63	1.85	0.292	1.88	0.283	1.4	0.15	5.7	0.07	-5	0.08	0.68	0.15	
VK32	4.67	0.701	3.86	1.28	0.547	1.57	0.32	1.95	0.46	1.31	0.198	1.37	0.204	0.8	0.08	0.4	0.05	-5	-0.05	0.18	-0.05	
VK33	8.11	1.326	7.2	2.1	0.694	2.3	0.43	2.62	0.55	1.54	0.233	1.5	0.237	1.2	0.16	2.1	0.36	-5	0.17	0.19	0.32	
VK34	14.3	1.997	9.88	2.75	0.808	3.3	0.64	3.78	0.84	2.43	0.379	2.44	0.361	2	0.28	1.6	0.07	13	0.87	0.79	0.17	
VK35	14.4	1.999	9.9	2.79	1.029	3.39	0.63	3.87	0.86	2.5	0.394	2.58	0.384	2.1	0.23	0.8	0.06	-5	-0.05	0.87	0.21	
VK3i	14.3	1.97	10	2.78	0.694	3.39	0.66	4.19	0.91	2.71	0.444	2.76	0.407	2.1	0.24	3	0.36	-5	0.09	0.86	0.2	
VK39	14.8	2.258	12	3.6	1.04	4.43	0.86	5.22	1.11	3.32	0.515	3.31	0.5	2.5	0.28	3.8	-0.05	-5	-0.05	0.61	0.14	
VK46	13.5	1.885	8.9	2.35	0.688	2.58	0.49	2.84	0.56	1.58	0.215	1.31	0.191	2.6	0.53	1.7	0.82	-5	0.08	1.3	0.31	
VK41	8.54	1.127	5.39	1.49	0.446	1.94	0.38	2.43	0.51	1.6	0.258	1.64	0.245	1.2	0.15	0.5	0.1	-5	0.09	0.62	0.14	
VK43	5.12	0.788	4.15	1.35	0.489	1.69	0.35	2.11	0.46	1.37	0.209	1.35	0.216	0.9	0.09	1.2	0.1	-5	0.07	0.23	0.06	
VK44	7.91	1.176	6.23	2.28	0.665	2.67	0.55	2.67	3.45	0.74	2.25	0.354	2.34	0.347	1.4	0.13	0.8	0.17	-5	0.19	0.6	0.14
VK46	18.1	2.747	14.9	4.44	1.506	5.3	0.97	5.62	1.13	3.24	0.465	2.81	0.4	3.2	0.35	0.8	0.08	5	0.05	0.88	0.2	
VK47	14	1.944	9.73	2.71	0.911	3.21	0.62	3.81	0.82	2.4	0.383	2.44	0.364	2	0.29	0.9	0.07	-5	0.17	0.79	0.18	
VK49	1.33	0.192	1.11	0.45	0.144	0.68	0.13	0.82	0.17	0.47	0.065	0.43	0.063	0.4	0.04	0.7	-0.05	-5	-0.05	0.09	-0.05	
VK51	10.9	1.77	9.5	2.97	0.997	3.88	0.75	4.67	0.99	3.08	0.462	3.02	0.453	2.1	0.22	1.2	0.1	-5	0.15	0.48	0.1	
VK52	6.92	1.034	5.51	2.03	0.757	2.78	0.55	3.29	0.69	1.9	0.264	1.71	0.237	1.6	0.13	1.5	0.14	-5	0.33	0.38	0.08	
VK54	1.47	0.234	1.3	0.45	0.155	0.73	0.15	0.88	0.18	0.51	0.074	0.45	0.061	0.5	0.03	1.4	-0.05	-5	0.08	0.09	0.08	
VK55	8.47	1.221	6.19	1.82	0.652	2.33	0.47	2.92	0.63	1.88	0.286	1.89	0.275	1.4	0.15	1.1	0.07	-5	-0.05	0.48	0.12	
VK56	6.6	1.02	5.75	2.09	0.738	3.24	0.6	3.68	0.74	2.05	0.319	1.89	0.278	1.5	0.11	0.7	0.07	-5	0.48	0.38	0.1	
VK58	9.9	1.474	7.85	2.67	1.03	3.76	0.72	4.38	0.9	2.52	0.37	2.3	0.332	2.1	0.18	0.8	0.06	-5	-0.05	0.53	0.12	
VK59	34.4	3.908	15.7	2.78	0.86	2.2	0.38	2.1	0.43	1.35	0.2	1.45	0.22	3.2	0.41	2.3	0.24	9	0.08	3.53	0.75	
VK60	1.71	2.406	12.2	3.41	1.042	4.24	0.81	5.04	1.08	3.24	0.493	3.19	0.49	2.5	0.34	2.7	0.06	-5	0.19	1.07	0.25	
VK61	4.7	0.735	4.17	1.47	0.519	1.8	0.34	2.16	0.43	1.25	0.189	1.16	0.168	1.1	0.09	1	-0.05	-5	0.07	0.24	0.06	
VK64	7.89	1.166	6.27	2.15	0.808	3.06	0.58	3.6	0.74	2.11	0.312	1.89	0.267	1.7	0.14	1	0.07	-5	0.27	0.4	0.09	
VK66	11.2	1.826	9.94	2.84	0.927	3.19	0.58	3.51	0.7	2.07	0.313	2	0.294	1.6	0.22	0.5	0.35	-5	0.17	0.26	0.06	
VK71	14.8	2.085	10.3	2.96	0.9	3.66	0.69	4.42	0.94	2.83	0.438	2.92	0.429	2.4	0.26	1.2	0.05	-5	0.12	0.89	0.22	
VK71	15.6	2.235	11.4	3.16	0.983	3.8	0.73	4.6	0.98	2.92	0.451	2.95	0.428	2.2	0.29	2.5	-0.05	-5	0.24	0.95	0.22	
VK73	22.4	3.133	15.5	4.14	1.229	4.66	0.88	5.27	1.1	3.35	0.521	3.32	0.496	3	0.37	2.2	0.1	-5	0.35	1.3	0.33	
VK77	7.34	0.834	3.35	0.69	0.448	0.96	0.18	1.25	0.31	0.97	0.139	0.88	0.127	0.2	0.04	1.3	-0.05	-5	0.63	0.3	0.37	
VK73	5.68	0.804	3.91	1.15	0.242	1.46	0.29	1.87	0.4	1.21	0.184	1.26	0.183	0.9	0.09	0.8	0.09	-5	-0.05	0.44	0.11	
VK79	0.9	0.125	0.59	0.15	0.053	0.16	0.03	0.19	0.04	0.12	0.017	0.12	0.017	-0.1	0.12	1.9	-0.05	-5	0.16	-0.05	0.05	
VK80	11.3	1.515	7.22	2.03	0.559	2.5	0.48	3.12	0.69	2.06	0.322	2.16	0.317	1.8	0.21	0.8	-0.05	-5	-0.05	0.91	0.23	
VK81	11.6	1.564	7.48	2.07	0.592	2.59	0.53	3.32	0.73	2.15	0.342	2.24	0.343	1.8	0.22	0.5	0.14	-5	-0.05	0.94	0.23	
VK81	2.02	0.33	1.92	0.82	0.334	1.29	0.25	1.44	0.3	0.87	0.132	0.79	0.111	0.6	0.04	2.2	-0.05	-5	0.8	1.3	0.06	
avg error	9.0	8.0	8.2	4.0				5.0		4.0		3.0		2.0	5.0	6.0	1.0			1.0	0	
sl. dev	0.0	0.0	2.5	0.0				0.0		0.0		0.0		0.0	0.0	0.0	0.0			0.0	0.0	



West Pilbara Geochem sample description

sample	E-W	N-S	Domain	unit	location	age (Ma)	description	IUGS classification
KB047	0484475	7703328	Roebourne	Ruth Well	Karratha Rd	>3265	foliated metabasalt	basalt
KB492	0497518	7690862	Roebourne	Regal	Pipeline Rd	2925	coarse metagabbro	tholeiitic gabbro
KB493	0496883	7691396	Roebourne	Andover	Pipeline Rd	2925	coarse metadiorite	monzodiorite
KB494	0495852	7692414	Roebourne	Andover	Pipeline Rd	2925	coarse dark gabbro	olivine gabbro
KB495	0493133	7694878	Roebourne	Regal	Pipeline Rd	2925	metagabbro	andesite
KB498	0484409	7705996	Roebourne	Regal	Karratha Rd	3265-3150	metabasalt	tholeiitic basalt
KB653	0481850	7704834	Roebourne	Regal	TomW	3265-3150	metabasalt	tholeiitic basalt
KB654	0481587	7705164	Roebourne	Regal	TomW	3265-3150	dark, homogeneous metabasalt	basalt
KB676	0483945	7693026	Roebourne	Ruth Well	RuthW	>3265	massive metabasalt	tholeiitic basalt
KB678	0483781	7692325	Roebourne	Ruth Well	RuthW	>3265	slightly foliated metagabbro	syenite
KB680	0473885	7696934	Roebourne	Regal	Mt Regal	3265-3150	metagabbro sill in metabasalt	tholeiitic gabbro
KB681	0473844	7696921	Roebourne	Regal	Mt Regal	3265-3150	metabasalt	tholeiitic basalt
KB682	0513170	7712036	Roebourne	Cleaverville	Prison	3020	gabbro sill in cleaverville fm	diorite
KB686	0507847	7707944	Roebourne	Regal	Rocky Ck	3265-3150	coarse vesicular metabasalt	tholeiitic basalt
KB689	0502499	7713903	Roebourne	Regal	Rocky Ck	3265-3150	andesitic metabasalt	tholeiitic basalt
KB691	0500043	7702940	Roebourne	Regal	Nickol W	3265-3150	metabasalt	tholeiitic basalt
KB696	0504488	7693182	Roebourne	Andover	Nickol W	2925	metagabbro	tholeiitic gabbro
KB698	0505700	7684837	Sholl	Sholl	Pipeline R	3120	tight colored pillowed metabasalt	andesite
KB700	0495689	7688621	Sholl	Sholl	Pipeline R	3120	green light colored coarse metagabbro	diorite
KB704	0516724	7687737	Sholl	Sholl	MtAda	3120	fine grained metagabbro, green	tholeiitic gabbro
KB707	0516309	7686763	Roebourne	Cleav	MtAda	3020	vesicular metabasalt	basalt

West Pilbara Geochem sample petrography

sample	description	metam	alt	plag	qlz	bio	chi	serp	hbl	act	trem	epid	cpx	opq
KB047	foliated metabasalt	amph	min	x			x		x	x				x
KB492	coarse metagabbro	grsch	min	x					x	x		x		
KB493	coarse metadiorite	grsch	min											
KB494	coarse dark metagabbro	grsch	min	x					x					
KB495	fine grained metagabbro	grsch	med	x			x		x	x				
KB498	metabasalt. tiny veins	amph	bad											
KB653	metabasalt, tiny veins	amph	bad											
KB654	dark, homogeneous coarse metabasalt	amph	min	x					x	x	x			
KB676	massive metabasalt	amph	med	x					x	x				
KB678	slightly foliated metagabbro	amph	bad	x			x		x					
KB680	metagabbro sill in metabasalt	amph	bad											
KB681	metabasalt, tiny veins	amph	bad	x					x	x		x		
KB682	gabbro sill in cleaverville fm	grsch	bad	x			x		x	x		x	x	
KB686	coarse vesicular metabasalt	grsch	med											
KB689	andesilic metabasalt. tiny veins	grsch	bad											
KB691	metabasalt	amph	min	x					x					
KB696	metagabbro	grsch	min	x			x		x	x		x	x	x
KB698	light colored pillowed metabasalt	grsch	min											
KB700	green light colored coarse metagabbro	grsch	min											
KB704	fine grained metagabbro, green	grsch	med											
KB707	vesicular metabasalt	grsch	med											

West Pilbara Geochem Major Elements

Sample	SiO2	TiO2	Al2O3	Fe2O3	FeO	MnO	MgO	CaO	Na2O	K2O	P2O5	LOI	Sum
KB047	50.76	0.79	12.69	8.6	3.68	0.19	9.91	8.14	3.19	0.4	0.31	0.92	100.00
KB492	50.39	1.8	12.97	9.78	4.19	0.21	5.73	10.22	1.95	0.33	0.2	1.78	100.00
KB493	65.21	0.61	14.6	3.79	1.62	0.11	2.4	4.95	3.62	1.38	0.09	1.43	98.60
KB494	51.44	0.91	15.84	6.49	2.78	0.17	7.35	7.02	3.7	1.41	0.1	2.48	99.20
KB495	54.92	0.65	12.45	7.82	3.35	0.18	7.12	9.16	2.25	0.6	0.1	1.02	98.60
KB498	48.21	1.01	14.69	8.81	3.78	0.21	5.6	12.42	2.11	0.09	0.32	2.33	99.10
KB653	51.6	1.35	14.56	8.57	3.67	0.21	6.81	9.23	3.12	0.1	0.12	0.28	99.20
KB654	48	1.22	14.88	9.67	4.15	0.25	7.45	10.51	2.53	0.2	0.1	0.59	100.00
KB676	50.33	1.06	13.83	7.58	3.25	0.19	9.13	8.59	2.53	1.05	0.14	1.96	99.90
KB678	54.82	0.91	8.47	8.39	3.59	0.19	8.97	8.85	3.1	11.6	0.1	1.06	99.10
KB680	49.22	1.38	14.62	9.43	4.04	0.21	6.82	10.44	2.49	0.15	0.16	0.60	99.90
KB681	49.15	1.32	14.27	9.2	3.94	0.22	6.74	10.8	2.63	0.23	0.12	0.95	100.00
KB682	56.31	0.79	13.9	7.55	3.23	0.16	4.45	7.5	3.15	0.65	0.11	1.84	99.50
KB686	51.29	1.62	15.12	9.1	3.9	0.34	4.31	8.86	2.7	0.21	0.13	1.99	99.10
KB689	49.72	1.26	14.18	9.34	4	0.23	5.72	10	1.33	0	0.11	3.67	99.20
KB691	49.06	1.26	14.85	8.99	3.85	0.2	7.12	8.52	1.52	2.08	0.13	1.98	99.80
KB696	51.39	0.4	17.49	4.45	1.91	0.12	7.26	10.61	2.89	0.75	0.05	2.47	99.30
KB698	54.17	0.9	14.51	4.63	1.98	0.18	3.19	8.45	3.4	1.24	0.17	6.95	98.80
KB700	55.37	0.49	13.75	6.43	2.76	0.17	6.71	8.11	2.05	1.19	0.1	2.56	100.00
KB704	51.73	0.27	16.29	5.68	2.43	0.15	8.72	7.63	1.8	0.83	0.06	4.13	101.00
KB707	39.88	0.89	15.97	7.37	3.16	0.27	3.91	12.58	0.07	3.18	0.18	12.19	98.40
BN02 std	52.32	0.92	17.21	9.09		0.17	5.69	10.44	2.90	0.68	0.12	0.47	100.00
BR std	38.42	2.64	9.97	12.97		0.24	13.55	13.84	2.99	1.38	1.07	2.94	100.00
OU4 sId	63.05	0.78	14.69	5.71		0.15	2.20	4.38	3.63	2.68	0.18	2.55	99.50
minerror	0.100	0.004	0.030	0.010		0.001	0.010	0.006	0.030	0.001	0.004	0.100	
avg 2s% error	0.202	1.095	0.320	0.113		0.756	0.145	0.111	32.681	1.932	19.187	9.749	
stdev of error	0.026	1.245	0.363	0.051		0.348	0.071	0.154	95.336	5.133	33.136	10.883	

West Pilbara Geochem Trace Elements

Sample	Li	Be	Sc	Ti	V	Cr	Co	Ni	Cu	Zn	Ga	As	Se	Rb	Sr	Y	Zr
KB047	63.90	0.44	32.45	4760.93	215.63	476.16	71.00	16933	86.55	123.87	5.49	0.46	0.70	33.03	109.36	17.42	49.60
KB492	54.02	0.83	39.41	10776.86	340.81	252.81	74.61	84.10	97.53	111.03	6.47	1.23	1.17	35.95	228.17	22.03	120.44
KB493	31.08	1.42	15.33	3681.62	9638	235.78	57.95	36.32	28.72	103.28	12.51	1.35	1.05	48.79	268.94	22.58	66.16
KB494	51.19	0.69	33.99	5478.22	195.69	474.05	5456	76.41	35.08	93.74	998	2.02	0.90	63.86	268.62	17.35	77.85
KB495	1790	0.76	3052	3888.65	206.51	656.14	8255	185.24	56.30	91.26	7.83	290	0.88	21.96	143.55	18.60	100.75
KB498	19.20	0.29	38.01	6027.98	282.36	391.90	80.00	140.06	161.10	97.26	5.54	0.71	1.25	2.23	142.79	20.55	7.74
KB653	853	0.52	40.11	8064.14	354.29	55462	8287	131.28	24.47	110.43	5.43	0.83	1.28	1.21	129.66	26.29	49.08
KB654	104.39	0.41	43.00	7312.68	355.01	290.56	65.28	131.97	11.31	114.71	5.69	0.85	1.13	14.12	133.26	24.35	32.70
KB676	95.22	0.56	32.93	6351.79	303.20	635.76	65.15	18869	21.51	63.03	10.81	2.61	0.94	40.22	218.90	19.95	76.85
KB678	39.89	0.97	23.91	5459.56	192.74	1064.92	85.56	299.82	193.62	112.99	13.02	1.91	0.95	36.94	222.46	13.59	108.93
KB680	8.43	0.49	38.43	8285.41	348.34	314.44	73.63	122.58	94.68	110.04	5.83	0.91	1.57	1.00	121.51	30.57	45.16
KB681	7.83	0.44	38.78	7900.89	366.73	814.59	78.72	137.32	136.96	117.93	5.77	1.28	1.99	3.73	103.14	26.22	26.70
KB682	10.03	0.87	30.04	4723.48	262.91	299.79	70.94	59.31	103.25	88.48	8.97	2.85	0.96	12.14	189.00	18.46	83.86
KB686	6.74	0.57	44.66	9716.60	434.12	520.44	90.78	103.99	175.44	139.42	6.34	1.50	1.86	7.31	161.11	32.69	36.11
KB689	22.42	0.51	40.66	7567.72	385.68	361.70	71.18	132.31	132.06	111.22	5.93	176.35	1.29	0.17	220.17	25.79	61.68
KB691	19.17	0.39	39.94	7544.28	36607	236.92	69.91	141.91	94.29	116.11	15.30	4.60	1.46	89.21	103.68	25.23	46.26
KB696	35.97	0.45	24.40	2379.85	143.92	388.73	138.97	191.39	31.92	64.35	7.97	16.33	0.60	40.89	269.08	8.03	59.73
KB698	14.60	0.56	25.26	5377.15	211.62	331.16	5825	85.91	50.76	7532	7.80	0.78	0.84	48.96	159.96	15.36	87.87
KB700	27.13	0.72	28.34	2957.29	199.36	650.74	71.45	119.52	59.02	95.28	8.71	323	0.76	39.91	166.57	14.67	81.39
KB704	27.45	0.35	3330	1610.72	165.60	738.89	62.43	125.38	30.64	60.87	6.68	5.70	0.61	32.19	378.42	11.60	41.84
KB707	33.71	0.76	26.40	5348.34	213.35	241.63	56.56	154.61	9.03	106.72	21.13	0.84	0.96	82.33	312.65	21.33	130.74
BN02 std	577	0.56	3456		236.88	78.95	140.20	35.24	86.64	78.45	608	114	0.93	2165	189.55	25.30	101.69
BR sid	11.68	1.68	2209		216.95	322.56	99.33	256.44	69.64	167.45	20.70	2.18	1.32	47.88	1335.03	28.67	278.37
OU4std	33.33	1.65	19.07		79.02	51.67	77.71	20.06	26.96	77.16	9.45	1.86	1.61	99.83	103.77	46.57	200.98
avg 2s% error	1.306	4.261	1.471	1.410	1.835	1.852	0.936	3.108	2.230	1.635	1.247	1.471	1.122	1.071	0.816	0.829	2.331
stdev of error	0.597	1.865	0.984	1.431	1.768	0.971	0.263	2.178	1.042	1.094	0.349	0.984	0.315	0.800	0.357	0.292	4305

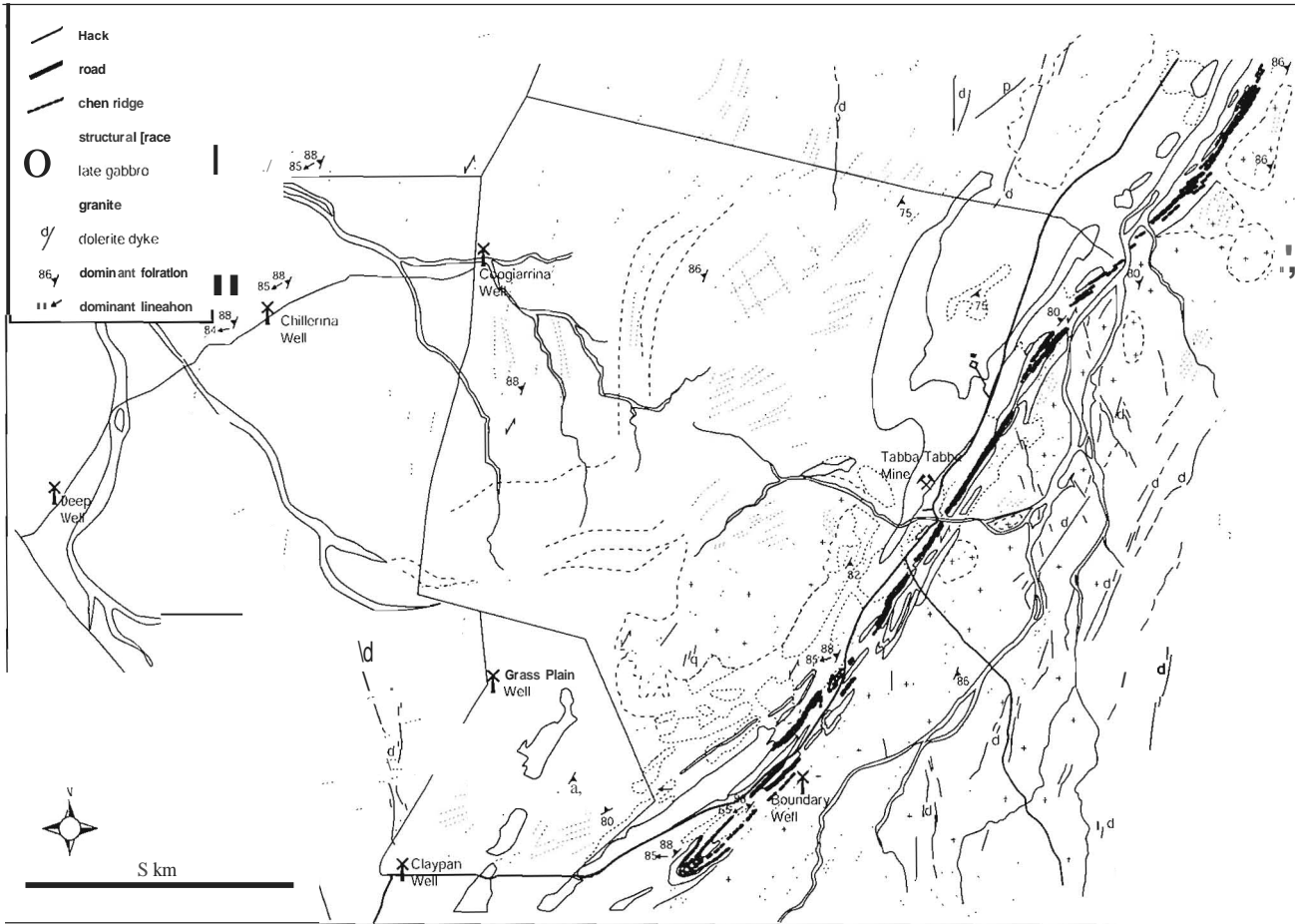
West Pilbara

Sample	Nb	Mo	Ag	Cd	Sn	Sb	Cs	Ba	La	Ce	Pr	Nd	Sm	Eu	Gd	Tb	Dy	Ho	Er	Tm
KB047	2.96	0.56	0.81	0.28	0.85	0.03	1.63	109.01	4.15	10.97	1.56	7.61	2.23	0.82	2.84	0.49	3.13	0.67	1.85	0.27
KB492	17.60	1.61	0.64	0.35	16.72	0.19	4.86	105.17	13.95	31.48	4.32	18.51	4.35	1.45	4.63	0.76	4.42	0.90	2.42	0.36
KB493	9.60	1.63	0.73	0.37	2.34	0.17	3.26	506.45	20.26	41.86	5.34	20.86	4.43	1.40	4.41	0.72	4.29	0.91	2.52	0.39
KB494	4.84	1.16	0.52	0.23	0.83	0.34	4.25	451.02	8.69	18.16	2.41	10.41	2.66	0.85	3.04	0.52	3.25	0.70	1.96	0.30
KB495	5.46	2.29	0.72	0.26	1.04	0.48	4.41	245.37	15.67	30.54	3.69	14.23	3.03	0.86	3.26	0.55	3.41	0.73	2.07	0.31
KB498	3.21	1.28	0.52	0.31	0.78	0.63	0.40	29.39	3.73	9.54	1.48	7.54	2.40	0.88	3.13	0.58	3.72	0.82	2.33	0.35
KB653	4.92	2.61	0.65	0.31	1.06	0.06	0.09	53.27	4.24	12.31	1.99	10.22	3.23	1.09	4.15	0.76	4.92	1.06	3.06	0.46
KB654	3.76	1.21	0.47	0.32	0.97	0.08	0.79	38.02	4.72	11.25	1.83	9.24	2.86	1.00	3.81	0.71	4.52	0.98	2.77	0.42
KB676	4.52	1.67	0.58	0.30	0.87	0.39	3.05	477.32	5.95	15.59	2.20	10.19	2.83	1.06	3.43	0.61	3.77	0.81	2.29	0.34
KB678	8.00	1.99	0.71	0.30	1.07	0.12	1.29	708.34	17.79	35.08	4.38	17.59	3.82	1.18	3.70	0.55	2.99	0.57	1.50	0.21
KB680	5.31	1.88	0.52	0.26	0.82	0.13	0.08	30.76	6.09	15.71	2.45	12.30	3.69	1.29	4.67	0.87	5.60	1.21	3.51	0.52
KB681	4.86	3.96	0.57	0.39	1.30	0.10	0.13	59.70	5.20	13.51	2.07	10.50	3.21	1.17	4.18	0.76	4.83	1.06	2.99	0.45
KB682	4.89	2.18	0.57	0.25	0.93	0.28	0.07	321.55	11.81	23.60	2.89	11.84	2.85	0.92	3.20	0.54	3.41	0.72	2.03	0.30
KB686	5.49	4.56	0.72	0.44	1.09	0.45	0.27	44.80	6.34	16.18	2.49	12.59	3.96	1.32	5.17	0.96	6.07	1.30	3.67	0.55
KB689	4.08	2.83	0.55	0.30	0.85	10.37	0.30	10.34	4.27	11.46	1.77	9.12	2.97	1.09	3.91	0.72	4.67	1.01	2.90	0.43
KB691	3.99	1.83	0.53	0.28	0.69	0.72	3.92	782.04	4.17	11.24	1.74	8.98	2.88	0.99	3.84	0.71	4.62	1.00	2.85	0.44
KB696	3.22	1.97	0.65	0.26	0.68	0.18	3.60	248.80	6.61	12.93	1.55	6.30	1.45	0.64	1.58	0.25	1.50	0.31	0.88	0.13
KB698	5.63	1.55	0.72	0.21	0.80	0.06	1.22	299.97	9.92	22.28	2.88	12.28	2.76	0.84	2.94	0.48	2.84	0.60	1.67	0.25
KB700	4.13	2.12	0.74	0.69	0.89	0.86	2.27	335.74	12.38	23.23	2.66	10.20	2.22	0.70	2.47	0.41	2.61	0.56	1.62	0.25
KB704	2.05	2.51	0.54	0.22	0.51	1.39	0.82	244.77	6.63	13.31	1.56	6.03	1.23	0.42	1.34	0.24	1.74	0.43	1.40	0.23
KB707	6.40	0.98	0.60	0.19	0.90	0.18	1.49	1170.58	11.30	23.36	2.94	12.47	3.12	1.04	3.67	0.62	3.85	0.83	2.45	0.39
BN02 std	4.02	1.13	1.41	0.26	1.00	0.08	0.69	116.12	8.27	18.56	2.53	11.28	3.11	0.94	3.77	0.67	4.32	0.95	2.72	0.41
BR std	130.97	2.32	1.59	0.38	1.94	0.15	0.74	1092.31	80.33	147.01	17.09	64.90	11.92	3.59	10.17	1.34	6.44	1.10	2.59	0.32
OU4 std	15.23	1.10	1.18	0.30	2.21	0.27	1.97	357.85	23.99	56.13	6.86	28.11	6.86	1.62	7.52	1.30	8.10	1.71	4.84	0.74
avg 2s% error	1.304	8.783	10.964	11.212	3.756	14.079	1.671	1.136	1.113	0.969	1.354	1.656	3.192	3740	2.574	2.895	3.103	3.001	3.315	4.803
stdev of error	0.790	4.252	5.113	3.664	2.670	7.501	0.893	0.555	0.374	0.310	0.514	0.763	1.865	2.561	1.350	2.188	1.789	2.031	2.410	3.203

West Pilbara									
Sample	Vb	Lu	Hf	Ta	Ti	Pb	Bi	Th	U
KB047	1.76	0.27	1.47	1.36	0.26	2.58	0.25	0.65	0.16
KB492	2.25	0.35	3.06	3.00	0.30	2.08	0.01	1.40	0.35
KB493	2.49	0.39	2.16	2.39	0.43	10.33	0.14	5.46	1.10
KB494	1.94	0.31	2.00	1.56	0.44	3.14	0.04	1.69	0.53
KB495	2.00	0.31	2.64	1.74	0.17	7.69	0.03	4.57	1.25
KB498	2.23	0.34	0.42	1.36	0.02	1.02	0.01	0.37	0.09
KB653	3.01	0.46	1.44	1.57	0.01	0.99	0.01	0.52	0.12
KB654	2.66	0.40	1.05	1.22	0.12	0.76	0.02	0.46	0.10
KB676	2.23	0.35	2.07	1.45	0.20	3.76	0.02	1.68	0.43
KB678	1.27	0.19	2.88	1.89	0.30	17.65	0.04	4.72	0.76
KB6S0	3.39	0.51	1.32	1.51	0.02	0.68	0.02	0.59	0.17
KB6S1	2.88	0.44	0.85	1.64	0.04	1.31	0.01	0.53	0.13
KB6S2	1.97	0.30	2.32	1.71	0.06	6.43	0.05	3.32	1.08
KB6S6	3.43	0.50	1.05	1.80	0.02	1.19	0.01	0.72	0.18
KB6S9	2.74	0.40	1.91	1.36	0.01	0.52	0.01	0.48	0.12
KB691	2.78	0.43	1.32	1.30	0.64	2.14	0.03	0.48	0.11
KB696	0.83	0.13	1.48	2.22	0.33	3.72	0.08	1.57	0.45
KB698	1.63	0.25	2.18	1.56	0.22	1.18	0.01	1.15	0.29
KB700	1.67	0.26	2.18	1.56	0.25	7.21	0.05	4.05	1.30
KB704	1.68	0.27	1.17	1.22	0.15	2.79	0.01	1.20	0.32
KB707	2.58	0.41	3.26	1.45	0.50	2.49	0.01	3.61	0.83
BNO1 sld	2.70	0.43	2.70	3.22	0.03	4.23	0.00	3.62	1.12
BR sid	1.85	0.26	5.90	13.14	0.04	4.86	0.01	9.87	2.46
OU4sld	4.72	0.73	5.41	3.71	0.46	14.75	0.09	7.88	2.14
avg 2s% error	3.658	5.833	3.074	3.002	6.450	1.954	7.329	1.563	3.060
slddev of error	1.805	10.393	2.067	1.432	5.666	1.293	4.784	1.139	3.533



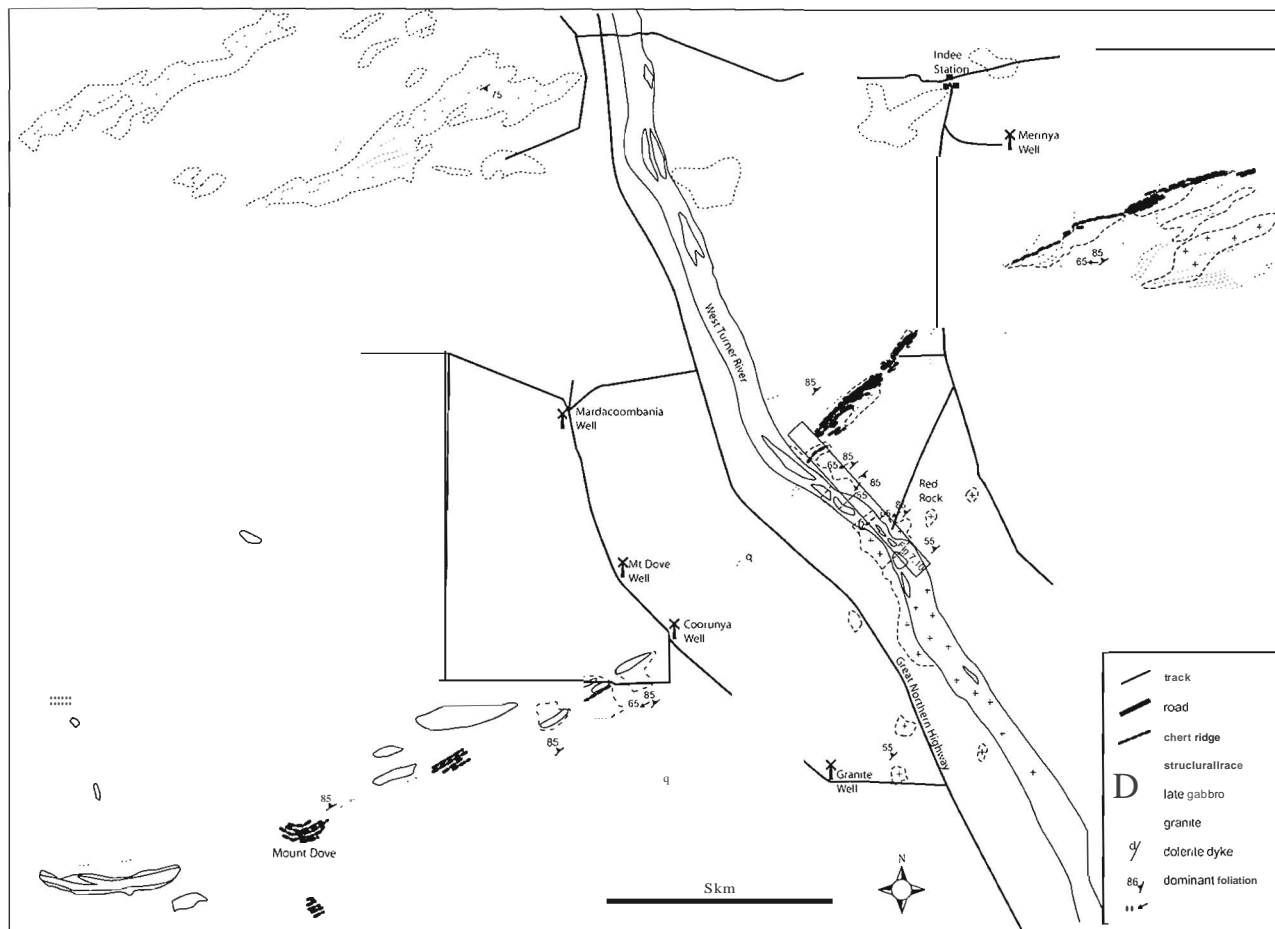
Aerial photograph interpretation, with added field structural and kinematic data. Location indicated in Figure 7.5. Full version on CD.



Aerial photograph of the area, with added field structural and kinematic data. location indicated in Figure 7.5. Full version on CD.



Aerial photograph interpretation, with added field structural and kinematic data. location indicated in Figure 7.5. Full version on CD.



Aerial photograph interpretation, with added field structural and kinematic data, location indicated in Figure 7.5. Full version on CD.

Tabba Tabba / Mallina Geochem samples - sample description

sample	10	batch	E-W	N-S	location	unit	age (Ma)	description	IUGS classification	Group
DL030	aus17	batch1	0664185	7693562	WTR	TT	?	massive ultramafics	tholeiitic basalt	unassigned mafics
DL031	aus34	batch1	0678386	7700278	ETR	TT	?	dark gabbro	komatiitic gabbro	Early mafic A
DL040	aus31	batch1	0708730	7727822	WalStn	TT	?	amphibolite	Fe-tholeiitic gabbro	intermediate schist
DL041	aus16	batch1	0696959	7707780	WalStn	TT	?	diorite	diorite	unassigned mafics
DL044	aus22	batch1	0693500	7705800	WalStn	TT	2930	dark gabbro	Mg-tholeiitic gabbro	Late Gabbro
DL046	aus23	batch1	0691739	7706018	WalStn	TT	2930	light colored gabbro	Mg-tholeiitic gabbro	Mal late gabbro
DL076	aus28	batch1	0663340	7692019	WTR	TT	3255	diorite	Fe-tholeiitic gabbro	Early mafic A
DL078	aus26	batch1	0663540	7691700	WTR	TT	3255	diorite	Fe-tholeiitic gabbro	Early mafic A
DL082	aus29	batch1	0663774	7691488	WTR	TT	3255	diorite	Fe-tholeiitic gabbro	Early mafic A
DL086	aus27	batch1	0663984	7691114	WTR	TT	?	light colored gabbro	Mg-tholeiitic gabbro	intermediate schist
DL101	aus25	batch1	0683981	7700065	ETR	TT	3235	silicified gabbro or diorite	Mg-tholeiitic gabbro	Early mafic B
DL108	aus30	batch1	0682340	7699634	ETR	TT	2930	amphibolite	Fe-tholeiitic gabbro	Mal late gabbro
DI130	aus15	batch1	0709438	7728007	Strelley	TT	?	amphibolite	Fe-tholeiitic gabbro	unassigned mafics
DL131	aus20	batch1	0706331	7725749	DonaldW	TT	2930	lale gabbro w-branch	Mg-lholeiitic gabbro	Late Gabbro
DL132	aus21	batch1	0707425	7725422	DonaldW	TT	2930	lale gabbro main body	Mg-tholeiitic gabbro	Late Gabbro
DL134	aus24	batch1	0705900	7722000	DonaldW	TT	2930	dark undeformed gabbro	Mg-lholeiitic gabbro	Late Gabbro
DL138	aus18	batch1	0701175	7718559	Mine fence	TT	2955	biotite granodiorite - sanukitoid	granodiorite	Mal sanukitoid
DL145	aus32	batch1	0700130	7718044	Mine	TT	2930	dark undeformed gabbro	Mg-tholeiitic gabbro	Late Gabbro
DL154	aus33	batch1	0700068	7711313	6MileW	TT	?	amphibolite	Fe-tholeiitic gabbro	intermediate schist
KB263	KB263	batch3	0678504	7699525	ETR	TT	3255	muscovite schist	dacite	musc schist
KB265	KB265	batch3	0678876	7699316	ETR	TT	3255	deformed granodiorite	diorite	musc schist
KB304	KB304	batch3	0663984	7691114	WTR	TT	?	coarse dark gabbro	komatiitic gabbro	musc schist
KB312	KB312	batch3	0663537	7691680	WTR	TT	3255	muscovite schist	rhyolite	musc schist
KB331	KB331	batch3	0683981	7700038	Pyr Isi E	TT	3235	s of chert silicified gabbro or diorite? Fresh	quartz-albite syenite	Early mafic B
KB430	KB430	batch3	0699853	7711500	6MileW	TT	3255	muscovite schist	rhyodacite	musc schist
KB547	KB547	batch2	0686000	7715607	Chillerina	Mal	2955	hbl diorite, round plag phenocrysts - sanukitoid	quartz monzodiorite	Mal sanukitoid
KB558	KB558	batch2	0685080	7706784	Wal	Mal	2955	hbl-diorite - sanukitoid (Wal stn)	quartz monzodiorite	Mal sanukitoid
KB560	KB560	batch2	0673939	7707736	WalStn	Mal	2930	gabbro hills W of Wal Stn, coarse plag-hbl	tholeiitic gabbro	Mal late gabbro
KB567	KB567	batch2	0691848	7711214	Wal	Mal	2955	biotite diorite - sanukitoid diorite	quartz monzonite	Mal sanukitoid
KB575	KB575	batch2	0669646	7710278	Walyanna	Mal	2930	gabbro (layered)	tholeiitic gabbro	Mal late gabbro
KB576	KB576	batch2	0669634	7710291	Walyanna	Mal	2930	light colored gabbro	tholeiitic gabbro	Mal late gabbro
KB581	KB581	batch2	0667043	7711896	Walyanna	Mal	2960	fine grained gabbro	tholeiitic gabbro	Millindinna
KB591	KB591	batch2	0658921	7687245	Mt Berghaus	Mal	2970	bedding parallel gabbro sill	tholeiitic gabbro	Early mafic A
KB592	KB592	batch2	0658480	7686580	Mt Berghaus	Mal	2970	bedding parallel mafic, very fine grained	tholeiitic basalt	Early mafic A
KB607	KB607	batch2	0602891	7678370	Mal	Mal	2955	diorite sanukitoid	diorite	Mal sanukitoid
KB635	KB635	batch2	0589447	7666628	Copper M H	Mal	2960	light colored meta-mafic, coarse. Millindinna	albite leuco gabbro	Millindinna
KB636	KB636	batch2	0588748	7666449	Copper M H	Mal	2960	dark colored mela-mafic, coarse. Millindinna	albite melano gabbro	Millindinna
KB779	KB779	batch3	0684277	7700096	BALBRYNA	TT	3235	gabbro with red dots	melano gabbro	Early mafic B
KB810	KB810	batch3	0682840	7699554	BALBRYNA	TT	3235	dark very very coarse gabbro	diorite	Early mafic B
KB815	KB815	batch3	0682840	7699554	BALBRYNA	TT	3235	gabbro with red dots	diorite	Early mafic B

Tabba Tabba / Mallina Geochem samples - petrographic description

sample	description	metam	alt	plag	Kfsp	qlz	bio	ms	chi	serp	carb	zo	ep	qt	hbl	act	trem	opq
DL030	massive ultramafics	amph	min						X	X	X							X
DL031	dark gabbro	amph	min							X	X					X		X
DL040	amphibolite	amph	min	X		X									X			X
DL041	diorite	amph	min															
DL044	dark gabbro	amph	bad															
DL046	light colored gabbro	amph	min	X		X									X	X		
DL076	diorite	amph	bad															
DL078	diorite	amph	med															
DL082	diorite	amph	min															
DL086	light colored gabbro	amph	min	X		X												
DL101	silicified gabbro or diorite	amph	min	X											X	X		
DL108	amphibolite	amph	min															
DL130	amphibolite	amph	bad	X												X		
DL131	late gabbro w-branch	amph	min	X					X						X	X		
DL132	late gabbro main body	amph	min	X					X						X			
DL134	dark undeformed gabbro	amph	med	X					X						X			
DL138	biotite granodiorite - sanukitoid	amph	min															
DL145	dark undeformed gabbro	amph	min															
DL154	amphibolite	amph	min															
KB263	muscovite schist	greensch	med	X		X		X	X									
KB265	deformed granodiorite	greensch	bad															
KB304	coarse dark gabbro	amph	min															
KB312	muscovite schist	amph	min															
KB331	s of chert silicified gabbro or diorite? Fresh	amph	min															
KB430	muscovite schist	greensch	min															
KB547	hbl diorite. round plag phenocrysts - sanukitoid	amph	min	X		X			X						X			
KB558	hbl-diorite - sanukitoid (Wal sin)	greensch	med															
KB560	gabbro hills W of Wal Sin, coarse plag-hbl	greensch	min															
KB567	Diorite diorite - sanukitoid diorite	greensch	min															
KB575	gabbro (layered)	greensch	med	X									X		X	X		X
KB576	light colored gabbro	greensch	med															
KB581	fine grained gabbro	greensch	bad															
KB591	bedding parallel gabbro sill	greensch	med															
KB592	bedding parallel mafic, very fine grained	greensch	min															
KB607	diorite sanukitoid	greensch	med	X	X	X							X					
KB635	light colored meta-mafic, coarse. Millindinna	greensch	bad															
KB636	dark colored meta-mafic, coarse. Millindinna	greensch	med	X						X	X		X				X	X
KB779	gabbro with red dots	greensch	min	X						X								
KB810	dark very very coarse gabbro	greensch	bad							X	X						X	
KB815	gabbro with red dots	greensch	med															

Tabba Tabba / Mallina Geochem samples - major elements

sample	SiO2	TiO2	Al2O3	Fe2O3	MnO	MgO	CaO	Na2O	K2O	P2O5	IOI	total
OL030	52.588	0.658	14.262	13.547	0.197	7.599	8.142	1.741	0.081	0.051	1.11	98.92
OL031	39196	0.077	1.915	7.183	0.064	37.808	0.872	0.010	0.005	0.003	12.87	99.53
OL040	38.719	0.125	3.053	8.209	0.126	34.129	2.271	0.010	0.008	0.005	13.34	100.28
OL041	66565	0.372	14.732	4.363	0.065	3.587	3.062	4.333	1.846	0.113	0.91	98.71
OL044	51.217	0.250	13.286	7.542	0.153	11.398	12.115	1.225	0.461	0.020	2.31	99.57
OL046	51.657	0.323	14.765	8.187	0.162	9.505	11.884	1.629	0.618	0.030	1.21	99.82
OL076	52.013	0.360	14.010	8.326	0.163	9.822	12.794	1.667	0.114	0.022	0.70	99.90
OL078	52.703	0.468	21.789	4.578	0.078	3.907	11.433	2.755	0.799	0.060	1.40	99.66
OL082	51.485	0.317	16.058	7.723	0.141	8.465	11.761	1.896	0.497	0.030	1.60	100.08
OI086	49.510	0.500	18.714	7.677	0.119	8.934	11.181	1.751	0.229	0.069	1.31	99.32
OL101	47.521	2.624	12.633	19.647	0.237	5.469	7.120	3.973	0.360	0.200	0.20	99.39
OL108	57.300	0.610	15.797	6.786	0.117	5.387	7.516	3.000	1.780	0.162	1.51	99.22
OL130	49.641	1.360	14.665	13.994	0.202	6.146	9.761	2.913	0.441	0.159	0.70	99.36
OL131	49.839	1.285	14.858	14.348	0.191	5.116	9.712	3.457	0.446	0.134	0.60	99.58
OL132	42.452	1.878	18.102	15.360	0.124	5.604	12.584	0.927	0.418	0.15	2.52	99.42
DL134	49.932	1.396	14.201	16.544	0.215	5.146	7.835	2.044	0.953	0.068	1.60	99.70
DL138	52.142	0.354	15.512	7.942	0.144	8.303	11.441	1.965	0.825	0.030	1.30	99.24
DL145	50.806	0.973	16.584	12.684	0.182	4.793	9.157	2.076	0.727	0.084	1.91	99.73
DL154	49.943	0.990	7.405	14.769	0.223	13.232	10.389	0.784	0.272	0.078	1.91	99.73
KB263	63.900	0.662	15.466	5.220	0.099	2.574	6.573	4.701	0.217	0.129	0.46	98.66
KB265	50.251	0.314	15.501	7.730	0.133	12.968	9.807	1.084	0.155	0.041	2.02	99.17
KB304	42.948	0.340	4.597	16.093	0.196	28.163	2.816	0.000	0.000	0.049	4.80	98.81
KB312	75.523	0.223	11.744	4.799	0.043	0.006	1.023	5.052	0.975	0.036	0.58	98.10
KB331	74.518	0.163	13.759	1.316	0.026	0.151	0.581	3.435	5.574	0.047	0.43	99.30
KB430	67.919	0.453	15.071	3.208	0.061	1.548	2.678	4.654	2.525	0.153	1.73	101.34
KB547	64.927	0.577	15.487	4.726	0.083	2.214	4.249	4.110	2.184	0.260	1.18	99.50
KB558	65.517	0.481	13.846	4.886	0.086	3.341	3.150	3.943	3.201	0.271	1.28	98.40
KB560	50.832	0.549	12.708	11.033	0.186	11.329	8.630	2.394	0.449	0.118	1.77	99.80
KB567	57.534	0.599	14.557	7.259	0.128	6.625	4.862	2.901	3.951	0.226	1.36	99.60
KB575	51.579	0.640	13.188	9.730	0.170	11.625	8.245	2.208	0.499	0.097	2.02	100.00
KB576	50.631	0.750	16.085	9.133	0.157	7.168	10.903	2.343	0.593	0.113	2.12	90.60
KB581	50.413	0.592	13.948	12.653	0.207	7.044	12.952	1.066	0.086	0.066	0.97	99.30
KB591	48.931	1.490	14.008	14.699	0.198	5.811	9.964	2.585	0.405	0.253	1.66	99.70
KB592	49.577	0.876	14.179	14.278	0.205	6.257	10.709	2.271	0.392	0.092	1.17	99.60
KB507	56.185	0.740	15.520	9.017	0.125	4.921	5.432	3.919	1.768	0.315	2.06	99.70
KB635	47.688	0.313	18.453	8.693	0.143	6.993	13.403	1.476	0.022	0.047	2.77	100.00
KB636	47.835	0.399	16.242	12.479	0.194	8.834	11.290	1.565	0.258	0.053	0.85	100.00
KB779	49.141	0.798	17.315	8.657	0.128	7.947	9.918	1.992	1.771	0.161	2.17	100.11
KB810	58.294	0.736	15.484	6.882	0.125	5.354	6.599	2.571	2.004	0.131	1.82	99.42
KB815	67.460	0.751	14.722	4.558	0.095	1.563	5.687	4.427	0.222	0.142	0.37	98.70
minerror	0.100	0.004	0.030	0.010	0.001	0.010	0.006	0.030	0.001	0.004	0.100	
avg 2σ% error	0.202	1.095	0.320	0.113	0.756	0.145	0.111	32.681	1.932	19.187	9.749	
stdev of error	0.026	1.245	0.363	0.051	0.348	0.071	0.154	95.336	5.133	33.136	10.883	

Tabba Tabba & Mallina Geochem - Trace Elements

sample	Li	Bc	Ti	V	Cr	Co	Ni	Cu	Zn	G.	As	Se	Rb	Sr	Y	Zr	Nb
OL03J			3946.08	44.08	1620.00	33.16	560.23	-10.00	-30.00	1.82	-5.00		-2.00	31.90	2.56	4.23	-0.50
OL031			461.57	174.26	1210.00	30.17	168.52	39.01	-30.00	6.68	-5.00		5.61	55.53	14.50	67.77	4.92
OL040			751.51	509.80	51.90	26.13	19.49	30.38	-30.00	9.87	-5.00		53.04	146.20	20.61	79.22	3.09
OL041			2229.06	36.85	1810.00	68.63	1810.00	-1000	-30.00	2.45	13.12		-2.00	7.12	1.91	5.10	-0.50
DL041			1499.09	123.46	141.32	26.29	79.00	-10.00	-30.00	9.59	-5.00		2.91	87.82	13.21	47.74	2.42
OL046			1935.53	107.46	55.14	20.13	45.92	35.27	-30.00	18.18	-5.00		27.61	231.23	16.17	88.03	4.83
DL076			2155.44	331.30	220.12	35.04	51.01	55.85	-30.00	15.18	-5.00		7.03	145.17	28.93	98.00	4.26
OL073			2804.63	701.54	25.30	31.35	16.20	20.35	78.42	15.90	-5.00		10.82	103.57	39.07	121.66	7.38
OL081			1900.14	310.67	45.74	42.71	53.22	48.81	76.95	17.40	-5.00		21.04	121.08	29.78	93.92	4.89
DL086			2997.70	133.68	84.11	23.25	67.32	18.33	70.32	16.72	-5.00		211.86	158.38	30.97	133.76	6.84
DL101			15730.19	115.53	234.07	27.42	161.91	13790	-3D 00	13.83	-5.00		21.20	270.71	6.16	17.54	1.21
OL103			3657.83	1060.00	50.69	47.71	643.11	272.94	46.11	20.12	-5.00		85.97	200.02	9.52	26.05	1.86
DL130			8155.56	330.84	68.96	32.08	-1500	53.89	75.19	12.46	-5.00		2.40	102.85	19.97	3704	1.52
OL.D1			7703.29	120.26	179.18	38.83	156.54	18.50	-30.00	10.80	-5.00		31.69	121.76	10.15	30.00	2.03
DL132			11256.77	136.08	108.05	43.97	141.67	46.95	54.40	13.04	-5.00		30.44	134.33	12.79	41.71	2.19
OL134			8369.88	128.89	307.12	41.53	657.38	72.28	71.04	14.58	-5.00		17.39	169.98	12.27	42.63	2.68
OL138			2122.03	57.96	236.99	12.85	70.41	-10.00	40.30	16.39	-5.00		73.84	282.31	13.39	118.50	6.79
DL146			5830.78	128.96	11476	33.58	120.94	32.14	40.52	13.50	-5.00		115.96	145.69	13.37	49.86	2.60
DL154			5932.76	256.92	65.14	39.05	23.85	29.53	63.22	17.72	-5.00		107.82	211.18	21.65	123.35	6.36
KB26J	12.28	1.54	3971.11	1.34	14.72	107.07	2.59	3.31	22.26	15.69			46.24	103.99	44.31	363.16	1620
KB26L	14.98	2.06	1882.84	79.13	27.67	132.97	40.94	1.16	49.92	17.31			2.46	247.00	34.56	155.42	13.20
KB304	392.99	11.21	2038.09	149.27	52.64	9202	140.34	7.03	111.86	16.53			248.37	147.26	29.10	73.90	7.66
KB311	12.87	1.93	1335.22	1.47	5.82	129.13	3.94	2.58	45.07	15.39			133.60	40.55	47.78	326.66	16.94
KB331	77.22	0.25	975.35	118.18	204.35	1151.6	443.51	212.27	55.87	15.33			26.43	263.08	6.08	12.24	0.94
KB430	96.83	1.87	2716.53	0.33	11.68	127.22	1.73	1.73	28.36	16.55			11142	54.27	50.19	349.03	19.81
KB547	25.73	1.83	3457.91	90.12	147.50	59.36	40.41	24.47	71.56	21.23	0.75	0.96	74.36	489.43	19.11	125.16	9.24
KB558	1600	2.23	2881.14	8349	21982	74.46	67.67	20.84	70.23	38.32	0.88	0.85	104.81	745.09	17.12	165.72	8.79
KB560	17.68	0.26	3289.49	153.09	663.74	69.84	149.03	55.06	91.29	5.74	0.61	0.61	14.23	158.56	10.94	35.00	2.09
KB567	10752	2.03	3591.63	120.46	345.36	55.09	151.20	5.89	100.55	12.95	0.78	0.97	206.46	459.77	20.43	48.87	6.15
KB575	19.30	0.35	3835.89	195.59	950.17	87.54	168.52	85.20	90.18	8.16	5.95	0.73	20.80	257.44	12.52	43.49	2.53
KB576	11.98	0.32	4497.97	193.39	494.64	75.50	94.32	73.19	75.73	8.05	0.76	0.66	18.15	327.98	11.97	28.90	2.52
KB581	8.16	0.14	3547.83	355.37	718.81	256.99	148.64	66.13	94.43	4.89	1.04	0.95	1.24	45.10	21.73	597	1.60
KB591	54.58	0.67	8930.30	398.54	173.63	106.96	112.50	206.49	128.46	8.63	14.85	2.05	19.24	38348	36.07	127.13	9.53
KB591	62.34	0.93	5248.76	289.07	231.79	88.75	153.79	130.17	102.02	6.42	1.92	0.98	21.34	170.82	18.47	34.26	4.01
KB601	32.18	1.85	4434.16	152.84	405.73	66.84	111.02	106.06	107.29	18.00	2.25	0.98	87.83	622.62	17.42	140.95	7.96
KB63S	21.95	0.06	1874.86	224.15	607.63	65.56	124.04	41.64	52.43	4.65	1.47	0.61	0.74	44.41	10.96	10.65	0.63
KB636	11.99	0.07	2392.74	264.30	459.58	78.65	277.51	35.67	70.72	4.71	0.84	0.85	13.24	48.94	15.12	17.18	0.79
KB779	9052	0.26	4782.03	94.06	469.11	94.08	360.87	15.53	51.63	15.07			19.41	219.15	5.53	7.22	0.71
KB810	6.00	0.58	4410.85	113.24	1658.97	168.82	2698.47	61.03	122.05	5.20			0.57	18.59	6.59	17.75	1.63
KB81S	11118	0.63	4503.64	86.19	404.59	100.31	515.52	5.80	60.86	12.44			24.43	146.95	6.25	11.93	0.87

Tabba

sample	Mo	A9	Cd	Sn	Sb	Cs	8a	La	Ce	Pr	Nd	Sm	Eu	Gd	Tb	Dy	Ho
DL030	-2.00	-0.50		-1.00	0.28	0A2	4.46	0.28	0.72	0.11	0.61	0.21	0.12	0.29	0.06	0.41	0.10
DL031	-2.00	-0.50		-1.00	0.59	0.27	32.98	4.28	1108	1.70	7.73	2.29	0.88	2.78	0.48	2.75	0.53
DL04Q	-2.00	-0.50		-1.00	-0.20	396	62 IA7	14.80	24.01	3.30	12.81	2.63	0.90	3.17	0.55	3.42	0.74
OLD41	-2.00	-0.50		-1.00	13.62	0.13	4.59	0A8	1.06	0.13	0.59	0.16	0.06	0.22	0.04	0.30	0.07
DL04.	-2.00	-0.50		-1.00	0.90	1.95	52.95	7.35	14.63	1.79	7.06	1.67	0.55	1.96	0.33	2.10	0A8
DL046	-2.00	-0.50		-1.00	1.40	1.52	27097	13.02	24.74	2.86	10.91	2.33	0.94	2.50	0.42	2.62	0.56
DL076	-2.00	-0.50		-1.00	-0.20	0.59	129.61	4.49	11.88	1.81	879	2.88	1.19	4.00	0.75	4.67	1.05
DL078	-2.00	-0.50		-1.00	-0.20	0.60	123.65	6.02	19.49	3.15	14.91	4.24	1.63	5.68	1.05	6.52	1.42
DL082	-2.00	-0.50		-1.00	-0.20	1.90	102.81	6.42	14.38	2.30	11.14	3.22	1.31	4.27	0.78	4.97	1.09
DL086	-2.00	-0.50		2.29	-0.20	26.24	324.83	2289	48.76	5.85	22.60	4.87	1.22	5.51	0.90	5.37	1.14
DL101	-2.00	-0.50		-1.00	-0.20	3.13	68.75	4.30	8.62	1.07	4.20	0.94	0.57	1.02	0.16	0.99	0.23
DL108	-2.00	-0.50		-1.00	0.33	8.80	125.51	3.78	8.22	1.11	4.88	1.30	0.64	1.63	0.28	1.66	0.36
DL130	-2.00	-0.50		-1.00	0.24	1.20	239.93	1.42	3.57	0.58	2.84	1.10	0.45	1.91	0.41	3.02	0.75
DL131	-2.00	-0.50		-1.00	-0.20	6.61	212.17	4.91	9A3	1.23	4.96	1.19	0.42	1.42	0.26	1.62	0.36
DL132	-2.00	-0.50		-1.00	-0.20	10.19	28935	6.18	12.60	1.64	6.61	1.58	0.56	1.80	0.32	2.06	0A5
DL134	-2.00	-0.50		-1.00	0.27	2.35	188.73	6.32	12.98	1.58	6.36	1.51	0.54	1.77	0.31	2.04	0.45
DL138	-2.00	-0.50		1.03	0.29	4.96	512A6	25.14	42.16	4.64	16.13	2.90	0.88	2.67	0.40	2.24	0.46
DL145	-2.00	-0.50		-1.00	-0.20	9.59	334.56	9.59	17.17	2.21	8.34	1.79	0.62	2.17	0.37	2.22	0.51
DL154	-2.00	-0.50		-1.00	-0.20	11.80	256.13	17.49	32.88	4.18	16.02	3.37	1.14	3.68	0.61	3.65	0.77
K8263	0.29		0.02	3.99	0.55	0.89	1023.96	50.75	95.16	11.12	41.07	8.11	1.86	7.56	1.18	7.25	1.47
K8265	0.08		0.05	2.93	0.17	1.23	234.05	38.27	72.52	8.46	31.62	6.01	1.61	5.85	0.92	5.61	1.14
K8304	0.09		0.14	2.76	0.17	36.42	364.57	30.09	50.31	6.94	26.37	5.06	1.15	4.88	0.77	4.71	0.97
K8312	0.16		0.07	4.25	0.20	1.54	401.58	54.54	95.91	12.85	48.06	9.41	1.73	8.15	1.29	7.92	1.68
KB331	0.03		0.06	0.30	0.12	3.80	71.57	4.18	8.66	1.07	4.54	1.02	0.55	1.04	0.17	1.01	0.21
KB430	0.12		0.05	3.67	1.03	5.21	617.80	56.83	113.89	12.72	46.71	9.13	1.48	8.30	1.33	8.26	1.64
KB547	0.72	0.77	0.28	1.48	0.05	1.24	98 IA6	55.90	93.14	11.61	41.22	6.82	1.60	5.50	0.74	3.77	0.72
K8551	0.68	1.03	0.31	1.90	0.09	1.10	1886.91	81.74	119.62	15.39	52.85	7.64	1.93	5.76	0.72	3.40	0.64
KB560	0.98	0.58	0.24	0.42	0.10	0.40	154.91	4.80	10.27	1.45	6.58	1.68	0.71	1.95	0.33	2.06	0.44
KB56)	0.91	0.61	0.33	1.16	0.04	14.15	579.21	34.21	76.99	8.64	33.19	6.9	1.73	5.65	0.80	4.19	0.82
K8575	1.08	0.97	0.32	1.15	0.20	0.98	301.06	5.73	120.9	1.68	7.71	1.96	0.82	2.27	0.38	2.37	0.51
KB576	1.16	0.73	0.28	0.44	0.09	1.10	264.30	5.49	11.73	1.63	7.50	1.93	0.87	2.20	0.37	2.28	0A8
KB58*	2.89	0.61	0.29	0.71	0.08	0.09	30.99	IA9	3.38	0.47	2.32	0.97	0.44	1.92	0.44	3A2	0.86
KB591	0.64	0.80	0.32	1.17	0.66	0.95	193.68	10.24	25.00	3.91	18.57	5.25	1.66	6.29	1.10	6.90	IA8
KB592	1.88	0.59	0.24	0.80	0.15	3.68	129.37	5.29	11.91	1.70	7.70	2.20	0.78	2.77	0.51	3.37	0.74
KB601	1.42	0.62	0.24	1.60	0.11	2.55	874.31	35.93	73.34	9.38	35.87	6.53	1.76	5.37	0.71	3.56	0.67
KB635	1.66	0.45	0.18	0.35	0.07	0.56	23.52	0.77	1.63	0.23	1.10	0.47	0.26	0.94	0.22	1.70	0.42
K8636	1.82	0.38	0.19	0.42	0.09	2.40	32.10	1.06	2.29	0.32	1.57	0.65	0.33	1.30	0.30	2.34	0.58
K8779	0.02		0.05	0.18	0.05	10.67	20.68	3.86	7.75	0.93	3.81	0.78	0.51	0.85	0.14	0.91	0.19
K88*0	0.04		0.04	0.73	0.25	4.15	3.41	4.38	9.36	1.14	4.67	1.02	0.29	1.06	0.17	1.09	0.22
KB815	0.02		0.04	0.26	0.07	14.56	17.80	3.43	6.84	0.82	3.37	0.77	0.41	0.86	0.15	0.95	0.21

Tabba											
sample	F'	Tm	Yb	Lu	Hf	Ta	Ti	Pb	Bi	Th	U
DL030	0.29	0.05	0.30	0.04	0.15	-0.10	0.05	5.70	0.20	-0.05	-0.05
DL031	1.54	0.20	1.29	0.19	1.96	0.36	0.11	-5.00	0.06	1.35	0.24
DL040	2.18	0.32	2.20	0.33	2.31	0.29	0.18	-5.00	0.10	2.83	0.49
DL041	0.22	0.04	0.24	0.03	0.14	-0.10	0.14	-5.00	0.22	0.10	-0.05
DL044	1.45	0.20	1.36	0.2'	1.36	0.16	0.08	-5.00	-0.06	1.82	0.44
DL045	1.68	0.25	1.61	0.22	2.43	0.31	0.32	11.49	1.61	3.59	0.87
DL076	3.16	0.45	2.95	0.46	2.66	0.27	0.31	-5.00	0.20	0.61	0.14
DL078	4.26	0.63	4.09	0.59	3.49	0.48	0.25	-5.00	0.13	1.24	0.31
DL082	3.25	0.48	3.21	0.49	2.60	0.31	0.66	-5.00	0.81	0.68	0.19
DL086	3.33	0.47	3.02	0.45	3.51	0A9	3.52	-5.00	10.08	3.64	0.65
DL101	0.67	0.09	0.59	0.10	0.48	-0.10	0.33	-5.00	-0.06	0.37	0.08
DL103	1.06	0.14	0.96	0.14	0.84	0.12	1.19	-5.00	4.44	0.38	0.10
DL13)	2.42	0.36	2.48	0.38	1.22	-0.10	0.32	5.83	0.07	0.21	-0.05
DL131	1.12	0.16	1.02	0.16	0.87	0.11	0.62	-5.00	0.57	1.12	0.25
DL132	1.41	0.19	1.37	0.21	1.21	0.13	0.79	8.99	0A6	1.56	0.38
DL134	1.32	0.19	1.28	0.19	1.19	0.16	0.81	23.48	0.76	1.66	0.38
DL133	1.35	0.20	1.35	0.20	3A3	0.62	1.20	24.67	0.74	6.37	0.88
DL145	1.51	0.22	1.44	0.22	1.56	0.17	1.76	-5.00	2.80	2.19	0.49
DL151	2.35	0.34	2.3'	0.35	3.21	0.45	1.53	-5.00	0.82	3.43	0.73
KB263	4.42	0.73	4.68	0.87	8.47	1.06	0.78	8.64	0.08	12.39	2.89
KB265	3.43	0.51	3.16	0A6	3.80	0.88	0.04	8.58	0.12	9.08	1.67
KB304	2.98	0A5	2.77	0.39	1.82	0.52	4.07	4.46	0.72	5.72	0.92
KB312	5.45	0.87	5.68	0.82	7.99	1.26	0.87	18.52	0.16	16.57	3.28
KB331	0.60	0.10	0.63	0.09	0.36	0.09	0.61	2.44	0.09	0.35	0.08
KB431	5.07	0.82	5.27	0.77	8.59	1.37	1.91	11.51	0.02	17.19	3.41
KB541	1.89	0.26	1.61	0.24	2.97	1.97	0.49	21.60	0.02	10.27	0.56
KB558	1.73	0.25	1.57	0.24	4.10	2.46	0.91	23.34	0.28	15.96	1.54
KB560	1.24	0.18	1.21	0.19	0.95	1.05	0.07	2.02	0.01	0.63	0.14
KB561	2.15	0.30	1.88	0.28	1.61	1.71	2.07	12.89	0.23	4.07	1.88
KB575	1.44	0.21	1.39	0.22	1.16	1.37	0.14	3.98	0.03	0.76	0.18
KB576	1.35	0.20	1.30	0.20	0.84	1.41	0.12	8.70	0.21	0.69	0.16
KB581	2.61	0A2	2.80	0A5	0.38	3.99	0.02	1.37	0.05	0.26	0.08
KB591	4.14	0.62	3.87	0.60	2.94	2.58	0.14	3.81	0.07	1.61	0.42
KB591	2.15	0.33	2.12	0.33	1.08	1.45	0.15	2.43	0.04	1.21	0.29
KB601	1.78	0.25	1.55	0.24	3.24	2.07	0.51	9.24	0.06	5.04	1.45
KB63i	1.32	0.21	1.45	0.23	0.38	1.09	0.01	0.68	0.01	0.41	0.03
KB633	1.82	0.29	1.99	0.32	0.56	1.06	0.09	1.29	0.02	0.15	0.06
KB779	0.58	0.09	0.62	0.10	0.20	0.09	0.62	1.82	0.29	0.23	0.05
KB810	0.67	0.10	0.66	0.10	0.48	0.11	0.09	0.46	2.93	0.66	0.16
KB815	0.70	0.11	0.74	0.12	0.33	0.09	0.63	1.34	DAD	0.46	0.10